Investigating the role of Asporin in musculoskeletal development.

Rachel Deborah Pearson

Biosciences Institute

Thesis submitted to Newcastle University for the Degree of Doctor of Philosophy

January 2024

Abstract

Understanding musculoskeletal development is of high importance, as it forms the foundation for understanding various skeletal disorders and can illuminate pathways involved in other musculoskeletal conditions including osteoarthritis (OA). This thesis focuses on the role of Asporin, a small leucine-rich proteoglycan (SLRP), expressed in the developing periosteum, perichondrium, tendons, and subchondral bone. Asporin possesses a unique ability among SLRPs to mineralise type I collagen fibres. A polymorphism associated with risk of OA and IDD was identified in GWAS studies increases Asporin function, moreover Asporin is significantly upregulated in OA cartilage in comparison to healthy cartilage. The study employs an *in vitro* approach utilising Asporin overexpression in cartilage and bone cells to replicate the conditions observed in OA. In addition, the research integrates the use of Asporin null mouse models and *col2cre* conditional knockout of Asporin to elucidate the role of Asporin in musculoskeletal development and specifically in cartilage and periosteal cells.

This research shows the effect of Asporin in the mineralisation of the ECM and reduction of sulphated proteoglycan in the overexpression model, interesting for the role of Asporin in OA pathogenicity. Phenotyping of the global mouse model demonstrates that Asporin is not essential for endochondral ossification or cartilage structure, highlighting modulation of Asporin expression as potential therapeutic target of OA with minimal off target effects. Further, studying of the role of Asporin in bone using µCT, histomorphometric analysis and histological techniques to gain a well-rounded understanding of its involvement in development showed that the loss of Asporin does not disrupt bone or spinal development nor affect the tendon structure. However, deletion of Asporin in type II collagen positive periosteal skeletal progenitor cells (under Col2Cre) hinders bone remodelling and appositional growth in the *col2cre* conditional Asporin knockout, suggesting a potential role for Asporin in bone homeostasis and fracture repair.

COVID-19 Impact Statement

The impact of the COVID-19 pandemic has had significant impact on my PhD, resulting in delays that affected the entire first year of my research. Specifically, the breeding of experimental mice has been considerably slower than anticipated, with unexpected additional costs as a result of the time taken to get the mice needed for the experiments, a large portion of our mice were culled, and mouse numbers had to be kept low leading to a lower-than-expected number of subjects for analysis and a much longer time to collect all the samples. Eventually, we have lost the complex genotypes necessary for this project and had to rederive them after the pandemic. Additionally, disruptions in the supply chain due to the pandemic further impeded progress by causing delays in crucial deliveries in turn resulting in experiments being lost and needing to be restarted or losing some entirely. This significant delay in my first year and the continued limitations with the mice had an understandable knock-on effect for the following two years, with all mouse work being completed in a significantly more limited timescale.

In order to mitigate this, I designed *in vitro* experiments in my first year. I planned and executed a project studying the effect of overexpressing Asporin in cartilage and bone cells to model the overexpression of Asporin detected in OA cartilage. This research forms the first chapter of my thesis.

The significant limitations to the mice were further impacted as the Post Doctoral project was also working with the same mouse lines. Therefore, only female mice were used in this study as the male mice were necessary for the PostDoc. Additionally, the license lapsed during the study at a critical time for my experiments, the new license was not implemented for 3 months, and this meant no studies could be carried out on the mice during this time, this include histomorphometry injections and X-rays, only tissue collection was permitted.

Although there were significant setbacks, I have tried to mitigate this and carry out extensive research with the samples available to me within the time frame.

Acknowledgements

I would like to first thank my lab group: my supervisor Dr Kasia Pirog for all of her support, guidance and knowledge throughout my PhD, Dr Francesca Brito, I couldn't have done it without you, your support, positive outlook on all my work and all the many fun memories together. Dr Ella Dennis thank you for all your help, advice, and friendship throughout my Undergraduate, MRes and PhD, thank you for kickstarting my enjoyment and passion for research and encouraging me to apply for this PhD. Marc Farcasanu thank you for being a constant ear for all my many rambles, for being just as sarcastic as me and a great friend throughout my time in the lab, Dr Anna Porter, you were a burst of bubbly energy that arrived just at the right time your enthusiasm and interest in the field and in my work was so refreshing.

To the rest of the Skeletal Research group, you have made my PhD so much more fun and enjoyable than I thought it could ever be! Thank you to all the Centre for Life colleagues and thank you to the Newcastle University Electron Microscopy Group for their help with processing the tendon samples for TEM and Microscope Support. BBSRC BB/R013942/1

To my family Mum and Dad, you have believed in me when I didn't, constantly encouraging me and reassuring me I can do it and to be brilliant. Thank you for being proud of me every step of the way, everything I do, or reach to achieve has only been possible as I knew you would always be there if things went wrong, thank you! Even when you haven't been sure how you can help, I can't even put into words just how much you have helped me through this entire PhD. To my sisters, Hannah and Leah, Hannah, you are my longest friend and my constant cheerleader, you have been the greatest support. Leah, you have made me laugh at my lowest and made Newcastle feel like home again, I have relied on you for so much and you have always been there for support. I can't thank you enough for it all, I truly couldn't have done it without you. To the family who were excited for me to start but are no longer here to see me finish, Grandma

Rose, Grandad Stan and Uncle Andy, thank you for all the encouragement through my life and instilling in me the confidence to do this PhD, I know you would have been proud to see me finish. Thank you to all my family.

Thank you to all my friends who have been there cheering me on especially Lucy, Charlotte, Kimberley, Lily and Tej thank you for filling my limited weekends and evenings out of the lab with fun and so many happy memories!

Finally, Lucas, thank you, thank you, thank you. You have been my absolute rock through this whole PhD, thank you for listening to me rant, cry and give entire talks on random bits of science that doesn't mean anything to you. You have got me through this, and I can't thank you enough for it all. You have made the toughest few years the absolute best years. I appreciate you so much and everything you have done for me.

Thank you all, I hope I make you all proud.

Table of Contents

List of Figures

Chapter 1. Introduction

1.1 Musculoskeletal development

The regulated differentiation of cells underpins all development. At 3 weeks post fertilisation, gastrulation occurs the first major differentiation of the development. During the gastrulation of the embryo three distinct germ layers are formed: the endoderm, ectoderm and the mesoderm. Endoderm, the inner germ layer proceeds to form organs including the colon, stomach, pancreas and intestines along with the inner lining of most of the organs including the lungs, liver and pancreas. The ectoderm is the outer layer which gives rise to the outer layers of the body such as the skin epidermis, hair and the nervous system. Finally, the mesoderm is the middle layer, cells derived from here form all other tissues and organs including the skin dermis, heart and crucially to this research, the muscle system, skeleton and bone marrow, from which blood originates[1]. The mesoderm allows the formation of bilateral symmetry observed in mammals.

Radial symmetry is observed in animals such as jellyfish, starfish and urchins, where multiple planes of symmetry all cross at one central point. Whereas bilateral symmetry refers to the singular plane of symmetry, through the centre of the body, the sagittal plane, resulting in identical formation of left and right sides of the body forming.

The musculoskeletal system comprises of bones, cartilage, skeletal muscle, connective tissue, tendons, and ligaments. The whole system is essential for movement and acts as a support structure for the soft organs in the human body. The development of organs and tissues in the human body is governed by various growth factors and signalling molecules capable of inducing differentiation of stem cells into different mature cell lineages. The musculoskeletal connective tissues originate from the mesenchyme in the differentiation process termed the mesengenic process (Figure 1.)[2].

During gastrulation, the primitive streak is formed, this establishes the cranial caudal axis[3].In initial formation of the skeleton the mesoderm folds to form three compartments: the paraxial mesoderm leads to the generation of somites to form the axial skeleton; the lateral plate mesoderm forms the skeleton of the limbs; and the cranial neural crest cells migrate and differentiate to the branchial arch and craniofacial bones and cartilage(Figure 2)[4, 5].

The mesoderm gives rise to the mesenchyme and the mesenchymal stem cells migrate and condense to begin the differentiation and formation of the skeleton. The differentiation of the mesenchymal stem cells is driven by specific transcription factors and by growth factor morphogen gradients that drive the patterning of the early embryo and drive the differentiation through a specific lineage[5]. During the condensation of the skeletal anlagen, these osteochondroprogenitor cells express RUNX2 or SOX9 for osteogenic differentiation or chondrogenic differentiation respectively[6]. The key drivers initiating skeletal development from the mesenchymal cells are RUNX2 and SOX9[6].

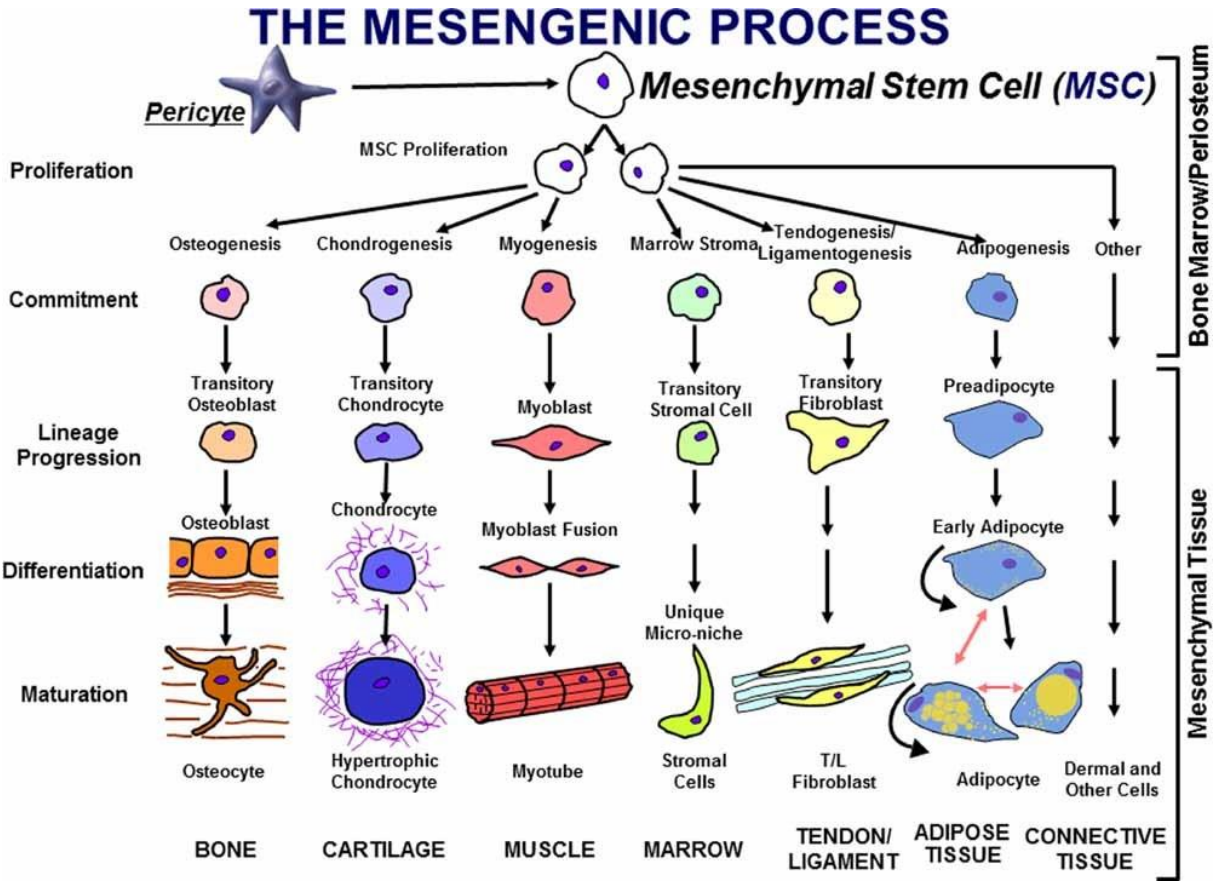

Figure 1. The mesengenic process*. Diagram of the differentiation lineages of mesenchymal stem cells (MSCs). MSCs are multipotent and can proliferate and differentiate into many cell types. Bone cells differentiate through osteogenesis, cartilage cells differentiate through chondrogenesis and fat cells (adipocytes) differentiate through adipogenesis* [2]*.*

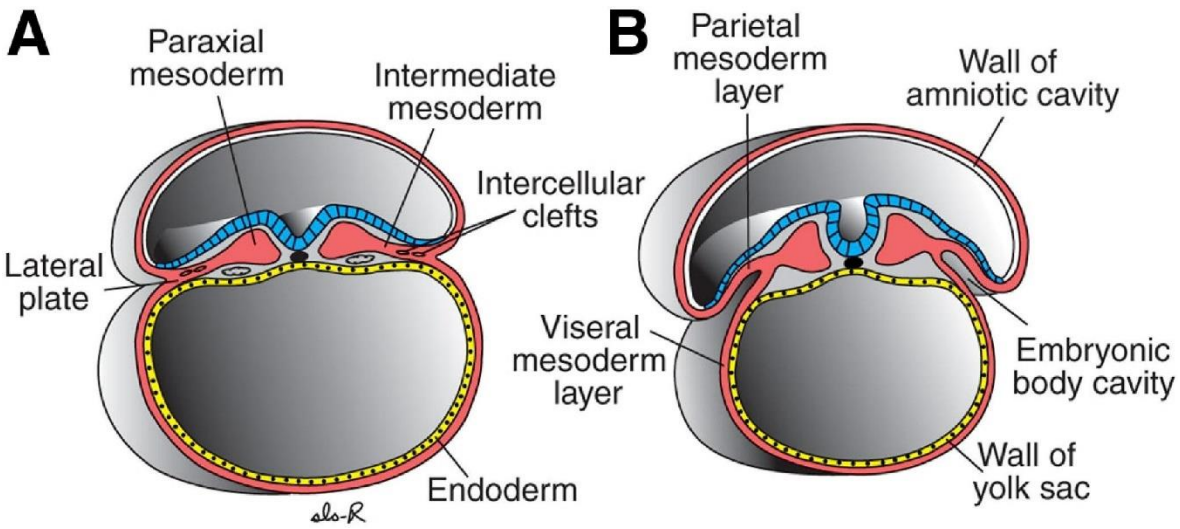

Figure 2. Gastrulation and formation of the three germ layers*. Cross section of the embryo 3 weeks post fertilisation. The ectoderm (blue) gives rise to the outer layers of the body such as skin. The paraxial mesoderm which gives rise to the sclerotome. The intermediate mesoderm gives rise to the urogenital system. The endoderm gives rise to the inner layers of the body and most other internal organs.(B) the paraxial mesoderm further differentiates to the parietal mesoderm which gives rise to the limb skeleton and the visceral mesoderm which gives rise to smooth muscle and muscular gut wall[7].*

1.1.1 Cartilage and bone cells

1.1.1.1 Chondrocytes

Chondrocytes are the only cell type found in cartilage. Chondrocytes differentiate from a mesenchymal condensation[8]. The osteochondroprogenitor cells found in the condensation express both *RUNX2* and *SOX9* transcription factors and sustained expression of these drives the osteogenic and chondrogenic lineages respectively. The key transcription factor for the induction of chondrogenic lineage differentiation is the expression of SRY-box 9 (SOX9), which has been shown to play an important role in the activation of cartilage specific genes and required for cartilage formation.[9]

Runt-Related Transcription Factor 2 (RUNX2) is the master transcription factor of osteoblast differentiation factor. It is important for both the maturation of chondrocytes and differentiation of osteoblasts. The RUNX family of genes share the conserved Runt domain, initially found in the drosophila melanogaster (fruit fly), a segmentation gene. The drosophila melanogaster body is built up of 14 segments, normal development patterning of the drosophila is dictated by pair-rule genes, each named by the phenotype resulting from the deletion of the genes. This conserved region is capable of forming a heterodimer with core-binding factor-β (CBFβ), a co-transcription factor[10].

Initially mesenchymal stem cells are stimulated by RUNX2 and drive to osteochondroprogenitor cells[6]. These cells differentiate into chondrocytes which make up the growth plate, the growth pate can be divided into layers of chondrocytes through different stages of the chondrocyte life. Runx2 is lowly expressed in the resting and proliferative chondrocytes. Runx2 expression is upregulated in prehypertrophic chondrocytes and this expression is sustained through differentiation to hypertrophic and terminal hypertrophic chondrocytes[10].

As explained, following the formation of mesenchymal condensations, mesenchymal stem cells differentiate to osteochondroprogenitor cells, where both SOX9 and RUNX2 are both expressed, cell fate of driving down the chondrogenic or osteogenic differentiation result is determined by the dominance of one gene over the other. The presence of both SOX9 and RUNX2 expression would be expected to drive the chondrocyte lineage and osteoblast lineage simultaneously. However, in early development the chondrogenic lineage is prioritised, this highlights that an inhibition of RUNX2 must be present to preferentially drive the chondrogenic lineage from the mesenchymal cells. Zhou et. al. Proposed that *SOX9*, in addition to its transcriptional activation effect driving chondrogenesis, must also have a transcriptional repressor effect for osteoblast differentiation[6].

SOX9 is a the master transcription factor driving the expression of chondrocyte-specific genes including type II collagen (*COL2A1) and* type XI collagen (*COL11A1*)[6]. Global ablation of SOX9 is embryonically lethal in mice and *Sox9*$^{+/-}$ heterozygous null mice results in perinatal lethality. Conditional targeting was therefore the only possible method for the study of knockout *Sox9* in mice[11]. Heterozygous loss-of-function mutations of SOX9 in humans leads to Campomelic dysplasia, a skeletal dysplasia characterised by shortened and bowed long bones, talipes equinovarus (clubfoot) and respiratory compromise resulting in neonatal lethality[12, 13]. Interestingly, when modelled in mice, it was found that all endochondral skeletal elements were smaller and thinner in the heterozygous mutant. Furthermore, the pre-cartilaginous mesenchyme was underdeveloped in the mutants, at E12.5 the chondroprogenitor cells around the notochord were still mesenchymal cells with little matrix whereas the chondroprogenitors of the wild-type were already forming the typical cobblestone arrangement of chondrogenic cells with deposited matrix[13].

To study the ability of SOX9 to modulate the transcriptional activity of RUNX2 in osteogenic stimulation Zhou et. al used COS7 cells which do not express RUNX proteins, containing a 6xOSE2-luc *Osteocalcin* reporter

plasmid. Osteocalcin expression is directly increased by Runx2 expression. When these cells were transfected with *RUNX2,* activity of the luciferase reporter increased over 150-fold, when transfected with both *RUNX2* and *SOX9*, the luciferase activity returned close to basal[6]. To further explore the modulation of RUNX2 transcription activity by SOX9 in chondrocyte maturation the cells were transfected with RUNX2 responsive 8xA-Min-Col10a1-luc, *type X collagen* reporter[6]. When these cells were transfected with *RUNX2,* activity of the luciferase reporter increased to almost 150-fold. When transfected with both *RUNX2* and *SOX9*, the luciferase activity returned close to basal[6].

SOX9 drives the mesenchymal stem cells (MSCs) expressing collagens I, III and V to differentiate to chondroprogenitor cells which express cartilage-specific collagens: II, IX and XI, then differentiate into chondrocytes. This process is called chondrogenesis[8]. The condensing mesechyme differentiates into cartilage anlage, forming template for the future long bones. The proliferation and maturation of the chondrocytes occurs in the structure called the cartilage growth plate and is driven by transcriptional activation by SOX9 inducing the expression of *SOX5* and *SOX6*. This trio of SOX transcription factors have been found to target and drive expression of type II collagen and aggrecan[14]. Additional signalling molecules driving the maturation include fibroblast growth factors (FGF), bone morphogenetic proteins (BMPs), and the Indian hedgehog (IHH) and parathyroid hormone related protein (PTHrP) and Wingless-Type MMTV Integration Site (WNT) signalling[15].

There are multiple stages of chondrocyte differentiation with resting, proliferating, and hypertrophic chondrocyte stages, then the final terminal differentiation stage leading to apoptosis which is the stage at which calcified cartilage is replaced by bone. Up to 50 % of the hypertrophic chondrocytes are able to transdifferentiate into osteoblasts and contribute to the trabecular bone formation[16].

1.1.1.2 Osteoblasts

Osteoblasts are bone forming cells that produce and secrete bone extracellular matrix proteins and drive the mineralisation of the ECM. MSCs first differentiate to osteochondroprogenitor cells which have the potential to differentiate into osteoblasts or chondrocytes. Osteoblast differentiation is driven by the expression of Runt Related Transcription Factor 2 (RUNX2). The continued expression of RUNX2 drives the differentiation of osteochondroprogenitor cells to preosteoblast, alongside the expression of β-catenin and osterix (SP7). Sustained expression of these transcription factors leads the preosteoblasts to produce bone matrix and differentiate into osteoblasts thereby losing the potential to differentiate down the chondrogenic lineage. RUNX2 keeps the osteoblasts in the immature stage, the expression of other transcription factors including ,MSX1, MSX2, DLX5, DLX6, TWIST, AP1, KNOX-20, SP3 and ATF4, SP7 (osterix) drives the maturation of osteoblasts where is BGLAP and SP7 are expressed and final transition driven by SP7 to osteocytes, where they begin to express SOST.[17]. Osteocytes selectively express sclerostin (SOST), considered a marker of osteocyte differentiation. SOST can modulate select bone morphogenetic proteins (BMPs) and bind to LRP5/LRP6 preventing canonical Wnt signalling.

To assess the role of RUNX2 in skeletal development, Komori *et. al.* disrupted the *Runx2* gene to create *Runx2*-deficient mice. *Runx2* null mice died shortly after birth. Interestingly, *Runx2* null mice had no mature osteoblasts, and a complete lack of ossification, however chondrocyte differentiation and cartilage formation still occurred and was close to normal[18]. *Runx2*$^{-/-}$ mice were dwarfed and dramatically delayed ossification until day 17.5 [18], due to preliminary calcification of the cartilage and lack of osteoblast recruitment. The calvaria of the *Runx2*$^{-/-}$ mice showed no intramembranous ossification occurred and a complete arrest of osteoblast maturation [18].

Osterix encoded by the *SP7* gene, is a transcription factor with three zinc finger motifs. Strong expression of osterix was found in the cells associated with bone trabeculae and cells involved in the formation of the bone collar in mouse embryo at E15.5[19]. In postnatal development, the secondary ossification centres, bone matrix cells, and cells of the endosteum and periosteum show sustained high osterix expression[19]. Osterix was also found to be weakly expressed in the prehypertrophic zone of the cartilage growth plate, but in no other zone of the growth plate[19].

Osterix is essential for osteoblast differentiation. Osterix null mice showed a complete lack of osteoblasts and therefore no bone formation[19]. Interestingly, the knock-out tissues still contained the preosteoblast cells, however, in the absence of osterix they expressed typical chondrocyte markers, suggesting they retained their potential to differentiate into both osteoblast and chondrocytes. Osterix was confirmed to act downstream of RUNX2, and *Runx2* null mice did not express osterix[18].

There are multiple populations of osteoblasts within the bones defined by their location: trabecular, endosteal and periosteal. Moreover, osteoblasts exist in different stages of differentiation: osteochondroprogenitors, pre-osteoblasts, immature osteoblasts, and mature osteoblasts, the final stage of differentiation of the osteoblast lineage are the osteocytes, (Figure 3). These are postmitotic osteoblasts that are embedded within their dense secreted matrix which comprises the final mature bone. Between 5 and 20 % of mature osteoblasts become osteocytes[20]. They are found in both cancellous and cortical bone where they can act as mechanosensory endocrine cells[21].

In the transition from osteoblast to osteocytes, secretion of type I collagen is ceased. Rather than the cells migrating into the bone, the osteocytes instead become entombed by the bone forming around them. In the cortical bone they sit within lacunae, cavities within the bone, this results in them being physically separated within the bone. However, they form an organised network within the bone, osteocytes have dendritic

extensions which travel through canaliculi facilitating their mechanosensing properties and connect to other osteocytes, osteoblasts and to other cells of the bone marrow.[22]

Metalloproteinase MMP14 plays a role in the differentiation of the osteocytes, and a deficiency in this metalloproteinase leads to collagen cleavage disruption. These MMP14 deficient mice have a greatly reduced osteocyte network, although the number of osteocytes is the same the network is disrupted[23]. E11 protein is expressed by early osteocytes, with a crucial role in osteocyte differentiation, the formation of the dendritic extensions, and additionally dendrite elongation in response to mechanical elongation[24]. During the encapsulation of osteocytes in the bone the dendrites are polarised to the mineralisation front, where the blood vessels invade. There are changes in the osteocyte dendrites in response bone formation; static and dynamic[24]. The balance of having enough connectivity for the successful function and viability of the osteocytes however, too many connections can reduce bone strength due to increased lacunae.[24] Additionally, osteocytes have primary cilium allowing direct fluid flow sensing in the lacunar cavity, further aiding the mechanosensing in the osteocytes[25].

Osteocytes account for more than 90% of the cells of the bone in the matrix and bone surfaces. Osteocytes are important coordinators of osteoclastogenesis and bone remodelling through the production and balance of osteoprotegerin (OPG) and Receptor Activator of Nuclear Factor Kappa β Ligand (RANKL)[26, 27]. SOST, the protein expressed exclusively by the osteocytes is a regulator of osteoclastogenesis and bone resorption, this system will be discussed in more detail in 1.1.3.2.5 Bone remodelling[28].

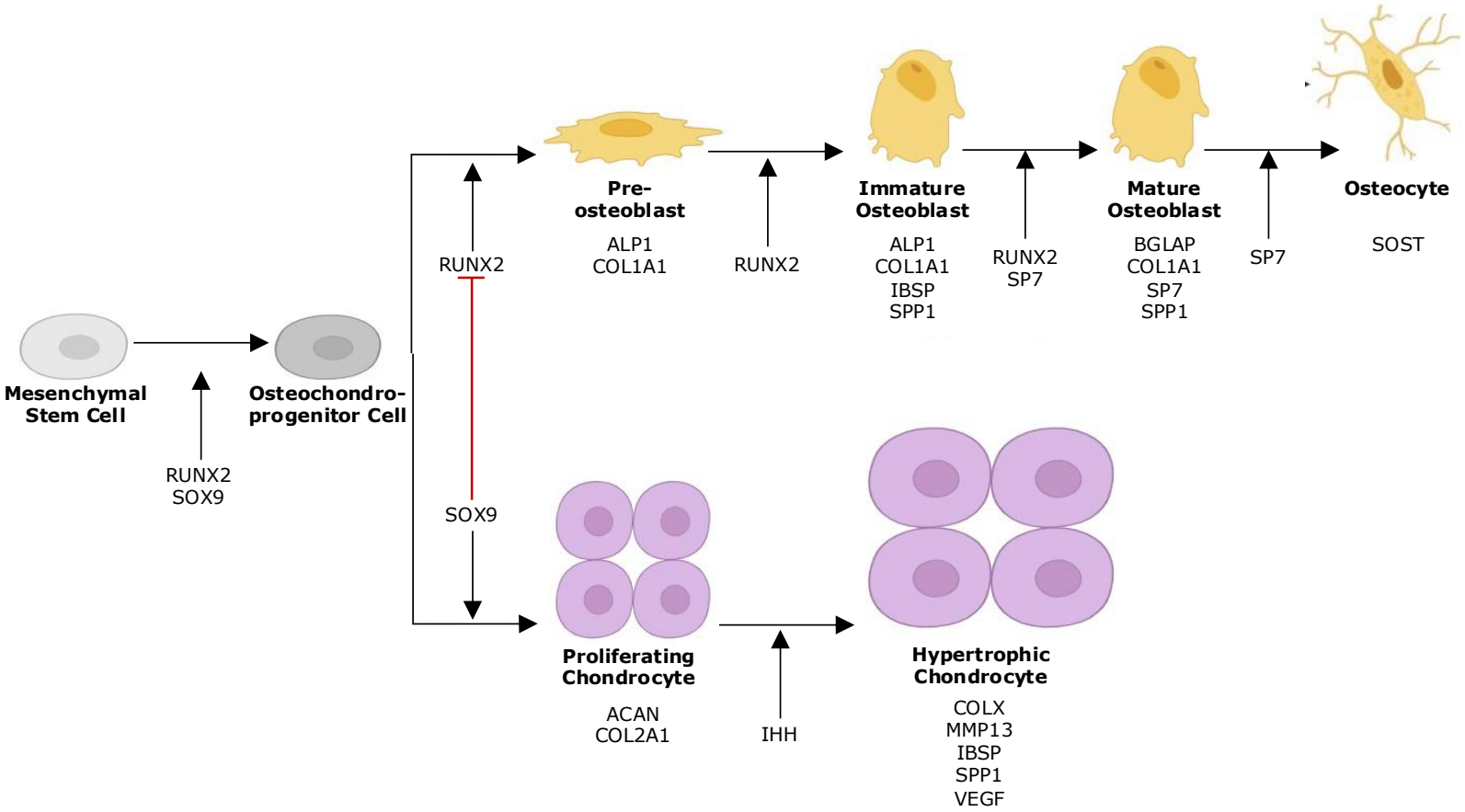

Figure 3. Osteoblastogenic and chondrogenic differentiation of MSCs. *Arrows shows critical transcription factors driving each stage of differentiation. The red block line shows transcriptional repressor at the initial stage of differentiation where SOX9 repressed RUNX2*.

1.1.1.3 Osteoclasts

Bone cells are derived from two lineages of multipotent cells: haematopoietic stem cells (HSCs) and mesenchymal stem cells (MSCs). HSCs give rise to osteoclasts (bone resorbing cells)(Figure 4)[29]. Bone homeostasis is maintained by the balance of osteoblast (bone forming cells) activity and osteoclast (bone resorbing cells) activity, termed bone remodelling. The dynamic turnover of bone is essential for appositional growth, adaptation to load, and restricting overproduction of mineralised bone and excessive bone formation. Osteoclasts are present in all mineralised tissues including teeth and found in mineralised cartilage[30].

HSCs differentiate to preosteoclasts through the action of Receptor activator of nuclear factor kappa-β ligand (RANK-L) and Macrophage colony stimulating factor (M-CSF) made by osteoblasts[29]. *RANK-L* null mice and osteopetrotic (op/op) mutant mice with a loss of function mutation in the *CSF-1* gene, showed inhibited osteoclastogenesis and lack of bone resorption[31, 32]. Both mouse models presented with osteopetrotic phenotypes *(osteo* – bone, *petra* – stone)*,* of high bone mass[31, 32]. Moreover, M-CSF stimulates the motility and cytoplasmic spreading of mature osteoclasts and induces the expression of receptor activator of nuclear factor kappa-β (RANK), the receptor for RANK-L[33].

Osteoclastogenesis is regulated by osteoprotegerin (OPG), a soluble receptor capable of binding RANK-L inhibiting its binding to RANK. The balance of OPG and RANK-L regulates osteoclastogenesis, therefore bone resorption and bone remodelling[34]. RANKL, OPG and RANK are all expressed by the hypertrophic chondrocytes and also by prehypertrophic chondrocytes at lower levels. Osteoclast differentiation is favoured in response to BMP2. BMP2 expression by prehypertrophic chondrocytes induces higher expression of RANKL from hypertrophic chondrocytes[35]. Hypertrophic chondrocytes also express low levels of OPG, lower than the levels of RANK-L thereby pushing the balance of OPG/RANK-L to increase osteoclastogenesis. OPG is predominantly secreted by osteoblasts and

regulated by a variety of factors including canonical Wnt/β-catenin signalling, promoting the ability of differentiated osteoblasts to inhibit osteoclastogenesis (Figure 4)[36, 37].

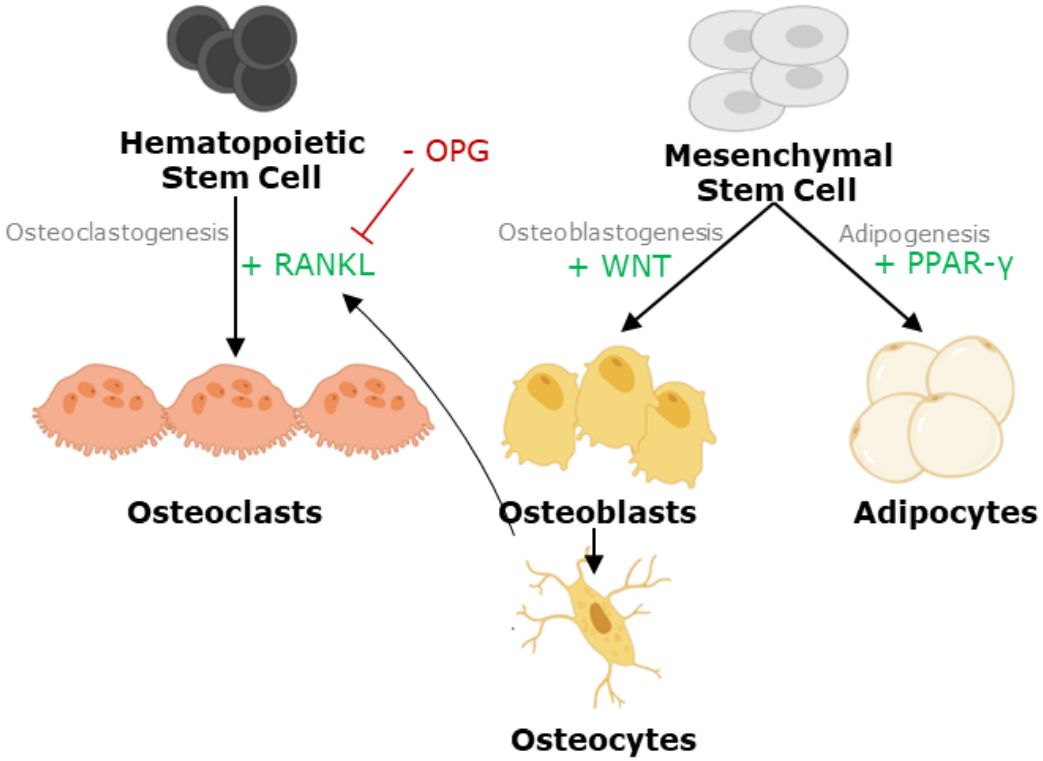

Figure 4. Osteoclastogenesis. *Osteoclasts are differentiated from HSC, driven by RANKL. RANKL binds the RANK receptors or preosteoclasts and maturation of the osteoclast occurs. RANKL is inhibited by OPG which acts as a decoy for the RANK receptor, inhibiting osteoclastogenesis. RANKL can be expressed by osteocytes in response to bone remodelling signals, osteogenic differentiation is driven by WNT signalling from MSCs, adipocytes are also MSC derived, and differentiation is driven by PPAR-γ. Adapted from Hawkes et.al* [38]

1.1.2 Articular cartilage

There are 3 classes of cartilage: hyaline, elastic and fibrocartilage. Hyaline cartilage is the most prevalent in the body, the precursor for bone and also found in the ribs, nose, trachea and articular cartilage. Fibrocartilage is found in joint capsules, ligaments and the intervertebral disc. Elastic cartilage is found in the external ear, larynx and epiglottis[39].

Articular cartilage is a form of hyaline cartilage that protects the ends of the long bones in the knee and hip and in all other diarthrodial joints, these are the free moving joints of the body including the elbow, wrist and shoulder. The diarthrodial joints, also referred to as synovial joints, are characterised by the presence of a joint capsule with the bone surface of the joint covered by hyaline cartilage, the articular cartilage and synovial fluid present in the cavity produced by the synovium[40]. The protective articular cartilage allows the bones to smoothly move against each other. Articular cartilage has no blood supply, nerves or lymphatic system, and is made up of chondrocytes embedded in the dense ECM containing water, collagen and proteoglycans[41].

There are 4 zones of the articular cartilage: the superficial zone, middle zone, deep zone, and calcified zone (Figure 5). The superficial zone is the thinnest, making up approximately 10-20% of the articular cartilage thickness. During movement, joints experience a combination of shear stress and compressive force. The superficial zone is in contact with the synovial fluid and is the main contributor to the tensile properties of the cartilage. It contains a high number of flattened chondrocytes and mainly type II and IX collagens, with collagen fibrils arranged in parallel to the articular surface to increase the tissue strength and withstand load. At the superficial zone, chondrocytes produce lubricin, which contributes to lubrication at the cartilage boundary alongside hyaluronic acid to reduce friction in joint movement[41].

The middle zone is the bridge between the superficial and deep zone, making up approximately 40-60% of the cartilage thickness. The collagen fibrils here have less uniform organisation, are organised in a mesh-like structure and are thicker than those of the superficial zone; chondrocytes are spherical and exist in lower numbers. These chondrocytes synthesise a greater amount of aggrecan [41]. The middle zone acts as a shock absorber in the articular cartilage as this is the first zone of resistance against compressive forces[42].

The deep zone accounts for ~30% of the articular cartilage thickness and is responsible for the greatest resistance to compressive forces. In this zone the collagen fibrils are the thickest and lie perpendicular to the articular surface. Chondrocytes in this zone arrange in columnar orientation, parallel to the collagen fibrils. The deep zone has the highest proteoglycan content and lowest water concentration[41].

In the calcified zone, the chondrocytes express markers of hypertrophy, vascularisation and innervation. The deepest calcified zone is necessary for the attachment of the cartilage to the bone, this is achieved by anchoring collagen fibrils of the deep zone. Hypertrophic chondrocytes, similar to the ones in the cartilage growth plate, are found in this zone[41].

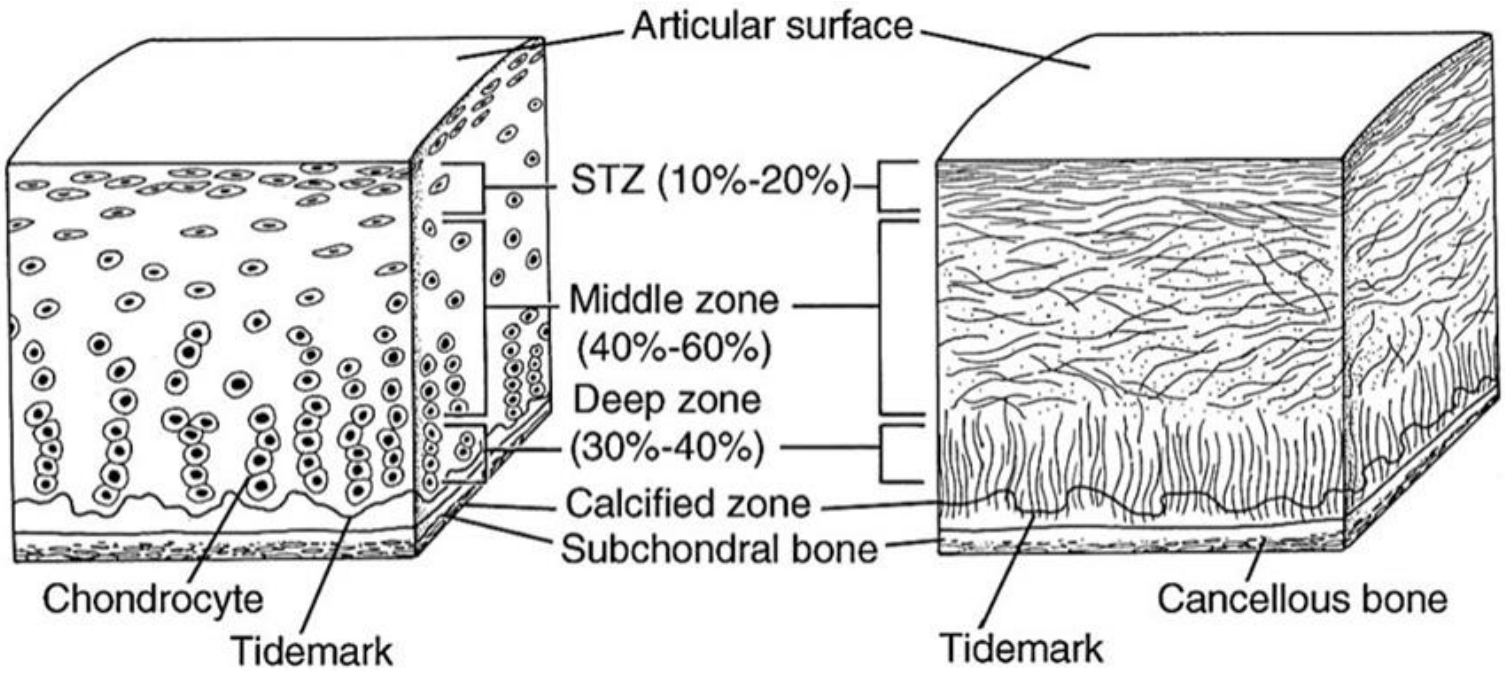

Figure 5. Schematic diagram of articular cartilage cross section[43]. *Arrangement of chondrocytes (Left) and collagen fibrils (Right) in the cartilage. Highlighting zones of the articular cartilage.Chondrocytes arrange in columns in the deep zone, in the middle zone they are more rounded and flatten in the articular surface. Collagen fibrils arrange perpendicular to the calcified bone in the deep zone, are disorganised in the middle zone and arrange horizontal to the articular cartilage in the STZ.*

1.1.3 Bone formation

Bone is divided into 3 categories, compact, cancellous and subchondral. Compact bone is the hard outer portion of bones, cortical bone is classed as compact bone. Cancellous bone (trabecular) is the porous honeycomb structured bone within the long bones. Subchondral bone is the smooth bone at the bone surface in the joints.

1.1.3.1 Intramembranous ossification

Intramembranous ossification (Figure 6) is the process by which flat bones, such as the craniofacial bones and part of the clavicle, are formed[5]. Unlike endochondral ossification, intramembranous ossification does not require a cartilage scaffold, instead, mesenchymal cell condensations form nodules which directly differentiate to osteogenic cells and then to osteoblasts. These cells secrete type I collagen and produce small leucine rich proteoglycans that binds calcium salts, hydroxyapatite. The calcified matrix traps the osteoblasts within it as they become osteocytes[5]. Osteocytes extend out and form canaliculi, creating a network between osteocytes of different layers of bone through these microscopic channels, crucial for mechanosensing, signalling and remodelling of the mature bone[44].

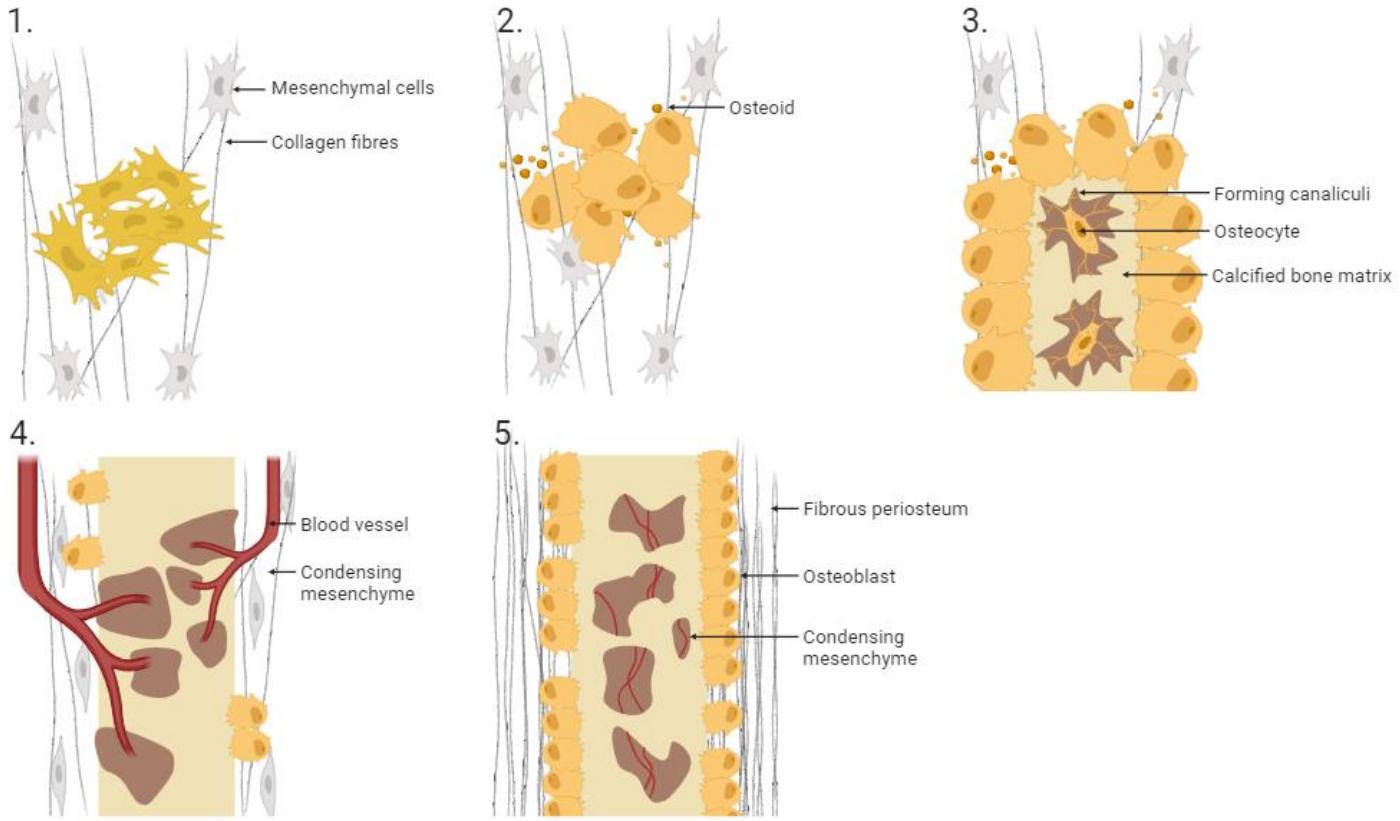

Figure 6. Process of intramembranous ossification[44]. ***(1)*** *Mesenchymal cells cluster and start to differentiate into osteoblasts.* ***(2)*** *Osteoblasts form an ossification centre and begin to secrete osteoid (bone matrix).* ***(3)*** *Bone matrix calcifies, osteoblasts become trapped within the ossification centre differentiate to osteocytes. Extensions of the osteocytes form canaliculi.* ***(4)*** *Bone matrix calcifies around blood vessels. Periosteum forms from condensing mesenchyme.* ***(5)*** *Periosteum formed, blood vessels enclosed in the bone and become red marrow. (Made in Biorender, adapted from Pearson Education, Inc)[45].*

1.1.3.2 Endochondral ossification

The process by which a cartilage scaffold is formed and replaced by bone is called endochondral ossification (Figure 7). This form of ossification is responsible for the development of long bones and all other bones of the body except for craniofacial bones and the clavicles. The cells in the mesenchymal condensations regulated by SOX9 differentiate into chondrocytes, which are the cells that make up the cartilage and secrete a matrix rich in type II collagen and aggrecan (Figure 7. A).[46].

This cartilage scaffold continues to grow and elongate through recruitment of more mesenchymal progenitors and proliferation of chondrocytes which mature and undergo hypertrophy due to the hypoxic environment induced by the deposition of the dense ECM within the condensation(Figure 7. B)[47]. The hypertrophic cells in the centre of the cartilage secrete angiogenic factors, including the vascular endothelial growth factor (VEGF) that attract blood vessel invasion into the cartilage template [5, 46].Osteoblasts (bone-forming cells) and osteoclasts (bone-resorbing cells) are brought into the cartilage matrix by these blood vessels, alongside the chondrocyte to osteoblast transdifferentiation pathway. The osteoblasts lay down bone matrix on the cartilaginous template to form trabecular bone while the osteoclasts degrade the extracellular cartilaginous matrix through the secretion of matrix metalloproteinases (MMPs) (Figure 7. C).

MMP13 is a key MMP for the degradation of the cartilage scaffold, it is expressed by terminal hypertrophic chondrocytes and the osteoblasts[48]. In *Mmp13*$^{-/-}$ null mice, trabecular bone density was increased, and hypertrophic zone height was increased resulting in the accumulation of cartilage matrix. The data suggested that MMP13 is the dominant collagenase in cartilage, cleaving type II collagen[48]. The degradation of cartilage by MMPs is critical for allowing the invasion of blood vessels and the bone formation process where the cartilage is degraded for it to be replaced by bone[49].

This leads to the formation of the primary ossification centre in the centre of the bone shaft. As the trabecular bone is laid down, the primary ossification centre splits the cartilage matrix into two distinct regions of differentiating chondrocytes which propagates towards the ends of the bone, epiphyses. Postnatally, there is a secondary blood vessel invasion to the terminal ends of the developing bone, resulting in secondary ossification centres (Figure 7. E). The scaffold can enlarge further by the continuous proliferation of chondrocytes, which change in shape and size and form columns of stacked cells, this structure is called the cartilage growth plate (Figure 7. G). The terminal hypertrophic zone of the growth plate directly above the ossification centre continues to secrete factors attracting the blood vessel invasion into the scaffold, the hypertrophic chondrocytes at this stage undergo apoptosis[50]. Postnatally, the growth plate continues to be responsible for linear bone growth until skeletal maturity is reached, which in humans is at puberty, where the growth plates fuse and the bone stops elongating[5]. However, in mice, the growth plates of long bones do not disappear with age, even after longitudinal growth stops[51].

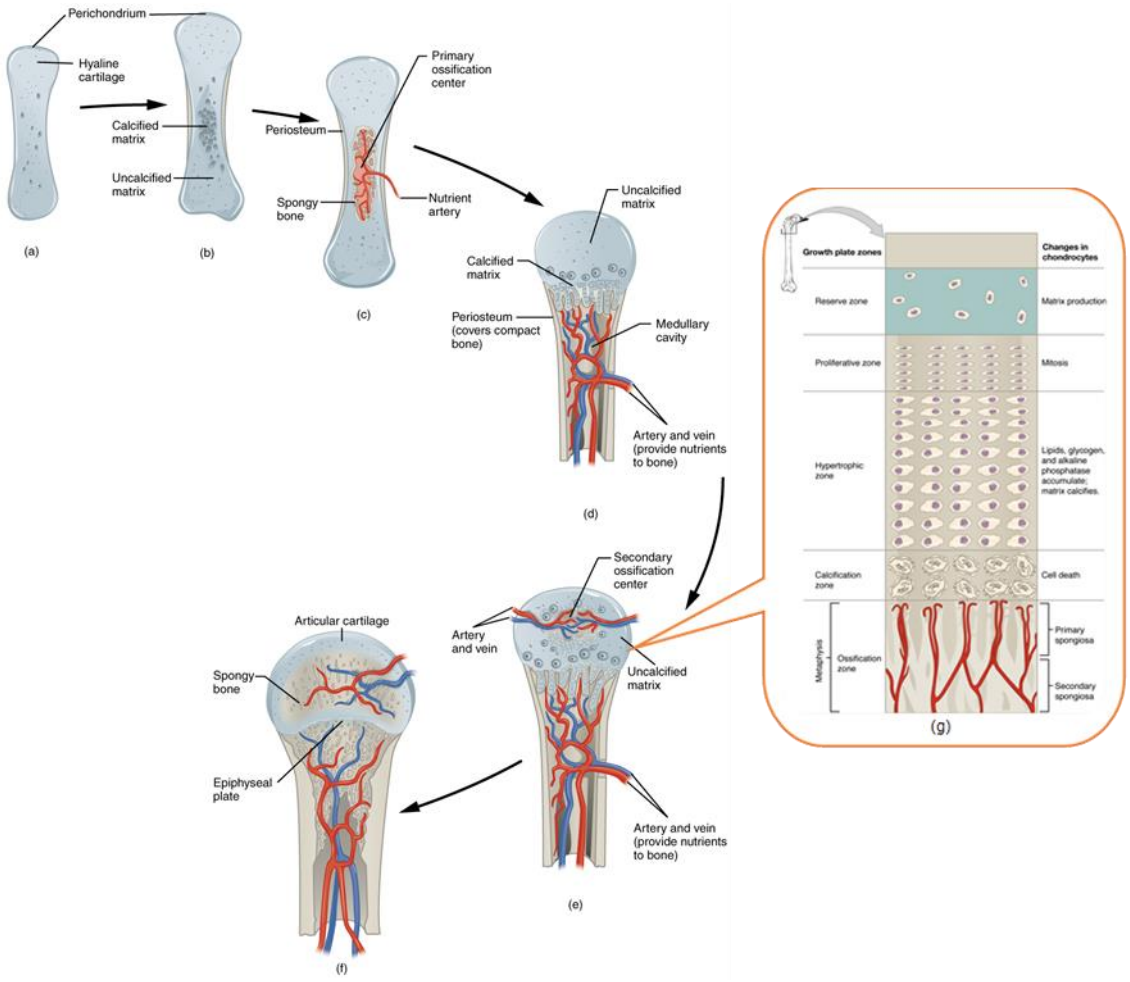

Figure 7. Process of endochondral ossification. *A) Mesenchymal condensation differentiates into chondrocytes, forming a hyaline cartilage. B) Perichondrium forms. C) Vascular invasion and formation of primary ossification centre. Perichondrium becomes periosteum D) Chondrocytes proliferate and cartilage continues to grow at ends of the bone (cartilage growth plate). E) Secondary ossification centres develop in the ends of the bone. F) Cartilage growth plate increasing, and the ossification centres fuse together, hyaline cartilage remains at the joint surface as articular cartilage. (Pearson Education Inc.*[45]*). G) Zones in the epiphyseal growth plate of long bones*[52]*.*

1.1.3.2.1 Organisation and regulation of the cartilage growth plate

Chondrocytes in the growth plate organise into five distinct structured zones, forming the cartilage growth plate. The progression of the chondrocytes through the five differentiation stages is regulated by a series of morphogens including Indian Hedgehog (IHH) and Parathyroid Hormone-related Protein (PTHrP), controlling the expression of *SOX9* and *RUNX2*, transcription factors responsible for the activation of specific genes in each zone (Figure 8)[52]. The five zones are the resting zone, proliferative zone, pre-hypertrophic zone, hypertrophic zone, and terminal calcification(Figure 8)[52].

In the resting zone, chondrocytes have a low proliferation rate, random organisation, are small and rounded, and express *COL2A1*, (type II collagen) and *ACAN (*aggrecan), crucial ECM components of the cartilage scaffold. As chondrocytes mature, they begin to proliferate rapidly, flatten in shape and organise into columns. At the bottom of the growth plate the chondrocytes undergo hypertrophy, whereby cells increase in size and become rounded, and the expression of type II collagen is stopped[52]. Hypertrophic chondrocytes stop dividing express type X collagen, osteocalcin (*BGLAP*) expression is upregulated and osteopontin (*SPP1*) expression increases two-fold[53]. The expression of these is necessary for the calcification of the cartilage matrix. Hypoxic conditions worsen as the matrix surrounding hypertrophic chondrocytes calcifies, resulting in the death of chondrocyte cells and interestingly transdifferentiation of some of the chondrocytes to an osteoblast lineage. During cell death chondrocytes express VEGF initiating the terminal calcification zone[16, 52].

The height of each zone is determined by the number of chondrocytes in each phase of the chondrocyte life cycle which is facilitated by differentially expressed morphogens driving several key signalling pathways through the zones. PTHrP is a paracrine hormone secreted by the perichondrium and in the early proliferative zone. PTHrP receptors are located on the cells in late proliferative zone and pre-hypertrophic zone.

Binding of PTHrP to the receptor prevents chondrocyte hypertrophy, keeping the cells above the hypertrophic zone in a proliferative state, and supressing the levels of IHH expression[54, 55]. IHH is a paracrine hormone expressed by cells that are no longer proliferating, in the pre-hypertrophic zone and hypertrophic zone. IHH can stimulate the production of PTHrP at the ends of bones through the binding of the Patched (Ptc) receptor. This feedback system maintains chondrocytes proliferating above the hypertrophic zone and balances minor signalling perturbations to retain a healthy growth plate.

PTHrP through WNT also has the capacity to induce intracellular influx of Ca^{2+} ions through the opening of L-type calcium channels. Calcium/calmodulin-dependent protein kinase II (CAMK2) activity, increases in response to calcium levels, increases in the transition from proliferative to prehypertrophic transition through β-catenin and RUNX2 transcriptional regulation. CAMK2 activity induces cell hypertrophy and the influx of Ca^{2+} promotes osteoblast proliferation, differentiation, consequently driving ossification and calcification of the growth plate. Furthermore, CAMK2 has been shown to increase the transcription activity of osterix. WNT and PTHrP signalling oppose CAMK2 activity.

Bone morphogenetic proteins (BMPs) play a crucial role in the regulating of bone growth. BMPs have been shown to play many roles in skeletogenesis, including induction of bone formation, deletion of interdigital mesenchyme, and regulation of chondrocyte differentiation[56, 57]. BMPs 2-5 and 7 are specifically expressed in the perichondrium and can modulate the IHH/PTHrP signalling axis by increasing the expression of IHH resulting in the increased expression of PTHrP and therefore elongation of the length of proliferating columns. BMPs 2 and 6 target the hypertrophic zone, increased levels of BMP2 lead to the delay in hypertrophic differentiation[57]. BMP 7 targets the proliferative zone and is necessary for proliferation and differentiation of chondrocytes.

Fibroblast Growth Factors (FGF) signalling can also modulate the growth plate homeostasis, and FGF receptors (FGFRs) are differentially expressed through the five zones of the growth plate. FGFR1 is expressed in the pre-hypertrophic zone and hypertrophic zone, FGFR2 is present in the perichondrium and FGFR3 is expressed in the proliferating zone and prehypertrophic zone. FGF signalling regulates the differentiation and proliferation of chondrocytes through suppression of IHH expression and acceleration of terminal differentiation of hypertrophic chondrocytes. FGFR3 contributes, along with PTHrP, to decrease in the chondrocytes in the pre-hypertrophic zone.

The terminal zone of the cartilage growth plate harbours cells undergoing apoptosis, leaving behind a calcified matrix of collagen fibres, and large clusters of aggrecan and hyaluronan glycosaminoglycans (GAGs)[52]. The recruitment of blood vessels through vascular endothelial growth factor (VEGF) signalling brings in osteoblasts and hematopoietic stem cells (HSCs) which give rise to osteoclasts as previously described. Osteoclasts stimulated by the RANK-L expressed by hypertrophic chondrocytes break down the calcified collagen matrix, thus allowing blood vessels to establish within the bone and bring more osteoblasts[52]. VEGF production is stimulated by oestrogen in both females and males, which spikes at puberty, promoting angiogenesis of the bone and therefore the entry of osteoblasts and osteoclasts, for crucial bone remodelling and formation of mature trabecular bone[51]. Oestrogen has also been identified for potential importance in growth plate fusion[51].

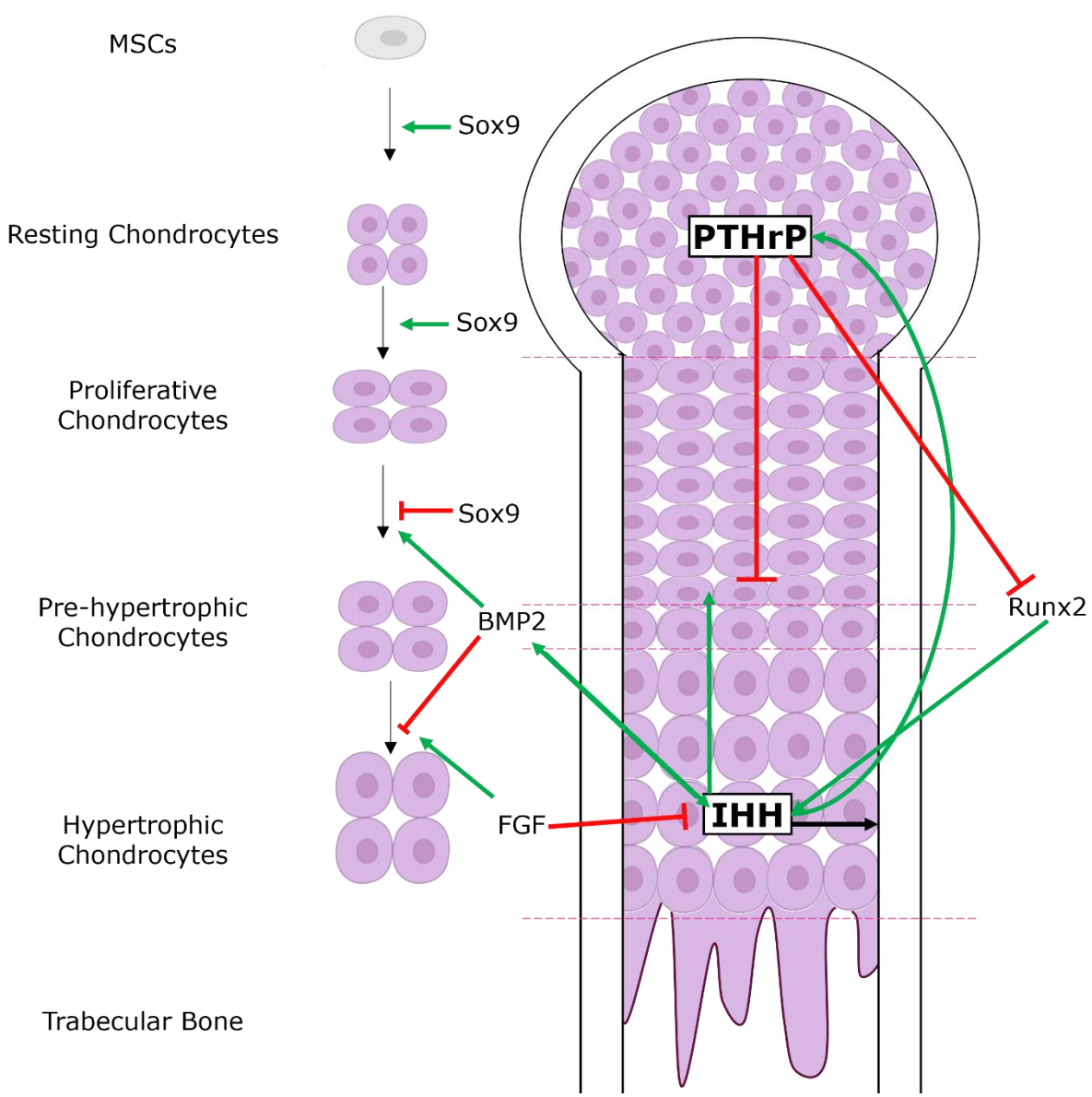

Figure 8. Paracrine regulation of the growth plate. *Ihh induces chondrocyte proliferation, maturation and the expression of PTHrP in the resting chondrocytes in the periarticular region. The negative feedback loop where PTHrP then inhibits Ihh keeps chondrocytes in the proliferative phase. There is a positive feedback loop of Ihh and Bmp2. Bmp2 induces Ihh which in turn induces proliferation of chondrocytes and represses terminally differentiated chondrocytes. FGF signalling works in opposition to Bmp2, supressing Ihh and driving the differentiation of prehypertrophic to hypertrophic terminal chondrocytes.Runx2 drives Ihh expression, this induces PTHrP which then supresses Runx2*[52].

1.1.3.2.2 Calcification of the cartilage matrix

The calcification of the matrix is coordinated by the expressed proteins by both the chondrocytes and the osteoblasts that have been brought into the hypertrophic zone to form the terminal calcification zone.

Osteocalcin (BGLAP) is the most abundant-non collagenous protein of the bone. During the calcification of the matrix when osteoblasts are brought into the hypoxic centre, osteoblasts mature and secrete BGLAP, it is also lowly expressed by hypertrophic chondrocytes. Osteocalcin is a calcium-binding peptide, it is a commonly used marker for bone formation. BGLAP possesses calcium binding Gla residues, this binds the calcium ions (Ca^{2+}) on hydroxyapatite. Interestingly, $Bglap^{-/-}$ null mice were viable and also had no initial skeletal defects, however at 6 and 9 months bone mass was increased. BGLAP is secreted as a prohormone which undergoes cleavage to form a 46 amino acid mature peptide and is γ-carboxylated. The mature protein has high affinity to hydroxyapatite binding calcium within the ECM however following the activation of osteoclast bone resorption, the acidic environment created de-carboxylates the osteocalcin which in turn reduces its affinity to hydroxyapatite, releasing the mineral and the BGLAP is subsequently released into the bloodstream[58, 59].

Osteopontin (SPP1) is a soluble ECM-associated glycoprotein and plays a role in bone metabolism and homeostasis. SPP1 is predominantly expressed by osteoblasts but also by osteogenesis progenitor cells, osteocytes and HSCs of the bone marrow[60]. Osteopontin has a very interesting role in the maintenance of bone mass induced by the sympathetic nervous system, this will be explained in 1.1.3.2.5 Bone remodelling[60].

1.1.3.2.3 Perichondrium

During endochondral ossification the perichondrium is a layer of mesenchymal stem cells that surrounds the forming growth plate. As the chondrocytes undergo to hypertrophy the perichondrium cells differentiate to osteoblasts. This encases the growth plate with bone, forming the bone collar. The periosteum is vascularised, and the blood vessels bring osteoprogenitor cells into the hypertrophic zone for the formation of trabecular bone and bone marrow cavity. The perichondrium is an essential source of osteoblasts for both cortical and trabecular bone formation[61]. Nakamura *et. al.* determined the localisation of Thy-1 positive cells, next to the hypertrophic zone and the periosteum of the developing bone. Thy-1 is expressed by MSCs and osteoblast lineages[61].

As the bone collar forms from the perichondrium, a layer of perichondrium cells remain on the outside of the bone, this is referred to as the periosteum.

1.1.3.2.4 Periosteum

Periosteum is the tissue surrounding the outer bone surface, periosteum is often investigated for its role in fracture healing. The periosteum is a layer of mesenchymal stem and progenitor cells, these are referred to a periosteal stem cells or skeletal progenitor cells. Studies have identified cathepsin K and periostin as markers of the periosteum[62]. The periosteal cells have been studied and they are found to be very heterogenic, including populations of type II collagen positive cells [63].

The periosteum is essential for facilitating appositional growth and as a reservoir of cells to be differentiated for bone remodelling.

1.1.3.2.5 Bone remodelling

Bone mass must be maintained through adulthood, for bone strength and integrity. The bone homeostasis is maintained through regulation of bone remodelling, whereby the amount of bone formed by osteoblasts which must equal the amount of bone resorbed by osteoclasts. Imbalances of the bone homeostasis are the root causes of multiple bone diseases including osteoporosis, characterised by bone fragility and deterioration of the bone microarchitecture[64]. The balance of osteoblast/osteoclast activity is influenced and modulated by endocrine, paracrine and mechanical factors.

Alongside elongation, bones also grow in diameter through the process called the appositional growth (Figure 9). Osteoblasts on the periosteal surface (outer surface of the bone) secrete bone matrix and osteoclasts on the endosteal surface (inner surface of the bone) at the inner surface break down the bone. Appositional growth is a mechanoresponsive process, whereby a higher mechanical load drives bones to grow in thickness, to withstand the increased load[65].

The cortical bone is made of cylindrical structures, osteons, surrounded by concentric lamellae forming a canal [66] filled with nerves and vasculature (Figure 10). The circumferential lamellae between the osteons are fibrous and become mineralised, encasing osteocytes where they can form lacunae (channels) and canaliculi (fluid-filled pipes). These are responsible for fluid shear stress (FSS), one of the keyways mechanical forces are sensed in the bone. Increased mechanical load is detected by the primary cilia on the osteocytes through detection of the fluid movement in the canaliculi of the bone. Through activating specific signalling pathways, this results in upregulation of the osteoblasts depositing periosteal bone and downregulation of the osteoclasts resorbing the endosteal bone, resulting in thicker bones[5]. This bone remodelling continues through life with the bones adapting to stress and load[5]. In the absence of mechanical forces, in

microgravity, it has been shown that bone formation is depressed and bone resorption increased[67].

The osteocytes translate the compressive or lack of compressive force to adapt bone growth promoting formation, stimulated by force or by WNT1 and IGF-1 osteocytes can stimulate osteoblast differentiation and proliferation via gap junctions and also stimulate osteoclastogenesis by expressing RANKL. Sclerostin (SOST) expressed by osteocytes can also regulate osteoblast and modulate osteoclast activity (Figure 11)[66].

Trabecular bone is also remodelled and adapted to load, in the arrangement and thickness of the plate-like and rod-like trabeculae, the structural components of trabecular bone, changes in response to increased mechanical force. In a study of the effect of military training on trabecular bone microarchitecture, O'Leary et. al. found trabeculae number, trabeculae thickness increased, and trabecular separation decreased over a course of 44 weeks of training[68]. Furthermore, cortical thickness and area was also increased following as a result of the training[68].

Bone mass is also regulated by the sympathetic nervous system, through local bone remodelling driven by β2-adrenergic receptor (β2AR) signalling. Experimental studies have shown activation of the sympathetic nervous system results in bone loss through increased resorption and decreased bone formation. Activation of sympathetic nervous system increases the *SPP1* expression and osteopontin protein levels in mouse plasma[60]. In *Spp1* null mice, the bone loss resulting from of activation of the sympathetic nervous system is inhibited. These mice show no reduction in osteoblastic activity and no increase to osteoclast activity[60].

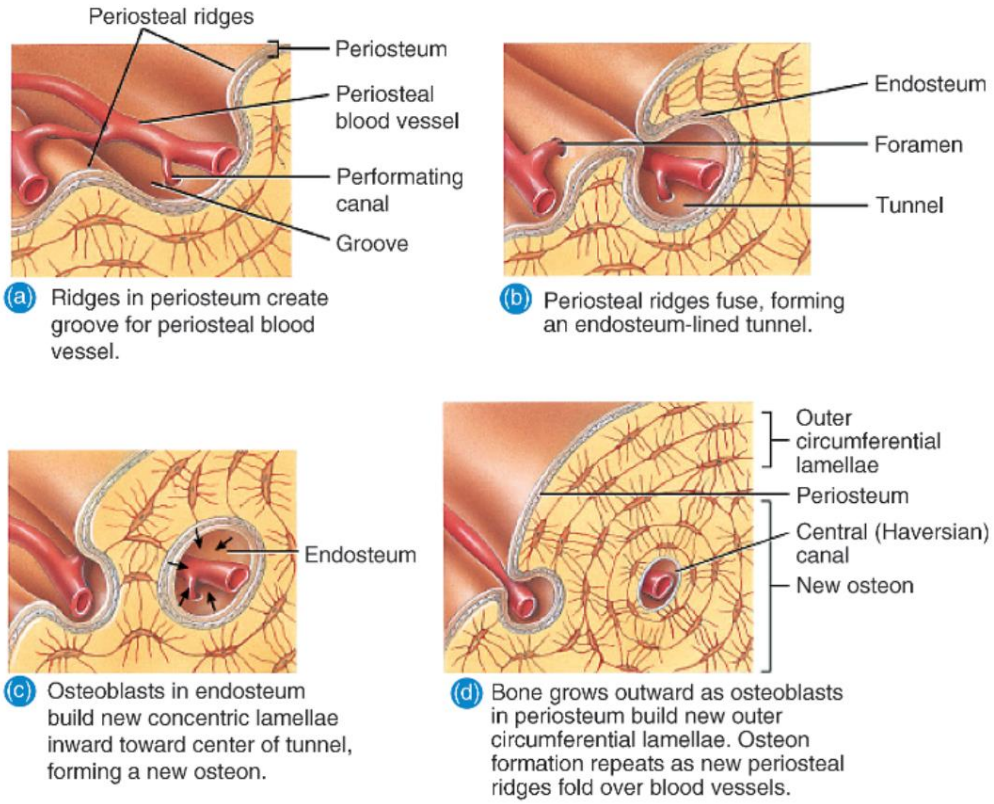

Figure 9. Appositional growth. *The periosteal cells are reservoirs of deposited mesenchymal cells, these differentiate to osteoblasts and begin to form ridges along the periosteal surface, these can then encompass blood vessels along the periosteum that are connected into the bone marrow. The vessels become trapped in the bone and the internal surface; the endosteum forms a circle around the vessel. The endosteum produces osteoblasts and deposit bone, this close circle of bone around the vessel is called an osteon where concentric circles of osteocytes and calcified bone are formed[69]. (Figure from Iles et.al.[69]).*

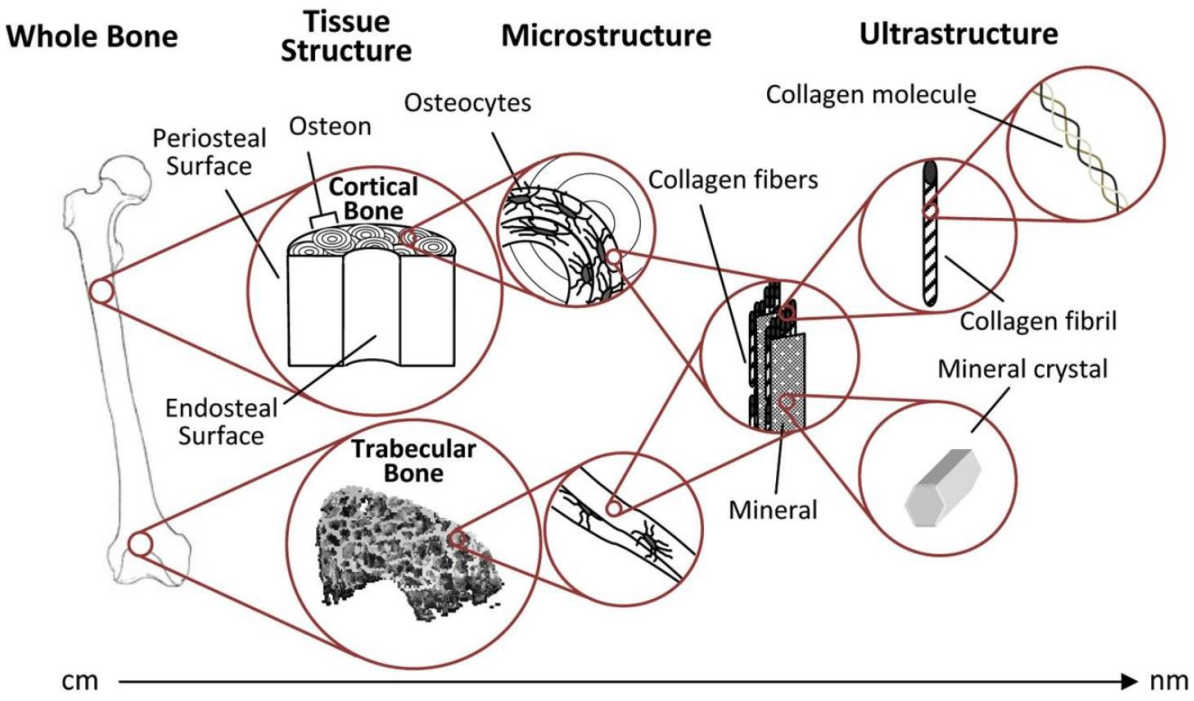

Figure 10. Hierarchical structure of bone. *Collagen molecules form collagen fibrils which alongside mineral crystals form mineralised collagen matrix. The mineralised collagen matrix forms connected plates and rods forming trabecular bone, found predominantly in the metaphysis and epiphysis of long bones and the vertebrae. The mineralised collagen matrix also forms organised cortical osteons made containing osteocytes, these osteons form compact bone surrounding the bone marrow, cortical bone[70].*

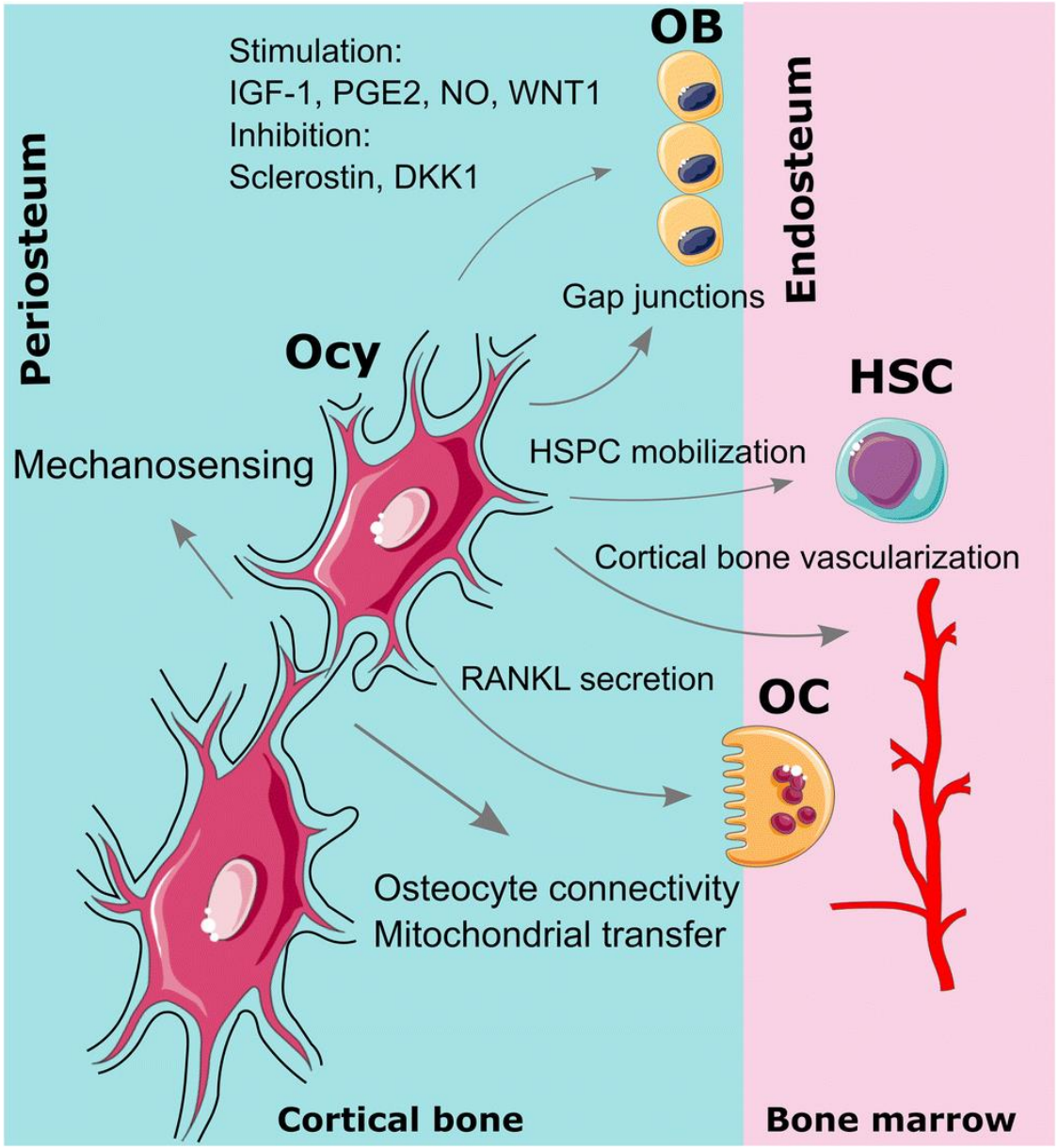

Figure 11. Osteocyte bone modulation capacity. *Osteocytes are embedded in the cortical bone they can modulate bone resorption and bone formation. They translate mechanic forces and cellular signals to modulate the bone environment, the dendrites are capable of mechanosensing. Osteocyte to osteocyte network is formed through the connection of dendrites through the lacunae. Osteocytes can stimulate osteoclastogenesis through the secretion of RANKL and can also regulate osteoblasts, the crucial cells of bone remodelling. Image from Wang et.al[71].*

1.1.3.3 Spine development

In a similar way to long bone growth, the spine develops from the mesoderm layer of gastrulation. The neural tube is formed from the convergence and closure of the neural folds of the ectoderm, triggered by the expression of Sox 1, Sox 2 and Sox3 from the cells of the neural plate (Figure 12). Somites give rise to the sclerotome under paired-box transcription factor *PAX1*, and therefore the skeletal system[72, 73]. Vertebral bodies develop from the Pax1 positive sclerotome ventral sclerotome cells migrate to the notochord and form the unsegmented perinotochordal sheath. BMP signalling in the sclerotome drives the expression of Nkx3.2 which upregulates SOX9 expression, which forms a positive feedback loop driving the expression of Nkx3.2, promoting chondrogenesis. A perinotochordal extracellular matrix of laminin, fibronectin and type I collagen is produced by the basement membrane of the notochord, requiring the expression of SOX5 and SOX6. Sox6. *Sox* 5/6 null mice did not develop the perinotochordal matrix[74].

The spine is a metameric structure, a linear series of body segments, vertebrae. The unsegmented perinotochordal sheath, proliferates as layers of PAX1-expressing sclerotome cells encompassing the notochordal rod. Sclerotome cells form condensations and form the precursor of the intervertebral discs (IVD), this is the beginning of metamerism. Sclerotome cells between these condensations form the vertebral bodies. Differential expression of PAX1 is the driving force of the separate formations of the IVD and the vertebral bodies. PAX1, is an inhibitor of chondrocyte maturation[75]. In the vertebral bodies PAX1 is down regulated, cells therefore upregulate genes that drive chondrogenesis, whereas in the IVD PAX1 expression remains high and chondrogenesis remains inhibited[73].

The process of endochondral ossification begins in the vertebral bodies where the process of chondrogenesis leads to the formation of a hypoxic environment, calcification of the cartilage matrix and the recruitment of blood vessel through expression of VEGF. As previously

described in endochondral ossification, the primary ossification site separates into two and two growth plates develop at either end of the vertebrae, vertebrae grow longitudinally[76]. Alike to long bone growth plates, the growth plates of mouse vertebrae do not fuse.

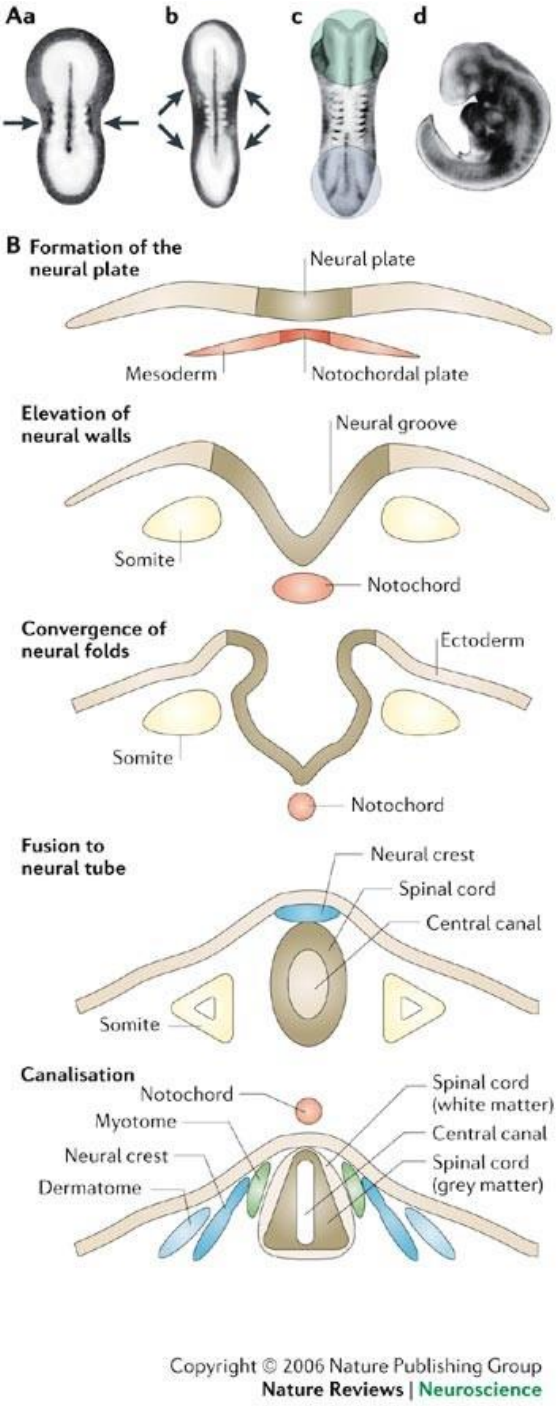

Figure 12. Formation of the neural tube. *The initial formation of the neural tube for the development and segmentation of the spine. The convergence of the neural folds is essential for correct spinal formation, conditions such as spina bifida occur as a result of incomplete neural tube closure. Image obtained from Blom et. al.* [77].

1.1.4 Bone marrow adipocytes

During the vascularisation of the hypoxic calcifying cartilage scaffold, hematopoietic stem/ progenitor cells (HSPC) are also brought into the matrix. The accumulation of these HSPCs alongside the retained reserve of mesenchymal stem cells (MSC), forms the bone marrow of the long bones. The bone marrow is an integral part of the bone, essential for bone health and for the function of the immune system. The bone marrow is part of the body's haematopoietic system and can produce and release both red and white blood cells into the bloodstream as required. Within the bone marrow, fat deposits of the bone marrow adipose tissue (BMAT) are formed through adipogenesis. BMAT has multiple roles within the body, acting as an energy reservoir and a role within the immune, paracrine, and endocrine systems. BMAT was originally thought to be an inert space filler in the bone marrow. However, more recent studies have found BMAT originates from skeletal lineages and has a role in bone marrow homeostasis and whole-body energy metabolism.

BMAT cells originate from the mesenchymal stem cells of the bone marrow. Mesenchymal stem cells (MSC), as previously discussed, can differentiate into multiple cell lineages determined by specific signalling morphogens and transcription factors. Osteoblastogenesis and adipogenesis are considered competitive processes, mediated by the relative activity of PPARγ and RUNX2. PPARγ and c/EBPα are the specific transcription factors that drive adipogenesis[38]. In age-related osteoporosis where bone volume is decreased there is also an increase in BMAT[78]. Furthermore, the activation of the ERK/MAPK pathway drives osteoblastogenesis and inhibits adipogenesis through the phosphorylation of RUNX2 and PPARγ. PPARγ null mice are embryonically lethal however in heterozygous $PPAR\gamma^{+/-}$ mice, bone marrow adipogenesis is decreased and osteoblastogenesis increases further highlighting the balance between the two differentiation axes.

1.1.5 Tooth development and the periodontal ligament

The stages of the tooth development are: growth and differentiation, epithelial proliferation, histological differentiation, organogenesis, mineralisation, eruption, wear and athropy[79]. During embryonic development, cranial neural crest cells forming the brain also migrate to the maxillary and mandibular anlage. These cranial neural crest cells form the oral ectoderm and are referred to as ectomesenchymal cells, which form the tooth except for the enamel[80]. The mesenchymal layer stimulates proliferation in the oral ectoderm, producing epithelial cells which form the dental laminae (Figure 13 A). Buds of these cells form the teeth anlage throughout the forming jaw. Neural crest mesenchymal cells surround the buds (Figure 13 C), and the enamel organ develops, containing the enamel knot, a cluster of nondividing epithelial cells that can be seen at the molar cap stage, condensations of the ectomesenchymal cells form the dental papilla (Figure 13 D). The enamel organ expresses RUNX2, TGF-β and WNT10a, which inhibits the proliferation of dental papilla cells and drives differentiation[81]. The differentiation to pre-odontoblasts and then to odontoblasts marks the start of dentinogenesis: the formation of dentin by odontoblasts of mesenchymal origin[79, 81]. Odontoblasts express BMP5 and FGF10 inducing amelogenesis to begin, the formation of enamel by ameloblasts derived from the epithelial cells. Terminal odontoblast differentiation is driven by TGF-β1, BMP2 and IGF1[82]. The mineral of dentin is hydroxyapatite and the mineral crystals found within the collagenous matrix. The signalling of differentiation and mineralisation of the tooth is very similar to that of ossification of the skeleton.

The periodontal ligament (PDL) is the soft connective tissue between the inner wall of the alveolar socket (tooth-supporting bone) and the roots of the teeth[83]. It consists of collagen bands (majority type I collagen), fibroblasts, cementoblasts, progenitor cells, bone associated cells, epithelial cell rests of Malassez and connective tissue cells[84]. Its role is to sense force applied on the tooth, including by orthodontic tooth movement and respond to it in order to maintain PDL width and preventing ankylosis where the

tooth root and alveolar bone attach[83, 85]. Cells of the PDL begin secreting osteoblast inhibiting factors, sclerostin (SOST) and Asporin, and osteoclast activating factors such as receptor activator of nuclear factor kappa-B ligand (RANKL) and interleukin-1 (IL-1), to prevent ossification of the PDL and ankylosis and maintain width of the PDL[85]. Sclerostin works as an osteoblast inhibiting factor, by inhibiting Wnt signalling[86]. Asporin works as an osteoblast inhibiting factor, inhibiting bone formation, binding directly to bone morphogenetic protein 2 (BMP-2), which in turn inhibits transforming growth factor beta (TGF-B)/Smad signalling[85, 87].

The PDL is responsible for tooth eruption, maintaining tooth support, sensory signals during (mastication) eating, as a shock absorber in the tooth and bone remodelling of the alveolar bone[88]. The PDL is a source of progenitor cells and periodontal stem cells able to differentiate to maintain the health of the tooth in multiple ways, such as osteoblasts/osteoclasts for bone remodelling, cementoblasts/cementoclasts for remodelling of the cementum the mineralised tissue at the tooth root and defence cells such as macrophages[84, 89]. Although the PDL is a connective tissue it is well vascularised, this is reflective of the high turnover rate of both the PDL cellular and extracellular elements[90]. Asporin has been determined to be frequently expressed in human PDL tissue and enhanced during PDL cell cytodifferentiation, into mineralising cells, osteoblasts and cementoblasts[90, 91]. During orthodontic tooth movement, the realignment of teeth for aesthetic or health reasons, the pressure exerted on the tooth results in bone resorption becoming dominant on the compressed and bone formation on the tension side[85]. The force on the tooth causes the root to shift to the alveolar wall reducing vasculature.

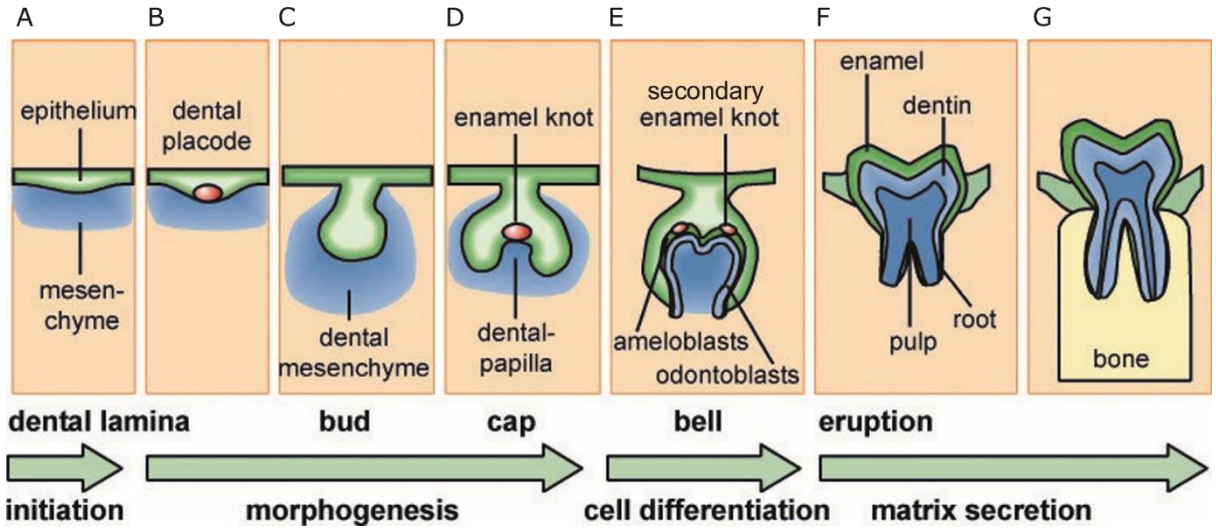

Figure 13. Tooth development. *The teeth are derived from the mesenchyme, which stimulates the oral ectoderm to proliferate initiating tooth formation, where it forms a laminae of epithelial cells at the mesenchyme which condense to for the bud, differentiation happens within the tooth and separate tissues of the tooth begin to form, the tooth is vascularised and the periodontal ligament provides support and is the mechanosensory of the tooth*[92]*.*

1.1.6 Tenogenesis

Tendons and ligaments are connective tissues that transmit force from muscle to bone and from bone to bone, respectively, and are crucial for orchestrating body movement. The development of tendons requires directional mechanical stimulus and presence of muscle tissue to act as an anchor as the tendons begin to form between the muscle and the bone[46]. The tendon-bone junction is named enthesis, and the myotendinous junction is where tendon collagen fibrils and muscle fibres intertwine. Tendons originate from the syndetome, the subdomain in the dorsolateral portion of the somite, between the sclerotome and the myotome, the syndetome is made of the tendon progenitor cells[93]. The transcription factor scleraxis (SCX) is believed to be a key regulator in progenitor cells for both tendon and ligament tissue formation. Tenomodulin (TNMD) is a specific marker of mature tenocytes, also present in periodontal ligament (PDL) cells, and is regulated by SCX and a second transcription factor, Mowhawk[94].

Foetal tendons consist of predominantly type I and type III collagen fibrils in addition to proteoglycans and tenocytes. Tenocytes are "specialised" fibroblasts that secrete and build the ECM of the tendon and its components. As the bones grow tendons stretch to grow longitudinally, and it is postulated that this occurs by bonds between the fibrils (interfibrillar bonds) releasing allowing the fibrils to slide over each other and then reform bonds, resulting in a more "stretched" tendon with less overlap of these fibrils[95]. Decorin, a Class I SLRP, is suspected to have a role in these interfibrillar bonds, by "decorating" the surface of collagen fibrils[96]. A study using NKISK, a competitive inhibitor of decorin binding, showed NKISK potentiated creep in rat tail tendons. In creep, tendons lengthen under tension and do not return to normal, therefore less resistance is detected when the tension is applied again[97]. It was suggested that decorin inhibition disrupted the intrafibrillar bonds between the collagen fibrils of the tendons[97]. Tendons with depleted decorin function

stretch and lengthen due to lack of the interfibrillar bonds to counteract the tension and maintain tendon integrity.

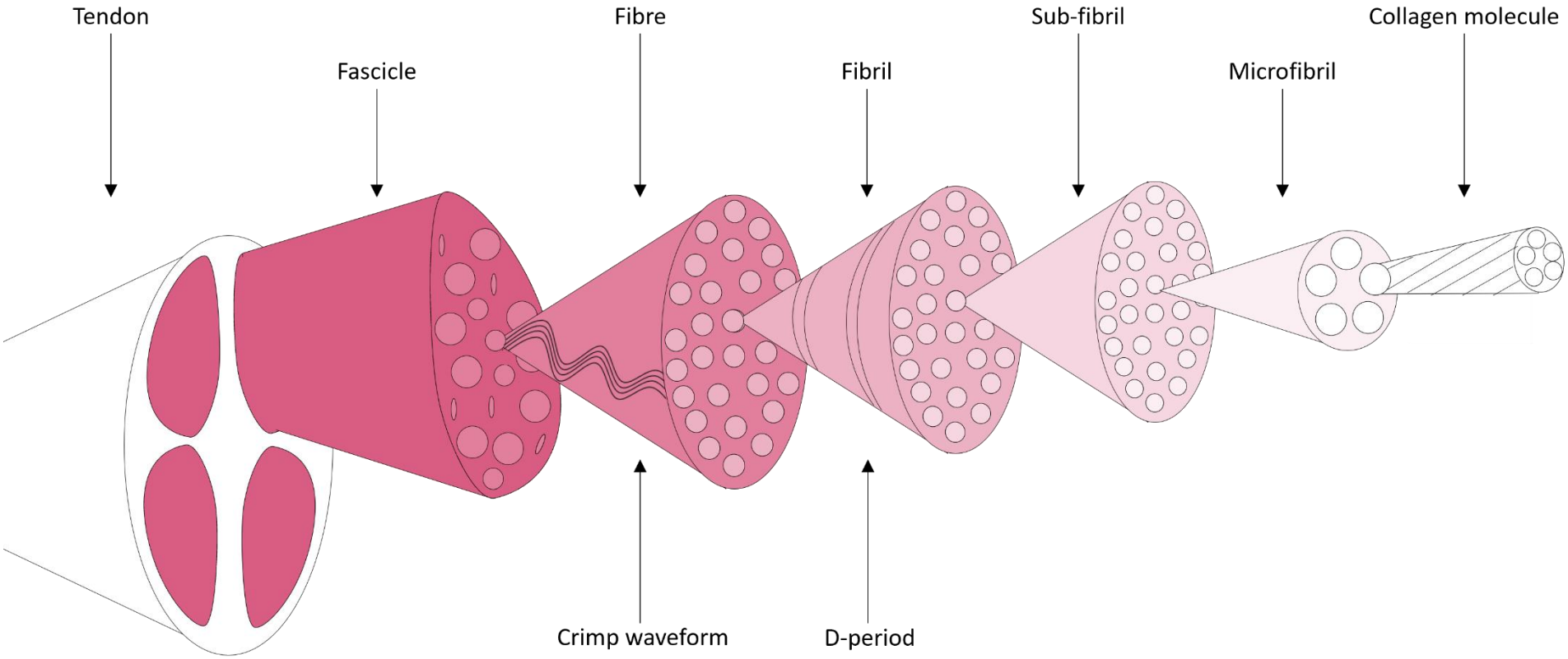

Figure 14. Hierarchical structure of tendon. *Tendons are a multi-level structure formed from collagen molecules binding to form microfibril of which many bind to form sub-fibril bind together to form fibrils, to fibres where they develop the crimp waveform, to fascicle to finally the full tendon structure. Adapted from Kastelic et al.[98] and Screen et al.[99].*

1.1.7 Myogenesis

Myogenesis is the term describing the development of the skeletal muscle system, which comprises of over 600 individual muscles across the full skeleton. Skeletal muscles are unique to cardiac and smooth muscle in that they can be controlled by the organism itself voluntarily allowing for movement and support.

The gross structure of the muscle comprises bundles of striated myofibers, made up of myocytes, which are tubular cells arranged in a line to form multinucleated syncytia and surrounded by epithelial cells forming a basal lamina[100].

The myotome is formed through the maturation of the lips of the dermomyotome, the cells of the myotome are committed to muscle cell lineage, expressing high levels of *MYOD* and *MYF5*[101]. Expression of these two basic helix–loop–helix (bHLH) transcription factors marks the terminal specification of muscle cell lineage[46]. The committed muscle cells join to form myocytes which then form the myofibers of the muscle[46].

1.2 Extracellular matrix function and components

The extracellular matrix (ECM) is a complex collection of macromolecules: collagens, non-collagenous glycoproteins, polysaccharides and proteoglycans[102]. All connective tissues are very ECM rich. The ECM harbours growth factors and cytokines that are essential for growth, turnover and differentiation, and acts as a scaffold for cells[102]. Cartilage ECM requires a collagenous network to maintain tensile strength of the cartilage matrix and proteoglycans, predominantly aggrecan, for the elasticity of the cartilage tissue and osmotic swelling[103]. Bone and tendon are primarily made of type I collagen which gives them their structural integrity, whilst proteoglycan and glycoproteins are responsible for bone mineralisation and tendon elasticity respectively.

The vast range of molecules mammalian ECM has led scientists to define key proteins of the ECM, which they have termed the "core matrisome"[104] comprising of approximately 300 proteins, including 43 collagen α-subunits, 36 proteoglycans and 200 proteoglycans. An additional group of ECM-affiliated proteins was also defined as proteins that are associated or interact with the ECM but are not considered ECM proteins. This list includes mucins, C-type lectins, galectins, semaphorins and plexins. Other components of the matrix that have been excluded from the "core matrisome" include ECM-modifying enzymes: proteases, cross-linking enzymes, growth factors and cytokines[104].

The ECM network is made up of proteins forming various complex interactions. Collagen fibrils are modified through cross-linking by disulphide bonding, transglutaminase cross-linking and through the effect of lysyl oxidases and hydroxylases[104]. Proteolytic enzymes present in the ECM can modify the ECM proteins. Collagens carry propeptide structures that must be cleaved by procollagen propeptidase, allowing the polymerisation of the collagen molecules[104]. Class I SLRPs, Asporin, decorin and biglycan carry N-terminal propeptide sequences that require protease cleavage[105].

Proteolytic enzymes of the ECM that contribute to regulation and ECM turnover include matrix metalloproteinases (MMPs), a disintegrin and metalloproteinase (ADAMs) and, a Disintegrin and Metalloproteinase with Thrombospondin motifs (ADAMTS)

1.2.1 Matrix metalloproteinases (MMPs)

Matrix metalloproteinases (MMPs) are a group of ECM enzymes, crucial for the maintenance and turnover of the ECM. MMPs are calcium-dependent zinc containing endopeptidases[106], capable of degrading collagens, elastins, gelatin, matrix glycol proteins and proteoglycans. To maintain homeostasis the MMPs are regulated by a combination of cytokines, growth factors and paracrine and endocrine hormones. In addition, MMP inhibitors (MMPIs) and tissue inhibitors of MMPs (TIMPs) closely regulate the expression and activity of MMPs.

MMPs are expressed as zymogens (propeptide MMPs) by connective tissues and pro-inflammatory cells, including fibroblasts, osteoblasts, endothelial cells, macrophages, neutrophils and lymphocytes[106]. These zymogens are then cleaved by proteolytic enzymes, generating active MMPs. This proteolysis regulates the levels of active MMPs there are three stages: activation of MMPs through proteolysis of zymogen, transcription of MMPs and inhibition of MMPs by TIMPs[106].

Dysregulation in MMP activity and expression disrupts the balance of MMPs and TIMPs. In pathological conditions the MMPs/TIMPs balance has shifted to increase MMP activity, resulting in increased tissue degradation[106]. MMPs have been implicated angiogenesis, apoptosis, bone remodelling, and inflammation, as well as arthritis, multiple sclerosis, Alzheimer's disease, nephritis, osteoarthritis and periodontal disease[106].

1.2.2 Collagens

Collagens are the most abundant protein in mammalian tissues. There are currently 28 identified mammalian collagen types[107]. The common

structure of collagens is the presence of a triple helix, made of 3 alpha chains, that can be made up as or homotrimers [107], heterotrimeric triple helices are more prevalent than homotrimeric triple helices[108].

Collagens are categorised into classic fibrillar collagens, network forming collagens, FACITs (fibril-associated collagens with interrupted triple helices), MACIT (membrane-associated collagens with interrupted triple helices) and MULTIPLEXINs (multiple triple-helix domains and interruptions)[108].

Type I collagen is the main building block of all tissues in the body, except for cartilage which is made up of predominantly type II collagen. Type I collagen is a fibrillar heterotrimeric collagen, made up of two α-1 chains and one α-2 chain whereas type II collagen is a fibrillar homotrimer collagen made of three α-1 chains. Collagens are a crucial component of the ECM forming supramolecular assemblies and providing main tissue structure. Collagen I is widely expressed in the majority of mammalian tissues including dermis, bone, tendon and ligament, and identified in the pathology of osteogenesis imperfecta, Ehlers-Danlos syndrome and osteoporosis[108]. Collagen II accounts for 85% of the collagen of articular cartilage, and changes to collagen II function, structure and expression have been identified for roles in the pathogenesis of osteoarthritis (OA)[109] and chondrodysplasias[108].

1.2.3 Proteoglycans

1.2.4 Small leucine-rich proteoglycans

Small leucine-rich proteoglycans (SLRPs) are a family of 17 proteins classified into 5 groups, determined by phylogenetic analysis (Figure 15). Their name is derived from the stretches of leucine-rich repeats (LRR) in the protein structure. SLRPs are proteins carrying glycosaminoglycan (GAG) chains in their structure. GAGs are linear polysaccharides, consisting of repeating disaccharide units of hexuronic acid linked to a hexosamine. The

sulphate groups of these GAGs give the proteins an overall negative charge (Figure 16). The five glycosaminoglycan chains are: heparan sulphate, keratan sulphate, chondroitin sulphate, polylactosamine sulphate and dermatan sulphate. GAGs are covalently attached to the proteoglycan molecule, either N-linked or O-linked. N-linked chains are attached to asparagine (Asn) present in Asn-X-Ser/Thr, O-linked chains are attached to functional hydroxyl groups on serine or threonine.

The classification of SLRPs is determined by their amino acid sequence organisation rather than function (Figure 15). Class I SLRPs includes decorin, biglycan and Asporin[110]. These SLRPs have a Cys residue cluster at the N termini, which form 2 disulphide bonds. Decorin and biglycan both have serine residues in the N-terminus and carry 10 LLRs. Decorin has one N-linked glycosylation site, biglycan has two, allowing the binding of chondroitin or dermatan sulphate chains. Asporin was formerly categorised into Class I, however it possesses a unique stretch of aspartate residues in its amino-terminal region, in place of the N-linked glycosylation sites, without the capacity to bind GAGs, therefore Asporin is not classed as a true proteoglycan. Asporin is actually more similar to the SLRPs in class II, III and V which contain a stretch of aspartic acid (Asp) residues, located in either the N- or C-terminal[110].

Class II SLRPs comprises fibromodulin, lumican, PRELP, keratocan and osteoadherin. Similarly, to class I, they each contain 10 LRRs. All class II SLRPs but PRELP carry polylactosamine or keratan sulphate chains bound to the LRR region. Their N-terminus contains sulphated tyrosine residues, whereas PRELP has a cluster of positively charged residues allowing the binding of heparan sulphate chains. Osteoadherin is further differentiated by its unique, large and very acidic C-terminal domain[111].

Class III of SLRPs consists of epiphycan, opticin and osteoglycin, each with 6 LRRs and sulphated tyrosine in their N-terminus. Epiphycan also carries chondroitin sulphate chain and at least three O-linked

oligosaccharides in the N-Terminus[112]. The N-terminus of opticin differs as it contains a cluster of O-glycosylation sites[113].

Class IV SLRPs are the chondroadherin and nyctalopin. Chondroadherin is similar in structure to Asporin and contains 10 LRRs but no N- or C- terminus extensions. Nyctalopin contains an N-terminus signal and a C-terminal glycophosphatidylinositol (GPI) anchor[114].

Class V has been termed the non-canonical class of SLRPs containing podocan (PODN) and podocan-like protein 1 (PODNL1). These have a different C-terminus cysteine cluster to the other SLRP classes however they carry 20 LRRs with homology to the class I and II SLRPs. Podocan can bind collagen I and can induce the p212 pathway, inhibiting cell growth, similarly to the other SLRPs.

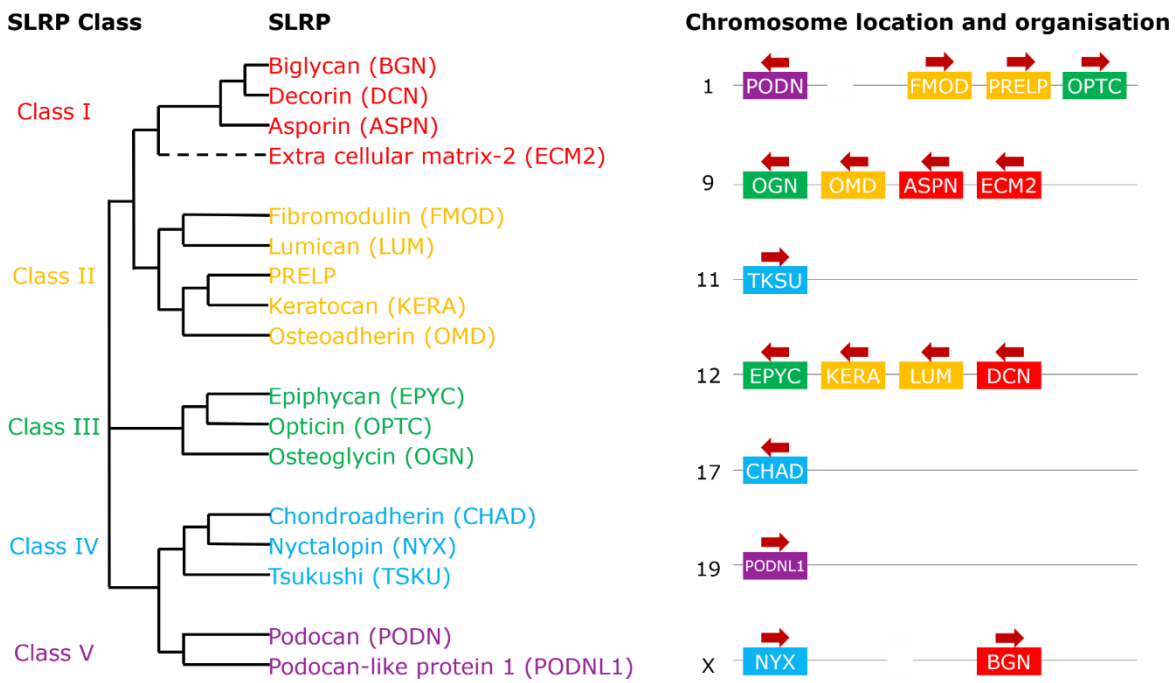

Figure 15. Classification of SLRPs and their human chromosomal location. *Asporin can be found in SLRP class I on chromosome 9 upstream of osteoadherin (OMD) and osteoglycin (OGN) and downstream of ECM2 (Adapted from[110]).*

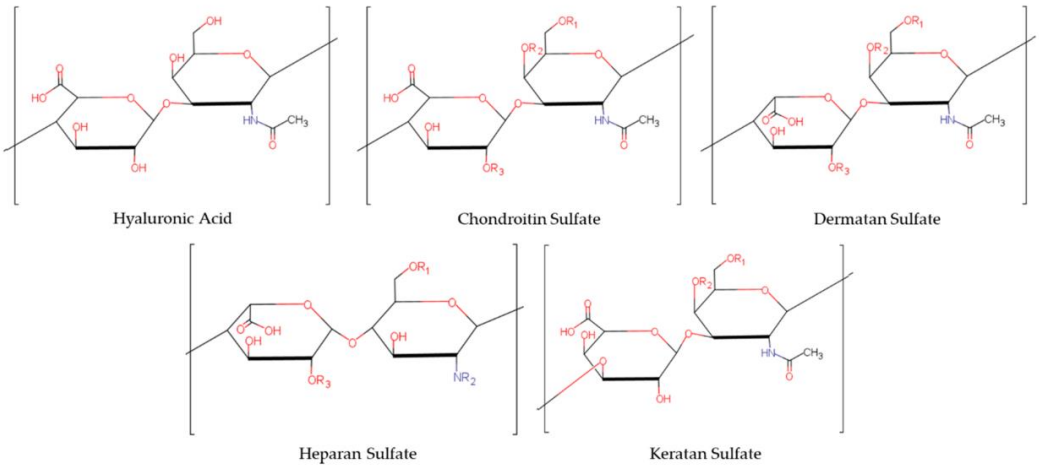

Figure 16 Structure of major glycosaminoglycans (GAGs) classes.

GAGs are unbranched polysaccharide chains made up of disaccharide units. The makeup of these chains is varied, and GAGs are classified based of the disaccharide chain composition. The 5 classes are: hyaluronic acid, chondroitin sulphate, dermatan sulphate, heparan sulphate and keratan sulphate. Image obtained from Sodhi et. al.[115].

1.2.4.1 Diseases linked to SLRPs.

Diseases linked to SLRPs commonly present with ocular abnormalities or have an ocular phenotype alongside the primary disease. Truncated decorin, missing 33 amino acids at the C-terminal, has been identified as a cause of congenital stromal dystrophy, characterised by opacities of the cornmeal stroma, predicted to alter the orthogonal arrangement of the collagen fibrils of the cornea, which provides transparency[116].

Loss of lumican or fibromodulin alters collagen architecture in the connective tissues. In fibromodulin null mice, Achilles tendons showed rough and irregular collagen fibrils, with on average thinner fibrils in the fibromodulin null mice than in the wild-type[117]. Interestingly in the fibromodulin null mice lumican content was increased four-fold within the tail tendon[117], potentially partially compensating for the loss of fibromodulin. Deletion of fibromodulin resulted in decreased tendon stiffness. Conversely, lumican null mice presented with thicker collagen fibrils resulting in an irregular collagen fibril organisation, and disorganised matrix in the cornea and skin. Similarly to fibromodulin null mice, this affected corneal clarity and also increased the laxity of skin[118].

In double knockout mice of fibromodulin and lumican, mice manifested with a phenotype akin to several features of the Ehlers-Danlos syndrome, they were smaller than their wild type littermates, presented with gait abnormality, joint laxity and age-dependent osteoarthritis[119]. The tendons of the fibromodulin-lumican double-null mice were significantly less stiff, the collagen fibril diameters showed less definition in the transition from small to large fibrils, resulting in irregularity in the organisation[119].

1.2.4.2 Asporin

Asporin (ASPN) is a member of the SLRP family of ECM proteins. Asporin is also referred to as periodontal ligament-associated protein 1 (PLAP-1) as it was first found to be expressed in the periodontal ligament (PDL). The gene *ASPN*, that encodes the Asporin protein is located on human chromosome 9 (chr9:92,456,205-92,482,506), and contains 8 exons, spanning 26 kilobases[87]. There are 3 type I SLRPs present in bone, cartilage, and the PDL: Asporin, decorin and biglycan; all three bind type I collagen and compete for the same binding site, however only Asporin binds calcium, and has been shown to increase calcium uptake by the osteoblasts[120].

1.2.4.2.1 Asporin protein structure

Asporin protein consists of a propeptide signal N-terminus, followed by a sequence of aspartate (Asp) repeats, 4 cysteine clusters, 10 LRRs and 2 cysteine clusters in the C-terminus (Figure 17).

Asporin's unique N-terminal sequence of a series of aspartate (Asp) repeats (Figure 17) means that it can bind other matrix constituents such as fibres of collagen to play a role in collagen metabolism and fibrillogenesis. This Asp repeat replaces the consensus sequences for glycosaminoglycan (GAG) chains to covalently bind, these are Ser-Gly motifs preventing Asporin from being classified as a true proteoglycan [121]. Asporin has one N-glycosylation site at Asn^{281}, giving Asporin the potential to bind N-linked oligosaccharides[121]. A potential O-glycosylation site at Ser^{54} was also identified.

The aspartate repeats in human Asporin is uninterrupted and consists of 13 residues whereas in mouse sequences there are interspersed amino acids through the repeats[121]. However, the clustering of aspartates in this region in the mouse protein still overall retains the negatively charged cluster in the protein structure, and the conservation of this site indicates an important function[121]. Interestingly, Asporin contains a putative

propeptide with a conserved region alike to the region present in biglycan and decorin. Pro-biglycan, the propeptide of biglycan, can be cleaved by bone morphogenic protein-1 (BMP1), the conserved cleavage site corresponds with the recognition sequence for BMP1.

Although the aspartate repeat found in Asporin is unique within SLRPs, it is found in other proteins. Interestingly osteopontin, a key component of the mineralised bone matrix and teeth, carries an aspartate repeat in the centre if the core protein. Osteopontin as previously mentioned inhibits hydroxyapatite (HA) formation and has a suggested role in bone mineralisation[122]. The aspartate repeat in osteopontin acts as a calcium ion binding domain in the protein to bind calcium ions and modulate the mineralisation of bone and teeth[122]. In Asporin this aspartate repeat gives the protein the capacity to bind calcium ions and promote the mineralising of type I collagen[123]. Whereas in decorin, another class I SLRP, lacking the aspartate repeat, decorin can bind but not mineralise type I collagen[123].

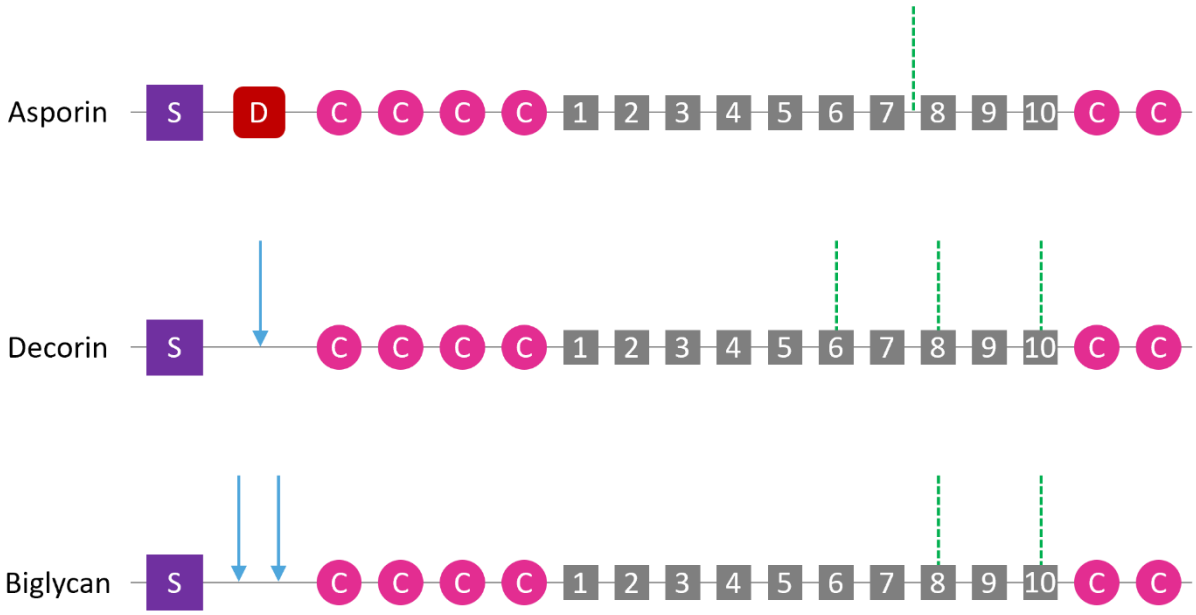

Figure 17. Schematic diagram of class I SLRPs: Asporin, decorin and biglycan. *Grey squares, leucine rich repeats (LRR). Arrows represent O-linked glycosylation site, present on decorin and biglycan, in Asporin this is replaced by a series of asp residues (D box), therefore it is not a true proteoglycan. S: signal peptide; C: cysteine region; dashed lines: putative N-linked glycosylation sites. (Adapted from L. Xu. Et. al. 2015)*[124].

1.2.4.2.2 Asporin expression

Asporin has been found in the developing bones of mice, specifically in the periosteum and perichondrium. However, it is not present in the trabecular bone, cartilage growth plate, articular cartilage, or skeletal muscle. Additionally, asporin is expressed in periodontal ligament (PDL) cells[87, 125]. A proteomics study by Onnerfjord found Asporin content was much higher in the meniscus than in the medial tibial condyle (end of the tibia bone) and the femoral head cartilage (cartilage in the hip joint) in adult joints[126].

Asporin is expressed during development and into adulthood, a broad screening of the presence of Asporin across adult and foetal tissue by hybridisation of a normal mRNA dot blot identified the highest signal levels in aorta and the uterus, with moderate expression levels in small intestine, heart, liver, bladder, ovary, stomach and within the adrenal, thyroid, and mammary glands. Low levels were also observed in the bone marrow. Similar expression patterns were observed in mouse foetal tissues (Figure 18).

High-density oligonucleotide arrays determined that gene expression levels of *ASPN* was highest in the cells of the uterus[127]. However, there were other cell types with increased Asporin expression: fetal liver, fetal lung, adipocytes and the small intestine (Gene report ID: 54829; Figure 7)[127]. Gene expression database (GXD) highlighted expression in the embryo mesenchyme in cartilage condensation, limb mesenchyme and strong expression in the musculoskeletal system and its components, (Figure 19)[128].

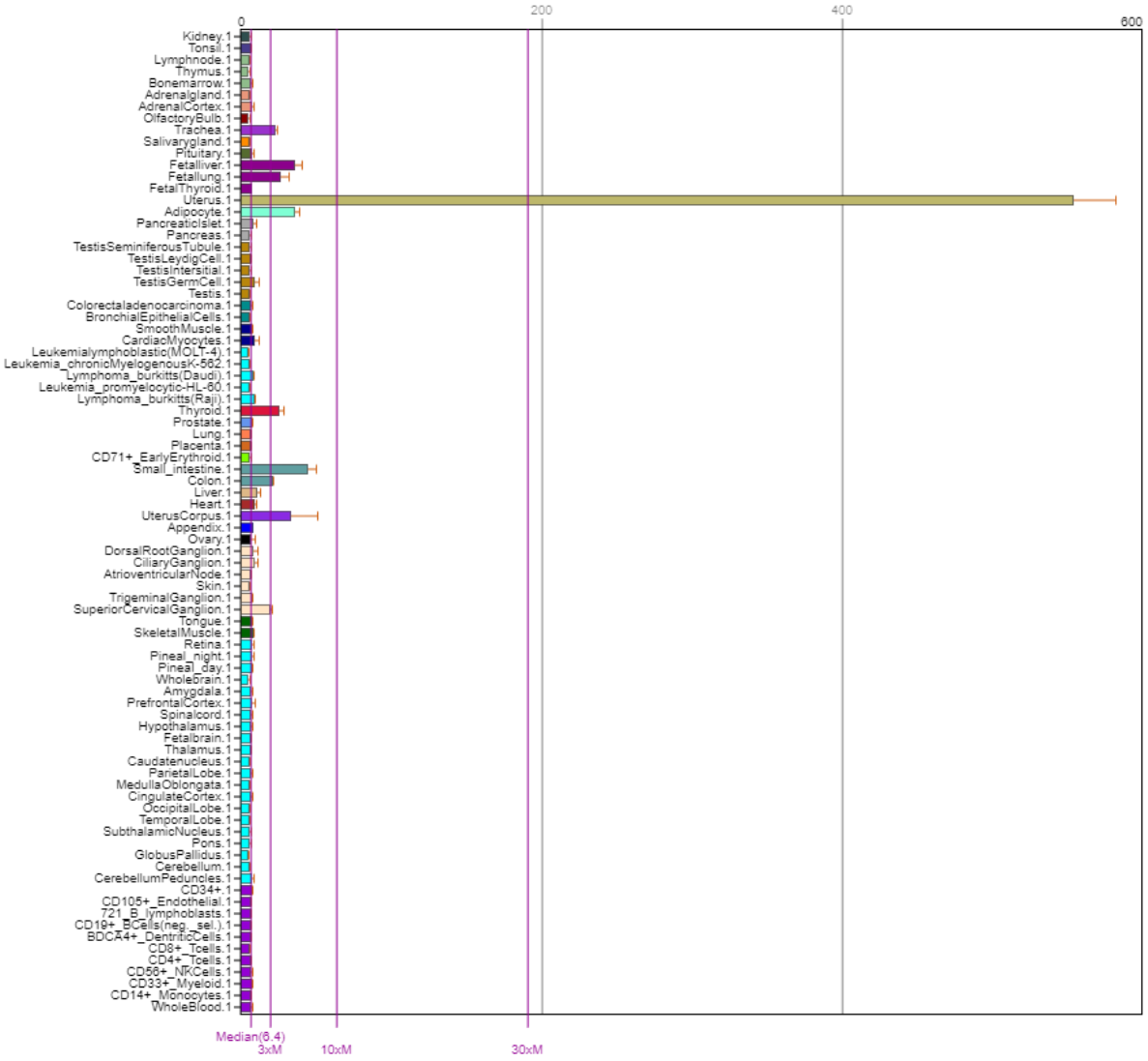

Figure 18. BioGPS Expression Data. *ASPN gene expression data from high-density oligonucleotide array in 79 human and 61 mouse tissues. Highest expression in uterus cells, fetal cell lines. (http://biogps.org/#goto=genereport&id=54829)*[127].

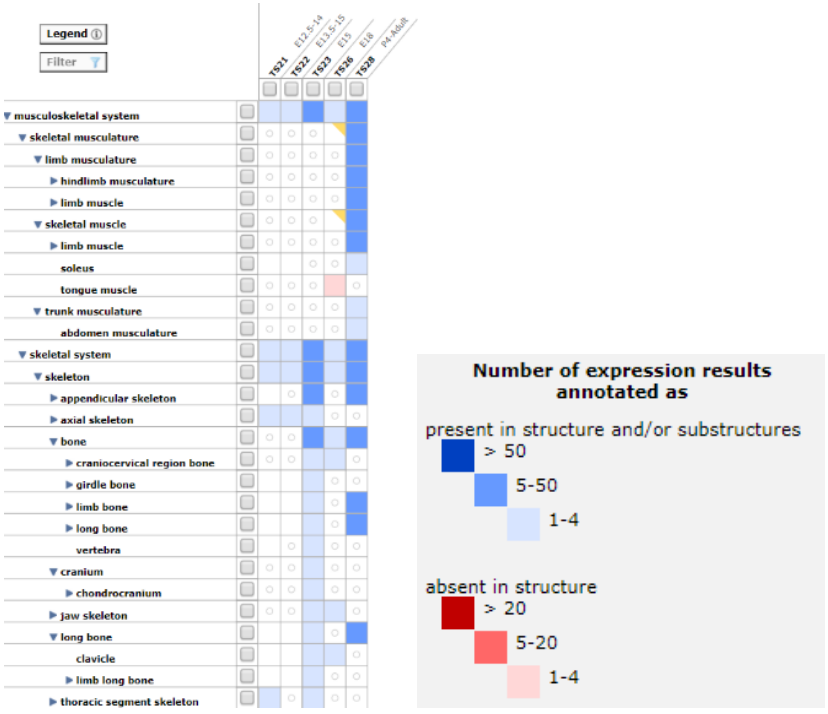

Figure 19. GDX Tissue x Stage matrix. To display expression of ASPN across musculoskeletal system across Theiler Stages 21-28 (MGI: 1913945)[128].

1.2.4.2.3 Asporin interactions

STRING database was used to identify interactions of ASPN with other proteins (Figure 20). This identified an interaction of Asporin with TGF-β family including TGF-β1, TGF-β2 and TGF-β3. Closely linked to the TGF-β family is mimecan (OGN) which alongside TGF-β1 and TGF-β2 induce bone formation[129].

Frizzled-related protein 3 (FRZB) and secreted frizzled-related protein 4 (SFRP4) are modulators of Wnt signalling, a pathway highlighted in articular cartilage degeneration in osteoarthritis (OA) models[129]. In rat models of injury and exercise-induced OA Wnt signalling pathways were excessively activated with increased protein levels of Wnt3a and β-catenin, however collagen II was reduced in these models[130]. Wnt signalling has been explored as a promising target for OA therapy with Wnt signalling inhibitor SM04690 having reached stage I clinical trials[130].

Two other notable interaction partners are Matrillin3 (MATN3) and cartilage intermediate layer protein 1 (CLIP), a major component of the extracellular matrix of cartilage as previously mentioned and a protein involved in cartilage scaffolding and possible TGF-β1 antagonist, respectively[41, 129].

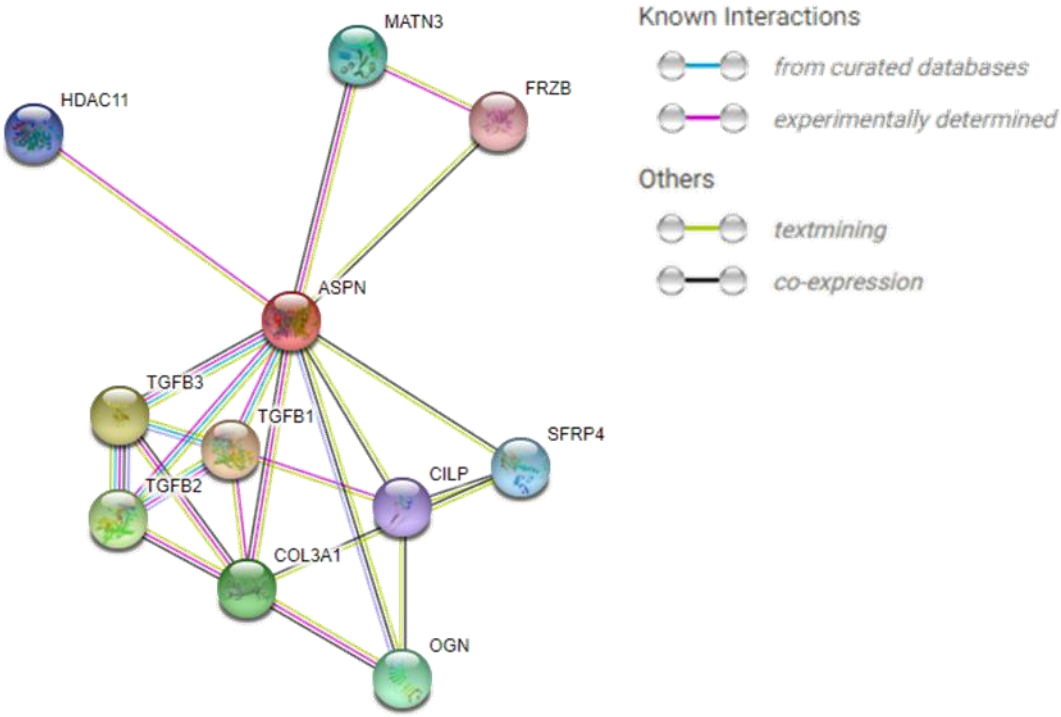

Figure 20. STRING network for ASPN protein. *Filtered for known interactions, from curated database and experimentally determined interactions, text-mining and co-expression. (https://string-db.org/cgi/network?taskId=b3BnJzmdWHVy&sessionId=bludjR4eShuL)*[129].

1.3 Asporin in age related diseases from ECM changes

1.3.1 Osteoarthritis

Osteoarthritis (OA) is an age-related condition that affects over 8.5 million people in the UK[131]. It is a progressive and painful disease and can become debilitating as it progresses, characterised by loss of articular cartilage in the joint and the subchondral bone becomes exposed resulting in inflammation[132]. OA is a long-term condition with no cure; all current treatments aim to slow the OA progression and to reduce the symptoms[133]. Finding early markers of OA and understanding the pathogenicity of the condition can help improve early intervention[132]. It is classed as a 'whole joint' disease due to pathological changes in all the tissues of the diarthrodial joint, the degradation of articular cartilage, thickening of subchondral bone, osteophyte formation, degeneration of the ligaments of the joint and synovitis, which is when the synovium of the joint becomes inflamed[133].

After significant loss of the cartilage, joint movement causes further damage and pain to the point where joint replacement is necessary for quality of life[132, 133]. The trauma at the ends of the bones can tip the homeostasis balance towards overproduction of bone and the formation of osteophytes (bone spurs), and bony lumps at the joint junction. These cause more friction at the joint and as a result more pain for the individual[132, 133].

OA is a multifactorial disease. Age, lifestyle, trauma, and genetics are all contributing factors to OA susceptibility.

1.3.1.1 Asporin and Osteoarthritis

Asporins role in osteoarthritis has been previously identified through human association studies in various populations. The connection is made

between polymorphisms in Asporin with varying numbers of D repeats[134]. As previously mentioned, the normal Asporin allele contains 13 aspartic acid repeats whereas Asporin alleles with 14 aspartic acid repeats (*ASPN* D14 allele) have been identified in individuals with OA of the knee in a Japanese population where the frequency of the D14 allele increased with the severity of the OA[134], [135]. 14 and 15 D-repeats were identified as a risk factor in a United States cohort in hand and knee OA. 15 D-repeats in a Greek cohort of knee OA was also identified as a risk factor of OA. Multiple associations have been made between these alleles and OA, however in UK and Spanish cohorts there was no significant association between Asporin and OA[124]. Ultimately, it has been shown in some cohorts that there is an increase in Asporin expression during OA therefore there is interest in investigating the effect or role of Asporin in OA.

In vitro studies of chondrogenesis in presence of recombinant Asporin in the culture medium have shown that Asporin is a negative regulator of chondrogenesis by inhibiting TGF-β function thus dampening TGF-β-induced aggrecan and type II collagen expression. Moreover, overexpressing Asporin D14 during TGF-β induced chondrogenesis of ATDC5 cells dampened chondrogenesis[135] and showed that Asporin D14, had a stronger inhibitory effect on TGF-β induced expression of aggrecan and type II collagen and therefore stronger inhibition of TGF-β-induced chondrogenesis[135].

It has been speculated that the polymorphisms in the Asp repeat of Asporin (D14) may affect conformation of collagen and as a result, its function[124, 134]. If this is true *in vivo*, the developing cartilage of the patients carrying the OA associated variant may be affected in but only come into effect later in life as cartilage breaks down tipping the balance towards more catabolism (breakdown) than anabolism (production) of the ECM. Asporin can bind directly to collagen and calcium to induce collagen mineralisation, by a similar mechanism to osteopontin (SPP1), a key marker of osteogenesis, to influence collagen hydroxyapatite crystal formation[123].

Other class I SLRPs, decorin and biglycan, and class II SLRPs, fibromodulin and lumican are also known to bind collagen, however Asporin is unique in its ability to mineralise collagen.

Another theory for the role of Asporin in OA pathogenicity is via the TGF-β signalling pathway, as many SLRPs have known roles in modulating TGF-B superfamily members. Decorin and biglycan the other two Class I SLRPs, have been identified for roles in TGF-β signalling. Decorin is shown to inhibit TGF-β and biglycan leading to overactive TGF-β signalling by decreased sequestration of TGF-β[124, 136]. The ratio of Asporin mRNA to TGF-β mRNA levels was found to be higher in OA patients in both cartilage and subchondral bone, moreover this ratio positively correlated with the OA severity[136]. Further supporting this, work by Nakajima *et. al.* showed that siRNA knockdown of Asporin in Normal Human Articular Cartilage (NHAC) cells resulted in increased expression of cartilage marker genes including TGF-β1, inferring Asporin may be an inhibitor of TGFβ signalling[137]. With the addition of recombinant Asporin they further demonstrated that Asporin inhibited TGF-β binding to both TGF-β RI and TGF-β RII. TGF-β-induced phosphorylation of Smad was also increased in a dose dependent manner of recombinant Asporin in NHAC cells.

In NHAC cells supplemented with TGF-β1, Asporin mRNA expression was upregulated. Moreover, siRNA knockdown of Smad3 was found to depress TGF-1-induced Asporin expression, whereas Smad3 overexpression promoted Asporin expression. This is suggested a regulatory loop between Asporin and TGF-β1[137], and regulation of Asporin by TGF-β in chondrocytes may be through the canonical TGF-β/Smad pathway[137].

1.3.2 Intervertebral disc disease

Intervertebral disc disease (IDD) is a musculoskeletal condition affecting the spine, characterised by degeneration of one or more of the fibrocartilage discs separating the vertebrae (bones of the spine)[138]. Like the articular cartilage, these discs provide cushioning between the bones and regulate and absorb pressure on the spine. IDD has similarities with osteoarthritis (OA), where the cartilage is worn down and degenerates leaving the bones prone to meeting and damaging each other[139]. Osteophytes (bone spurs) develop on the edges on the vertebrae causing more pain and without the fibrocartilage disc to absorb pressure and separate the vertebrae nerves spinal nerves can be pinched where these vertebrae meet, causing numbness and weakness[138, 139].

The most widely accepted cause of IDD is the accumulation of changes in the proteins making up the extracellular matrix of the discs. As Asporin is an ECM protein, it has been investigated for a role in IDD. Studies have shown Asporin expression to be increased in degenerated intervertebral discs, but its regulation during the disc development and degeneration is unknown[140]. Polymorphisms within the aspartic acid rich region of Asporin, together with an increase in ASPN expression, have been implicated in the susceptibility to the intervertebral disc degeneration (IDD)[87, 110, 124].

Individuals with 14 Asp residues allele of ASPN had an increased risk of lumbar disc degeneration and OA[140]. Asporin was also more highly expressed in the nucleus pulposus (inner core of the vertebral disc) of individuals with IDD[140], with a positive correlation of the more severe the degeneration the stronger the Asporin expression. Pro-inflammatory cytokines TNF-α and IL-1β are upregulated in IDD, work with primary human nucleus pulposus showed that IL-1β upregulated Asporin expression via the NF-κB p65 pathway. In the IDD model, Asporin is more highly expressed, this may be through upregulation of IL-1β[140]. The Asporin promoter was found to contain at least 2 p65 binding sites[124, 140]. This study

highlights a common pathway of increase in inflammatory cells and interaction between Asporin and TNF-α in the pathogenesis of the disease[140, 141].

1.3.3 Asporin and tooth health

The most understood role of Asporin is in the periodontal ligament (PDL), where it negatively regulates PDL differentiation and mineralisation to prevent ossification and maintain the tooth supporting system[142].

A study by Ueda *et. al.* investigated changes to the PDL during pressure of tooth movement using centrifugation to mimic the compressive force (CF) exerted by orthodontic tooth movement *in vitro,* on human periodontal ligament (hPDL)[85]. Cells were centrifuged at confluency and RNA was extracted and analysed by qPCR. CF-treated hPDL cells showed increased *ASPN* mRNA and lower *SOST* mRNA in comparison to control hPDL cells[85]. The CF-treated hPDL cells were also exposed to varying levels of CF: 40, 90, 135, 160 x g. Interestingly, *ASPN* mRNA expression increased in 40 x g and more so in 90 x g, however, was decreased in 135 x g and 160 x g. Asporin is therefore predicted to have a role in prevention of ossification in the PDL[85].

Periodontitis is a severe gum infection where the infection damages soft tissue and can progress to the degradation of the bone that supports teeth, known as alveolar bone[143]. In a study investigating periodontitis in rats, Asporin expression was reduced and degradation of PDL collagen was increased[141]. Inflammatory cells were observed in the degrading alveolar bone of the periodontitis rats, acute periodontal inflammatory infiltration, with Asporin-positive inflammatory cells having infiltrated in pits of the alveolar bone surface, interacting with CD68+ cells and mediating collagen destruction and alveolar bone resorption[141].

In this periodontitis model alveolar bone destruction and acute periodontal inflammatory infiltration is further induced by administration of TNF-α. In the TNF-α induced group increased numbers of Asporin-positive inflammatory cells were found in multinucleate cells in pits of the alveolar bone, identified to be osteoclasts by TRAP staining[141]. This study concluded

a role for Asporin-positive inflammatory cells in pathogenesis of periodontitis, mediating osteoclast activity in the alveolar bone[141].

1.4 Conclusions

OA and IVD variants in Asporin and/or exposure to recombinant Asporin in the medium hinder chondrogenesis. Asporin has also been shown to influence collagen mineralisation and regulate TGFβ signalling in the pathological conditions. Modulation of the Asporin expression therefore presents an exciting therapeutic avenue for several age-associated conditions, including OA and IVD. However, Asporin is also present in healthy developing connective tissues, including healthy cartilage and bone. As many repair mechanisms revert the cells to their more juvenile state in an attempt to increase anabolism and ECM production, it is therefore important to analyse the effect of Asporin deletion on skeletal development and homeostasis.

1.5 Aims

1. To analyse the effect of Asporin overexpression on the TGFβ independent chondrogenesis and osteogenesis
2. To study the effect of Asporin deletion on cartilage (growth plate, articular cartilage, IVD) development and homeostasis
3. To assess the effect of Asporin deletion on tendon mechanical properties and health
4. To study the effect of Asporin deletion on bone metabolism in the long bones and in the vertebrae

Chapter 2. Materials and Methods

2.1 Materials

The consumables, histology slides and tissue culture plastics used in the experiments in this thesis were purchased from Fisher Scientific, unless stated otherwise.

Cell culture media and supplements were obtained from Gibco and purchased through ThermoFisher Scientific.

cOmplete™, Mini EDTA-free Protease Inhibitor Cocktail Tablet obtained from Roche purchased through Merck.

Mr. Frosty™ Freezing Container was purchased from ThermoFisher Scientific.

DH5-α Competent Cells were obtained from ThermoFisher Scientific.

S.O.C medium and DNase I (RNase-free) (18047019) were obtained from Invitrogen™ and purchased through ThermoFisher Scientific.

RNase H (EN0202) was obtained from ThermoFisher Scientific.

Chemicals were procured from Merk (formerly Sigma Aldrich), and ethanol, methanol and xylene were purchased from VWR.

Vector® Nuclear Fast Red solution and ImmEdge® Hydrophobic Barrier PAP Pen were obtained from Vector Labs.

Primary and secondary antibodies used in the immunohistochemistry experiments, primary antibodies used in Western blotting and Mounting Medium with DAPI - Aqueous, Fluoroshield (ab104139) were purchased from Abcam. Antibody dilutions and incubation conditions are given in Appendix E.

4-12% NUPage Bis Tris precast gels and the MES buffer were purchased from Fisher Scientific.

Membrane was manufactured by GE Healthcare.

Secondary antibodies used in Western blotting and the REVERT™ Total protein stain came from LI-COR®.

Primers were purchased from Eurofins Genomics.

Power SYBR® Mastermix was acquired from Applied Biosciences.

10X Biomix™ Red and Hyperladder™ 100 bp came from Bioline.

ReliaPrep™ RNA Tissue and Cell Miniprep Systems, GoScript™ Reverse Transcription System and DeadEnd™ Fluorometric TUNEL System were obtained from Promega.

QIAprep Spin Miniprep kit was obtained from QIAgen.

Dissecting tools: Swann Morton scalpels, Dumont Watchmakers forceps and dissecting scissors were purchased through Avantor™ VWR™.

MicroAmp™ Optical 96-Well Reaction Plate and MicroAmp™ Optical Adhesive Film were obtained from Applied Biosystems™ and purchased through ThermoFisher Scientific.

D-profile tungsten carbide knife was obtained from Histoline.

Fast-Read® 102 Counting Chamber Slides were obtained from Immune Systems Ltd.

All experiments are carried out at room temperature unless stated otherwise.

2.2 In vitro methods

2.2.1 Cell culture of ATDC5 and U2OS cell lines

Mouse chondrogenic ATDC5 cells (ECACC: 99072806) were maintained in complete D-MEM (Dulbecco's Minimum Essential Media) supplemented with 10 % foetal bovine serum and 1 % penicillin/streptomycin (Appendix F). Human osteogenic U2OS cells (ECACC: 92022711) were maintained in complete α-MEM supplemented with 10 % foetal bovine serum and 1 % penicillin/streptomycin (Appendix F). Cells were cultured at 37 °C and 5 % CO_2 and media was changed every 2-3 days, cells were passaged at ~80 % confluency.

2.2.1.1 Passaging cell lines

At ~80 % confluency the cell monolayer was washed with PBS and trypsinized (Trypsin-EDTA 0.05%) for 5 minutes at 37 °C. Trypsin was neutralised with equal volume of medium, centrifuged at 1,000 x g for 5 minutes. Supernatant was removed and the cell pellets were resuspended in appropriate medium and either passaged, frozen or seeded for experiments.

Cells were passaged at 1 in 10 dilutions. Briefly, the cell pellet was resuspended in 10 mL of the appropriate medium and 1 mL was transferred to each T75 (75 cm^2) flask and 9 mL of medium was added.

2.2.1.2 Freezing cell lines

Following trypsinization and centrifugation, the cell pellet was resuspended in 1 mL of freezing medium, comprised of 10 % (v/v) dimethyl sulfoxide (DMSO) in appropriate media (Appendix F). Cell suspension was

transferred to a cryovial and placed in a Mr. Frosty™ Freezing Container filled with 2-isopropanol and placed in the -80 °C freezer overnight. Cryovials were then removed from the Mr Frosty™ and stored at -80 °C.

2.2.1.3 Thawing cell lines

Cells were removed from – 80 °C freezer and defrosted to room temperature. Cells were transferred to T75 flask and 9 mL medium was added and cells were incubated as previously described for 24 hours to allow the cells to adhere. Medium was then replaced with fresh medium to remove dead cells and residual DMSO.

2.2.1.4 Cell counting for seeding

Cells were counted using Fast-Read® 102 Counting Chamber Slides (Kova International). Following trypsinization and centrifugation, supernatant was removed, and cell pellet was resuspended in 10 mL of appropriate medium. A 100 µL aliquot of cells was diluted with 100 µL trypan blue to identify dead cells on the counting chamber slide. 9 µL of cell suspension with trypan blue was pipetted into the chamber slide and the number of cells in each square was counted, the volume in each 4 x 4 square is 0.1 µL (Figure 21). The calculation for cells/ mL detailed in the Fast-Read® 102 Counting Chamber Slides protocol was used.

$$counts/mL = \frac{total\ counts}{number\ of\ complete\ 4\ x\ 4\ grids\ counted} \times 10^4 \times sample\ dilution$$

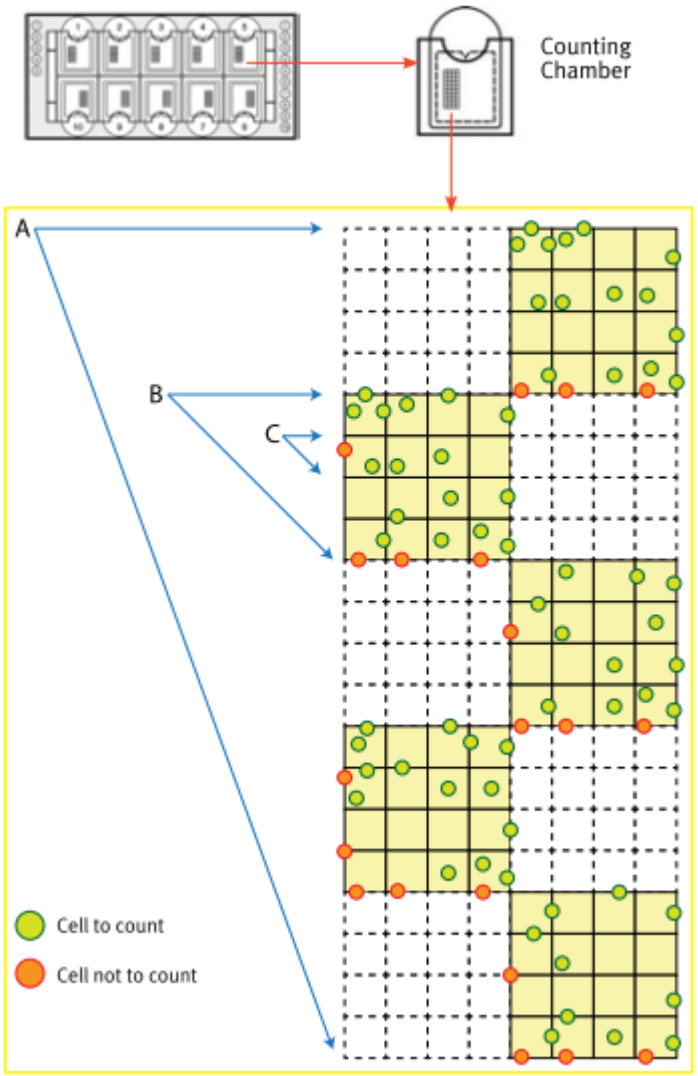

Figure 21. Fast-Read® 102 Counting Chamber Slides counting method. *Cells counted in the 4 x 4 counting grids (B), 10 per chamber (A). Image obtained from Biosigma Fast-Read® 102 protocol*[144]*.*

2.2.2 Primary cell extraction and analysis

2.2.2.1 Extraction and culture and differentiation of mesenchymal stem cells

Mice were culled at 9 weeks of age, femur and tibia were removed, leg bones were separated at the knee joint, and all tissue was removed from the bone. Ends of the bones were cut at either end of the bone shaft and to expose bone marrow (Figure 22). Tibia and femur of each leg was placed into a 500 µL Eppendorf tube pierced with an 18G needle at the bottom inside a sterile 1.5 mL Eppendorf tube with 125 µL of complete α-MEM (Appendix F) (Figure 22). The Eppendorf tubes were centrifuged at 800 x g for 3 minutes. The bone marrow was flushed out of the bone and into the α-MEM. The settled bone marrow was resuspended into the complete α-MEM. Cells were counted as previously described and seeded directly into 12 well plates at 0.5×10^6 per well for mineralisation studies.

2.2.2.2 Extraction and culture of primary osteoblasts

Following extraction of the bone marrow, the remaining tibia and femur bones were cut into 2 mm fragments (bone chips) with a sterile scalpel in Hank's buffered saline (HBS). Fragments were transferred to a T25 (25 cm^2) flask containing 5 mg/mL collagenase and incubated in a 37 ^oC oven on a nutating mixer (GyroMini – Labnet) at 20 rpm for 1 hour. The supernatant was discarded, and bone chips were washed three times in HBS to separate the chips. 5 mL of complete α-MEM was added to the T25 flasks and incubated at 37°C and 5% CO_2, left undisturbed for 5 days. Media was removed and bone chips were washed in PBS, 5 mL of fresh complete α-MEM was added, and cells that migrated out of the chips were grown to confluency for one month with media changed every 3 days.

At confluency the bone chips were removed, and the cell monolayer was washed with PBS and trypsinized for 5 minutes at 37°C. Trypsin was quenched with equal volume of media, centrifuged at 1,000 x g for 5 minutes and the cells were seeded in 24 well plates for mineralisation studies.

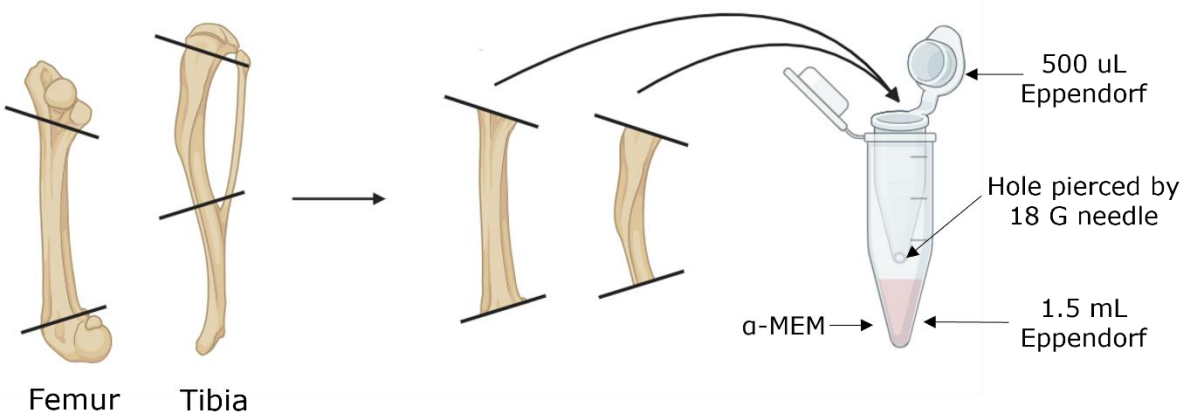

Figure 22. Set up for the extraction of bone marrow from mouse bones. *Femur and tibia were cleaned and cut at the sites shown on the figure. The cut bones were then placed into the 500 uL Eppendorf. The 500 uL Eppendorf is pierced at the bottom with an 18 G needle and placed withing a 1.5 mL Eppendorf containing α-MEM.*

2.2.3 Cell differentiation protocols

2.2.3.1 Mineralisation of bone cells in monolayer

For mineralisation studies, the cells were counted as previously described and seeded in 24 well plates at 0.05 x 10^6 cells per well, in 12 well plates, or at 0.1 x 10^6 cells per well for bone marrow derived cells. At confluency the medium was changed to osteogenic differentiation medium (Appendix F). Cells were cultured for 21 days at 37°C and 5% CO2 and osteogenic media was changed every 2-3 days.

2.2.3.2 Mineralisation of cartilage cells in monolayer

For mineralisation studies the cells were counted as previously described and seeded in 24 well plates at 0.05 x 10^6 cells per well, in 12 well plates, or at 0.1 x 10^6 cells per well for bone marrow derived cells. Cells were grown to confluency in cartilage mineralisation medium 1 (Appendix F) for 6 days, medium was then changed to cartilage mineralisation medium 2 (Appendix F), and cells were cultured for further 21 days at 37°C and 5% CO2 and cartilage mineralisation medium 2 was changed every 2-3 days.

2.2.3.3 Mineralisation assay

To assess calcium deposition in the mineralising cultures, the cells were stained with Alizarin Red S and the stain was extracted and quantified by spectrophotometry. Briefly, media was removed, and the monolayer was washed three times with 1 x PBS and fixed in 4 % formaldehyde for 20 minutes at room temperature. Cell monolayers were then stained for 30 minutes with 40 mM Alizarin Red S solution (Appendix A) with gentle agitation, then washed three times with distilled water. The water was

removed, and slides were left to dry overnight. Once dry cells were scanned on a Nikon flatbed scanner.

To extract the stain, 10% acetic acid (Appendix A) was added to each well and incubated at room temperature on a shaker for 30 minutes. Cells were then scraped off the plate and transferred to 1.5 mL Eppendorf tubes. Tubes were vortexed for 30 seconds and then heated to 85 ^{o}C for 10 minutes forming a slurry. The extracts were cooled on ice for 10 minutes and vortexed again. The slurry was then centrifuged for 15 minutes at 20,000 x g. The supernatant was removed and transferred to a new Eppendorf tube and neutralised with 75 µL of 10 % (v/v) ammonium hydroxide to pH 4.1-4.5 (Thermo-Scientific).

Standards for the quantification of the Alizarin Red S stain were made up and loaded in triplicate on a 96 well flat-bottomed plate, standards are outlined in Appendix G. For quantification, 50 µL of each sample was ran in duplicate. Absorbance was quantified on a Varioskan LUX Multimode Microplate Reader (Thermo Scientific), and absorbance measured at 405 nm optical density. Alizarin Red S stain concentration was calculated from the standard curve of absorbance. Linear regression coefficient was calculated and $R^2 > 0.99$ was accepted for the standard curve.

A Student's unpaired two tailed T-test was used to analyse significant differences between samples and statistical significance was given by $p<0.05$.

2.2.3.4 Chondrogenesis of cells in monolayer

For chondrogenesis studies the cells were counted as previously described and seeded in 24 well plates, at 0.05 x 10^6 cells per well in complete DMEM medium (Appendix F). At confluency medium was changed to chondrogenic differentiation medium (Appendix F), the cells were

cultured for 21 days at 37 °C and 5% CO_2 and chondrogenic medium was changed every 2-3 days.

2.2.3.5 Proteoglycan assay

To assess sulphated proteoglycan (sGAG) deposition, the cell monolayers were stained with Alcian Blue and quantified by spectrophotometry.

Media was removed and the monolayer was washed three times with 1 x PBS and fixed in 95 % methanol for 20 minutes. Cells were then stained overnight with 1% Alcian blue in 0.1 M HCl (Appendix A). Cells were washed three times with distilled water. All water was removed, and slides were left to dry overnight. Once dry, the wells were scanned on a Nikon flatbed scanner.

To extract the stain, 6 M guanidine-HCl (Appendix A) was added to each well and incubated at room temperature on a shaker for 3 hours. Cells were then scraped off the plate and transferred to Eppendorfs. Tubes were vortexed for 30 seconds and then heated to 85 ^{o}C for 10 minutes forming a slurry. Cells were cooled on ice for 10 minutes and vortexed again. The slurry was centrifuged for 15 minutes at 20,000 x g. The supernatant was removed and transferred to a new Eppendorf tube.

Standards for the Alcian blue stain were made up and loaded in triplicate on a 96 well flat-bottomed plate, standards are outlined in Appendix A. For quantification 50 µL of each sample was ran in duplicate. Absorbance was quantified on a Varioskan LUX Multimode Microplate Reader (Thermo Scientific), and absorbance measured at 630 nm optical density. Alcian blue stain concentration was calculated from the standard curve of absorbance.

A Student’s unpaired two tailed T-test was used to analyse significant differences between samples and statistical significance was given by $p<0.05$.

2.3 Molecular biology

2.3.1 Generation of overexpression vector

2.3.1.1 Bacterial transformation and culture

Asporin cDNA ORF clone DNA (Genscript) (Clone ID: OHu29011) (vector map outlined in Appendix D) was resuspended in 100 µL TE buffer according to GeneEZ^{TM} protocol. 2 µL of DNA was transformed in 50 µL of DH5α competent cells. Briefly, 50 µL of DH5-α competent cells were thawed on ice, under aseptic conditions 2 µL of Asporin ORF clone DNA was added and gently pipette mixed and kept on ice for a further 30 minutes. Cells were heat shocked by incubating for 45 seconds at 42 ^{o}C and immediately placed back on ice for 2 minutes. 250 µL of prewarmed Super Optimal broth with Catabolite repression (SOC) media was added and incubated in a shaking incubator, 225 rpm at 37 ^{o}C for 1 hour. Transformed cells were plated on LB Agar plates (Appendix A) with 100 µg/ mL ampicillin and incubated in a 37 ^{o}C oven overnight. Individual colonies were aseptically picked and added to 5 mL of LB broth containing 100 µg/ mL ampicillin (Appendix A) and grown overnight in a shaking incubator, 225 rpm at 37 ^{o}C.

2.3.1.2 Miniprep extraction of ASPN ORF DNA.

To extract ASPN ORF plasmid DNA, QIAprep Spin Miniprep Kit was used according to manufacturer's instructions and plasmid DNA was eluted in 50uL of water. The concentration of the extracted DNA was assessed using the NanoDrop™ 8000 Spectrophotometer at 260 nm, absorbance at 280 nm is also measured and the ratio of 260/ 280 nm is used to assess quality of the DNA.

2.3.1.3 Transfection of cells overexpression of Asporin

ATDC5 and U2OS cells in T25 flasks were transfected with ASPN ORF plasmid to overexpress Asporin in the cell lines. Briefly, 200 µL of OPTIMEM and 2 µg of plasmid DNA were combined, and in a separate 15 mL sterile falcon tube 200 µL of OPTIMEM and 16 µL of Lipofectamine were combined. Tubes were left to equilibrate at room temperature for 5 minutes. The first solution was added to the falcon containing the second solution and 3.6 mL of OPTIMEM was added and incubated for 15 minutes at room temperature.

Media was removed from the cells and washed with PBS. After the 15 minutes the OPTIMEM/DNA/Lipofectamine solution was added to the confluent cells and incubated for 24 hours at 37°C and 5% CO_2. Media was removed and fresh complete medium was added, 24 hours later T25 flasks were split into three T25 flasks, and selection media was added. Geneticin was used for the selection of ASPN ORF plasmid positive cells.

Optimum antibiotic concentration in selection media was determined to be 0.6 mg/mL for both ATDC5 and U2OS by a kill curve, where cells were seeded in a 24 well plate at 0.05 x 10^6, varying concentrations)0.05, 0.1, 0.2, 0.3, 0.6, 0.75, 1.0, 1.25, 1.5 mg/ µL) of Geneticin in media was added to cells, alongside antibiotic free control wells. Optimum antibiotic concentration was determined by the lowest concentration required to kill all cells after 1 week of incubation.

2.4 Protein methods

2.4.1 Lysate collection

Media was removed from cells and monolayer was washed with phosphate buffered saline (PBS). Cells were trypsinized and centrifuged at 1,000 x g for 5 minutes, supernatant was removed, and cell pellet was resuspended in PBS. Cells were centrifuged again at 1,000 x g for 5 minutes and resuspended in 100 µL of RIPA buffer (Appendix A) and snap frozen in liquid nitrogen. Lysates were defrosted and vortexed for 20 seconds, snap frozen in liquid nitrogen and again defrosted and vortexed. Lysates were then centrifuged at 8,000 x g for 5 minutes at 4 ^{o}C. Supernatant was removed and transferred to a clean Eppendorf; lysates were stored at -80 ^{o}C until needed.

Protein concentration of the lysates was assessed using the Pierce™ bicinchoninic acid assay (BCA) Assay kit according to manufacturer's instructions, using the kit standards to plot the standard curve for absorbance. Absorbance was quantified on a Varioskan LUX Multimode Microplate Reader (Thermo Scientific), and absorbance measured at 562 nm optical density.

2.4.2 Western blotting

Western blot samples were made up to final volumes in 5 x sodium dodecyl sulphate (SDS)-PAGE sample buffer with 0.05 M dithiothreitol (DTT) (F.C.) using 1 M dithiothreitol (DTT) stock to reduce disulphide bonds (Appendix A). Samples were denatured by heating to 95 ^{o}C for 5 minutes, cooled on ice and were loaded alongside Precision Plus™ dual colour protein colour marker (Bio-Rad) into precast 4-12% NuPAGE® Bis-Tris gels. GSamples were elecrophoretically resolved at 150 V for 90 minutes in 1 x Running buffer and electroblotted at 30 V for 90 minutes onto nitrocellulose membrane (Amersham) in 1 x Transfer buffer using the XCell SureLock Mini-Cell® Electrophoresis System. Membrane was blocked in 5 % Bovine Serum Albumin (BSA) in 1 x PBS with 0.05 % Tween-20 (PBS-T) (Appendix A) for 1 hour on a rocker. Membrane was washed three times with PBS-T for 5 minutes, then incubated with primary antibody diluted 5 % BSA in 1 x PBS containing 0.02 % sodium azide (Appendix A) overnight at 4 ^{o}C on a rocker. Membrane was washed three times with PBS-T for 5 minutes, then incubated secondary antibody diluted in 5 % BSA/ 0.02% sodium azide/ 1 x PBS for 1 hour on a rocker, in a dark box. Membrane was washed three times with PBS-T for 5 minutes. Membranes were imaged on a LI-COR® Odyssey CLx Imaging System. All solutions are outlined in Appendix A, antibody dilutions are outlined in Appendix E.

2.5 Analysis of gene expression

2.5.1 Ribonucleic acid (RNA) extraction

Media was removed from cells and the monolayer was washed with phosphate buffered saline (PBS). Cells were trypsinized and pelleted by centrifugation at 1,000 x g for 5 minutes, supernatant was removed, pellet was resuspended in PBS and centrifuged as previously, and supernatant was removed. Cell pellets were snap-frozen in liquid nitrogen and stored at -80 °C until required. RNA was extracted from the cell pellet using the ReliaPrep™ RNA Cell Miniprep System (Promega) according to manufacturer's protocol with in-column DNA digestion. Cell pellets were passed through an insulin needle in the first step of kit, the lysis buffer, to ensure efficient RNA extraction. The resulting RNA was eluted in 15 µL RNase free water.

Prior to cDNA generation, the concentration of the extracted RNA was assessed using the NanoDrop™ 8000 Spectrophotometer at 260 nm, absorbance at 280 nm is also measured and the ratio of 260/ 280 nm is used to assess quality of the RNA.

2.5.2 Reverse transcription polymerase chain reaction (RT-PCR) and quantitative polymerase chain reaction (qPCR)

cDNA was prepared from RNA, using the GoScript™ Reverse Transcriptase system (Promega) according to manufacturer's instructions. Reverse transcription was carried out on a Labnet International MultiGene™ OptiMax Thermal Cycler. 50- 150 ng of RNA was combined with 0.5 µg Oligo(dt)15 primers and 0.5 µg random primers for 5 minutes at 70°C in the Thermal Cycler. Tubes were removed and place on ice immediately for 5 minutes. Each tube was then made up to 1X GoScript™ reaction buffer, 2.0 mM magnesium chloride, 20 Units (U) Recombinant RNasin® ribonuclease inhibitor, 20 U GoScript™ reverse transcriptase, and ran in the thermal cycler with the cycling conditions described in Appendix B.

Prior to qPCR, cDNA was treated with 2 U RNase H for 20 minutes at 37°C to digest the RNA template. cDNA was diluted as necessary in nuclease free water to concentration of 5 ng/ µL.

Quantitative real time PCR (qPCR) was performed using Power SYBR® green according to manufacturer's protocol. A standard qPCR reaction mix consisted of 10 µL Power SYBR® Green Master Mix, 10 pmol of forward and reverse primers, 1 µL cDNA and 7 µL nuclease free water. Samples were run in duplicate and normalised to the expression levels of the housekeeping gene *18S*. qPCR reactions were carried out on a QuantStudio™ 3 Real-Time PCR System, 96-well machine. Primer sequences and cycling conditions are outlined in Appendix B. Melt curve was carried out at the end of the qPCR protocol and melt curves were assessed to check for single product amplification. Ct (cycle threshold) values were obtained from the Quantstudio 3 analysis software, normalised Ct values were calculated and expressed as $2^{-(Ct_{GOI}-Ct_{Houskeeper})}$. ANNOVA was used to analyse significant differences between samples with Tukey's post-hoc analysis to and statistical significance was given by $p<0.05$.

2.6 Generation and maintenance of the mouse models

2.6.1 Breeding strategy of the mouse model

All animal experiments were carried out under Home Office granted licenses and procedures. All procedures were in accordance with the Animals (Scientific Procedures) Act 1986 and the EU Directive 2010/63/EU and after the local ethical review and approval by Newcastle University's Animal Welfare and Ethical Review Body (AWERB). Breeding and phenotyping experiments were performed under licence P8A8B649A.

Asporin null ($Aspn^{-/-}$) mice were obtained from The European Conditional Mouse Mutagenesis Program (EUCOMM) ($Aspn^{tm1a(EUCOMM)Hmgu}$) generated with "knockout-first" conditional allele targeting, allowing generation of both Asporin null and col2cre conditional knockout mice. Mice were generated on a C57BL/6J background.

There are 8 exons present in Asporin, in the targeted Asporin knock-out allele exon 4 was spanned by 2 loxP sites and a FRT flanked lacZ/ neomycin-resistant cassette, containing a third loxP site, inserted in the intron between exons 3 and 4 (Figure 23) disrupting the Asporin gene.

Mice carrying the targeted allele were crossed with *Actin-flp* mice (Jackson Laboratories) resulting in the excision of the neomycin-resistant cassette restoring the wild-type Asporin allele. These mice were then crossed with mice expressing *Cre* under the Collagen 2 promoter[145], subsequently excising exons 2 and 3 in the *Asporin* allele in cells expressing Collagen 2.

2.6.2 Genotyping the mouse models

Ear or tail biopsies were used to genotype the mice. Biopsies were incubated in 75 µL of HotShot lysis buffer pH 12 (Appendix A) at 95 ^{o}C for 30 minutes. Samples were cooled and incubated at 4 ^{o}C for 10 minutes. 75 µL of neutralising buffer pH 5 (Appendix A) was added to the samples and vortexed. To prepare Polymerase Chain Reaction (PCR) mix 3 µL of DNA was combined with 25 µL of BioMix™ Red (Bioline) with 0.1 uL of each primer and made up to a final volume of 50 µL with nuclease free water. PCR reactions were carried out on a Labnet International MultiGene™ OptiMax Thermal Cycler. For Asporin global knockout genotyping, samples were combined with Ef, Er and Kr primers (Figure 23). For FLP genotyping, samples were combined with Flp forward and reverse primers. For Asporin flipped genotyping, samples were combined with Ef, Er and Kr primers, additionally Nr primer was used to confirm the genotype. For Col2*Cre* genotyping, samples were combined with Cre forward and reverse primers, additionally Ef, Er, Kr and Nr primer were used to confirm the genotype. For conditional Col2*Cre* Asporin knockout mice samples were combined with Ef, Er and Nr primers, additionally Kr primer was used to confirm the genotype. Water samples were included in every genotyping experiment as controls to exclude contamination.

Location of primers are outlined in Figure 23; thermocycler protocol and primers sequences are outlined in Appendix B.

PCR samples were samples were elecrophoretically resolved on 1.5 % (w/v) agarose gel in 1 x TAE buffer containing 0.5 µg/mL Ethidium bromide for DNA intercalation (Appendix A) and electrophoresed for 40 minutes at 100 V, alongside 5 µL of 100bp Hyperladder™ (Bioline) for identification of PCR DNA product size. Gel was visualised on a Bio-Rad Gel Doc System.

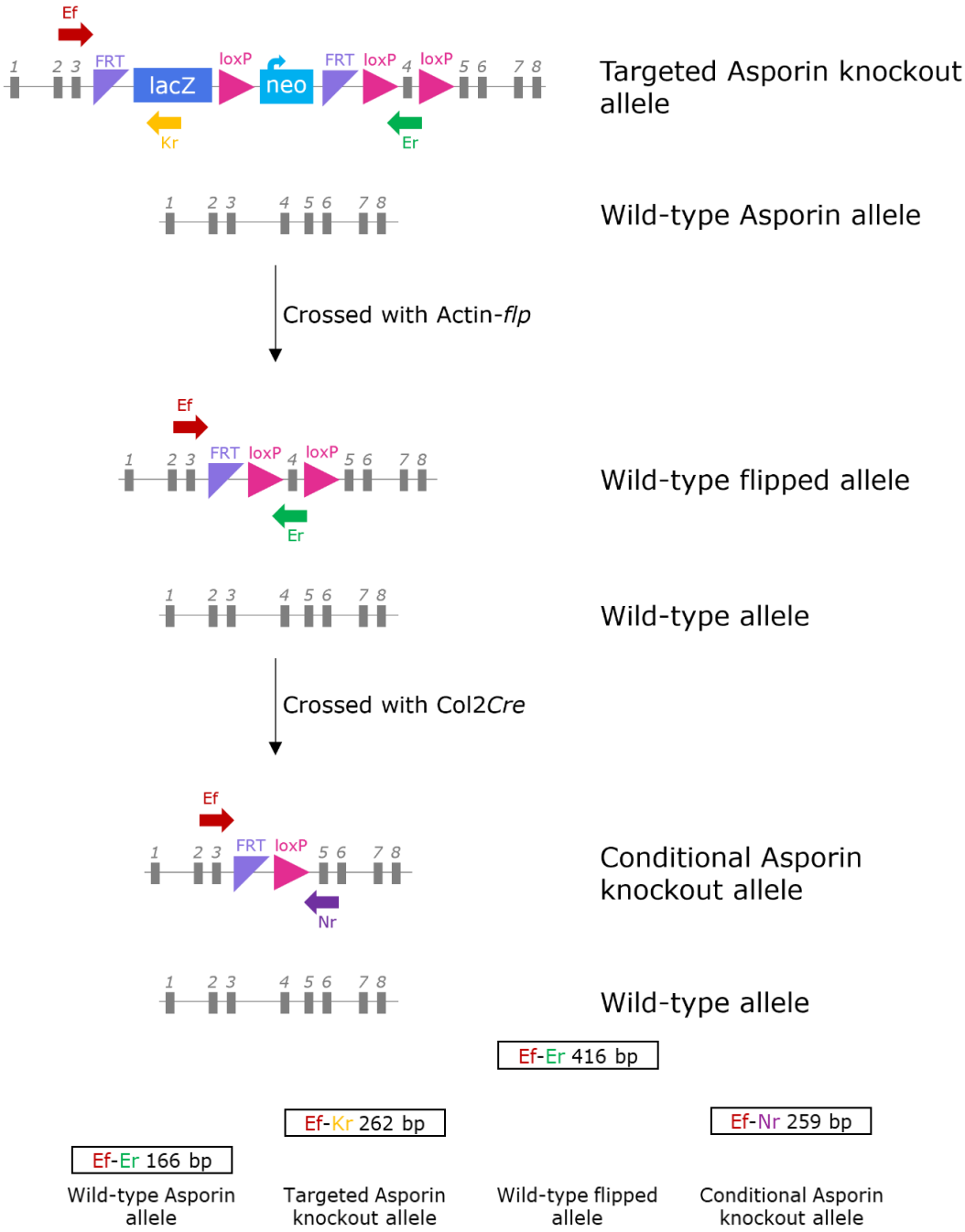

Figure 23. Allele maps and expected band sizes for the generation of Asporin mouse models. *Wild-type Asporin allele has primer sites for Ef and Er. Ef-Er product is 166 bp. Targeted Asporin knockout allele (KO) has primer sites for Ef, Er and Kr. In the targeted knockout allele, the Ef-Kr band is too large for PCR therefore no product is made. Ef-Er product is 262 bp. Wild-type flipped allele has only Ef and Er primer sites as Kr has been excised out by the FRT sites through Flp-recombinase. Ef-Er is the only product at 416 bp. Conditional Col2Cre Asporin knockout allele has primer sites for Ef and Nr primers the Er primer site has been excised out by the loxP sites, the Ef-Nr product is 259 bp. If Cre excision has not worked, then there will be no Ef-Nr product as it will be too large.*

2.7 Phenotyping methods of mouse models

2.7.1 Whole body skeletal preparations

P2 mice were sacrificed with anaesthetic overdose, euthatyl and death confirmed by jugular snip. Whole bodies were scalded in tap water and skin removed and fixed in 95 % EtOH for 3 days. Whole preparations were stained for 24 hours with Alcian blue for skeletal preparations (Appendix A), then rinsed twice in 95 % EtOH and fixed for 48 hours in 95 % EtOH. Tissue was cleared in 1 % KOH (Appendix A) for 6 hours and stained with Alizarin Red for skeletal preparations (Appendix A) for 3 hours. To remove remaining tissue skeletal preparations were cleared for up to 48 hours in 2 % KOH, until only cartilage and bone remained.

For storage of the skeletal preparations, skeletal preparations were taken through decreasing concentration of 2 % KOH in glycerol. 80:20 2 % KOH:glycerol solution, 60:40 2 % KOH:glycerol solution, 40:60 2 % KOH:glycerol solution each for 24 hours, before being stored in 20:80 2 % KOH:glycerol solution.

Skeletal preparations were imaged on a Nikon Flatbed scanner and long bone measurements were carried out in ImageJ 1.52i software[146].

2.7.2 X-Ray and bone measurements

For longitudinal bone measurement studies mice were X-Rayed at 3, 6, 9 and 12 weeks of age. Where possible the same mice would be used through the study. Mice were anaesthetised with 5% isoflurane in a red induction box once righting reflex was absent, mice were transferred to isoflurane mask and following paw pad and tail reflex check and X-rayed for 5 seconds at 23 kV, using the Faxitron X-Ray radiography system. Bone measurements were carried out in ImageJ 1.52i software[146]. Tibia, femur, L5 vertebrae length, pelvis, inner canthal distance (ICD) and skull length were measured. Measurements are outlined in Figure 24. Left and right tibia and femur measurements were averaged for each mouse.

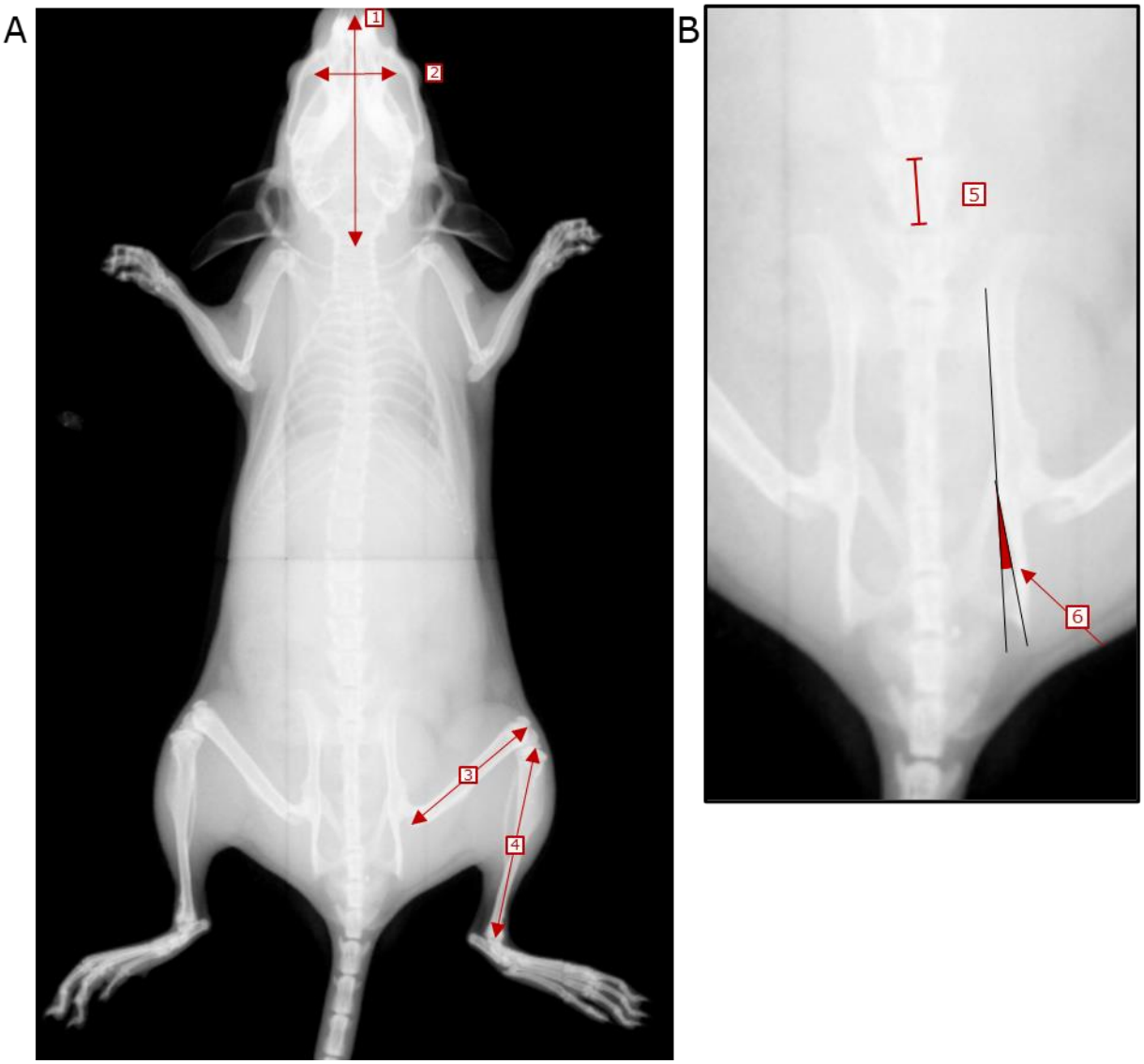

Figure 24. X-Ray bone measurements. *Representative X-ray image to demonstrate the measurements taken for analysis.* ***A****) whole body image: 1) Skull length, 2) inner canthal distance (ICD), 3) femur length, 4) tibia length,* ***B****) Magnified pelvic and spine region of 5) L5 vertebrae length and 6) Pelvis angle.*

2.7.3 Structural analysis of tissues

2.7.3.1 Preparation of tissues for μCT, and three-point bending

Mice at 12 weeks were sacrificed by exposure to carbon dioxide in line with Schedule 1 of ASPA 1986 to preserve the spine, severing of the femoral artery was performed for secondary confirmation of death. Skin was sprayed with 70% ethanol and removed. Excess tissue was removed from the hip joint and hind limbs were dislocated at the hip and removed. Tissue around the spine was removed, and lumbar spine was cut below the hip and below the ribcage. For μCT left leg and spine samples were fixed in 4% paraformaldehyde for 24 hours and then stored in 70% ethanol until scanned for μCT. Right legs were stored in 70% ethanol until destructive three-point bend tests were carried out.

2.7.3.2 Micro-computed tomography (μCT) and analysis

Left legs and spines were scanned by Histology Shared Research Facility at University of Liverpool, using a SkyScan 1272 system (Bruker) by μCT with aluminium filter thickness of 0.5 mm and X-ray source at 50 kV and 200 μA. For trabecular scans of leg bones and spine a rotation step size of 0.3 ° with 4.5 μm pixel size and a resolution of 4032 x 2688 was used. For cortical scans of leg bones, a rotation step size of 0.5 ° with 9.0 μm pixel size and a resolution of 2016 x 1344 was used.

Images were reconstructed for tibia, femur and spine using SkyScan NRecon software (Bruker) which generated cross-sectional slices from the raw images, with the following parameters Smoothing: 1, Misalignment compensation: -2.0, Ring artifacts reduction: 5 and Beam-hardening correction: 38 %. Reconstructed images were then opened in SkyScan DataViewer to produce 3D computational models of the bones and spine. Legs and L5 vertebrae were oriented as outlined in Figure 25 and Figure 26 respectively, and Volume of Interest (VOI) was selected and exported,

encompassing the whole width of bone and the Region of Interest (ROI), and the whole L5 vertebrae, optimised by Rob Van 't Hof[147].

To quantify metrics of the bone VOIs were opened in CTAn (Bruker) and Region of Interest for analysis was determined. For trabecular bone analysis, the ROI of leg bones were 200 slices immediately proximal to the femoral growth plate and 200 slices immediately distal to the tibial growth plate, outlined in Figure 25. For cortical analysis, the ROI of leg bones were 100 slices immediately distal to the trochanter of the femur and 100 slices proximal to the tibio-fibular junction of the tibia, outlined in Figure 25. For L5 vertebrae the ROI was between both growth plates of the vertebrae and a 0.9 mm circle to select exclusively the trabecular bone.

CTAn macros developed by Rob Van 't Hof[147], detailed in Appendix G were used to separate trabecular bone from cortical bone and then the same macro was used to quantify metrics of the trabecular and cortical bone according to the ASBMR guidelines[148]. For L5 vertebrae a trabecular bone macro was used, detailed in Appendix G.

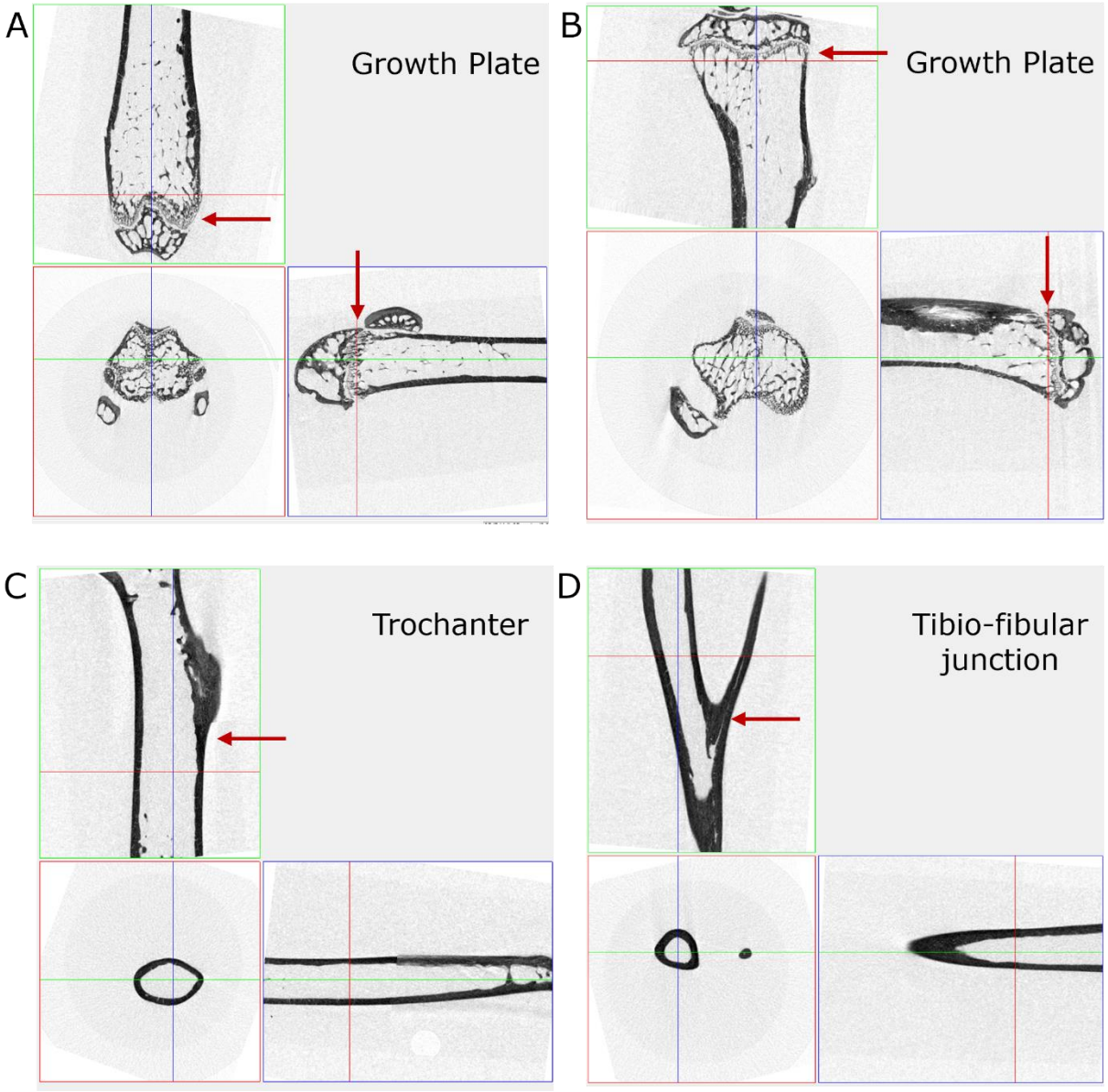

Figure 25. Representative images from Data-Viewer software. *Images of femur (A) and tibia (B) in correct orientation with growth plate landmark for selection of region of interest for trabecular analysis. Images of femur (C) and tibia (D) in correct orientation with trochanter and tibio-fibular junction landmarks for femur and tibia respectively for selection of region of interest for cortical analysis.*

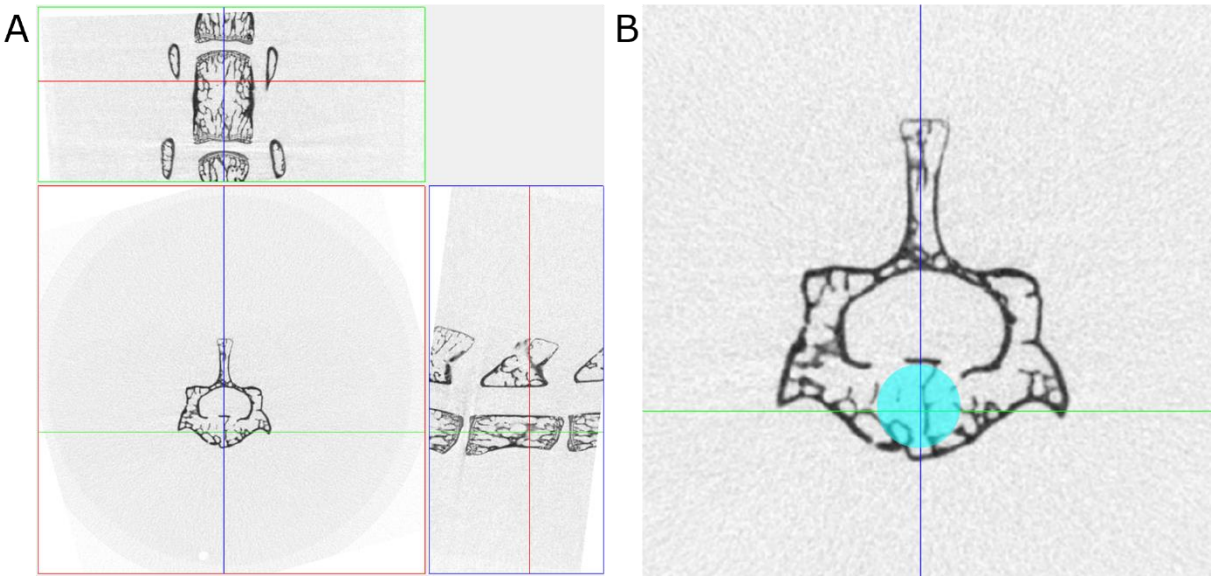

Figure 26. Representative images from Data-Viewer software. *Image of L5 vertebrae in correct orientation for selection region (A) with blue circle highlighting the region of interest for trabecular analysis (B).*

2.7.3.3 Three-point bending

Destructive three-point bend tests were carried out on tibia and femur of 12-week-old mice on a UniVert CellScale Tester, using the compression mode and 3-point bend setup.

Bones were placed across 2 plinths 8 mm apart; force was applied to the centre of the bone. The magnitude of force parameters used was displacement control mode for compression, with ramp function and stretch magnitude of 3mm for 30 seconds with no rest duration and no preload. Force (N) and displacement (mm) measurements were taken every 0.1 seconds (Figure 27).

Raw data was used to plot force/ displacement graphs. To calculate Stiffness (N/mm) was calculated by the gradient of the graph at the start of application of force. $Stiffness = \frac{\Delta\, Change\ in\ force}{\Delta\, Change\ in\ displacement}$. Maximum force (F*max*) was identified as the peak of the force displacement graph.

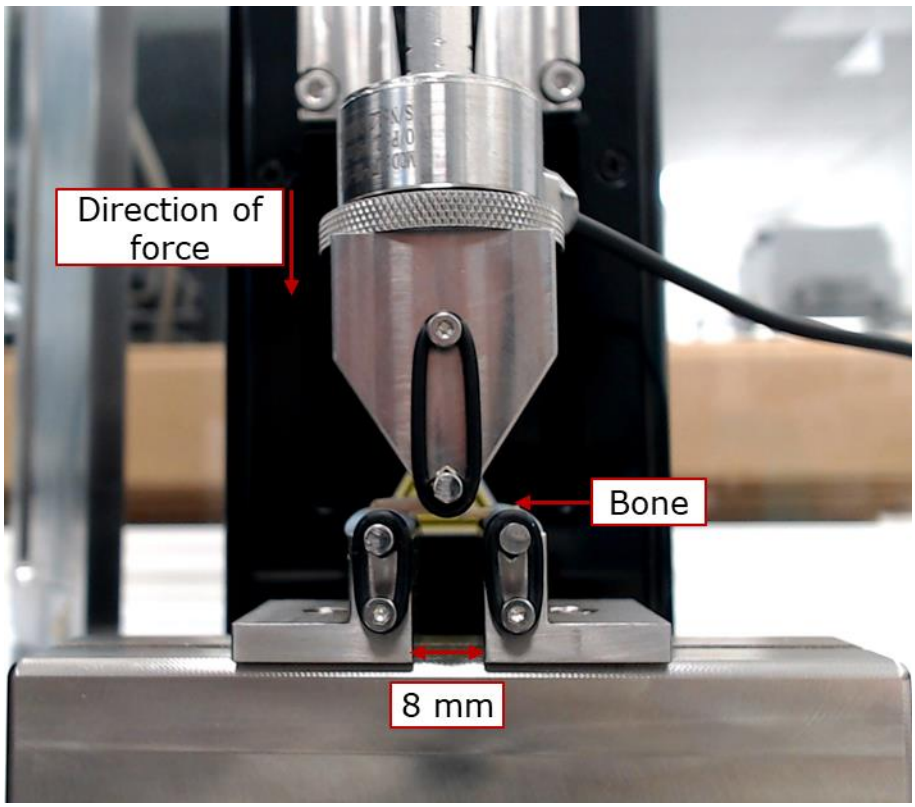

Figure 27. Set up of tibia bone on UniVert CellScale tester for destructive three-point bend test. *Tibial bone was laid horizontally across the two plinths, 8 mm between the two base points. Downwards force was applied in the direction of the arrow.*

.

2.7.3.4 Preparation of Achilles tendons for transmission electron microscopy (TEM) and test to failure.

9-week-old and 12-week-old wild-type and Asporin null mice were sacrificed as previously described for transmission electron microscopy (TEM) and test to failure experiments respectively. Achilles tendons were separated from muscle with tweezers and cut at the join to the calcaneus (heel bone), Achilles tendon identified in Figure 28. For test to failure experiments tendons were frozen in phosphate buffered saline at -20 ^{o}C. For transmission electron microscopy tendons were fixed in 2% (v/v) glutaraldehyde for 24 hours and passed to the Newcastle University Electron Microscopy Research Services Unit for processing.

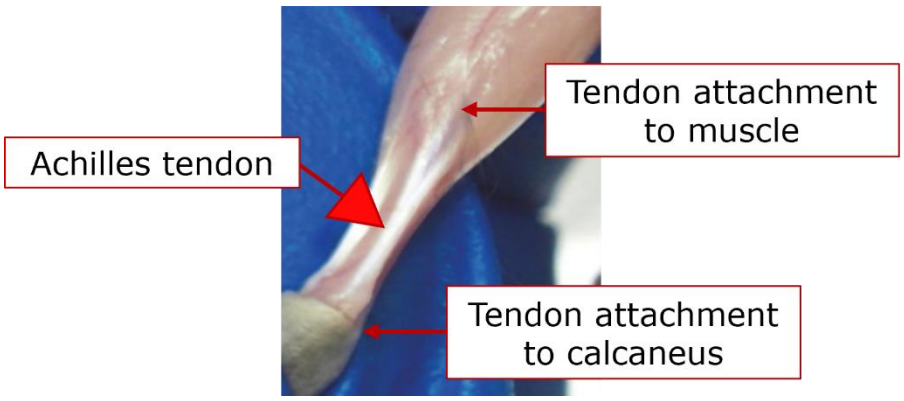

Figure 28. Identification of mouse Achilles tendon. *Arrow indicates the Achilles tendon and the places where the tendon is cut is highlighted the attachment of the tendon to the muscle and the attachment of the attachment to the calcaneus (heel bone). Image published by Zhang et. al.*[149]

.

2.7.3.5 Transmission electron microscopy (TEM) of Achilles tendon

Newcastle University Electron Microscopy Research Services Unit processed the samples according to the following protocol. Tendon samples were washed three times in 0.1 M sodium cacodylate buffer for 30 minutes per wash, then fixed again in 2 % (w/v) osmium tetroxide in distilled water for 1 hour at room temperature. Tendon samples were then rinsed in water twice and immersed in 2 % uranyl acetate for 2 hours, then rinsed again in water twice before washes with increasing concentrations of acetone (25 %, 50 %, 75 %) for 30 minutes per wash, followed by two 1 hour incubations in 100 % acetone. Samples were embedded using the TAAB epoxy resin kit according to manufacturer's instruction. Samples were incubated in 100 % resin for 2 days to ensure full penetration of the tissues with resin. Samples were then placed into a mould and into a 60 ^{o}C oven overnight to polymerise the resin.

Samples were sectioned to ultrathin 70 nm sections on a Leica EM UC7 ultramicrotome using a diamond knife. Sections were stretched with chloroform and mounted onto Pioloform0filmed copper grids. Grids were then stained with 2 % aqueous uranyl acetate and lead citrate solution.

Collagen fibrils and tenocytes were imaged using a Hitachi HT7800 Transmission Electron Microscope.

2.7.3.6 Test to failure of Achilles tendons

Achilles tendons of 12-week-old wild-type and Asporin null mice were stretched to failure on a UniVert CellScale Tester, using the tension mode and setup.

Tendons were gently defrosted and sandwiched at either end between two slices of ultra fine sandpaper within the clamps. This was carried out as quickly as possible to minimise the tendon drying. The length of tendon

between the two vertical clamps to be tested was 1 mm, with the calf end of the tendon fixed in the upper clamp and the foot end fixed in the lower clamp. The magnitude of force parameters used was displacement control mode for tension, with ramp function and stretch magnitude of 60% for 60 seconds with no rest duration and no preload. Force (N) and displacement (mm) measurements were taken every 0.1 seconds (Figure 29).

Raw data was used to plot force/ displacement graphs. To calculate Stiffness (N/mm) was calculated by the gradient of the graph at the start of application of force. $Stiffness = \frac{\Delta\, Change\ in\ force}{\Delta\, Change\ in\ displacement}$. Maximum force (F*max*) was identified as the peak of the force displacement graph.

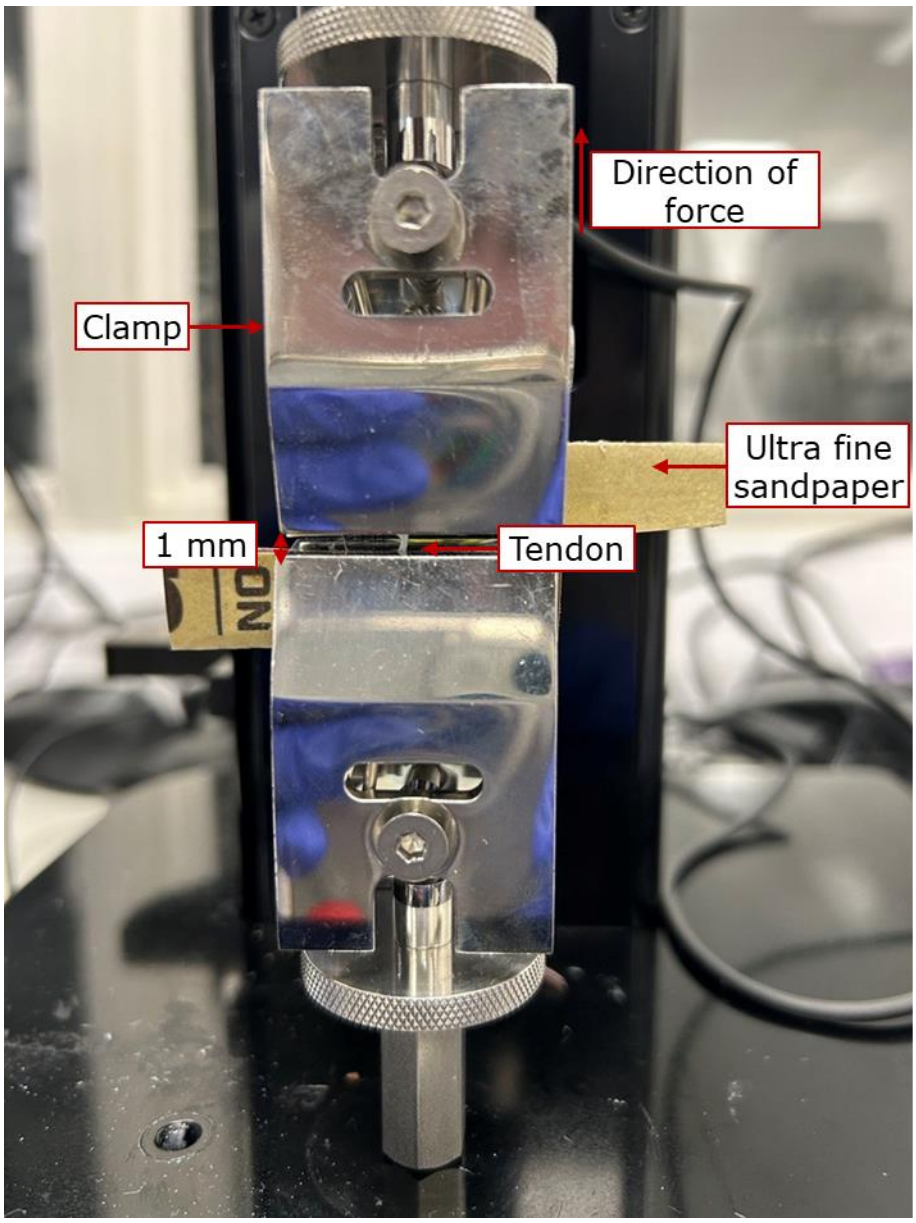

Figure 29. Set up of Achilles tendon on UniVert CellScale tester for test to failure tension test. *Tendon was sandwiched between two pieces of ultra fine sandpaper at the top and at the bottom of the tendon and clamped at either end with 0.1 mm distance between the two clamps. Tendon was set up vertically and the direction of force was upwards where the upper clamp is moved up by the Univert System, shown by the arrow on the figure.*

.

2.7.4 Histological analysis of cartilage

2.7.4.1 Preparation of mouse tissues for histological analysis of cartilage

Legs (tibia and femurs) were dissected from 3-week-old mice as previously described, for histological staining legs were fixed in 4% PFA and for immunohistochemical staining legs were fixed in 5% acetic acid: 95% ethanol for 24 hours.

Bones were decalcified in 20% (w/v) EDTA pH 7.4 (Appendix A) for 2 weeks at room temperature with constant gentle agitation. Legs were washed for 1 hour in running tap water and processed overnight (Appendix C) in Thermo Scientific™ STP 120 Spin Tissue Processor. Processed samples were embedded in Lamb wax paraffin blocks; lateral side of the joint was at the front of the block.

Legs were sectioned to 6µm sagittal sections using a Thermo Scientific™ HM 355S automatic microtome. Wax sections were collected on positively charged slides and left to dry overnight, to fix sections they were heated on 60 ^{o}C hot plate until wax melted and removed and left to cool before staining.

2.7.4.2 Toluidine blue staining

Toluidine blue staining was performed to analyse deposition of sulphated proteoglycans of the growth plate and articular cartilage. 3-week-old formaldehyde-fixed limb sections were dewaxed in two 5 minute incubations of xylene and rehydrated through decreasing concentrations of ethanol (100 %, 90 %, 70%, 50%) (v/v) followed by two 5 minute washes in distilled water.

Slides were stained with 0.04 % (w/v) toluidine blue pH 3.75 (Appendix A) for 10 minutes, followed by two 5 minute washes in distilled water to remove excess stain. Slides were counterstained with Nuclear Fast Red solution for 10 minutes, followed by two 5 minute washes. Slides were quickly dehydrated in 95 % and 100% ethanol each for 2 minutes. Slides were cleared in xylene and mounted in DPX mountant.

Once mountant was dry (overnight), the slides were imaged using a brightfield camera on a Zeiss Axioimager 2 microscope at a magnification of 20 x, images were tiled and stitched using the ZEISS Zen Blue Software.

2.7.4.3 Immunohistochemistry

As previously described, 3-week-old acetic acid-ethanol-fixed limb sections were dewaxed in xylene and rehydrated through a decreasing series of ethanol, followed by two washes in distilled water.

Slides were washed twice in phosphate buffered saline (PBS) for 3 minutes. For intracellular unmasking slides were placed in a citrate buffer (Appendix A) boil, for 20 minutes. Citrate buffer was heated to boiling point in a microwave and then slides were added to the buffer and microwaved at 160 W for 2 minutes every 5 minutes to maintain the temperature. Slides were then placed in PBS and left to cool followed by two further washes in PBS for 5 minutes. Individual sections were outlined with ImmEdge™ pen, from this point all work was carried out in a darkened humidified chamber. Slides were blocked for 1 hour in donkey serum in 1 % (w/v) BSA in 1x PBS solution at room temperature. Slides were incubated in primary antibodies diluted in 1 % BSA/1x PBS solution overnight at 4 ^{o}C (dilutions outlined in Appendix E). Slides were then washed twice in 1 % BSA/1x PBS for 5 minutes followed by incubation for 1 hour in secondary antibody diluted in donkey serum/1 % BSA/1x PBS solution (dilutions outlined in Appendix E). Slides were then washed three times in 1x PBS for 5 minutes and mounted in Fluoroshield Mounting Media with DAPI, media was left for 5 minutes before coverslips were added. Negative controls were carried out for all

experiments as all other sections however without primary antibody. All solutions are outlined in Appendix A, antibody dilutions in Appendix E.

Slides were imaged on a Zeiss Axioimager 4 at 20 x magnification using DAPI and AlexaFluor™ 488 and 594 filter sets.

2.7.4.4 Proliferation analysis

Ki67 was used as a marker of proliferation in the growth plate and articular cartilage[150, 151]. Ki67 assay was optimised to, citric buffer boil Appendix A. Ki67 immunohistochemistry was performed as previously described.

Slides were imaged using Zeiss Axioimager 2, fluorescent microscope at 20x magnification. Ki67 positive cells in the growth plate, articular cartilage and vascular invasion front were counted using the Watershed Segmentation program in ImageJ 1.52i software[146], and expressed as a percentage of the total number of cells in each zone.

Ki67 was performed on 3 slides per mouse (9 sections), 3 mice per genotype. A Student's unpaired two tailed T-test was used to analyse significant differences between samples and statistical significance was given by $p<0.05$.

2.7.4.5 Terminal deoxynucleotidyl transferase deoxyuridine triphosphate (dUTP) nick end labelling (TUNEL) assay

To analyse cell death, TUNEL assay was carried out according to DeadEnd™ Fluorometric TUNEL System protocol, on formaldehyde fixed samples. Sections were dewaxed in xylene, re-hydrated through decreasing concentrations of ethanol. Citric buffer boil was performed for antigen

unmasking as previously described. Manufacturer's protocol details the use of Proteinase K for the unmasking step, however this has been shown to generate false positive therefore the assay was optimised to use citric buffer boil[152]. 5.5 units/ mL DNAseI was added to one section per experiment for the positive control, DNaseI fragments the DNA generating nick ends and therefore will be labelled by TUNEL assay kit. Nuclei were counterstained with DAPI.

Slides were imaged using Zeiss Axioimager 2, fluorescent microscope at 20x magnification. TUNEL positive cells in the growth plate, articular cartilage and vascular invasion front were counted using the Watershed Segmentation program in ImageJ 1.52i software[146], and expressed as a percentage of the total number of cells in each zone.

TUNEL was performed on 3 slides per mouse, 3 mice per genotype. Student's unpaired two tailed T-test was used to analyse significant differences between samples and statistical significance was given by $p < 0.05$.

2.7.5 Histological analysis of bone

2.7.5.1 Preparation of mouse tissues for histological analysis of bone

Following µCT the 12-week-old left legs and spines were then used for bone histology. Legs and spines were dehydrated through an increasing series of ethanol (70 %, 90%, 100%), and then infiltrated with methyl methacrylate (MMA) Embedding Solution 1 (Appendix A) for 24 at 4 ^{o}C. Bones were transferred to a fresh Solution 1 and incubated for a further 24 hours at 4 ^{o}C. Legs and spines were then embedded in MMA Embedding Solution 2 (Appendix A) in sealed glass vials, vials were placed in water at 4 ^{o}C for 72 hours to aid polymerisation.

Samples were broken out of the glass vials and sectioned to 5 µm sections on a Thermo Scientific™ HM 355S automatic microtome using a D-profile tungsten carbide knife (Histoline). Sectioning solution (Appendix A) was used to aid smooth sectioning; this was applied to the front of the sample and the blade to guide the section down. The sections were collected on positively charged slides. Stretching solution (Appendix A) was added to the sections for 5 minutes then sections were gently stretched, this was repeated 2 more times. Once fully stretched plastic coverslips were placed on the slides. Slides were placed on top of one another and clamped at either end using G-clamps to keep sections flat as they fixed. Slides were placed in a 60 ^{o}C oven for 72 hours to securely fix the sections to the slide.

2.7.5.2 Toluidine blue staining for osteoblasts

Toluidine blue staining was used to analyse osteoblasts at the trabecular bone surface. Slides were de-plastified in two 10 minute incubations in 2-methoxyethyl-acetate (MEA), reagent grade, 98 % slides were then rehydrated through decreasing concentrations of ethanol (100 %, 90 %, 70 %, 50 %) followed by two 5 minute washes in distilled water. Slides were then stained with 1 % (w/v) toluidine blue pH 4.5 (outlined in

Appendix A) and washed with distilled water to remove to remove excess stain. Slides were dehydrated through increasing concentrations of ethanol (50 %, 70 %, 90 %, 100 %), cleared in xylene and mounted in DPX Mountant.

Bioimaging Unit at Newcastle University imaged the tibiae using a brightfield camera on a Zeiss Axioscan 7 microscope at a magnification of 10 x, images were tiled and stitched using the ZEISS Zen Blue Software.

Osteoblasts were analysed in a 100 µm by 300 µm area, 100 µm from distal from the tibial growth plate, 3 mice per genotype. Osteoblasts, the cuboid cells along the bone surface were counted in ImageJ 1.52i software[146]. Total osteoblast count and osteoblast count per bone surface were calculated. A Student's unpaired two tailed T-test was used to analyse significant differences between samples and statistical significance was given by $p < 0.05$.

2.7.5.3 Von Kossa/Van Gieson staining

Von Kossa/van Gieson staining was performed to analyse the calcification of bone. As previously described, slides were de-plastified in MEA and rehydrated through a decreasing series of ethanol, followed by two washes in distilled water. Slides were incubated in 1% (w/v) silver nitrate (Appendix A) for 10 minutes followed by a 10 minute wash in distilled water. To reduce to silver nitrate slides were exposed to ultraviolet (UV) light, by adding water droplets to keep samples from drying and placing slides on a DarkReader transilluminator (ClareChemical) for 30 minutes. To remove unreacted silver nitrate, slides were incubated in 5% thiosulphate (Appendix A) for 5 minutes and then washed for 10 minutes in tap water. Slides were stained with Van Gieson counterstain (Sigma-Aldrich) for 2 minutes followed by a rinse in distilled water to remove excess stain. Slides

were then dehydrated as previously described through a series of increasing ethanol, cleared in xylene, and mounted in DPX mountant.

Bioimaging Unit at Newcastle University imaged the tibiae using a brightfield camera on a Zeiss Axioscan 7 microscope at a magnification of 10 x, images were tiled and stitched using the ZEISS Zen Blue Software.

Osteoid deposition was analysed using the open-source software OsteoidHisto, developed by Rob Van 't Hof, according to the developer protocol[153]. 3 mice per genotype. A Student's unpaired two tailed T-test was used to analyse significant differences between samples and statistical significance was given by $p < 0.05$.

2.7.5.4 Goldner's Trichrome

Goldner's Trichrome staining was performed to analyse bone marrow fat. Sections were de-plastified and rehydrated as previously described followed by two washes in distilled water.

Slides were stained with freshly made Weigert's Iron Haematoxylin solution of equal parts solution A and solution B (Sigma-Aldrich) for 30 minutes followed by 10 minutes wash in running tap water to remove excess staining. Slides were then stained with Ponceau-acid fuchsin solution or 30 minutes and quickly rinsed with 1% (v/v) acetic acid in water. Slides were stained in Phosphomolybdic Acid–orange G solution for 5 minutes and again rinsed quickly in 1% (v/v) acetic acid and stained with Light Green solution for 15 minutes, slides were rinsed in 1% (v/v) acetic acid for 5 minutes. Slides were immersed in 2-isopropanol three times, then immersed in 100% ethanol twice and mounted in DPX mounting media. All solutions are outlined in Appendix A.

Bioimaging Unit at Newcastle University imaged the tibiae and spines using a brightfield camera on a Zeiss Axioscan 7 microscope at a

magnification of 10 x, images were tiled and stitched using the ZEISS Zen Blue Software.

Bone marrow fat was quantified in a 100 um by 300 um area, 100 μm from distal from the tibial growth plate, 3 mice per genotype. Fat deposits, the circular spaces in the bone marrow were counted and area of deposits were quantified in ImageJ 1.52i software[146]. Total fat deposit count, fat deposit area and total deposit area were calculated. A Student's unpaired two tailed T-test was used to analyse significant differences between samples and statistical significance was given by $p < 0.05$. Mann-Whitney U test was performed to assess the difference in distribution of fat deposit size in the bone, $p < 0.05$.

2.7.5.5 Safranin O staining

Safranin O/Fast Green staining was used to assess integrity of cartilage growth plate and intervertebral discs. Sections were de-plastified and rehydrated as previously described followed by two washes in distilled water.

Slides were placed in Weigert's Iron Haematoxylin solution for 10 minutes followed by two brief washes in distilled water and dipped in 0.5% acid alcohol (Appendix A), to clean excess staining leaving only nuclei stained, and immediately into running tap water for 10 minutes to stop the reaction.

Slides were then stained with 0.06 % (w/v) Fast Green solution for 5 minutes; slides were briefly washed in 1 % acetic acid (v/v) in water before being stained with 0.1 % (w/v) Safranin O solution for 5 minutes. To prevent loss of staining slides were dehydrated quickly in 95 % ethanol for 1 minute followed by two washes in 100 % ethanol for 1 minute. Slides

were cleared in xylene and mounted in DPX mountant. All solutions are outlined in Appendix A.

Bioimaging Unit at Newcastle University imaged the tibiae and spines using a brightfield camera on a Zeiss Axioscan 7 microscope at a magnification of 10 x, images were tiled and stitched using the ZEISS Zen Blue Software.

2.7.5.6 Tartrate-resistant acid phosphate (TRAcP) staining

Tartrate-resistant acid phosphate (TRAcP) staining was used to analyse osteoclasts in undecalcified bone. Sections were de-plastified and rehydrated as previously described followed by two washes in distilled water. 100mL of TRAcP solution 1 was preheated to 37 ^{o}C, 1 mL of TRAcP solution 2 was added. Slides were placed into this solution for 45 minutes at 37 ^{o}C. 1.8 mL of TRAcP solution 3 was combined with 1.8 mL TRAcP solution 4 and mixed by inversion and left for 2 minutes, solution was a pale red colour. If solution had turned bright fuchsia after the 2 minutes the solution was discarded. The pale red solution (TRAcP solution 3 and 4) was added to 100mL of TRAcP solution 1, preheated to 37 ^{o}C. Slides were placed into this solution for 20 minutes at 37 ^{o}C. All solutions are outlined in Appendix A.

Slides were immediately placed in distilled water to stop the reaction. Slides were counterstained with Aniline blue solution (Appendix A) to stain bone tissue. Slides were dehydrated quickly in 95 % ethanol for 1 minute followed by two washes in 100 % ethanol for 1 minute. Slides were cleared in xylene and mounted in DPX mountant.

Sections were imaged using a brightfield camera on a Zeiss Axioscan 4 microscope at a magnification of 20 x, images were tiled and stitched using the ZEISS Zen Blue Software.

Osteoclasts were analysed using the open-source software TrapHisto, developed by Rob Van 't Hof, according to the developer protocol[153]. 3 mice per genotype. Osteoclast number, osteoclast number per bone surface and osteoclast surface per bone surface were calculated. A Student's unpaired two tailed T-test was used to analyse significant differences between samples and statistical significance was given by $p < 0.05$.

2.7.5.7 Immunohistochemistry of undecalcified bone

For localisation of perilipin in bone marrow fat, protocol was adapted and optimised from Torgersen et. al[154]. Slides were de-plastified and rehydrated as previously described followed by two washes in distilled water. For epitope retrieval slides were boiled in 10 mM Tris-HCL pH 10 (Appendix A) for 3 minutes. Slides were cooled and blocked in 5 % milk/1x TBS (Appendix A) for 1 hour.

Slides were incubated in primary antibodies diluted in 2 % milk/1x TBS solution overnight at 4 ^{o}C (dilutions outlined in Appendix E). Slides were then washed 3 times in 2 % milk/1x TBS for 15 minutes followed by incubation for 1 hour in secondary antibody diluted in 2 % milk/1x TBS solution (dilutions outlined in Appendix E). Slides were then washed three times in 1x TBS for 15 minutes and mounted in Fluoroshield Mounting Media with DAPI, media was left for 5 minutes before coverslips were added. All solutions are outlined in Appendix A, antibody dilutions in Appendix E.

Slides were imaged on a Zeiss Axioimager 4 at 20 x magnification using DAPI and AlexaFluor™ 488 and 594 filter sets.

2.7.5.8 Dynamic histomorphometry of bone

Double injection of alizarin complexone and calcein green was used to assess bone formation. Mice were injected intra-peritoneally (IP) with 30 mg/kg alizarin complexone and 20 mg/kg calcein green in 2% (w/v) sodium

bicarbonate pH 7.4 solution (Appendix A), 8 days and 1 day before culling at 12-weeks-old respectively. Mice were euthanised by exposure to carbon dioxide. Left tibiae were dissected and fixed in 4% formaldehyde for 24 hours before being stored in 70% ethanol until processing and embedding in methyl-methacrylate and sectioned, as previously described.

Calcein blue staining was used to counterstain bone for analysis of bone formation. Sections were not de-plastified and placed in 0.1 % calcein blue pH 8 (Appendix A) for 3 minutes followed by three 5 minute washes in distilled water. Slides were then dehydrated as previously described through a series of increasing ethanol, cleared in xylene, and mounted in DPX mountant.

Bioimaging Unit at Newcastle University imaged the tibiae using a fluorescent camera on a Zeiss Axioscan 7 microscope at a magnification of 20 x. Custom filter sets were used to image the fluorescent dyes, Alizarin complexone 495/515 mm, calcein green 530-560/580 nm and calcein blue was imaged using the DAPI filter. Images were tiled and stitched using the ZEISS Zen Blue Software.

Bone histomorphometric analysis was carried out using a custom analysis program to quantify bone formation parameters, developed by Professor Rob van' t Hof[153], through ImageJ 1.52i software[146]. Analysis was performed on matched sections 3 per genotype. A Student's unpaired two tailed T-test was used to analyse significant differences between samples and statistical significance was given by $p<0.05$.

2.8 Protein analysis of mouse tissue

Mouse tissues of ear notches, tail tips, skin and xiphoid were collected and snap frozen in Eppendorfs. Mikro-Dismembranator S (Satorius) homogeniser vessel with ball bearing was precooled in a liquid nitrogen bath. Tissues were transferred to the vessel 200 µL RIPA buffer (Appendix A) was added and tissues were homogenised at 2000 rpm for 2 minutes.

Homogenised tissues lysates were defrosted and vortexed for 20 seconds, snap frozen in liquid nitrogen and again defrosted and vortexed. Lysates were then centrifuged at 8,000 x g for 5 minutes at 4 ^{o}C. Supernatant was removed and transferred to a clean Eppendorf; lysates were stored at -80 ^{o}C until needed.

Protein concentration of the lysates was assessed using the Pierce™ bicinchoninic acid assay (BCA) Assay kit according to manufacturer's instructions, using the kit standards to plot the standard curve for absorbance. Absorbance was quantified on a Varioskan LUX Multimode Microplate Reader (Thermo Scientific), and absorbance measured at 562 nm optical density.

Lysates were made up for Western blot samples and Western blot were carried out as previously detailed.

Chapter 3. Overexpression of Asporin in cartilage and bone cells.

3.1 Introduction

A polymorphism in the aspartic acid region of the human *ASPN* gene has been shown to correlate with osteoarthritis risk in several populations[155, 156]. Wild-type Asporin has also been shown to be upregulated in osteoarthritis both in humans and in mice. RNA sequencing data obtained from Prof David Young at Newcastle University (unpublished) of unaffected neck of femur control cartilage versus osteoarthritic neck of femur articular cartilage highlighted an approximately seven-fold upregulation of Asporin in the osteoarthritic data set, Figure 30. Furthermore, human microarray data collected by Dr Mary Goldring mined and plotted by Professor Francesco dell'Accio (unpublished), found ASPN expression was significantly upregulated in the osteoarthritis knee cartilage samples versus normal knee cartilage samples ($p = 0.00002$), this was both male and female samples, highlighting that the elevated Asporin expression in OA was independent of sex, Figure 31. Secondary stratification of Age vs ASPN expression in Normal and OA samples found Asporin expression was increased in the OA samples independent of age, Figure 31. Further data obtained from Prof David Young (unpublished) showed an upregulation in Asporin in the articular cartilage of mice following induction of osteoarthritis through surgical destabilisation of the medial meniscus (DMM) surgery in comparison to controls, by Log_2FoldChange 1.421 (Adjusted $p = 0.000785$), Figure 32. These datasets are further supported by consistent data by Liu et. al. where expression levels of Asporin were increased in OA-damaged articular cartilage and as a result of DMM-induced OA mouse model[157].

Chondrogenesis studies have been previously performed in the presence of exogenous recombinant Asporin in the medium and showed that exogenous Asporin can downregulate chondrogenesis and inhibit TGF-β1 function in NHAC cells[137]. Further experiments with cells stimulated with TGF-β1 to drive chondrogenesis and mimic the OA environment in Normal

Human Articular Cartilage (NHAC) cells showed Asporin expression was induced[137].The effect of the upregulation of Asporin expression in cartilage and bone progenitor cells has not been previously assessed.

Mineralisation is an important part of endochondral ossification; hypertrophic chondrocytes of the cartilage growth plate undergo apoptosis as the secreted extracellular matrix mineralises. This hypoxic environment, together with growth factors and ECM remodelling factors secreted by the hypertrophic cells, drives the recruitment of blood vessels and osteoblasts to form calcified bone. Mineralisation of the articular cartilage is a common feature of the osteoarthritis pathology [158]. Additional features of osteoarthritis (OA) include cartilage hypertrophy and tidemark duplication, accompanied by upregulation of type X collagen and MMP13. These changes lead to alterations in chondrocyte differentiation that resemble the processes observed in the growth plate during endochondral ossification, where cartilage undergoes hypertrophy[159]. Tidemark replication describes the change to the cartilage/bone junction, in healthy articular cartilage the tidemark is the zone of calcified cartilage between the bone and the uncalcified articular cartilage. During tidemark replication the hypertrophy drives an advancement of the calcification front, where the previously uncalcified zone is calcified, the previously calcified zone of cartilage is degraded, and the subchondral bone thickens and extends into the previously calcified zone[159]. Moreover, during the progression of osteoarthritis, osteophytes (bony spurs) develop from the chondro-synovial junction, where the periosteum, a reserve of mesenchymal and osteochondroprogenitor cells reside. The formation of osteophytes has been shown to be similar to the process of fracture repair, which periosteum is heavily involved in in the bone[160].

Cartilage mineralisation occurs through the mineralisation of the collagen fibrils by the binding of hydroxyapatite ($Ca_{10}(OH)_2(PO_4)_6$), the mineral form of calcium apatite[161]. Asporin has been shown to have a high affinity for collagen, however decorin competes with Asporin to bind collagen and inhibits Asporin-collagen interaction. Although they can both

bind collagen, Asporin is the only SLRP capable of binding the Ca^{2+}, therefore Asporin is the only SLRP that can mineralise collagen fibrils[123]. The upregulation of Asporin in the cartilage of OA and DMM-induced OA models and the unique ability of Asporin in the SLRP family to bind and mineralise collagen fibrils suggests a role of Asporin in OA cartilage mineralisation and osteophyte formation[123].

To analyse the effect of Asporin overexpression on chondrogenesis and on the mineralisation of cartilage and developing bone, two commercially available immortalised cell lines were used - a chondrogenic cell line, ATDC5, and osteogenic cell line, U2OS[162, 163]. ATDC5 cells are derived from mouse teratocarcinoma cells, they have capacity to differentiation analogous to that of chondrocytes[162]. U2OS are an osteoblast-sarcoma which demonstrate similar gene expression to that of human osteoblasts[163]. Human Asporin was overexpressed in the cells using an open reading frame (ORF) *ASPN* cDNA containing mammalian expression vector (Clone ID: OHu29011) (Appendix D). The cells were driven through differentiation for chondrogenesis, and with mineralising media (containing Beta-glycerophosphate) to model cartilage mineralisation and osteogenic differentiation[164-166]. Beta-glycerophosphate (BGP) is routinely used in ATDC5 differentiation studies in order to induce cartilage mineralisation[164]. The use of beta-glycerophosphate has been shown to induce rapid chondrogenic differentiation with the production of a mineralised ECM previous studies required over 34 days of culture followed by 21 days in mineralising media to produce the same results[164]. BGP provides the phosphate needed to produce hydroxyapatite[166]. Alkaline phosphatase (ALP) produced by the hypertrophic chondrocytes hydrolyses the BGP releasing the inorganic orthophosphate, sodium phosphate co-transporters then take up the orthophosphate and produce hydroxyapatite[167]. High levels of orthophosphate have been shown to induce apoptosis of hypertrophic chondrocytes, the terminal stage of chondrocyte differentiation.

Chapter aims:

- To study the effect of overexpression of Asporin on chondrogenesis of ATDC5 cells
- To study the effect of *ASPN* overexpression on mineralisation of ATDC5 derived cartilage
- To study the effect of *ASPN* overexpression on early bone mineralisation using the USOS2 immature osteoblast cell line

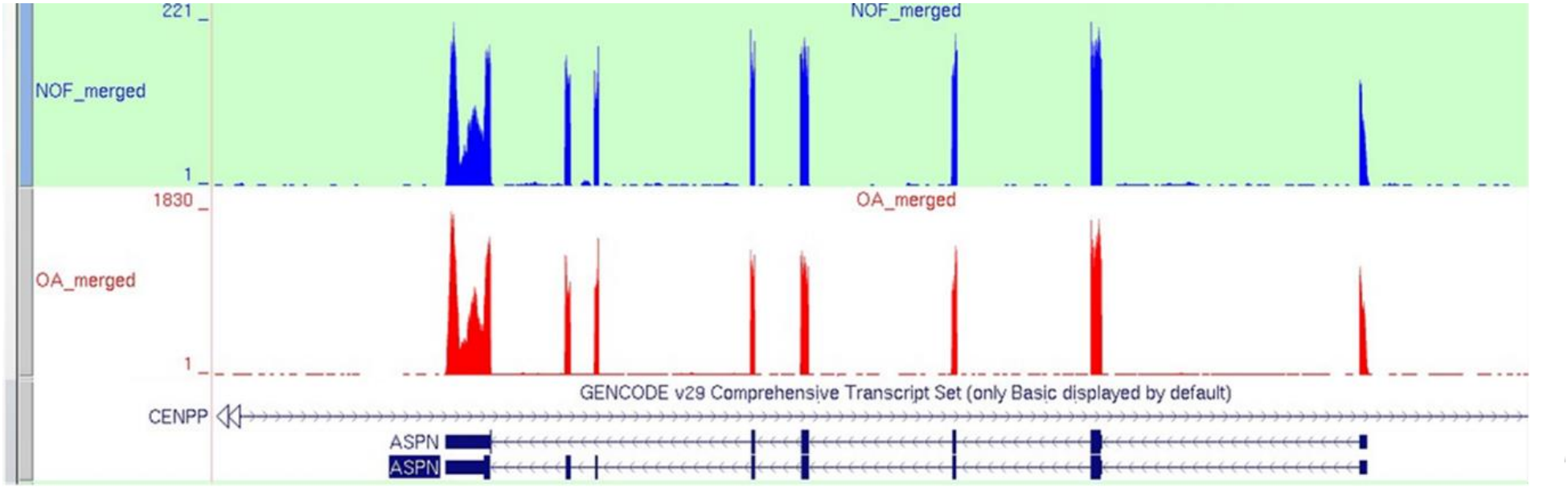

Figure 30. RNAseq data showed a significant increase in the expression of Asporin in OA patients. *RNAseq data was inputted into the UCSC genome browser, unaffected neck of femur (NOF) dataset against OA dataset showed an increase in expression of Asporin (fold change >7). All exons were present in the increased expression. Unpublished data from Professor D. Young.*

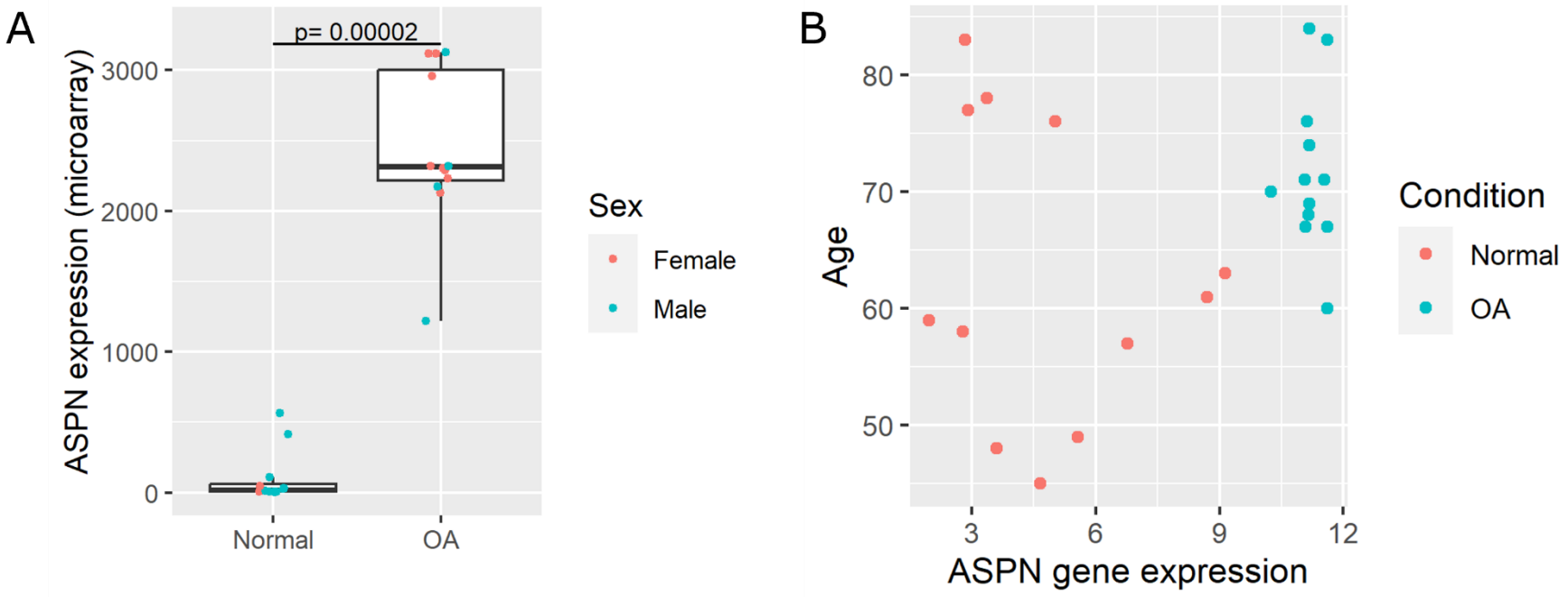

Figure 31. Asporin expression was significantly upregulated in OA samples, independent of gender and irrespective of age. *Stratification of Asporin expression data by sex and by age. Asporin was found to be significantly upregulated in the OA samples in both male and female samples (p = 0.00002)* ***(A)****. ASPN was increased in the OA patients irrespective of the age on the individuals* ***(B)****. Data Mining by Professor F. dell'Accio from Dr M. Goldring human microarray data.*

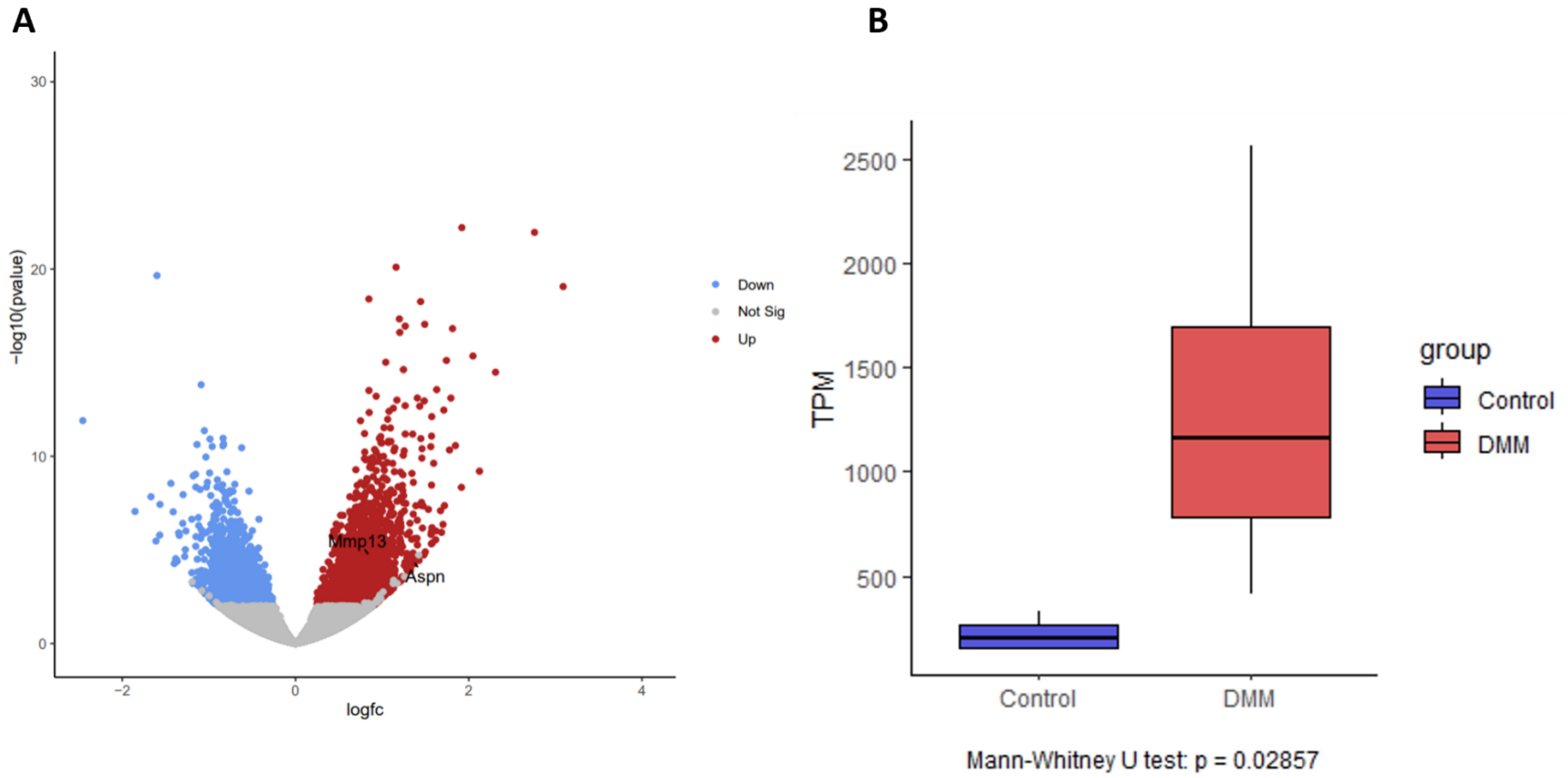

Figure 32. Asporin expression is upregulate following DMM induction.

RNAseq analysis of articular cartilage of mice following OA induction by destabilisation of the medial meniscus (DMM) surgery. Asporin is significantly upregulated by Log_2FoldChange 1.421 (Adjusted p = 0.000785) in the DMM surgical group in comparison to the control group. Unpublished data from Professor D. Young.

3.2 Preparation of the *ASPN* overexpression plasmid

Lyophilised GenScript ASPN ORF plasmid DNA (Clone ID: OHu29011) (vector map in Appendix D) was resuspended in TE buffer and transformed into DH5α cells, cell colonies successfully transformed with the ASPN ORF plasmid that survived on the selective ampicillin were picked and cultured in liquid broth cultures to amplify the DNA. ASPN ORF plasmid DNA of the clone was extracted was extracted by Miniprep (QIAgen) of selected DH5α cells. ATDC5 and U2OS cells were transfected with 2mg of ASPN ORF Plasmid DNA was transfected with lipofectamine. Cells successfully transfected with the plasmid DNA survived Geneticin selection, and untransfected and no-DNA transfection controls were used in the selection to verify Geneticin selection was effective. The ATDC5 and U2OS cells expressing the vector (OE) and untransfected controls (WT) were used for the following studies.

3.3 Asporin cDNA is successfully and consistently overexpressed in chondrogenic and osteogenic cell lines.

To determine the effect of the overexpression of Asporin on differentiation and mineralisation of cartilage and bone, ATDC5 chondrogenic cell line and U2OS osteogenic cell line were transfected with human Asporin ORF overexpression vector (Genscript).

Overexpression of human *ASPN* (h*ASPN*) was confirmed at an mRNA level by quantitative RT-qPCR, using human *ASPN* specific primers to differentiate from the endogenous mouse Asporin expression in ATDC5 cells. mRNA was sampled at day 1, 7, 14 and 21 of the culture using of the experiment. In the chondrogenic ATDC5 cells, by ANOVA and Tukey's post-hoc analysis, hASPN was overexpressed from Day 1 wild type cells by 31.1-fold ($p<0.05$) to day 14 and 81.2-fold to day 21 ($p<0.0001$) and by 81.2-fold ($p<0.0001$) between WT and OE cells at day 21 (Figure 33 A). By ANOVA and Tukey's post-hoc analysis, *hASPN* was overexpressed in mineralising ATDC5 cells from Day 1 wild type cells by 135-fold ($p<0.01$) to day 14. Additionally, overexpression of h*ASPN* in the mineralising ATDC5 cells was 117.5-fold ($p<0.01$) at day 14 (Figure 33 B). Primers specific to mouse *Aspn* gene were used to check the endogenous levels of Asporin expression during ATDC5 chondrogenesis.

Overexpression of *ASPN* was also confirmed in osteogenic U2OS cells, by ANOVA and Tukey's post-hoc analysis of WT an OE at each time point whereby Asporin was overexpressed 14.6-fold ($p<0.01$), 16.5-fold ($p<0.001$) and 14.1-fold ($p<0.01$) at day 1, 7 and 14 respectively. By ANOVA and Tukey's post-hoc analysis, hASPN was overexpressed from Day 1 wild type cells by 22.3-fold ($p<0.01$) to day 1 OE cells, 23.2-fold ($p<0.001$) to day 7 OE cells and 19.67-fold ($p<0.01$) to day 14 OE cells (Figure 33 C). Fold changes were lower in the U2OS cells in comparison to ATDC5 cells, however U2OS cells are a human cell line and Asporin is expected to be expressed in the WT cell line during osteogenesis.

To confirm overexpression of Asporin at protein level 30 ng of protein was electrophoretically resolved. SDS-PAGE gel electrophoresis followed by Western blotting for Asporin and GAPDH loading control Protein from mineralising ATDC5 cells and mineralising U2OS cells was used to verify the sustained overexpression of Asporin after 21 days of culture in differentiation media. Overexpression was confirmed in both ATDC5 cells (Figure 33 D) and U2OS cells (Figure 33 E).

Additionally, endogenous mouse Asporin expression was assessed by qPCR in chondrogenic WT ATDC5 cells and in cells overexpressing Asporin. Mouse Asporin was expressed in low levels in chondrogenic WT ATDC5 cells and OE ATDC5 cells with no significant difference in the expression of mouse Asporin between the WT and OE cells (Figure 34)

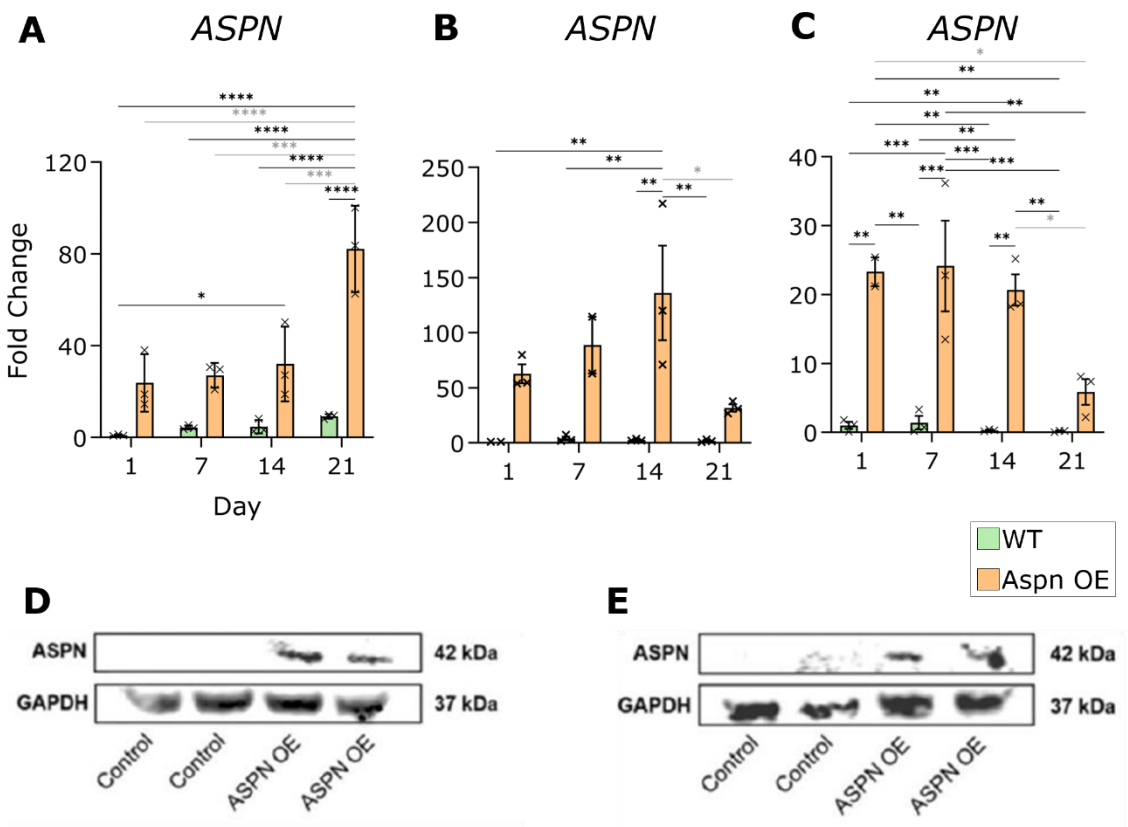

Figure 33. Human ASPN is overexpressed for 21 days of chondrogenic and mineralising culture. *RT-qPCR confirmed overexpression vector consistently upregulated ASPN in chondrogenic ATDC5 cells (**A**), mineralising ATDC5 cells (**B**) and osteogenic U2OS cells (**C**). Expression levels were normalised to 18s. 2-way ANOVA was carried out between WT and OE and across each timepoint (n=3) and denoted by *=p<0.05, **=p<0.01, ***=p<0.001. Overexpression of Asporin at protein level was confirmed by Western Blotting in mineralising ATDC5 cells (**D**) and U2OS cells (**E**) after 21 days of culture. Error bars represent standard error of the mean.*

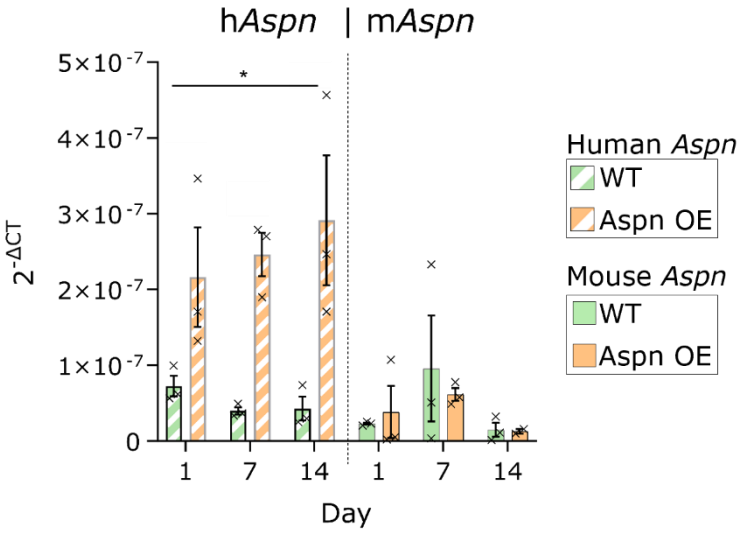

Figure 34. Mouse ASPN is expressed in low levels in chondrogenic culture of WT ATDC5 cells. *RT-qPCR assessed human and mouse Asporin expression at day 1, 7 and 14 in chondrogenic ATDC5 cells. Expression levels were normalised to 18s. 2-way ANOVA was carried out between WT and OE and across each timepoint (n=3) and denoted by *=p<0.05. Error bars represent standard error of the mean.*

3.4 Overexpression of Asporin dysregulates proteoglycan networks in the extracellular matrix produced by ATDC5 cells.

3.4.1 Overexpression of Asporin decreases proteoglycan deposition during ATDC5 chondrogenesis.

To study the effect of overexpression of Asporin on the deposition of the extracellular matrix of cartilage, ATDC5 cells were transfected with h*ASPN* ORF expression vector. WT (no vector controls) and overexpressing (OE) cells were plated and grown to confluency in chondrogenic medium supplemented with 1% insulin/transferrin/selenium and 1 % sodium pyruvate then stimulated to drive collagen production and ECM deposition stimulated with ascorbic acid at day 6[164]. Cells were cultured for a further 21 days and assessed at day 1, 7, 14 and 21.

Cell monolayers were stained with Alcian blue, a sulphated proteoglycan specific stain. Sulphated proteoglycan deposition was visibly decreased in the OE cells in comparison to the WT cells (Figure 35 A). At day 1, 7, 14 and 21, Alcian blue stain was extracted from the monolayers and quantified using absorbance measurement. By ANOVA and Tukey's post-hoc analysis across time points, sulphated proteoglycan decreased from day 1 WT cells 35.1% ($p<0.05$) to day 14 OE cells and significantly reduced in the OE cells by 43.7 % ($p<0.05$) at day 14 compared to WT cells (Figure 35 C). Sulphated proteoglycans are crucial for cartilage integrity, stabilising and organising collage fibrils and a role in regulation of growth factor signalling[168]. The decrease in deposition in the ASPN OE cells suggests a role of Asporin in cartilage integrity.

To assess mineralisation of the differentiating ATDC5 monolayer cultures, Alizarin red staining (ARS) was performed. ARS is an anionic dye that binds to cationic metals including calcium the cationic ion of hydroxyapatite ($Ca_5(OH)(PO_4)_3$), the main mineral of mineralised bone. Alizarin red stains the calcium deposits red when bound to the cations,

however the staining of the cells in this experiment appeared brown, suggesting background staining rather than staining of calcium deposition in the monolayer (Figure 35 B). The quantification of the ARS showed no difference in mineralisation between the WT and ASPN OE cultures (Figure 35 D).

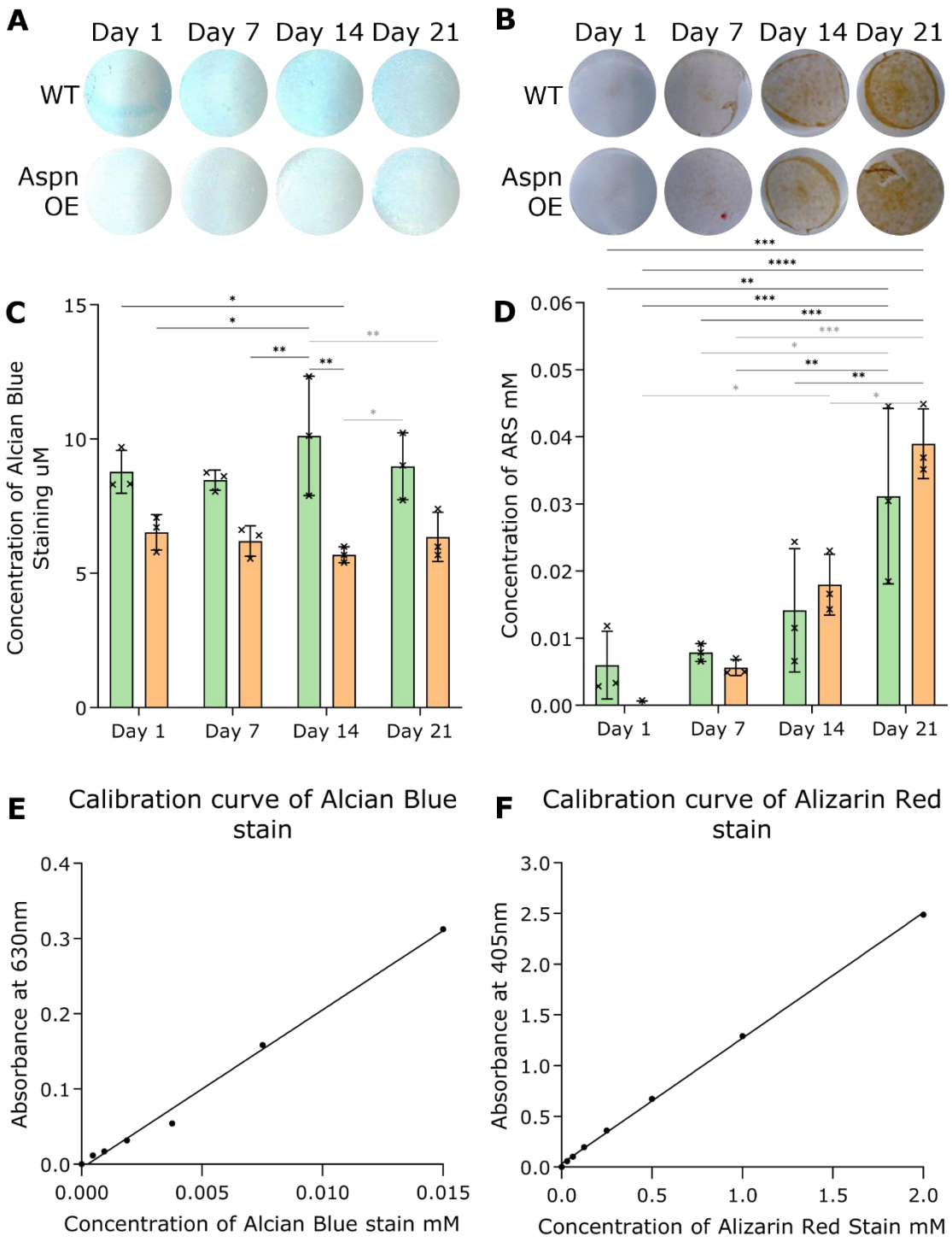

Figure 35. Overexpression of Asporin inhibits sulphated proteoglycan deposition in ATDC5. *Alcian blue and Alizarin Red staining of monolayer ATDC5 cells through chondrogenic differentiation of ATDC5 throughout 21-day cell culture in chondrogenic medium without beta-glycerophosphate (BGP). Comparison of wild-type ATDC5 (WT) and ATDC5 overexpressing Asporin (ASPN OE). Cells were stained with 1% Alcian blue (**A**) or 40mM Alizarin Red stain (ARS)(**B**). Semi-quantitative measurement of sulphated proteoglycan deposition through quantification of Alcian blue stain read by spectrophotometry at 630 nm(**C**). Semi-quantitative measurement of calcium deposition through quantification of Alizarin red stain read by spectrophotometry at 405 nm(**D**). Concentration of stains were calculated*

*from calibration curve of standards of serial dilutions of Alcian blue stain (**E**) and standards of serial dilutions Alizarin red stain (**F**). 2-way ANOVA was carried out between WT and OE and across each timepoint (n=3) and denoted by *=p<0.05, **=p<0.01. Error bars represent standard error of the mean.*

3.4.2 Overexpression of Asporin inhibits the expression of Decorin during ATDC5 chondrogenesis.

To assess the effect of overexpression of Asporin on chondrogenesis and the extracellular matrix production, mRNA levels of chondrogenic markers and extracellular matrix proteins were assessed by RT-qPCR. Chondrogenic differentiation markers were selected and assessed for the different stages of the differentiation, *Sox9* an early marker, *Ihh* a mid differentiation marker and *Col10a1, Mmp13*, *Runx2* for late markers.

Overexpression of Asporin led to a decrease in the Alcian blue staining of the chondrogenic OE monolayers. Aggrecan is a key component of the cartilage extracellular matrix. Interestingly, aggrecan expression, was comparable between the WT and OE cells at day 1, 7 and 21 of chondrogenesis, however, it was dramatically increased (1812 %, $p<0.001$) in the OE cells compared to the WT controls at day 14. Aggrecan is a large aggregating chondroitin sulphate and is important to the function of the articular cartilage contributing to the ability of cartilage to resist compressive load and mediating chondrocyte-chondrocyte interaction and chondrocyte-ECM interactions[169]. Aggrecan degradation is a feature of osteoarthritis, with breaking down of the protein aggregates and the degradation of the protein itself[169].

Expression of decorin, a member of the SLRP family of proteins shown to bind to aggrecan and modulate the structural integrity of the cartilage ECM by increasing its interaction with type II collagen fibrils, was decreased significantly in ASPN OE ATDC5 cells at 21 98.8 % ($p<0.001$) respectively (Figure 36).

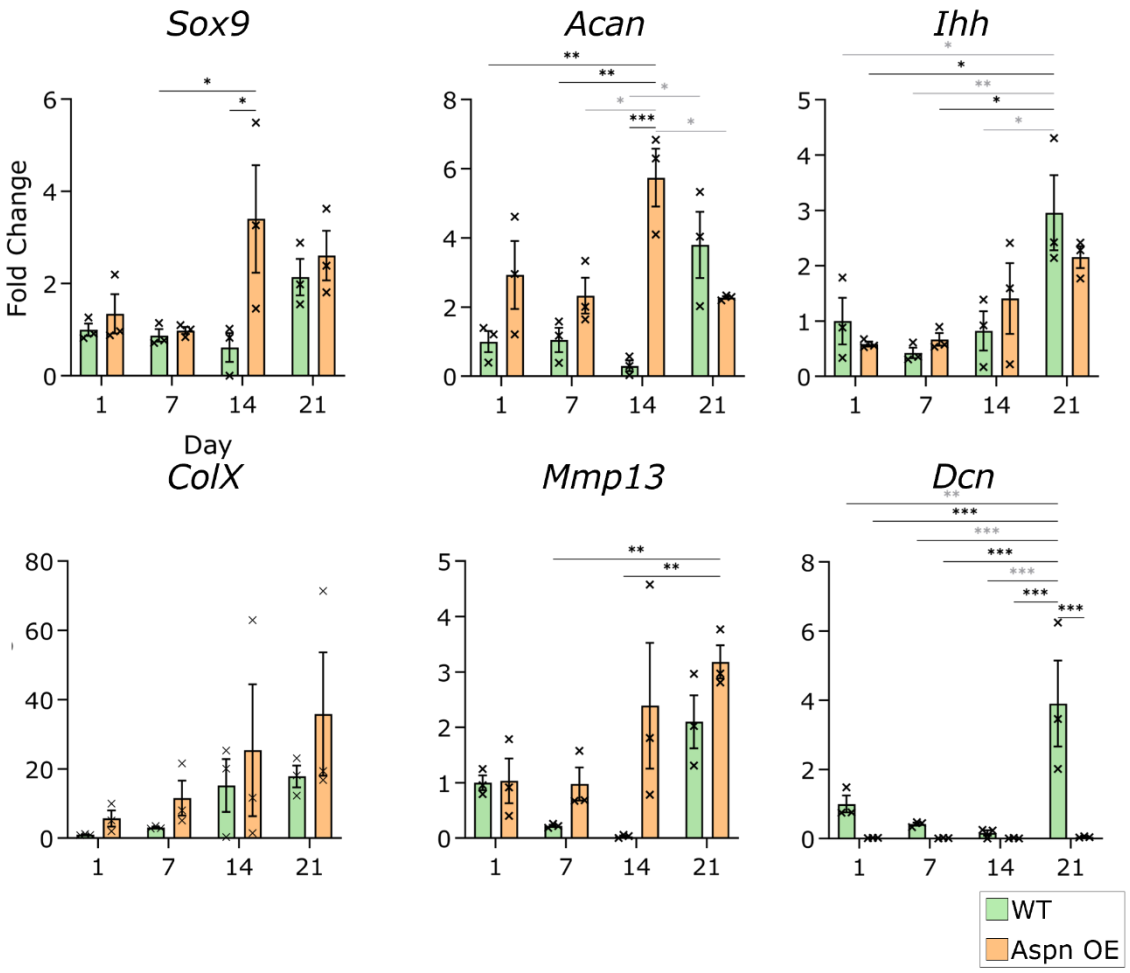

Figure 36. Asporin overexpression supresses the expression of Decorin during chondrogenesis. *Chondrogenic markers were assessed by rt-qPCR. Decorin is supressed in Asporin overexpression ATDC5 at day 1, 7 and 21. Aggrecan expression is upregulated at day 14 in the Asporin overexpression ATDC5. Expression levels were normalised to 18s. 2-way ANOVA was carried out between WT and OE and across each timepoint between WT and OE(Black *) and within the genotype between each time point (Grey *), (n=3) and denoted by *=p<0.05, **=p<0.01, ***=p<0.001. Error bars represent standard error of the mean.*

3.4.3 Overexpression of Asporin promotes hypertrophic and terminal differentiation of ATDC5.

Chondrogenic differentiation proceeds to hypertrophy and terminal chondrocyte differentiation. At this stage of differentiation chondrocytes begin to express genes involved in osteoblast differentiation, these are classed as osteogenic markers. These transcription factors drive osteoblast differentiation in developing bone. For the assessment of the terminal differentiation and mineralisation early markers *Sp7*, *Runx2* were measured and late markers of osteoblastogenesis *Sost and Bglap* were tested by qRT-PCR to assess the effect of Asporin overexpression on chondrogenesis.

Asporin overexpression upregulated *Runx2* a master regulator of osteogenic differentiation by ANOVA and Tukey's post-hoc analysis, *Runx2* was increased in day 21 OE cells by 45.8 % ($p<0.05$) in comparison to day 14 WT cells this was not observed in the day 14 to day 21 WT cells (Figure 37). This is interesting preliminary data as by Student paired T-test at day 7 and day 21, by 75.5 % ($p<0.05$), 32.6 % ($p<0.001$) respectively *Runx2* expression was upregulated in the OE cells in comparison to WT cells.

SPP1 is involved in the mineralisation of the matrix and regulated by RUNX2. SPP1 (osteopontin) is a non-collagenous bone protein, involved mineralisation of the matrix, capable of binding hydroxyapatite and in the attachment of osteoclasts to the mineralised matrix. In ASPN OE ATDC5 cells, *Spp1* expression is upregulated at day 14 by 3053 % ($p<0.05$).

SP7 (osterix) is another master regulator of osteogenic differentiation however it has also been shown to be expressed by hypertrophic chondrocytes at low levels, in ASPN OE ATDC5 cells *Sp7* expression was decreased at day 21 by 81.4 % ($p<0.01$) in comparison to day 1 WT cells, whereas there was no significant difference in expression from day 1 to day 21 WT cells.

BGLAP (osteocalcin) is a marker of osteoblast differentiation, *Bglap* expression was decreased at day 21 in the OE cells by 78 % ($p<0.05$). SOST is a late marker of osteoblast differentiation expressed by osteocytes however it is also expressed by hypertrophic chondrocytes, RUNX2 can supress the expression of SOST.

The upregulation of *Runx2* and the expression changes in downstream transcription factors expression *Spp1* and *Bglap*, suggests a role for Asporin in modulating the RUNX2 axis of chondrocyte differentiation and osteoblast differentiation.

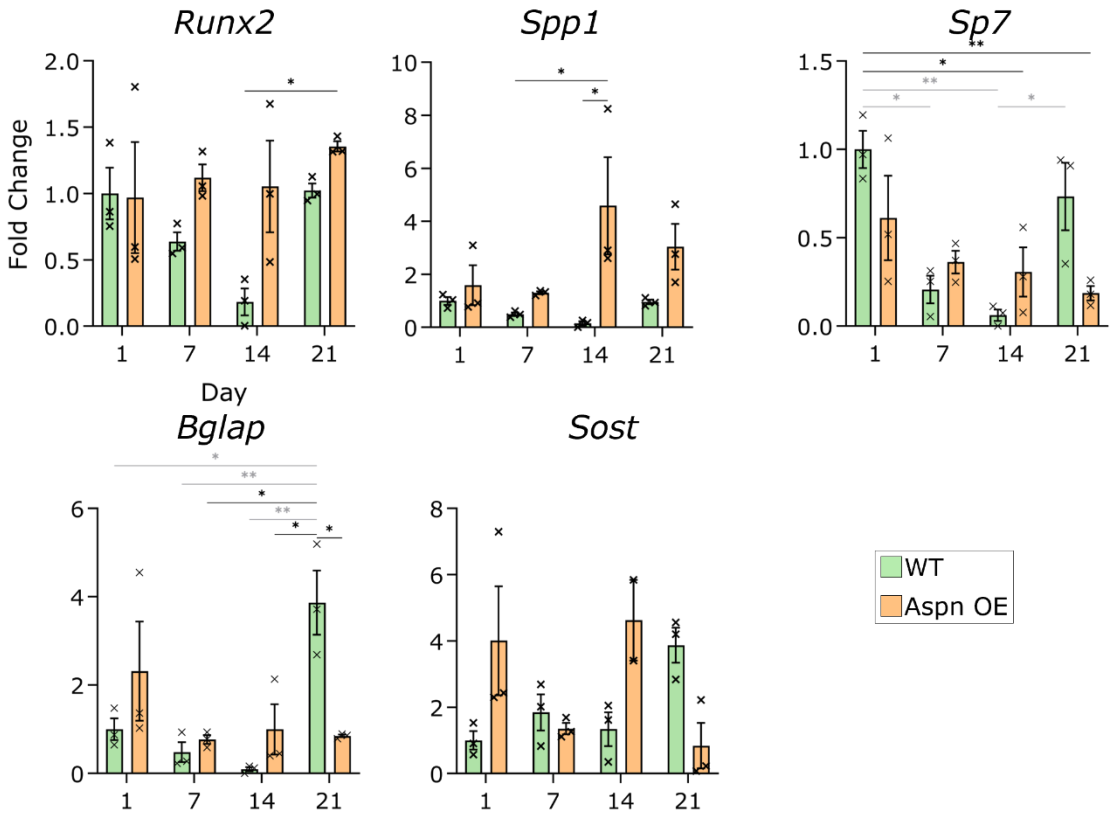

Figure 37. Overexpression of Asporin upregulates Runx2 and Spp1 expression and supresses Bglap. *Osteogenic markers were assessed by RT-qPCR. Runx2 expression is upregulated at day 7 and 21 in the Asporin overexpression ATDC5. Spp1 was upregulated at day 14. At day 21, Bglap was downregulated. Expression levels were normalised to 18s. 2-way ANOVA was carried out between WT and OE and across each timepoint between WT and OE (Black *) and within the genotype between each time point (Grey *), (n=3) and denoted by *=p<0.05, **=p<0.01, ***=p<0.001. Error bars represent standard error of the mean.*

3.5 Overexpression of Asporin accelerates cartilage mineralisation.

3.5.1 Asporin overexpression increases calcium deposition in mineralising ATDC5 monolayer.

To study the effect of overexpression of Asporin in the mineralisation of the extracellular matrix of cartilage, ATDC5 cells were transfected with h*ASPN* ORF expression vector, WT and OE cells were plated and grown to confluency in chondrogenic differentiation media supplemented with 1% insulin/transferrin/selenium and 1 % sodium pyruvate for 6 days. Cells were then cultured for a further 21 days supplemented with BGP and ascorbic acid to drive the mineralisation of the deposited ECM and collagen production and assessed at day 1, 7, 14 and 21. As discussed previously BGP provides the phosphate for the formation of hydroxyapatite the mineral for the calcification/mineralisation of the cartilage ECM.

Mineralising ATDC5 cell monolayers were stained with Alcian blue as described previously and showed no overt difference in the sulphated proteoglycan deposition (Figure 38 A). No difference was found between WT and ASPN OE ATDC5 cells in the quantification of the extracted Alcian blue stain either (Figure 38 C).

To assess mineralisation of the ATDC5 cell monolayer, Alizarin red staining (ARS) was used. ARS was visibly increased in the ASPN OE ATDC5 at day 7, 14 and 21 (Figure 38 B). At day 7, 14 and 21, the extracted and quantified ARS levels were significantly increased 945.7 % ($p<0.001$), 453.7 % ($p<0.0001$) and 29.3 % ($p<0.0001$) respectively, compared to the WT cells (Figure 38 D).

The significant increase in the Alizarin Red staining in the Asporin OE cells supports a potential role of Asporin in the mineralisation of cartilage during osteoarthritis.

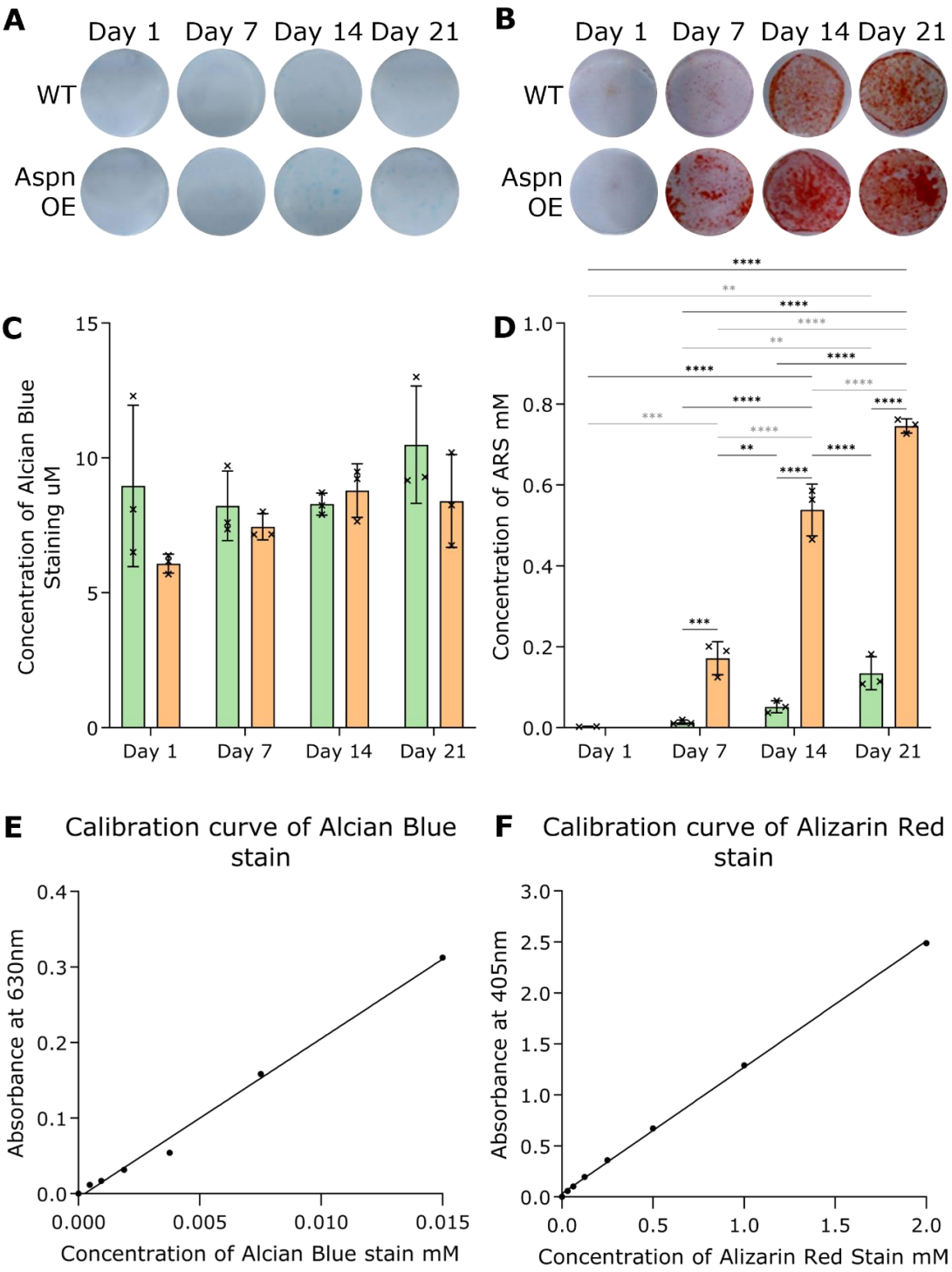

Figure 38. Overexpression of Asporin accelerates mineralisation in ATDC5. *Alcian blue and Alizarin Red staining of monolayer ATDC5 cells throughout mineralising 21-day cell culture in chondrogenic medium supplemented with beta-glycerophosphate (BGP), to induce mineralisation. Comparison of wild-type ATDC5 (WT) and ATDC5 overexpressing Asporin (ASPN OE). Cells were stained with 1% Alcian blue (**A**) or 40mM Alizarin Red stain (ARS)(**B**). Semi-quantitative measurement of sulphated proteoglycan deposition through quantification of Alcian blue stain read by spectrophotometry at 630 nm (**C**). Semi-quantitative measurement of calcium deposition through quantification of Alizarin red stain read by*

*spectrophotometry 405 nm (**D**). Concentration of stains were calculated from calibration curve of standards of serial dilutions of Alcian blue stain (**E**) and standards of serial dilutions Alizarin red stain (**F**). 2-way ANOVA was carried out between WT and OE and across each timepoint, between WT and OE(Black *) and within the genotype between each time point (Grey *), (n=3) and denoted by *=p<0.05, **=p<0.01, ***=p<0.001, ****=p<0.0001. Error bars represent standard error of the mean.*

3.5.2 Cartilage and OA markers are increased by Asporin overexpression in the mineralising ATDC5 cultures.

Key steps in the mineralisation of the cartilage growth plate and laying down of bone in endochondral ossification is the degradation of the cartilage to allow the infiltration of blood vessels with osteoblasts and osteoclasts from the perichondrium, the expression of type I collagen and the subsequent mineralisation of the collagen fibrils. In order to assess the effect of Asporin overexpression on the differentiation of mineralising ATDC5 cells, expression of chondrogenesis markers (*Sox9, Ihh, Mmp13, Col10a1*) was assessed by qRT-PCR in OE and WT cells at day 1, 7, 14 and 21 of culture.

Sox9 expression in the OE cell was not significantly different at any time point to the WT cells. However, expression does increase in the OE cells from day 7 to 14.

Ihh is a key morphogen secreted by prehypertrophic chondrocytes responsible for the organisation of the zones of the growth plate through the differentiation of the chondrocytes in the PTHrP feedback loop, described in Chapter 1, PTHrP Ihh is regulated by *Sox9* and a downstream target of *Runx2*[170]. Ihh expression has also been implicated in OA pathology because of its role in regulation of chondrocyte hypertrophy and *Mmp13* expression, Ihh is found to be upregulated in OA cartilage[171, 172]. Interestingly, *Ihh* expression was upregulated in the day 14 ASPN OE cells 411.96 % ($p<0.01$) compared to the WT mineralising cells.

Collagen X is expressed specifically by the hypertrophic chondrocytes, *Col10a1* expression was downregulated at day 7, 88.1 % ($p<0.0001$), and there was no difference in *Col10a1* expression between the OE and WT cells at day 14 and day 21. COL10A1 is important for the cartilage-bone transition, expressed by the hypertrophic chondrocytes.

MMP13 is a matrix metalloprotein that is responsible for the turnover of the cartilage ECM. MMP13 is the primary collagenase in the primary and secondary ossification centres of endochondral ossification and targets type II collagen and aggrecan[48]. and upregulation of MMP13 leads to accelerated articular cartilage degradation in OA[173].

In the ASPN OE mineralising ATDC5 cells M*mp13* expression was upregulated at day 7, 14 and 21, by 2322.4 % ($p<0.0001$), 587.3 % ($p<0.001$) and 288 % ($p<0.05$) respectively, compared to the WT cells. This highlights a very interesting avenue for an effect of Asporin overexpression in OA cartilage. MMP13 is expressed by terminal hypertrophic chondrocytes and cleaves type II collagen[48], the degradation of the cartilage is necessary for the invasion of blood vessels. However, it is also highlighted for its pathogenic role in OA, MMP13 has been shown to be elevated in osteoarthritic cartilage, where degradation is increased further accelerating the loss of cartilage and progression of OA[173]. As Asporin has been shown to be upregulated in OA cartilage and has been shown here to upregulate the expression of MMP13, Asporin may be a therapeutic target in OA to reduce the activity of MMP13.

Type I collagen is significantly increased in the overexpression of Asporin from day 1 to day 7. Type I collagen, the main building of all tissues in the body except cartilage, it is expressed at high levels in early osteoblast differentiation (Figure 3). Type I collagen is used as a marker of early osteoblasts. The formation of bone is from the mineralisation of cartilage, as discussed, Kalamajski et. al. demonstrate Asporin binds Type I collagen[123].

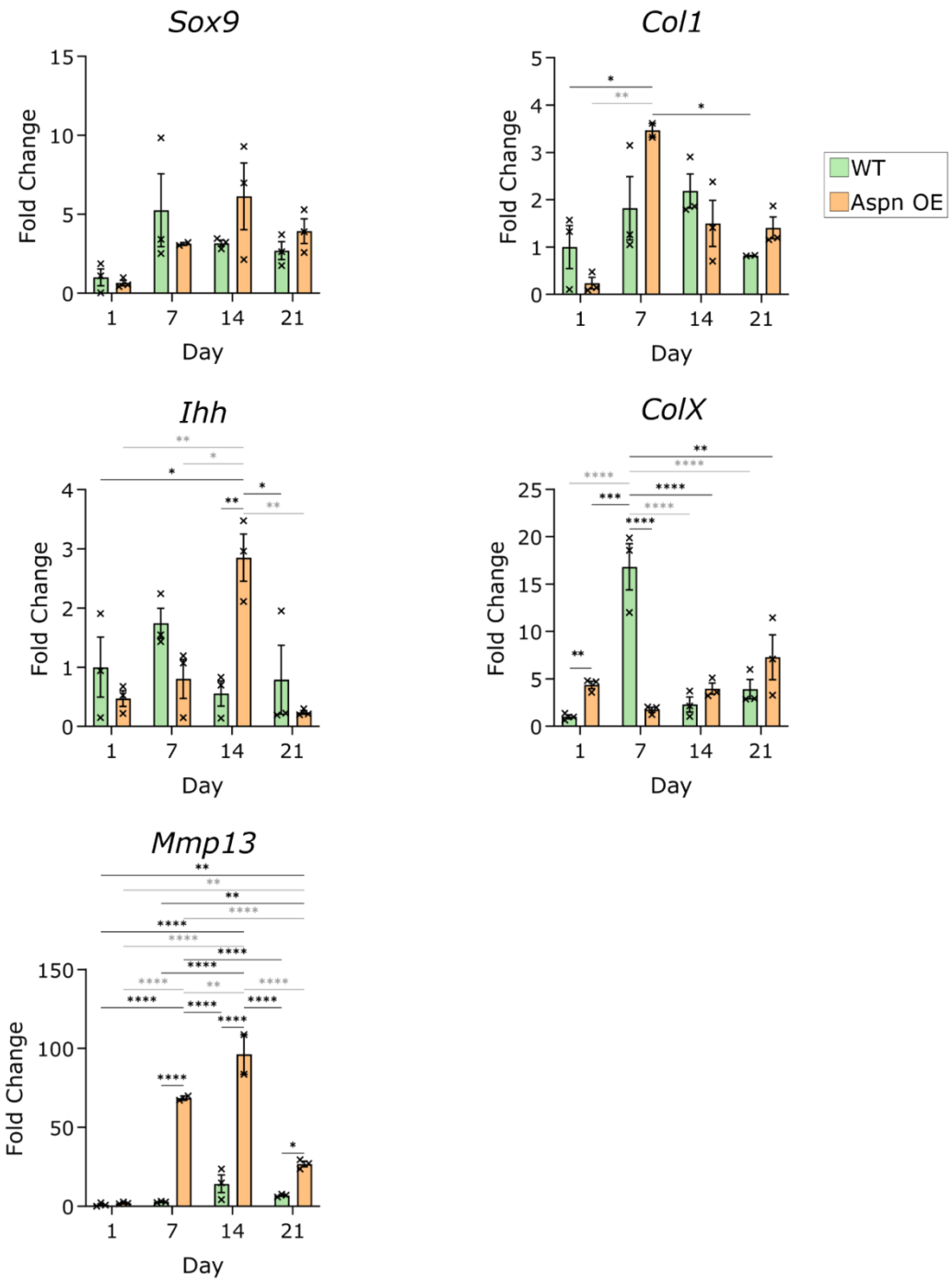

Figure 39. Asporin overexpression upregulates cartilage degradation enzyme Mmp13 in mineralising cartilage. *Osteogenic markers were assessed by rt-qPCR. Mmp13 is significantly upregulated in the OE cells, Mmp13 is a major enzyme targeting cartilage for degradation, a previous study by Wang et al.[1] found that deletion of Mmp13 resulted in decreased ColX induction, here we see upregulation of Mmp13 and no suppression of ColX at the later differentiation time points. Expression levels were normalised to 18s. 2-way ANOVA was carried out between WT and OE and across each timepoint, between WT and OE (Black *) and within the genotype between each time point (Grey *), (n=3) and denoted by *=p<0.05, **=p<0.01, ***=p<0.001. Error bars represent standard error of the mean.*

3.5.3 Asporin upregulates Runx2 expression in mineralising ATDC5 cells.

To explore the reason behind the increased mineralisation of the cartilage monolayer in BGP cultured ASPN OE ATDC5 cells, osteogenic markers were assessed by RT-qPCR to determine gene expression changes during chondrogenesis and cartilage mineralisation in presence of BGP.

RUNX2, the master regulator of osteoblast differentiation was increased at day 14 in the ASPN OE ATDC5 590.1 % ($p<0.05$) from day 1 OE cells, whereas there was no significant difference in the expression between day 1 and day 14 WT cells (Figure 40).

SPP1, capable of binding hydroxyapatite and regulated by RUNX2 In ASPN OE ATDC5 cells, *Spp1* expression was upregulated at day 14 by 3680 % ($p<0.05$) from day 1 WT cells, whereas there was no significant difference in expression between day 1 and day 14 WT cells. Interestingly, the increase of *Spp1* correlated with the increase in mineralisation of the cell monolayer (Figure 40). *Sost, Sp7* and *Alp* expression in the OE cell was not significantly different at any time point to the WT cells. There were changes between the expression of the genes within the cell type, *Bglap* expression peaked at day 14 in the OE cells, however there was no difference in the expression of *Alp* between the WT and OE or between the day points of the cells.

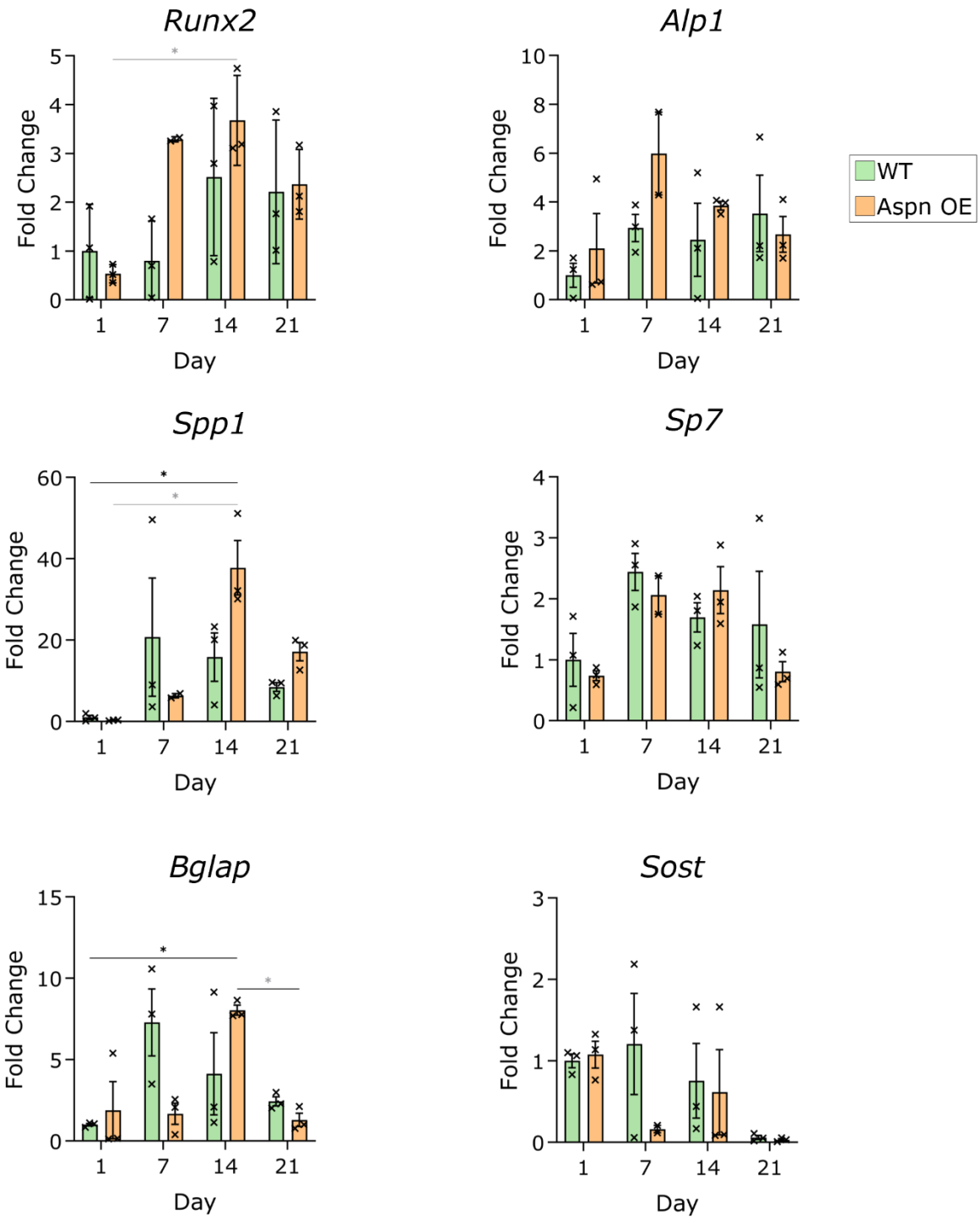

Figure 40. Overexpression of Asporin upregulates Bglap and Spp1 expression. *Osteogenic markers were assessed by rt-qPCR. Bglap expression is upregulated at day 14 in the Asporin overexpression ATDC5. Spp1 was upregulated at day 14. Expression levels were normalised to 18s. 2-way ANOVA was carried out between WT and OE and across each timepoint, between WT and OE (Black *) and within the genotype between each time point (Grey *), (n=3) and denoted by *=p<0.05, **=p<0.01, ***=p<0.001.Error bars represent standard error of the mean.*

3.6 Overexpression of Asporin in mineralising ATDC5 cells leads to changes in the balance of the OPG/RANKL pathway.

During end stage chondrogenesis and cartilage mineralisation the recruitment and modulation of osteoblastogenesis is essential for endochondral ossification. As discussed previously the RANKL and OPG balance regulates the activation of osteoclastogenesis. Osteoclastogenesis is initiated by the binding of RANKL (secreted by the osteoblasts) to the RANK receptor on osteoclast progenitor cells. Osteoprotegerin (OPG) is a decoy receptor of RANKL secreted by several cell types, including the osteoblasts and chondrocytes. Increased OPG binds RANKL preventing RANKL from binding to the RANK receptor, thus inhibiting osteoclastogenesis. The OPG/RANKL balance has been shown to be active in OA pathology[174]. In primary human OA chondrocytes cultured grown *in vitro,* supplementation with human OPG resulted in an upregulation in *MMMP13* expression[174].

To assess the modulation of the elements of this pathway by Asporin overexpression in mineralising cartilage cells, *Opg* and *RankL* mRNA expression levels were assessed by RT-qPCR. Interestingly, in the chondrogenic unmineralized cartilage (ATDC5 cells cultured without BGP), *Opg wa*s upregulated at day 21 in the ASPN OE ATDC5 cells, by 339.8 % ($p<0.05$) (Figure 41 A). In the mineralising chondrocytes, *Opg wa*s upregulated at day 14 in the ASPN OE ATDC5 cells, by 490.1 % ($p<0.01$) (Figure 41 B).

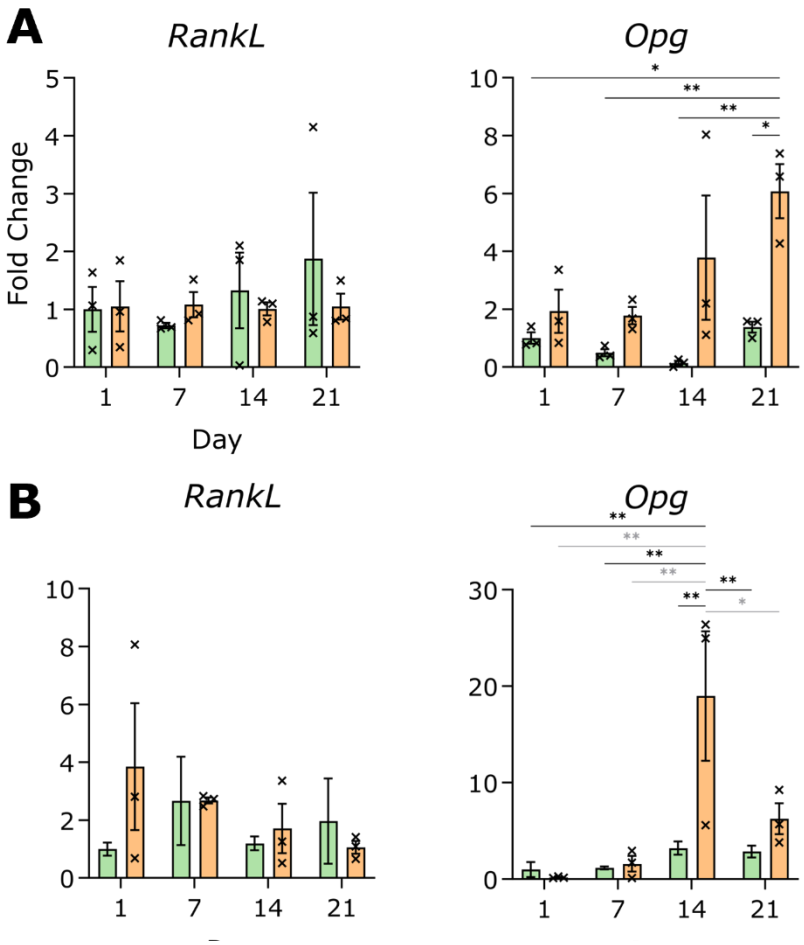

Figure 41. Asporin overexpression upregulates Opg in chondrogenic ATDC5 cells.

Activators of the osteoclastogenesis differentiation, RankL and Opg were assessed by rt-qPCR. Opg is significantly upregulated in the OE chondrogenic cells at day 7 and 21 ***(A)****, but not during mineralisation* ***(B).*** *Opg is an inhibitor of osteoclastogenesis during skeletal development. Expression levels were normalised to 18s. 2-way ANOVA was carried out between WT and OE and across each timepoint, between WT and OE (Black *) and within the genotype between each time point (Grey *), (n=3) and denoted by *=p<0.05, **=p<0.01, ***=p<0.001. Error bars represent standard error of the mean.*

3.7 Overexpression of Asporin effect on mineralisation of U2OS cells.

To assess the effect of overexpression of Asporin on osteogenic differentiation and mineralisation, U2OS osteogenic cells were transfected with Asporin overexpression vector. WT and ASPN OE cells were seeded, grown to full confluency, cells were then cultured for 21 days in osteogenic medium to drive mineralisation of the cell monolayer. The osteogenic media contained BGP as previously discussed, which provides the phosphate necessary for the formation of hydroxyapatite the mineral component of the calcification of bone. In contrast to previous studies TGFβ supplementation was not used in order not to affect the endogenous levels of Asporin in the cultured cells[175]. No significant differences were observed between WT and OE at the same time points in any of the genes assessed (Figure 42).

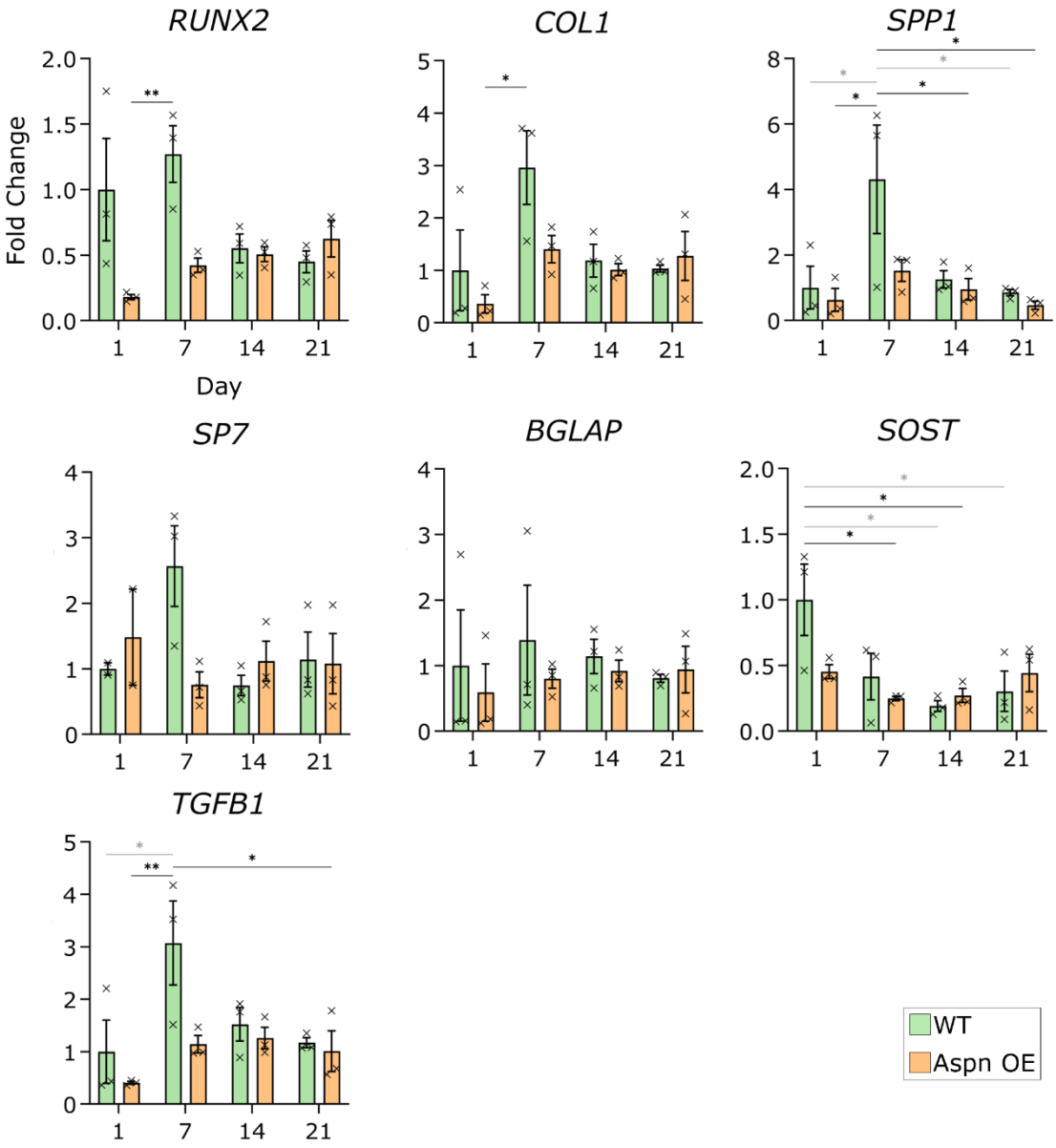

Figure 42. Osteogenic markers were assessed in U2OS cells overexpressing Asporin. *Osteogenic markers were assessed by rt-qPCR. Expression levels were normalised to 18s. 2-way ANOVA was carried out between WT and OE and across each timepoint, between WT and OE (Black *) and within the genotype between each time point (Grey *), (n=3) and denoted by *=p<0.05, **=p<0.01, ***=p<0.001. Error bars represent standard deviation.*

3.8 Discussion

Overexpression of Asporin resulted in the increased mineralisation of the ECM. *Runx2* expression was altered in all cells overexpressing Asporin, highlighting the role for Asporin in modulating *Runx2* in mouse cells. Upregulation of Runx2 is a hallmark of OA animal models and also in OA human cartilage samples. The current hypothesis for the role of Runx2 in OA is in the regulation of matrix degradation enzymes in the articular cartilage[176]. *Runx2* is involved in late stage chondrogenic differentiation and has been shown to regulate *Col10a1, Spp1* and *Mmp13* in chondrocytes and *Ihh* a regulator of chondrogenic differentiation is a reported downstream target of Runx2. The total ablation of Runx2 is embryonically lethal. However, in the study by Chen et. al., through using a mouse model with mutated Runx2, deleting exon 8, resulted in disrupted chondrocyte development and failed endochondral ossification[170]. In the mutated $Runx2^{\Delta E8/\Delta E8}$ mouse model expression of *Ihh* expression was significantly reduced[170].TGF-β has been reported to induce *Runx2* expression. RUNX2 is the master regulator of osteoblast differentiation. It is expressed by terminal chondrocytes, however it is not necessary for the vascular invasion, instead it is essential in the transdifferentiation of chondrocyte to osteoblasts.

Qin et. al. generated a mouse model of *Col10a1 cre* targeted ablation of *Runx2* to delete Runx2 specifically in hypertrophic chondrocytes[177]. Interestingly, the transdifferentiation of terminal chondrocytes to osteoblasts was significantly reduced and furthermore the apoptosis of hypertrophic chondrocytes was increased. In the embryonic and neonatal stages, the reduction of transdifferentiation affected trabecular bone formation[177]. Despite this, there was no difference to the trabecular bone formation at 6 and 20 weeks of age. Qin et. al. confirmed through cell lineage tracing the osteoblasts originating from the perichondrium/periosteum were responsible for the formation of normal trabecular bone post-birth[177]. In $Runx2^{-/-}$ null mice there was a total absence of perichondral osteoblasts, however in the conditional mice there

were perichondral osteoblasts and *Vegfa* expression in the perichondral osteoblasts was sufficient to vascularise the cartilage growth plate[18, 177].

In the *Col10a1 cre* targeted ablation of *β-catenin* in hypertrophic chondrocytes, transdifferentiation of chondrocytes to osteoblasts was reduced, reducing trabecular bone formation in embryonic development and furthermore the mice presented with increased bone resorption with an increase in the ratio of RANKL to OPG, driving osteoclastogenesis[178].

The increase in *Runx2*, essential for transdifferentiation and *Col1a1*, early transdifferentiating marker, the increase in expression at day 14 from day 1 in h*APSN* overexpressing ATDC5 (OE) cells that is not observed in the WT cells from day 1 to day 14, could be indicative of accelerated transdifferentiation in the h*APSN* overexpressing ATDC5 (OE) cells following the supplementation of mineralising media[177]. Moreover, the increased mineralisation in the OE ATDC5 cells could also indicate Asporin has a role in the mineralisation of cartilage. This could be due to the accelerated transdifferentiation and the ATDC5 adopting osteogenic properties, however it is also interesting to consider, as Kalamajski et. al. confirmed, Asporin is capable of mineralising type I collagen, the increase in mineralisation in the OE ATDC5 could be a combined result of the upregulation of type I collagen mRNA, with more type I collagen expected to be present and the abundance of Asporin, the mineralisation of the number of mineralised fibrils are increased and therefore increased Alizarin Red stain in the OE cell monolayers.

Most interestingly for these results is the increase in Mmp13 expression in the mineralising cartilage. In the presence of BGP, the mineralising ECM cells significantly upregulated the expression of *Mmp13*. MMP13 is the main matrix metalloproteinase, important for the turnover of the cartilage matrix for maintenance and for the infiltration of blood vessels along with osteoblasts and osteoclasts during the mineralisation of the matrix[23].

Mmp13 has been identified in OA cartilage for a pathogenic effect, increase Mmp13 drives the degeneration of the articular cartilage through the breakdown of type II collagen and aggrecan. The overexpression of Asporin upregulated Mmp13 may highlight a role of Asporin in the pathology of OA, through the dysregulation of the homeostasis of cartilage turnover.

Spp1 expression is upregulated in the mineralising OE cells at day 14 in comparison to day 1 WT cells, whereas this upregulation was not observed in the day 14 WT cells from day 1 WT cells. *Spp1* is an early marker of osteogenic differentiation and a driver of the mineralisation of the cartilage matrix. This is another likely contributing factor to the increased mineralisation of the cartilage observed in the mineralising OE cells.

The U2OS mineralisation experiments provide interesting preliminary data for the role of Asporin in osteogenic differentiation in bone cells, from day 1 to 7 *TGF-β1* expression increases in the WT cells that is not observed in the OE U2OS cells, however there is no significant difference in the expression of *TGF-β1* between OE and WT U2OS at any time point. However, interestingly RUNX2 and SP7 expression are trending toward being reduced at day 7 in the OE cells ($p=0.0521$ and $p=0.0853$). Osteoblast differentiation is regulated by RUNX2 expressed by endochondral bone and the perichondrium, RUNX2 induces SP7 expression, therefore the reduction of *SP7* expression may be a result of lack of induction due to reduced *RUNX2* expression[17]. However, this reduction in *RUNX2* expression is interesting as this is the opposite of what is observed in the OE ATDC5 both mineralising and non-mineralising chondrogenic cells. RUNX2 drives osteogenesis however there is no overt difference in the OE cells in comparison to the WT cells. There are limitations to the use of U2OS cells. They have similar transcriptional patterns to osteoblasts through differentiation[163]. However, they lack the capacity to mineralise, unlike other osteoblast cell lines such as SaOS2 cells. This difference is important as a very interesting feature of Asporin is the ability to mineralise type I collagen[123]. Future work, employing a different cell line such as SaOS2

would be interesting to assess whether Asporin modulates mineralisation of bone cells and whether the changes observed in the mineralisation of ATDC5 OE cells where calcium deposition was increased is upheld in bone cell mineralisation.

The chondrogenic cartilage experiments using the ATDC5 cells focused on the effect of Asporin overexpression on the stability and homeostasis of the ECM. The initial culturing of the cells for 6 days in the chondrogenic media initiates chondrogenesis and formation of the ECM. The following 21-day culture supplemented with ascorbic acid promotes cartilage ECM deposition and type II collagen production[164]. This experiment tested chondrogenesis without a mineralising stimulus (BGP).

Runx2 expression is also increased at day 7 and 14 in the h*ASPN* OE cells in comparison to the WT cells, the increase in Runx2 without the presence of BGP to drive mineralisation demonstrates this change to the Runx2 is a consistent effect of the overexpression of Runx2. As discussed Runx2 can drive the chondrogenesis of ATDC5[179]. Additionally, as Kalamajski et. al. demonstrated that Asporin and decorin compete for the binding of type I collagen, interestingly these data show the overexpression of h*ASPN* supresses decorin expression, this lack of decorin coupled with the abundance of Asporin would suggest there would be low competition to the Asporin-type I collagen interaction[123].

The significant reduction of sulphated proteoglycan in the chondrogenic cartilage experiments is surprising as there was no difference in the expression levels of the main cartilage proteoglycan aggrecan in the Asporin OE cells. In a study by Lee et. al. overexpressing Asporin in mice increased GAG production in the nuclear pulposus, the central portion of the IVD[180]. Type II collagen and aggrecan expression was increased by the overexpression and an increase in the phosphorylation of Smad2/3, this is indicative of increased Tgf-β signalling.

Interestingly, the overexpression of Asporin by vector rather than supplementation of recombinant Asporin supressed expression of decorin across all 21 days of culture, in the work by Kalamajski et. al. addition of recombinant hASPN did not inhibit decorin expression, however supplemental Asporin was a potent inhibitor of decorin-collagen binding [123]. This was very interesting to find as both Asporin and decorin compete for type I collagen binding, however Asporin is a more potent inhibitor of decorin-collagen interactions than decorin as an inhibitor of Asporin-collagen interactions[123]. Considering the increased Asporin and decreased decorin that is demonstrated in these experiments it can be hypothesised that Asporin will bind the majority of the type I collagen fibrils with extremely low levels of competition. Decorin is described as a physical linker in the ECM, with a key role in increasing the molecular adhesion of aggrecan-aggrecan and aggrecan-collagen II fibrils forming the aggrecan network of the ECM[181]. Decorin for this reason is important for the integrity of the aggrecan network of cartilage ECM. This process has been shown to modulate the ECM integrity with no direct effect on chondrocyte differentiation or the synthesis of aggrecan[181].

The significant reduction in decorin expression, can be predicted to reduce the integrity of the ECM and the formation of an aggrecan network. Alcian blue stains sulphated proteoglycan and aggrecan is the main constituent of cartilage ECM. The loss of Alcian blue staining may be a result of the loss of the network of aggrecan and not in fact as a result of modified chondrogenesis. Moreover, decorin is successfully stained by Alcian blue, the loss of Alcian blue may also be a result of the loss of decorin in the cells overexpressing Asporin.

Asporin-collagen interactions have been shown to be inhibited by decorin, without the presence of decorin, Asporin is able to bind collagen fibrils without competition. Asporin overexpressing cells had significantly increased Alizarin Red Staining, a semiquantitative method for assessing mineralisation. The binding of Asporin and its ability to mineralise collagen

fibrils, suggests that in the presence of BGP, the phosphate needed for formation of hydroxyapatite for mineralisation of cartilage Asporin will mineralise type I collagen, and compete with decorin to bind type I collagen[123]. With the suppression of decorin and overexpression of Asporin, the increase of mineralisation of the monolayer is a result of lack of competition in collagen fibril binding and in the presence of BGP the binding results in the mineralisation of the fibrils.

To further investigate this balance between Asporin and decorin it would be interesting to look at protein to protein interactions as it has been previously shown they compete for type I collagen binding[123]. Decorin could also be overexpressed in these cells to determine if there is a reciprocal effect of decorin overexpression supressing Asporin expression. It would be an opportunity to look in OA cartilage, to determine if there is a suppression of decorin *in vivo* and investigate if there is an impact of this suppression on OA progression and cartilage integrity. This could be carried out using IHC on OA-induced animal models sections and compare decorin expression.

Spp1 expression was low in the WT cells with expression peaking at day 21. Whereas *Spp1* expression is significantly increased in the chondrogenic OE ATDC5 cells at day 14. SPP1 has been found to be highly expressed in osteoarthritic cartilage and subchondral bone of OA patients[182]. This is an interesting result as the overexpression of h*ASPN* upregulated the expression of *Spp1,* as both Asporin and SPP1 have been shown separately to be highly expressed in OA cartilage it would be interesting to look at a connection between the two and whether there is a driving force or connected pathway between the two in the pathology of OA.

In chondrogenesis, hypertrophic chondrocytes begin to express drivers of osteogenic differentiation SP7, SOST, and BGLAP. Interestingly, in the OE cells *Sp7* and *Bglap* expression levels were all downregulated at day 21. This would indicate they are not reaching the hypertrophic stage[183]. Most interesting will be to focus on the effect on Sost in future work,

downregulation of *Sost* expression in the chondrogenic ATDC5 cells. SOST is expressed by osteocytes and in low levels by hypertrophic chondrocytes. Although by ANOVA analysis of the data there is no significant difference observed, in Student t-test of WT vs OE at each time point this preliminary data indicates in the OE cells, *Sost* expression is significantly decreased at day 21 compared to the WT cells, whereas the WT cells peak in *Sost* expression at day 21. SOST is a negative regulator of bone formation, expressed primarily by osteocytes in the regulation of bone resorption, increased SOST has been shown by Jiao et. al. to supress β-catenin and increase the RANKL/OPG ratio, promoting osteoclastogenesis[184]. SOST suppression was also shown to increase bone density and bone volume and OPG expression was increased, inhibiting bone resorption[184]. Suppression of *Sost* expression was observed in the chondrogenic OE cells and the decrease in *Sost* expression at from day 1 to day 7 of the mineralising OE ATDC5 cells.

This finding is very interesting when considered with the increase in mineralisation of the monolayer. To explore this further, OPG/RANKL ratio was assessed. There was a significant increase in the expression of *Opg* in the chondrogenic OE cells at day 14 in comparison to the WT cells. Furthermore, *Opg* expression is increased in the mineralising OE cells from day 1 to 14 and from day 7 to 14. This has highlighted an interesting effect of the overexpression of Asporin modulating the SOST and OPG pathway. With increased OPG expression, OPG acts as a decoy to the RANKL receptor, this blocks the receptor and inhibits osteoclastogenesis and consequently bone resorption[35].

Endogenous mouse Asporin was low in the ATDC5 cells with no difference in the expression between WT and OE cells, this could be indicative that there is no positive feedback signalling from the human Asporin overexpression on mouse Asporin in these cells. There was no significant difference between the mouse Asporin levels and the human Asporin expression in the WT cells. This is due to the very low expression

levels of both human and mouse Asporin in WT ATDC5 cells, as the human primers target a region present in only the human Asporin sequence.

U2OS cells were studied frequently in osteogenic differentiation experiments as an early osteogenic cell line with fibroblast morphology, this was used to look mimic initial differentiation of osteoblasts from MSCs. However, work has been carried out to show that U2OS is not necessarily the best cell line to model mineralisation and osteogenic differentiation. If repeated, using SaOS2 cell line would be preferred as this has been shown to have a more similar differentiation pathway and gene expression panel to that of classic osteogenic differentiation in development[163].

ATDC5 cells are a robust cell line frequently used in cartilage modelling due to their capacity to be driven through chondrogenic differentiation ad their potential to be mineralised[162, 164]. However, in assessing gene changes through qPCR of the WT cells they do not follow the expected trend of cells undergoing chondrogenesis. It would be expected for there to be minimal expression of type X collagen at the start of chondrogenesis which would then increase significantly after 14 days of culture and increase further by day 21[164]. However, in chondrogenic ATDC5 cells (Figure 39) there was no significant difference in type X collagen expression across the time points. Furthermore, there was a lot of variability between the samples in the qPCR data particularly in the *Sox9* expression data at day 14 (Figure 39). *Sox9* is the master regulator of chondrogenesis, cells undergoing chondrogenesis would have an early and significant expression of *Sox9* at day 1 and day 7, this was not observed across the time points, the variability in the data points poses concern for whether the cells are in fact undergoing chondrogenesis. Another, repeat of the chondrogenesis in WT ATDC5 would be beneficial to make sure the cells are capable of chondrogenesis, these were a late passage and therefore the possibility they have lost differentiation capability.

Chapter 4. Asporin knockout in cartilage

4.1 Introduction

Upregulation of Asporin has been implicated in the pathobiology of osteoarthritis. In order to understand the role of Asporin in ageing and degenerative disease, it is first essential to look at its role in cartilage development. As previously discussed in Chapter 3, the overexpression of Asporin was shown to modulate mineralisation in bone and cartilage cells. In the context of development, the epiphyseal growth plate is the main regulator of the skeletal growth. This chapter describes the study of the growth plate and the longitudinal bone growth in Asporin wild type (C57BL/6 colony) and Asporin null (C57BL/6 $ASPN^{-/-}$ colony) mice in order to obtain an overall picture of the role of Asporin in cartilage development. The development of the articular cartilage was also studied to investigate potential developmental changes that might shed light on the role of Asporin in Osteoarthritis.

Chapter aims:

- To confirm the global knockout of Asporin and the conditional knockout of Asporin under the type II collagen promoter in cartilage specific knockout mice (generated by Dr Francesca Brito and described in the Methods chapter) using protein was extracted from skin, tail tips and the xiphoid cartilage.
- To assess the effect of the global and cartilage-specific deletion of Asporin on hyaline cartilage (articular and growth plate) morphology, expression of key molecules, cartilage proliferation and apoptosis, and endochondral ossification.

4.2 Western blotting confirmed global knockout of Asporin.

For the confirmation of global knockout of Asporin skin tissue and tail tip were collected, and protein extracted, 30 ng of protein was electrophoretically resolved. SDS-PAGE gel electrophoresis followed by Western blotting for Asporin and GAPDH loading control confirmed knockout of Asporin in all tissues of the global knockout (Figure 43).

The conditional knockout of Asporin" was developed using mice expressing *Cre* recombinase under the type II collagen, with the aim of creating a mouse line with a cartilage specific knockout of Asporin. The conditional allele contains loxP sites that flank exon 4 of Asporin deletion of which would lead to a frame shift and production of non-functional protein. Asporin was detected in the ear notch samples of Col2Cre KO mice, likely because there was skin present in the sample. It was also detected in the tail tip sample and in the skin samples from the Col2Cre KO mice. However, in the cleaned xiphoid, which is exclusively made up of cartilage and perichondrium, Asporin was not detected in the samples collected from Col2cre knockout mice. Genotyping was used to confirm the Cre floxed Asporin null mice using primers detailed in 2.6.2.

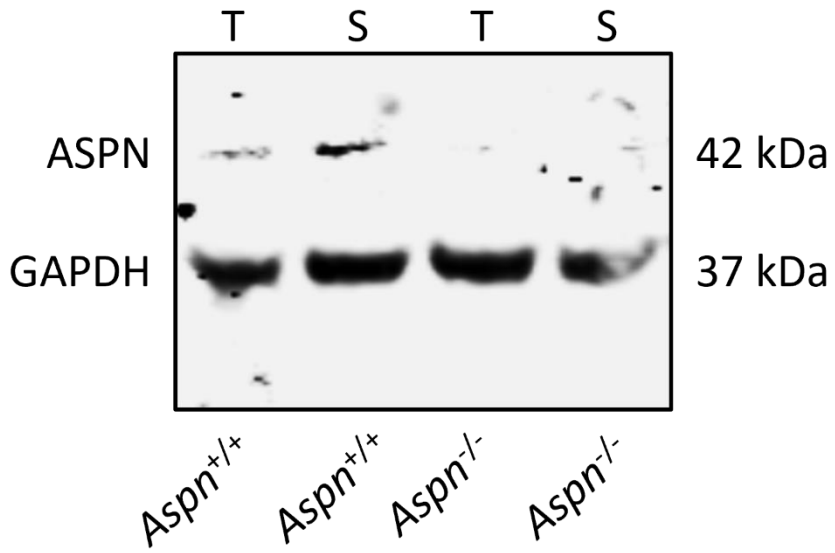

Figure 43. Western blotting confirms successful global knockout of Asporin. *Asporin is not present in any tissue of the global knockout mouse (KO). Asporin is present in all tissues of the conditional knockout mouse (cKO) except for the xiphoid made of exclusively cartilage. ASPN (Asporin) 42 kDa, and GAPDH 37 kDa was also probed to confirm equal loading of proteins. T (tail tip), S (skin). Tissues were collected at 3-weeks of age. N = 3 per genotype.*

4.3 Endogenous expression of Asporin and confirmation of global knockout of Asporin.

To determine the localisation of the wild type Asporin and to further confirm the of global deletion of Asporin, immunohistochemical staining of three-week old tibial growth plates was performed.

Wild type Asporin was detected in the bone of the secondary ossification centre and in the perichondrium and was confirmed to be absent in the global knockout (KO) tibia (Figure 44). Moreover, it was not present in the articular cartilage at 3 weeks of age, further confirming the low levels of Asporin expression in the developing and healthy articular cartilage that was reported in the human samples.

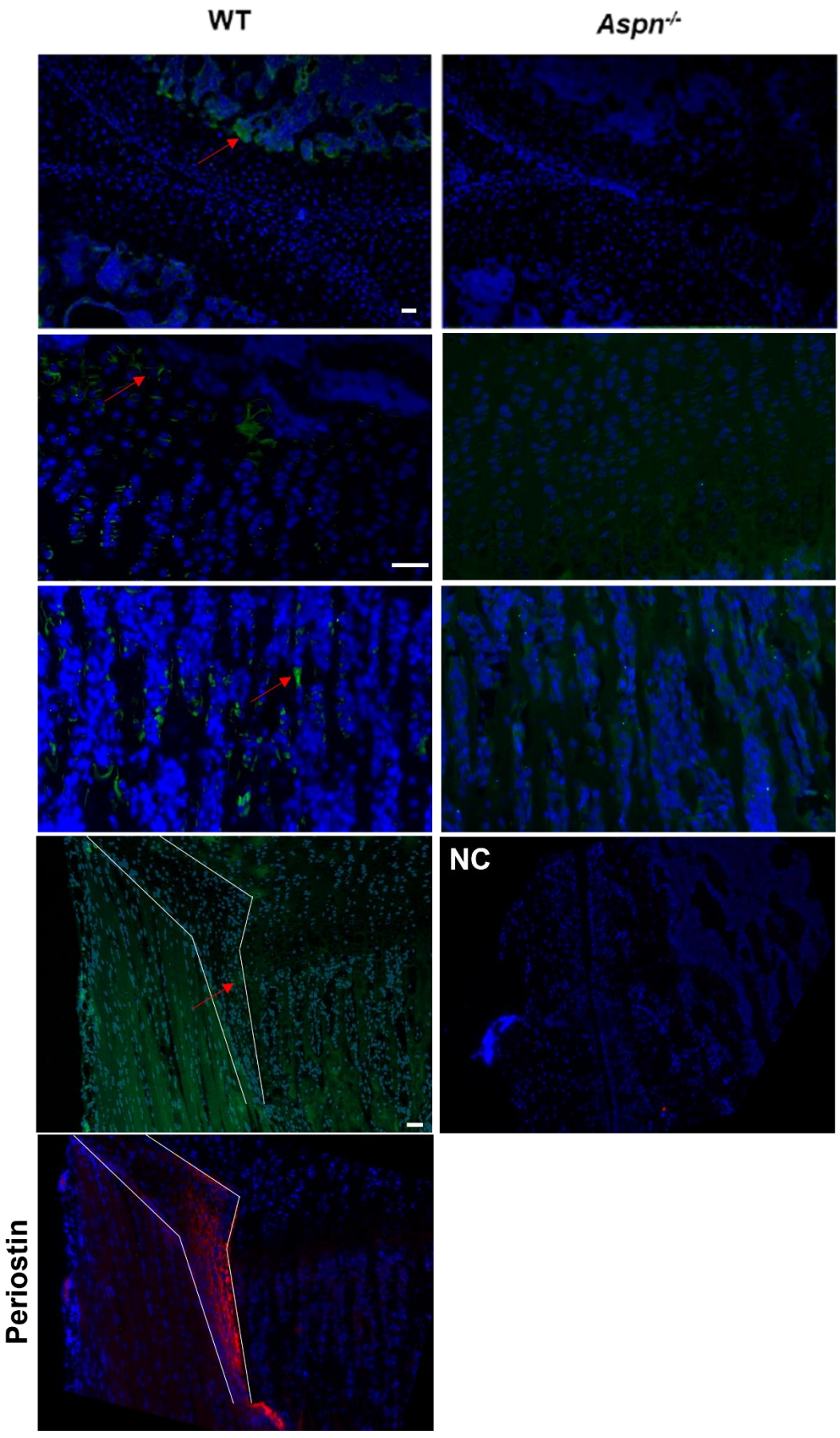
WT
Aspn-/-
NC
Periostin

Figure 44. Endogenous Asporin is localised to the secondary ossification centre, the calcification zone and the periosteum*. Immunohistochemistry to visualise the expression of Asporin in the tibial growth plate and articular cartilage of knee joints of 3 week old mice. Periostin IHC to localise periosteum to verify Asporin expression in the periosteum. Key: blue fluorescence - DAPI counterstain of nuclei, green fluorescence – Asporin staining, with red arrows to highlight examples of Asporin expression, red fluorescence – periostin staining, protein expressed in the periosteum. White border highlights the periosteum on the section. NC – Negative Control. Scale bar 100 µm.*

4.4 Role of Asporin in the 3 week old growth plate.

4.4.1 Loss of Asporin has no effect on early skeletal development.

To assess overall skeletal changes in early development of Asporin KO mice, whole skeletal preparations of wild type and knockout mice were performed at postnatal day 2 (P2). The staining with Alcian blue (detecting proteoglycans) and Alizarin red (binding calcium) allows for the distinction of bone and cartilage in developing skeletons.

There were no observable differences in the amount of cartilage detected at the ends of the long bones, bowing of the legs or overall morphology of individual skeletal elements. Measuring of the long bones showed no difference in the size of the mice as a result of the loss of Asporin (Figure 45).

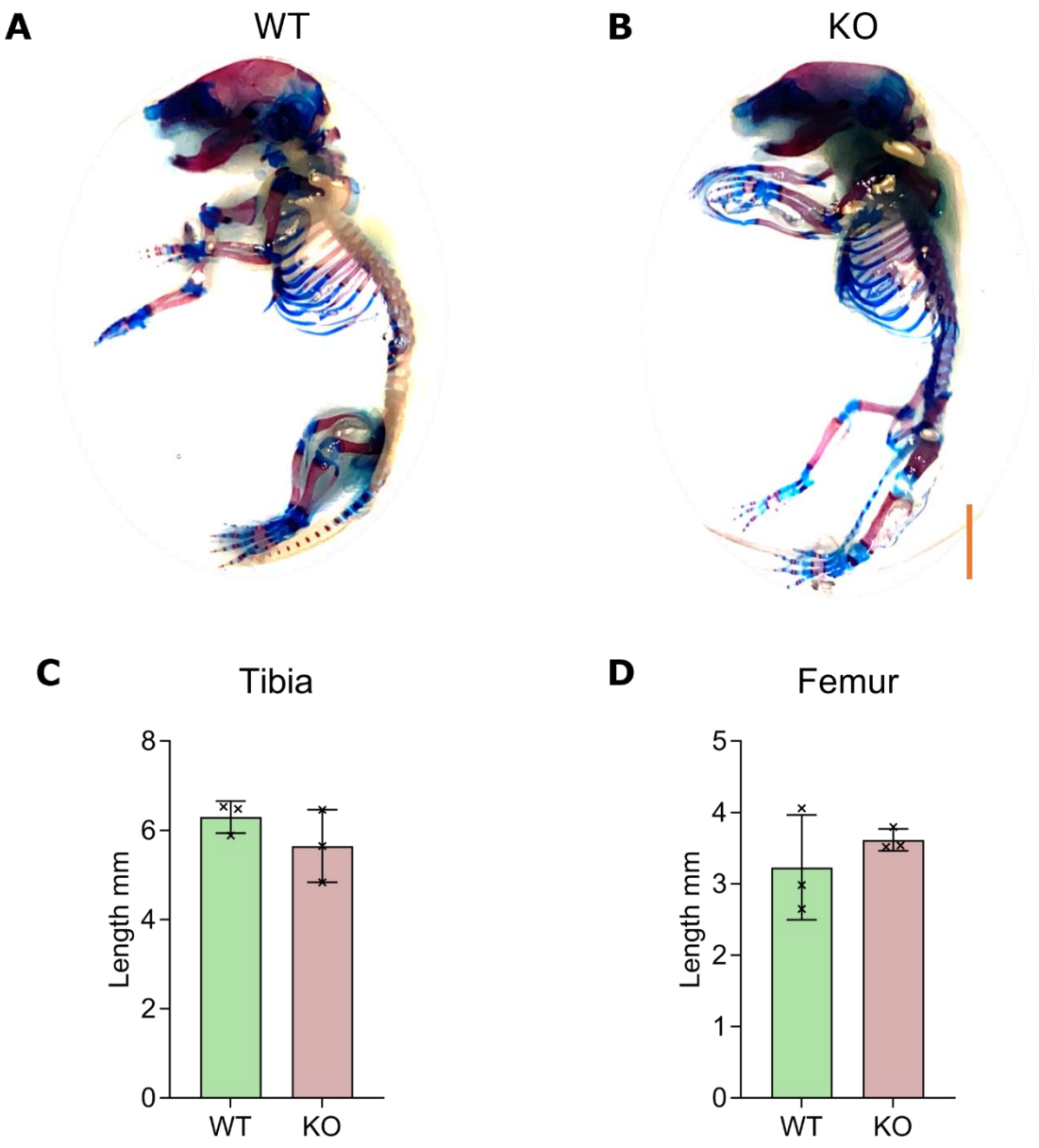

Figure 45. Global knockout of Asporin has no effect on overall skeletal development. *Whole P2 skeletons of wild type (WT) (**A**) and global Asporin knockout (KO) (**B**) mice were stained with Alcian blue and Alizarin red to visualise bone and cartilage in the developing skeleton. There were no differences in the length of the tibia (**C**) and the femur (**D**) of the mice. Student t-test were carried out between WT and KO (n=5) and denoted by *=p<0.05.Error bars represent standard deviation. Scale bar 0.5 cm.*

4.4.2 Loss of Asporin has no effect on longitudinal bone growth (endochondral ossification).

To study the effect of the loss of Asporin on bone development, both endochondral and intramembranous ossification were assessed using longitudinal bone measurements. Mice were X-Rayed at 3, 6, 9 and 12 weeks of age. Each set of measurements was key for the assessment of skeletal growth, long bone measurements of the femur and tibia were used to investigate differences in endochondral ossification. Inner canthal distance (ICD) measurement in the skull was used to investigate the intramembranous ossification. Skull lengths, determined by a combination of endochondral and intramembranous ossification, we also measured. A common feature in mouse models of skeletal dysplasia is a hip dysplasia where the hip bone is flared, therefore the angle of the hip flare was also measured.

Endochondral ossification was unaffected by the loss of Asporin. There was no significant difference in long bone measurements of the tibia or femur in the global Asporin knockout and wild type mice, nor the conditional Col2Cre Asporin knockout and conditional wild type mice at any of the ages (Figure 46 & 47). The angle of the hip flare was not significantly different in the global and conditional knockout of Asporin mice in comparison to the relative wild type controls, indicating that there is no hip dysplasia phenotype in the Asporin knockout (KO) and Col2Cre Asporin knockout (cKO) mice.

Moreover, intramembranous ossification was also not affected by the loss of Asporin. There was no significant difference in the global Asporin knockout and wild type mice, nor the conditional Col2Cre Asporin knockout and conditional wild type mice in the inner canthal distance or skull length in any of the ages that were investigated.

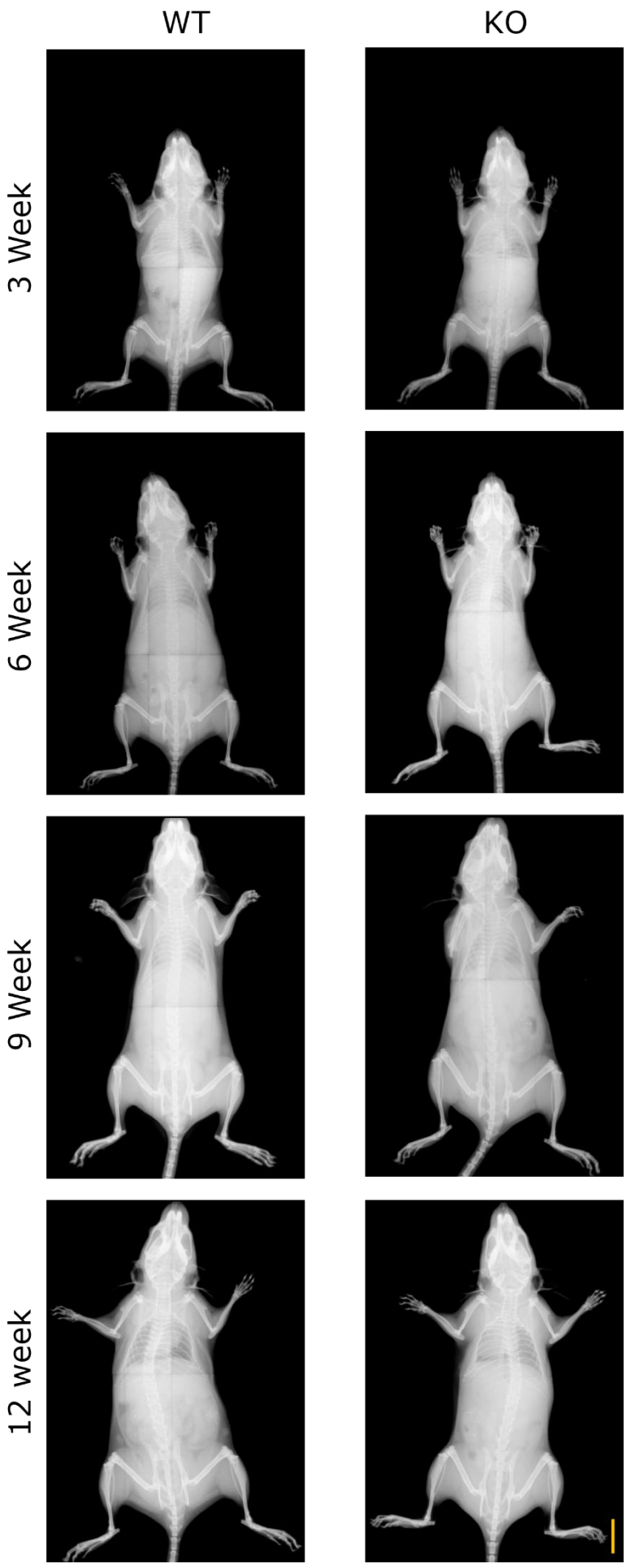
WT
KO
3 Week
6 Week
9 Week
12 week

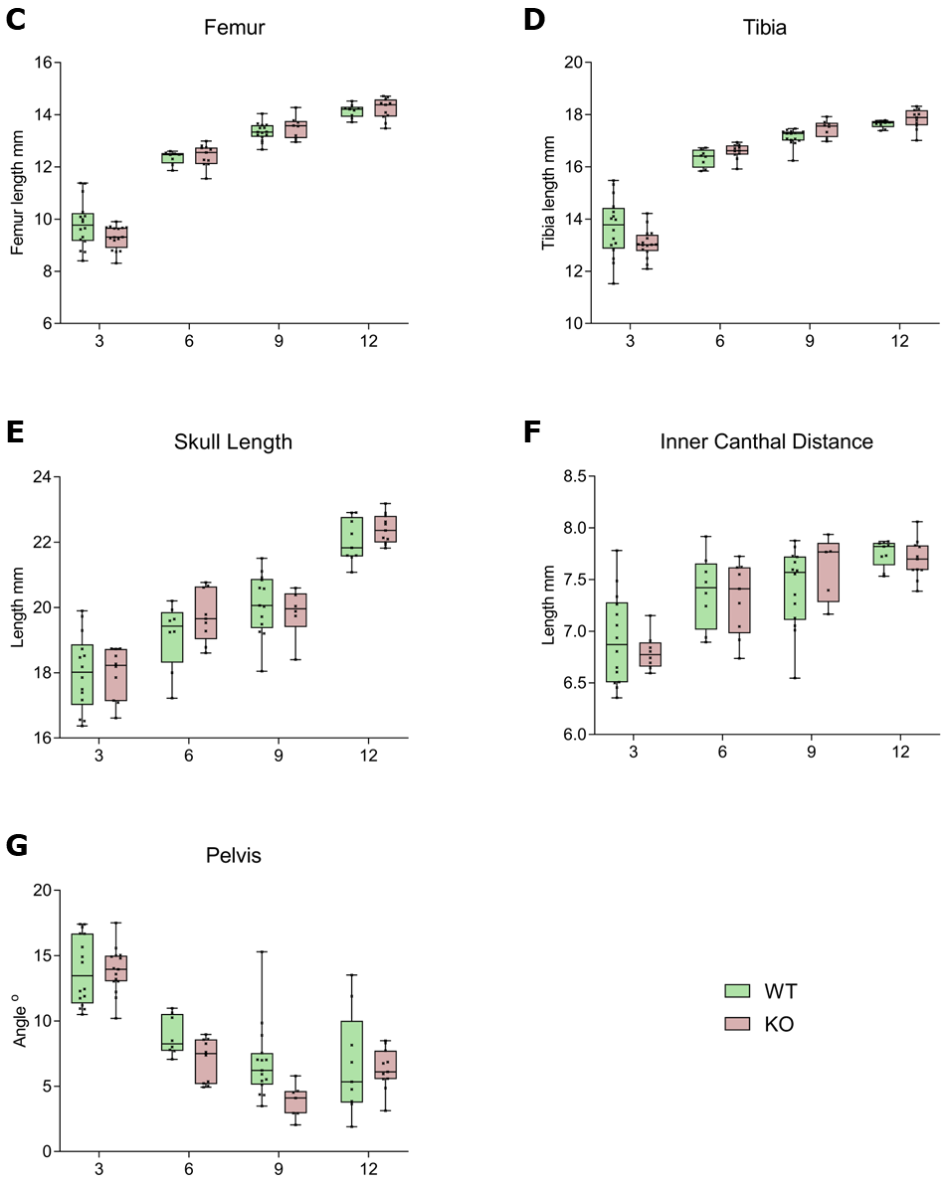

Figure 46. Global loss of Asporin has no effect on endochondral or intramembranous ossification measurements. *Asporin null mice did not appear to be different in size in comparison to the wild type mice. Representative X-Ray images of wild type (**A**) and Asporin null (**B**) mice, at 3, 6,9 and 12 weeks. Mice were X-rayed and measured using femur and tibia lengths to determine differences in endochondral ossification and skull length and inner canthal distance (ICD) to determine differences in intramembranous ossification. Asporin null mice showed no difference to the wild type mice at any time point in the length of the femur (**C**), tibia (**D**), skull length (**E**) and ICD (**F**). To determine the presence of a hip dysplasia the angle of the hip bone was measured, there was no difference in the angle indicating there was no hip dysplasia in the global knockout (**G**). Student t-test were carried out between WT and KO (n = number of x on the graph) and*

*denoted by *=p<0.05.Error bars represent min to max. Scale bar 1 cm.*

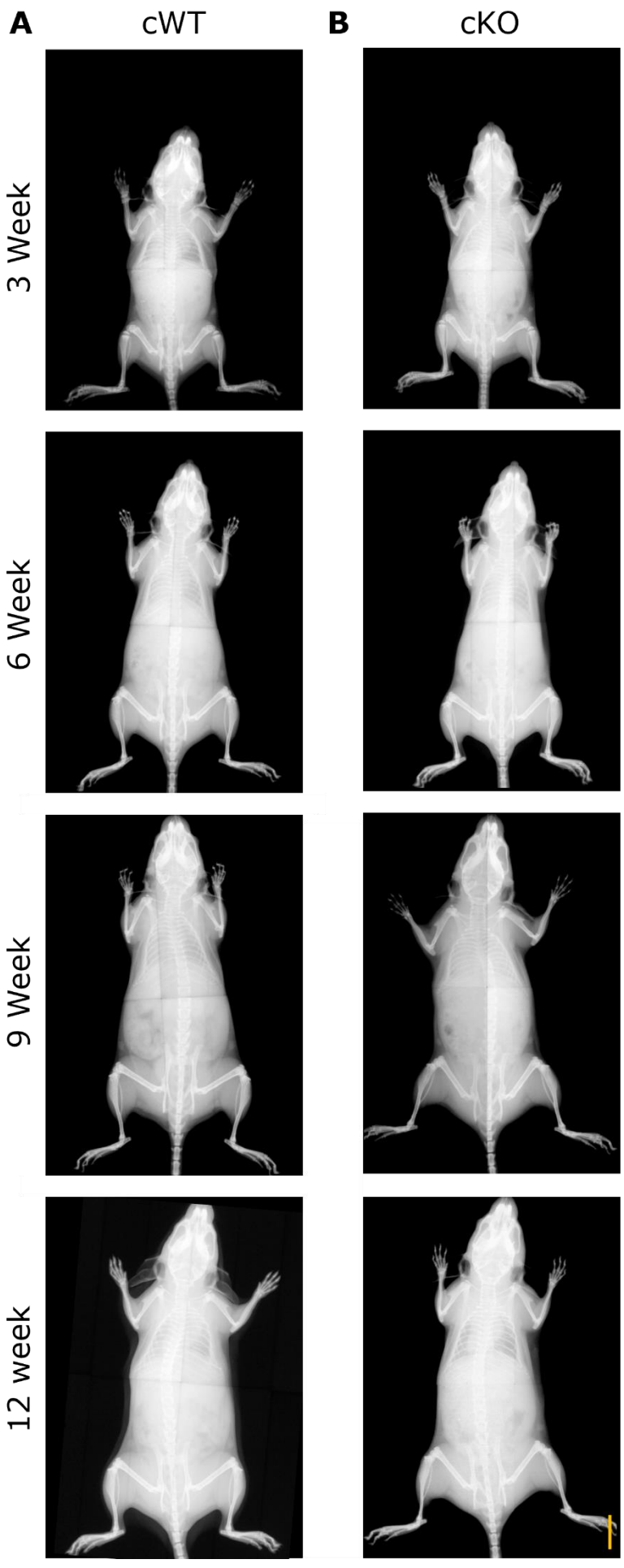
A
cWT
B
cKO
3 Week
6 Week
9 Week
12 week

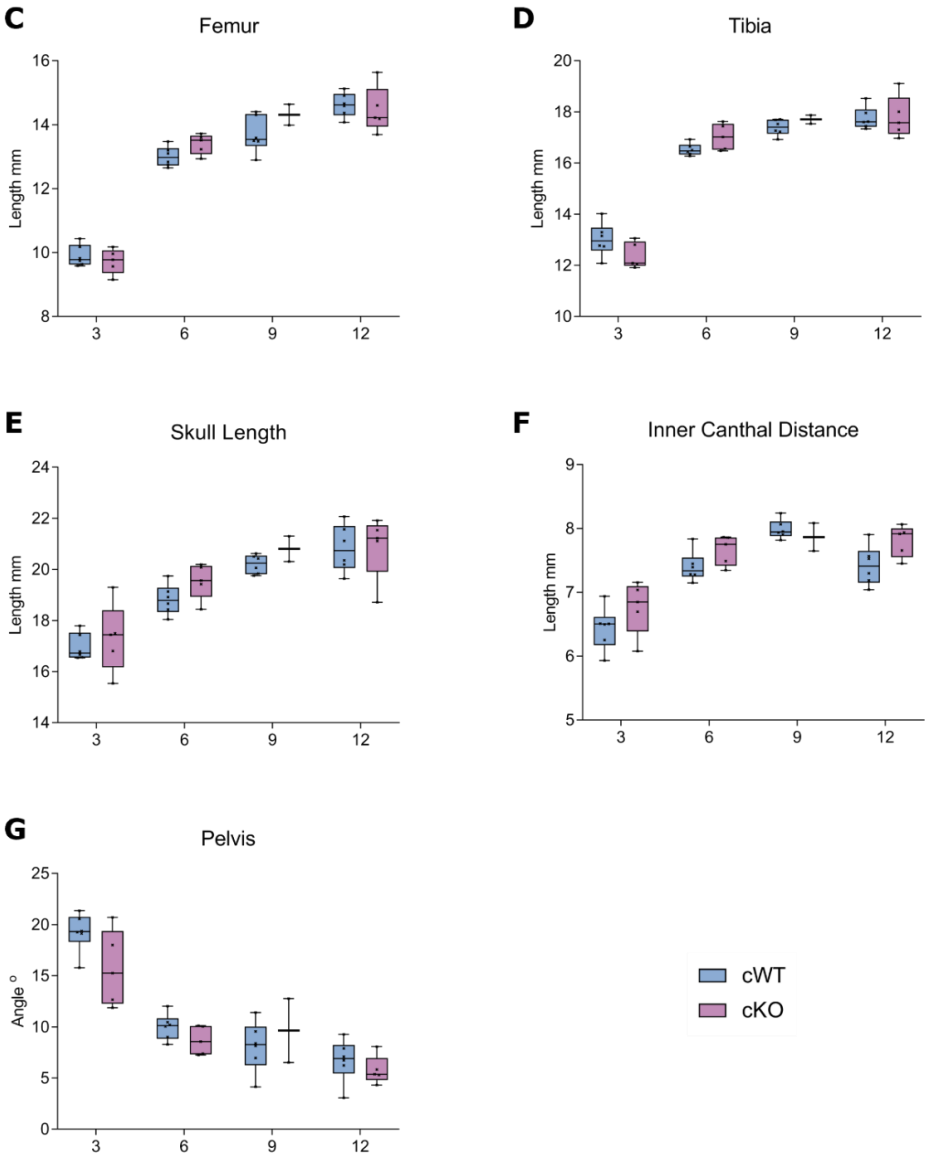

Figure 47. Conditional loss of Asporin has no effect on endochondral or intramembranous ossification measurements. *Col2cre Asporin knockout mice did not appear to be different in size in comparison to the conditional wild type mice. Representative X-Ray images of conditional wild type (**A**) and Col2cre Asporin knockout (**B**) mice, at 3, 6,9 and 12 weeks. Mice were X-rayed and measured using femur and tibia lengths to determine differences in endochondral ossification and skull length and inner canthal distance (ICD) to determine differences in intramembranous ossification. Col2cre Asporin knockout mice showed no difference to the conditional wild type mice at any time point in the length of the femur (**C**), tibia (**D**), skull length (**E**) and ICD (**F**). To determine the presence of a hip dysplasia the angle of the hip bone was measured, there was no difference in the angle indicating there was no hip dysplasia in the global knockout (**G**). Student t-test were carried out between cWT and cKO (n = number*

*of x on the graph) and denoted by *=p<0.05. Error bars represent min to max. Scale bar 1 cm.*

4.4.3 The morphology of the cartilage growth plates of global and conditional knockout mice is not affected by the deletion of Asporin.

To investigate characteristics of the cartilage growth plate Toluidine blue staining carried out on 3-week paraformaldehyde fixed hind-limb sections to assess the sulphated proteoglycan deposition in the growth plate. Sulphated proteoglycans are core proteins with long chains of glycosaminoglycans attached (GAGs) such as aggrecan, that contribute to the strength and integrity of the extracellular matrix of the cartilage growth plate[41]. The concentration of sulphated proteoglycans is low in the proliferative zone and very high in the hypertrophic zone where chondrocytes increase synthesis of proteoglycans expanding the cartilage matrix[41]. As discovered in Chapter 3, the overexpression of Asporin was found to decrease in the proteoglycan deposition in developing cartilage constructs, it was interesting to assess if there was a change as a result of the loss of Asporin.

However, the global Asporin knockout tibia showed proteoglycan deposition similar to that of the wild type controls at 3 weeks of age. Equally, in the Col2Cre conditional Asporin knockout the sulphated proteoglycan deposition was similar to that of the conditional wild type control (Figure 48). There was no difference in the organisation of the growth plate zones between the wild type and global Asporin knockout tibia growth plate. Equally there was no difference between the conditional wild type and the Col2cre conditional Asporin knockout (Figure 48).

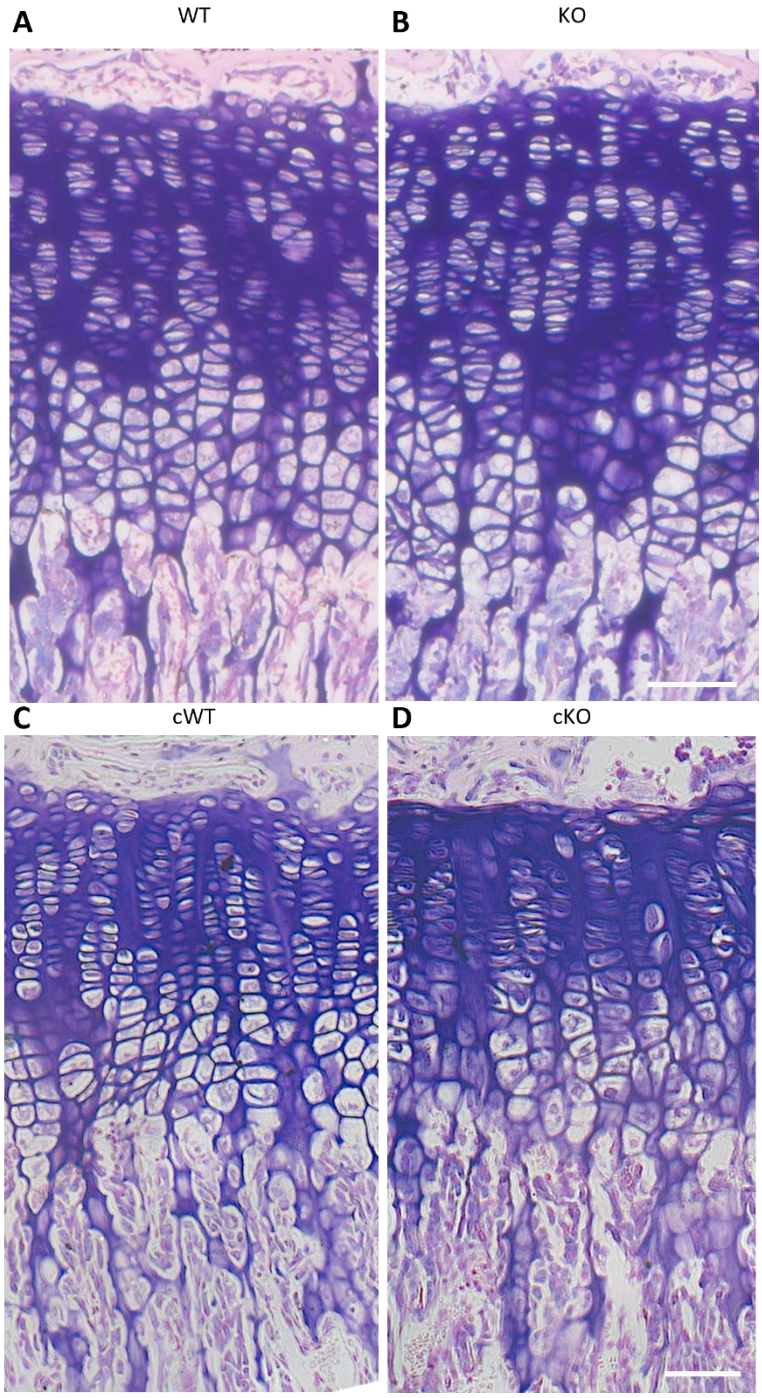

Figure 48. Toluidine blue staining shows no difference in proteoglycan deposition. *Toluidine blue staining to visualise proteoglycan deposition in the cartilage growth plate, shows no observable difference to the deposition of proteoglycan or the organisation of the growth plate zones in the global knockout (**A**) relative to the wild type (**B**) or in the Col2cre conditional Asporin knockout (**C**) relative to the conditional wildtype (**D**). Scale bar 100 µm.*

4.4.4 Loss of Asporin does not affect type II and type X collagen expression and localisation in the growth plate.

To determine the effect of global and conditional deletion of Asporin on the deposition of key ECM molecules, Type II and Type X collagen, immunohistochemical staining of three-week old tibial growth plates was performed.

Type II collagen is the main structural collagen of the growth plate and the key component of hyaline cartilage[185], and involved in the signalling pathway regulating chondrocyte proliferation and differentiation within the growth plate. Type II collagen is expressed by resting and proliferative chondrocytes, in parallel with aggrecan, forming the ECM, crucial for the structure of the growth plate. Type II collagen disorders are a diverse group of disorders, including severe skeletal dysplasias, achondrogenesis type II and hypochondrogenesis and mild skeletal dysplasias such as mild spondyloephiphyseal dysplasia (SED), where mutations result in disruption in the synthesis and/or the organisation of type II collagen[186]. Changes to type II collagen can result in ECM abnormalities including under-sulphation of proteoglycans[186].

The localisation of type II collagen was undisrupted in the global knockout growth plate cartilage (Figure 49), the expression was comparable to that of the wild type. Similarly, the conditional Col2Cre knockout of Asporin also showed type II collagen expression comparable to that of the conditional wild type (Figure 49). The expression of type II collagen in the conditional wild type highlights the regions targeted by the Asporin knockout.

Type X collagen, is a marker of hypertrophic chondrocytes, Type X collagen mutations is implicated in Metaphyseal chondrodysplasia, Schmid type, the mutation results in ER stress in the chondrocytes of the growth plate disrupting hypertrophic chondrocyte differentiation, consequently long

bone growth is disrupted and individuals present with short limbed dwarfism[186, 187].

The localisation and expression of type X collagen was normal in the global knockout tibiae and in the col2cre conditional Asporin mouse relative to the respective wild-types.

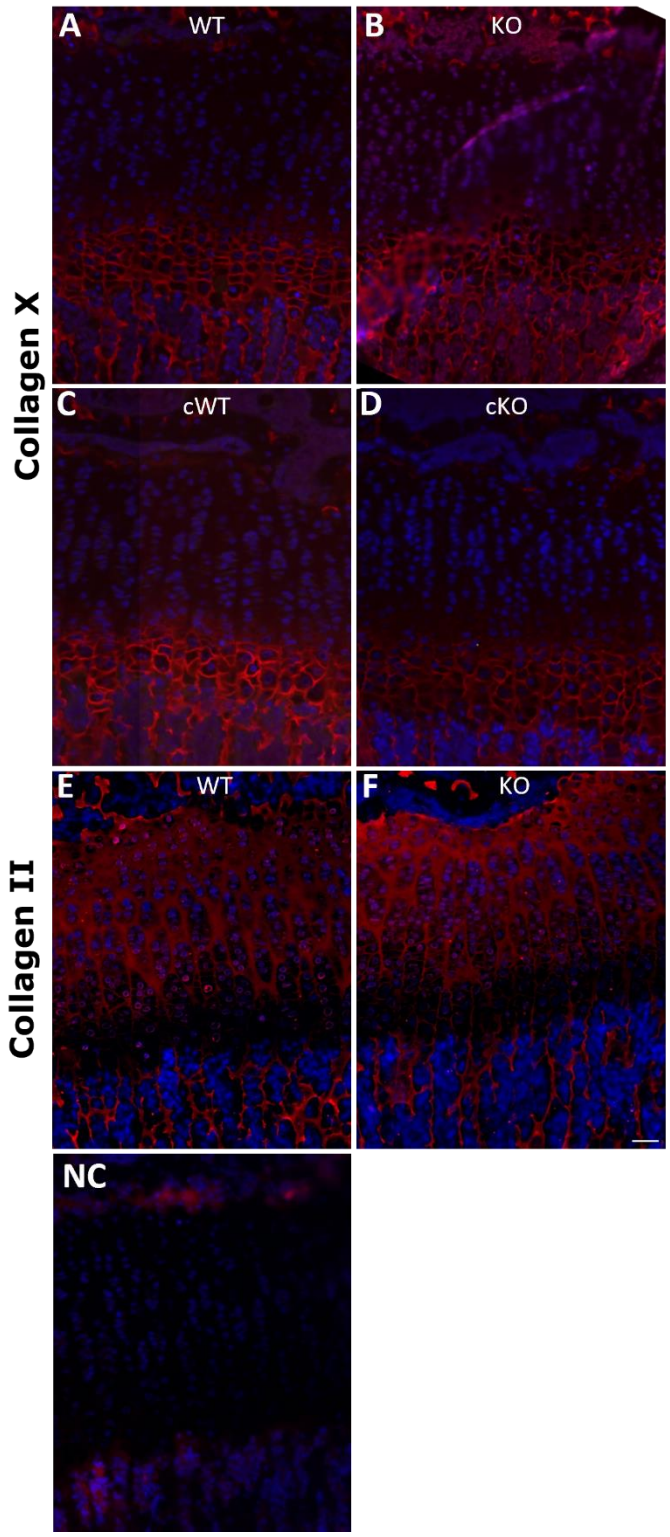

Figure 49. Type X collagen and type II collagen expression and localisation in the cartilage growth plate is not affected by the loss of Asporin. *Type X collagen and type II collagen IHC on 3 week old mice tibiae determined there was no difference in the expression or localisation of type X collagen in*

*the cartilage growth plate in the global knockout (**B**) relative to the WT (**A**) or in the conditional Asporin knockout (**C**) relative to the conditional wild type (**D**).Additionaly, there was no difference in the expression or localisation of type II collagen in the cartilage growth plate in the global knockout (**F**) relative to the WT (**E**). n=3 per genotype. Key: blue fluorescence - DAPI counterstain of nuclei, red fluorescence A, B, C and D - type X collagen staining, red fluorescence E and F – type II collagen staining. NC – Negative Control, some red fluorescence observed due to chondrocytes auto fluoresce red. Scale bar 100 μm.*

4.4.5 Global loss of Asporin has no effect on proliferation and apoptosis in the growth plate.

To assess proliferation and apoptosis in the growth plate, Ki67 and TUNEL (terminal deoxynucleotidyl transferase dUTP nick end labelling) assays are used to quantify these processes respectively.

Ki67 is a nuclear protein expressed in active phases of the cell cycle, however in resting cells in the G growth phase it is not present, this allows for the identification of proliferating cells. Immunohistochemistry for Ki67 was performed on 3-week paraffin embedded tibia sections to measure proliferation in the growth plate. Ki67 positive cells were counted and expressed as a percentage of the total cell number of cells stained with DAPI nuclear counterstain.

No difference was found in the quantification of Ki67-positive cells, in the global Asporin knockout relative to the wild type in the growth plate.

During apoptosis, DNA is broken down, fragmented, along with the degradation of proteins, cell structures and the overall breakdown of the cell. The TUNEL assay exploits the exposed the fragmented DNA ends in apoptotic cells to allow for quantification of apoptosis. In the TUNEL assay, fluorescently labelled dUTP bind to the fragmented ends of the DNA, labelling the fragment, this allows for the identification of apoptotic cells, TUNEL-positive cells[188]. This was performed on 3-week paraffin embedded tibia sections to measure apoptosis in the growth plate and vascular invasion front and the TUNEL positive cells were expressed as a percentage of total number of cells stained by DAPI nuclear counterstain.

As expected, the majority of cell death occurred at the vascular invasion front (Figure 50) in the wild type and KO cartilage growth plates. No difference was found in the quantification of TUNEL-positive cells, in the global Asporin knockout relative to the wild type in the growth plate and the vascular invasion front.

The combined use of these two experiments gives complementary information on the balance of proliferation and apoptosis in the growth plate. Both processes are tightly regulated as discussed in chapter 1 to ensure proper growth plate formation and function and therefore proper endochondral ossification.

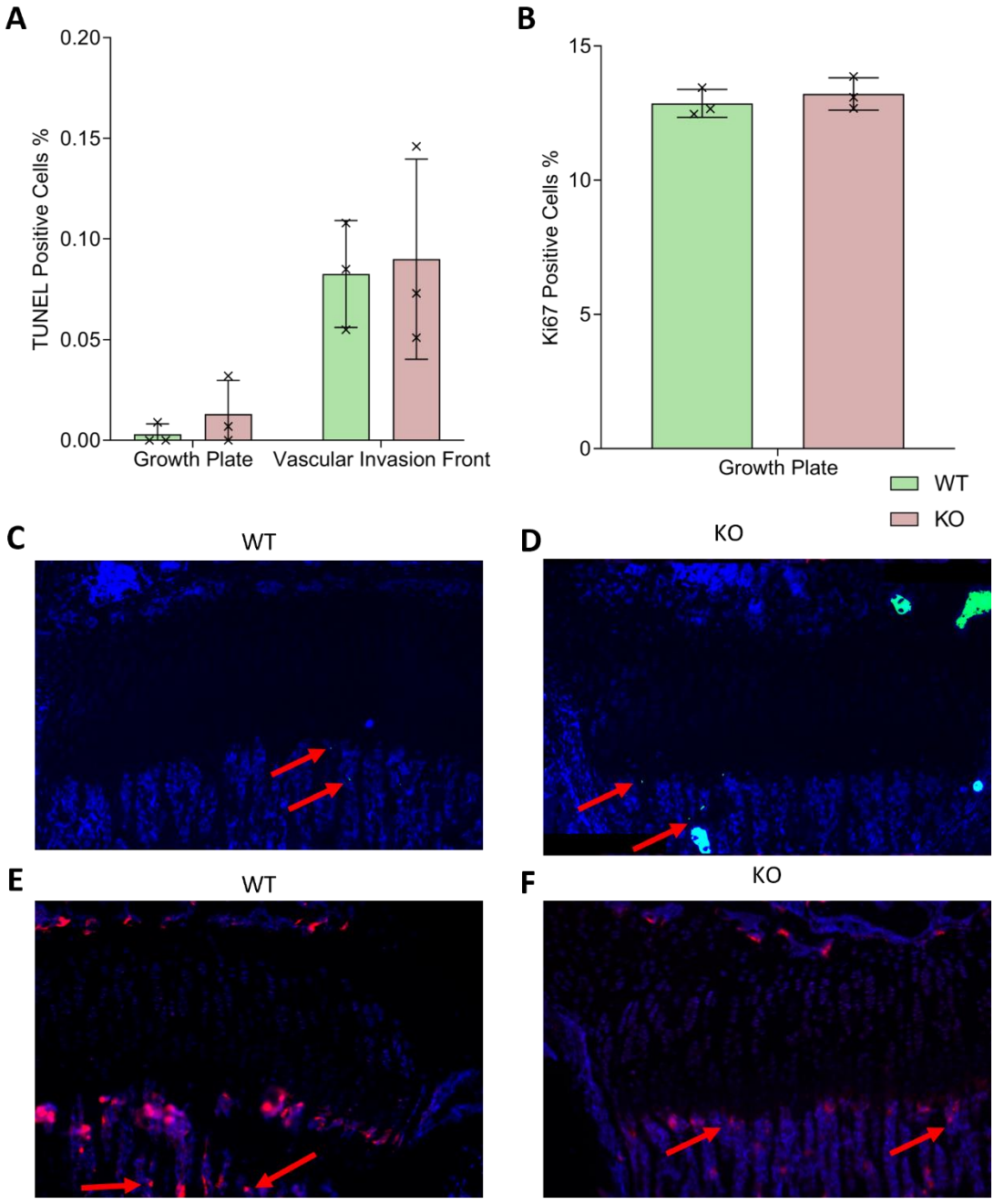

Figure 50. Global loss of Asporin does not affect apoptosis or proliferation in 3 week old tibiae. *Quantification of TUNEL assay determined there was no difference in apoptosis of cells in the growth plate and the vascular invasion front in the global Asporin knockout relative to the wild type (**A**). Quantification of Ki67 immunohistochemistry determined there was no difference in Ki67 positive cells in the growth plate of the global Asporin knockout relative to the wild type (**B**). Error bars represent Standard deviation. 3 Sections per tibiae, 3 per genotype (n=3).*

*Representative images of TUNEL IHC assay in WT (**C**) and KO (**D**) tibiae. Representative images of Ki67 IHC in WT (**E**) and KO (**F**) tibiae. Key: blue fluorescence - DAPI counterstain of nuclei, green fluorescence – TUNEL staining, with red arrows to highlight examples of TUNEL positive cells, red fluorescence – Ki67 staining, with red arrows to highlight examples of Ki67 positive cells.*

4.5 Role of Asporin in 3 week old articular cartilage.

4.5.1 The morphology of the articular cartilage of global and conditional knockout mice is not affected by the deletion of Asporin.

jThe changes to the sulphated proteoglycan deposition as a result of overexpression of Asporin in Chapter 3. The global ablation of Asporin and the cartilage specific knockout of Asporin is interesting to assess if Asporin is involved in sulphated proteoglycan deposition or whether it is only the overexpression that can modulate the deposition.

However, the global Asporin knockout articular cartilage showed proteoglycan deposition similar to that of the wild type controls at 3 weeks of age. Equally, in the Col2Cre conditional Asporin knockout the sulphated proteoglycan deposition was similar to that of the conditional wild type control (Figure 51). There was no difference in the organisation of the articular cartilage between the wild type and global Asporin knockout tibia growth plate. Equally there was no difference between the conditional wild type and the Col2cre conditional Asporin knockout (Figure 51).

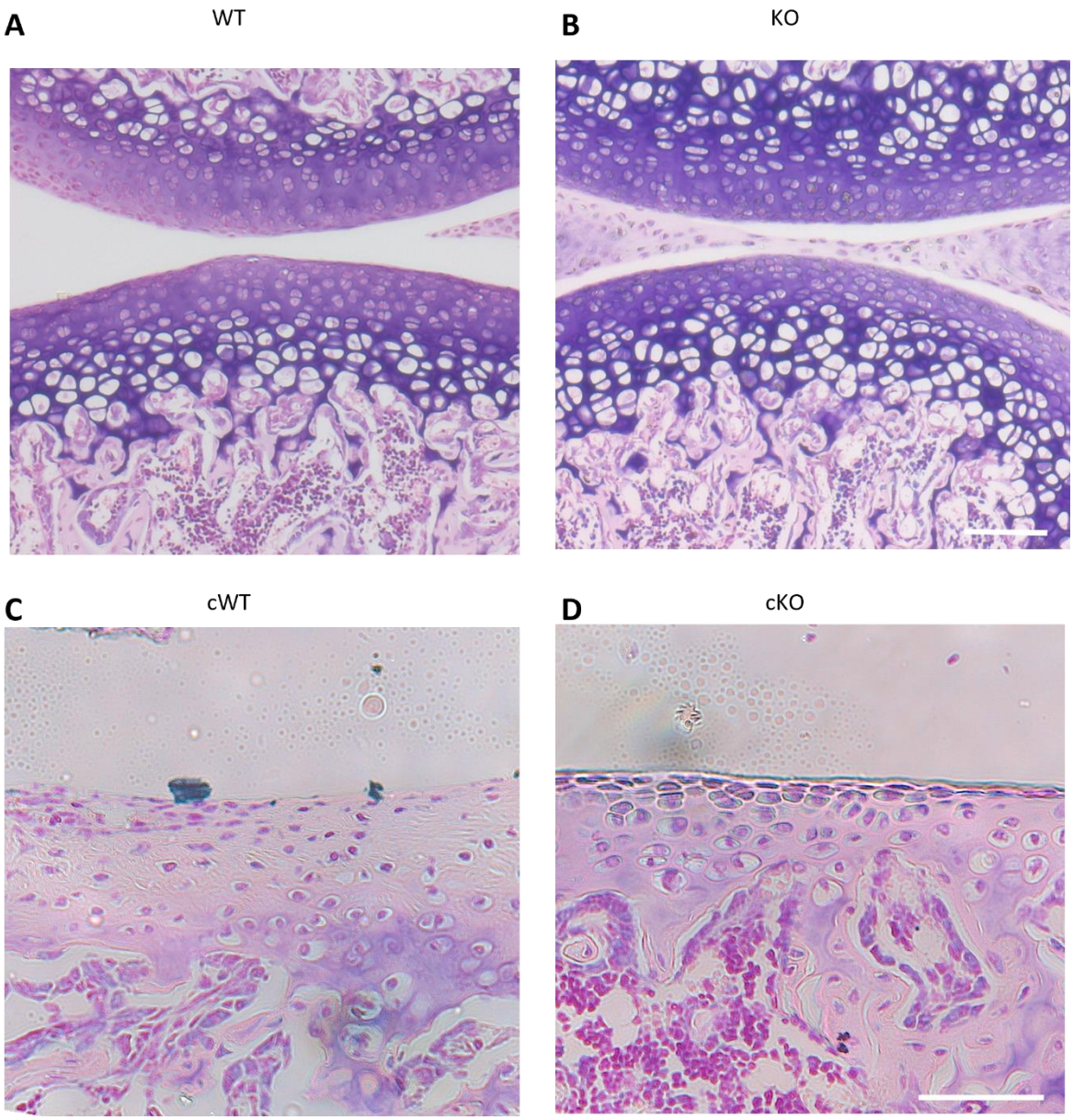

Figure 51. Toluidine blue staining shows no difference in proteoglycan deposition. *Toluidine blue staining to visualise proteoglycan deposition in the articular cartilage, shows no observable difference to the deposition of proteoglycan or the structure of the articular cartilage in the global knockout (**A**) relative to the wild type (**B**) or in the Col2cre conditional Asporin knockout (**C**) relative to the conditional wildtype (**D**).Scale bar 100 µm..*

4.5.2 Global loss of Asporin has no effect on proliferation and apoptosis in the growth plate.

TUNEL assay and Ki67 apoptosis IHC was also quantified in the articular growth plate. During OA pathogenesis, chondrocytes have well documented patterns, Sandell et. al summarised these into 5 categories "(1) proliferation and cell death (apoptosis); changes in (2) synthetic activity and (3) degradation; (4) phenotypic modulation of the articular chondrocytes; and (5) formation of osteophytes." Due to the overexpression of Asporin in OA cartilage, assessing the loss of Asporin may elucidate the pathways in which this overexpression is pathogenic in OA[189].

Apoptosis of chondrocytes of the articular cartilage is a feature of osteoarthritic cartilage. 3 week old mice with no surgical intervention would not be anticipated to show features of OA. To assess the likelihood of Asporin knockout being chondroprotective and its role in cartilage, measuring cell death in the articular cartilage in young mice is important as reduction of TUNEL positive cells, cells undergoing apoptosis, may indicate a chondroprotective phenotype. Articular cartilage cannot regenerate therefore the maintenance of healthy chondrocytes producing the ECM is crucial to retain healthy cartilage. The proliferative activity of articular cartilage chondrocytes has been shown to be increased in OA chondrocytes, though at a very low level, whereas healthy articular cartilage chondrocytes have essentially no proliferative activity. Changes to the dynamic balance of apoptosis and proliferation can be detrimental to cartilage health.

No difference was found in the quantification of Ki67-positive cells, in the global Asporin knockout relative to the wild type in the articular cartilage. Additionally, no difference was found in the quantification of TUNEL-positive cells, in the global Asporin knockout relative to the wild type in the articular cartilage.

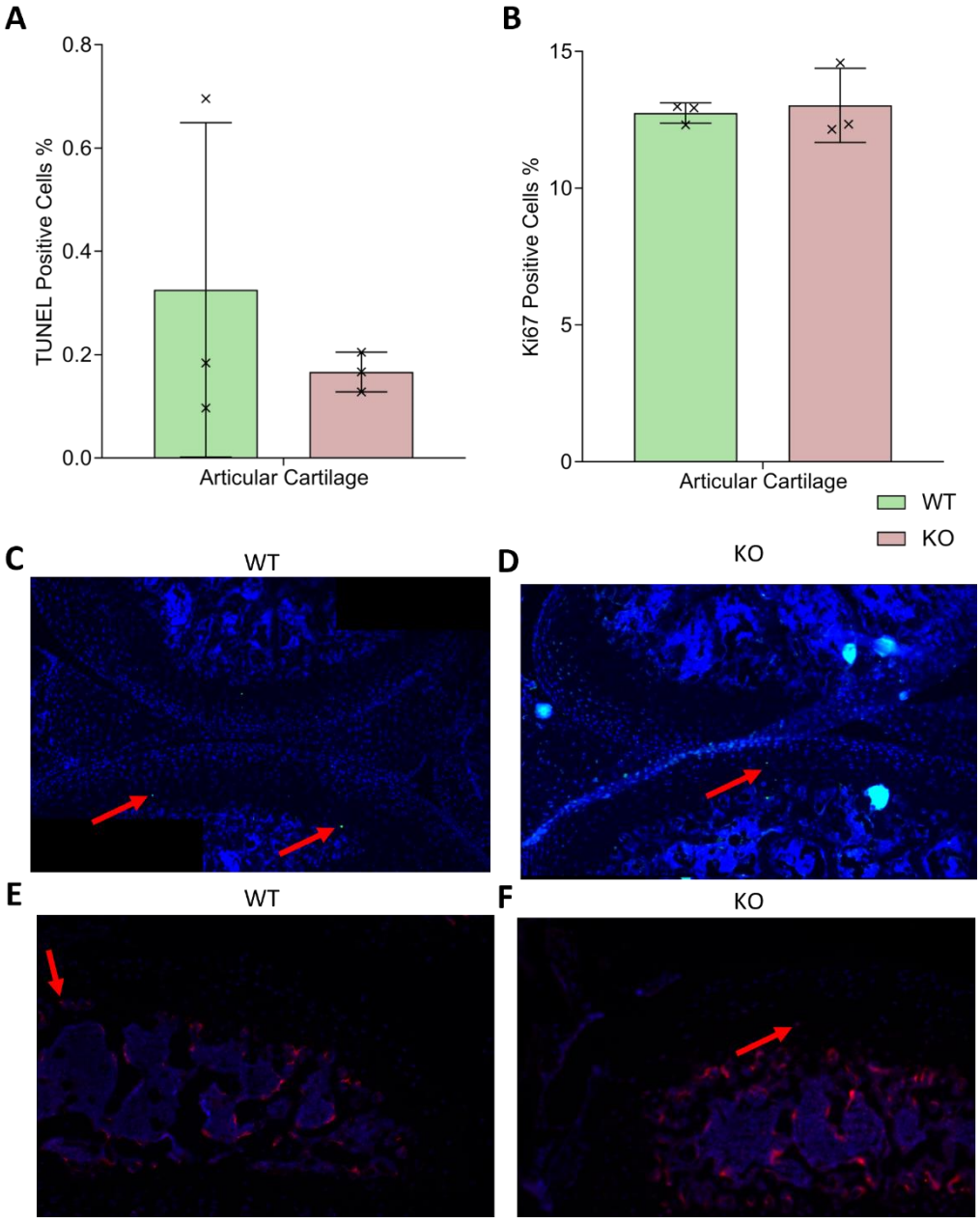

Figure 52. Global loss of Asporin does not affect apoptosis or proliferation in 3 week old articular cartilage.

*Quantification of TUNEL assay determined there was no difference in apoptosis of cells in the articular cartilage in the global Asporin knockout relative to the wild type (**A**). Quantification of Ki67 immunohistochemistry determined there was no difference in Ki67 positive cells in the articular cartilage of the global Asporin knockout relative to the wild type (**B**). Error bars represent standard deviation. 3 Sections per tibiae, 3 per genotype (n=3).*

*Representative images of TUNEL IHC assay in WT (**C**) and KO (**D**) tibiae. Representative images of Ki67 IHC in WT (**E**) and KO (**F**) tibiae.. Key: blue fluorescence - DAPI counterstain of nuclei, green fluorescence – TUNEL staining, with red arrows to highlight examples of TUNEL positive cells, red fluorescence – Ki67 staining, with red arrows to highlight examples of Ki67 positive cells.*

4.5.3 Loss of Asporin global has no effect on type II collagen expression articular cartilage.

Type II collagen is the main component of the articular cartilage, OA is characterised by the degradation and loss of the articular cartilage. This is a loss in type II collagen however additionally to there being loss there can also be damage to the type II collagen fibrils, it has been shown by Tschaikowsky et. al. there is a loss of thick type II collagen fibres and an increase in type I collagen fibres, normally present in fibrocartilage.

If Asporin is to be used as a potential target of OA and has been identified to be overexpressed in OA it is therefore interesting to look at the effect of the global loss of Asporin on articular cartilage. To elucidate potential pathways of its pathogenicity in OA but additionally the possible off target effects of targeting Asporin as a chondroprotective therapeutic target.

IHC of type II collagen in the articular cartilage in the global Asporin knockout was alike to that of the wild type articular cartilage. Loss of Asporin does not appear to disrupt the type II collagen expression or localisation in the growth plate.

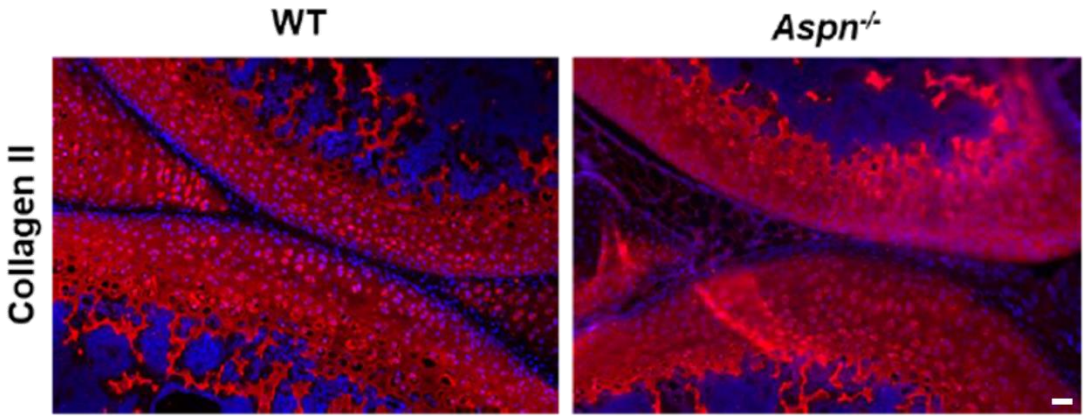

Figure 53. Global loss of Asporin does not affect type II collagen expression and localisation in the articular cartilage. *Type II collagen IHC determined there was no difference in the expression or localisation of type II collagen in the articular cartilage in the global Asporin knockout relative to the wild type. Key: blue fluorescence – DAPI counterstain of nuclei, red fluorescence – type II collagen staining. N=3 per genotype. Scale bar 100 μm.*

4.6 Discussion

This chapter aimed to characterise a skeletal phenotype resulting from the global knockout of Asporin and from the Col2cre conditional Asporin knockout, focusing specifically on the development and homeostasis of the hyaline cartilage.

Western blotting confirmed the global knockout of Asporin in all tissues (KO) and the knockout of Asporin under the type II collagen promoter in the Col2cre Asporin conditional knockout (cKO). The Western blot analysis of tail tip and skin samples from both global and knockout (KO) mice was poor, primarily due to difficulties in protein extraction caused by contamination from fur. Future experiments should focus on isolating tissues more effectively, such as obtaining pure skin or cartilage samples, to avoid contamination. Additionally, Asporin is expressed in a wide range of tissues, including the heart, which may have served as a more suitable tissue for confirming the Asporin knockout, given its higher expression levels in this organ[127]. Nevertheless, the knockout of Asporin was confirmed at the DNA level through genotyping, which validated both the global and conditional knockout alleles. This experiment validates the following experiments assessing the role of Asporin in all tissues through the global knockout (KO) and the role of Asporin specifically in the cells expressing type II collagen through the conditional Col2cre knockout (cKO). This was further verified by immunohistochemistry which showed Asporin deletion in the subchondral bone and the periosteum of Asporin KO mice. However, the histological analysis of the global and conditional cartilages highlighted no difference in the morphology and organisation of the growth plate, and articular cartilage at 3 weeks of age furthermore no changes were identified in the deposition of sulphated proteoglycans or the expression of key ECM molecules, determined by immunocytochemistry. Taken with the lack of difference in the whole-body skeletal preparations and the multi-timepoint long bone measurements confirms indicates Asporin is dispensable in endochondral ossification and development of articular cartilage. Furthermore, the lack of difference in the skull measurements, highlights a

lack of a key role in the early intramembranous ossification. Considering proliferation and the apoptosis within the 3-week tibiae was unaffected in the global knockout. All these experiments considered Asporin can be concluded to be not essential in the growth plate and endochondral ossification.

Global and conditional loss of Asporin had no effect on the structure of the articular cartilage H&E highlighted no real differences in the structure and organisation of the articular cartilage. Furthermore, the same was found in the toluidine blue staining to visualise the sulphated proteoglycan cartilage structure and the deposition amount. As discussed in Chapter 3 the overexpression of Asporin, modelling the overexpression found in OA cartilage, the amount of sulphated proteoglycan in the cartilage cells was significantly reduced. Studies were therefore designed to look at the effect of global Asporin knockout and a cartilage specific knockout. Although, the knockout is not always the converse phenotype of the overexpression, it is interesting to assess changes if any to identify possible pathways of Asporin function which may in turn highlight pathways of its pathogenicity in OA. In Chapter 3 the loss of sulphated proteoglycan was discussed that in the OE cells, decorin was significantly downregulated, this is an important protein, described as a physical linker for binding aggrecan, type I and type II collagen and facilitates the formation aggrecan-aggrecan molecules and aggrecan-type II collagen fibrils[181]. The lack of sulphated proteoglycan deposition was discussed that it may be a result of the lack of formed aggrecan network resulting in the reduction. The work by Kalamajski et. al. discussed that Asporin is a potent inhibitor of decorin binding type I collagen and that both compete to bind the fibrils[123]. It could be hypothesised that in this work studying the loss of Asporin there would therefore there would be no inhibition of decorin. The decorin should therefore function as normal and contribute to the formation of a strong, well-connected network of aggrecan-aggrecan and aggrecan-type II collagen fibril complexes in the hyaline cartilage.

In assessing the role of Asporin as a therapeutic target for OA the results shown here are promising, the knockout of Asporin does not appear to have a detrimental impact on the formation and structure of the growth plate or importantly the articular cartilage. As previously mentioned, the increased proliferation of articular chondrocytes, which are normally non-proliferative or at extremely low levels and the increase in apoptosis of articular chondrocytes are a common reaction pattern of the articular chondrocytes in response to OA. In a therapeutic target, change to increase proliferation or apoptosis in the cartilage would be a major off target effect, exacerbating the OA damage and potentially accelerating the progression of OA. In the articular cartilage data, there is no difference in the articular chondrocytes in proliferation or apoptosis.

Thes results demonstrate that the global knockout of Asporin does not have a detrimental effect on the articular cartilage or furthermore in the growth plate, expression, and localisation of the structural proteins of the growth plate or the structure itself of the growth plate and articular cartilage.

Asporin is often investigated for its role in osteoarthritis, where Asporin expression is upregulated and has been shown to suppress both Aggrecan and type II Collagen through the modulation of TGF-B[135, 137]. Asporin and the osteoarthritis susceptibility polymorphism in Asporin has been shown to inhibit chondrogenesis and Asporin has been previously linked to collagen fibrillogenesis[123]. With these evidenced connections between Asporin and chondrogenesis and factors of the cartilage, the lack of a phenotype in these mice was surprising.

Considering this lack of phenotype, it is reasonable to conclude Asporin is dispensable in growth plate function and consequently the long bone growth and trabecular bone structure.

Immunohistochemistry of 3 week old legs confirmed the co-localisation of Asporin with periostin and its localisation in perichondrium

and periosteum of developing bones, which was previously only published for foetal mouse limbs E15.5[175]. This was an interesting discovery as it highlights a new targeted tissue in the conditional knockout of Asporin. Periosteal cells are heterogenic tissue of cells with stem cell potential, COL2-positve cells have been identified in the periosteal cells [63]. The targeted deletion of Asporin under the type II collagen promoter would therefore delete Asporin in these COL2 positive periosteal cells. As discussed, the periosteal cells are important for cortical bone formation, bone remodelling through the production of osteoblasts and the activation of osteoclastogenesis[63]. Considering the conditional knockout of Asporin will also target knockout in the COL2 positive cells of the periosteum it will be interesting to determine an effect if any of this deletion in bone remodelling and the cortical bone.

Further investigation of the implications of the global and conditional knockout of Asporin in periosteal cells is necessary. This investigation could include TUNEL and apoptosis quantification studies observing changes to the periosteum. Additionaly, cell lineage tracing experiments would be very interesting to trace the col2cre knockout cells within development and determine if there is a role of Asporin in bone remodelling.

Chapter 5. Bone

5.1 Introduction

Chapter 4 discussed the role of Asporin in cartilage development and endochondral ossification through the study of 3-week-old articular and growth plate cartilage. Longitudinal bone growth was not affected by the deletion of Asporin, however the role of Asporin in trabecular and cortical bone structure is not fully understood. Previous studies have shown that exogenously added recombinant Asporin can modulate mineralisation of mesenchymal stem cells and primary osteoblasts, and results in Chapter 3 show that overexpression of Asporin has an impact on mineralising cartilage. Moreover, expression of Asporin has been reported in the developing perichondrium prenatally (E15.5), a structure which supports and modulates both homeostasis, and the results in Chapter 4 further confirm the expression of Asporin in postnatal perichondrium and periosteum. Targeting Asporin could potentially be therapeutic for osteoarthritis, therefore the role of Asporin in bone must be studied for potential off target effects of such therapy.

Studies confirmed that the skeletal progenitor cells in the periosteum include populations of type II collagen positive cells. The localisation of Asporin in the periosteum highlights a very interesting avenue for exploration. As the conditional knockout is under a type II collagen promoter, Asporin will be knocked out in these populations of skeletal progenitor cells. The role of these cells in bone remodelling and cortical bone growth will make the conditional knockout novel work. The work in Chapter 3 demonstrated there are no overt differences to growth and growth plate structure, therefore it can be assumed it does not have an obvious role in early bone formation. This chapter will explore its effect in bone remodelling and bone structure at 12-weeks of age, where growth has plateaued and at this age it is bone remodelling and appositional growth occurring rather than growth in length[190].

Chapter aims.

- To investigate the role of Asporin in development of trabecular and cortical bone using a global knockout mouse model of Asporin and a mouse model with a tissue specific deletion of Asporin, with *Cre* expression driven by the *Type II Collagen* promoter for a Col2cre Asporin knockout.
- To study the effect of Asporin deletion on early differentiation events in the osteogenic lineage using mesenchymal stem cells extracted from wild type and Asporin null mice.

5.2 Analysis of the effect of the global deletion of Asporin on bone microarchitecture and osteoblast and osteoclast activity.

5.2.1 Global loss of Asporin has no effect on the microarchitecture of mouse trabecular bone at 3 months of age.

μCT analysis has not been carried out on Asporin null and conditional mice previously and despite several studies showing that Asporin promotes collagen mineralization by the osteoblasts, the role of Asporin in the bone architecture remains largely unknown[123]. Trabeculae are the rods and planes of bone that form the interconnected network of cancellous bone, these trabeculae surround bone marrow. The parameters used for trabecular bone analysis include percentage bone volume (the volume of bone calculated as a percentage of the whole tissue volume, excluding cortical bone), trabecular number (the total number of trabecular), trabecular thickness (the average thickness of the trabeculae), and the trabecular separation (the distance between the trabeculae)[147].

The number, thickness and separation all impact the strength of the bone and health of the bone due to changes in the bone volume to the bone marrow volume ratio. Enough bone mass is crucial for strength but too much bone can result in less bone marrow which is necessary for bone homeostasis and recovery. Narrow bone marrow can also have immune implications, as the bone marrow is a source of new blood cells and immune system cells, when it is too narrow it cannot function as normal[191]. In individuals with osteopetrosis due to incorrectly formed and small bone marrow cavity, they present with anaemia due to the blood cells not forming normally, additionally the immune system also becomes compromised due to the immune cells not forming normally.[191]. The pattern factor is a determinant of the shape of the trabeculae, whereby a lower number means a higher proportion of rod like trabeculae and a higher number indicates a higher proportion of plane like trabeculae. Finally, the Structure Model

Index (SMI) is calculated based on the previous parameters and gives an overall prediction of the likelihood of the bone to break under load.

Interestingly, despite the known roles of Asporin in collagen mineralisation, the uCT analysis of the 12-week mice tibiae and femur of the global knockout and wild type mice showed no differences in the trabecular bone architecture (Figure 54). All of the structural parameters in the Asporin null bones were similar to the wild type controls with no statistically significant differences found.

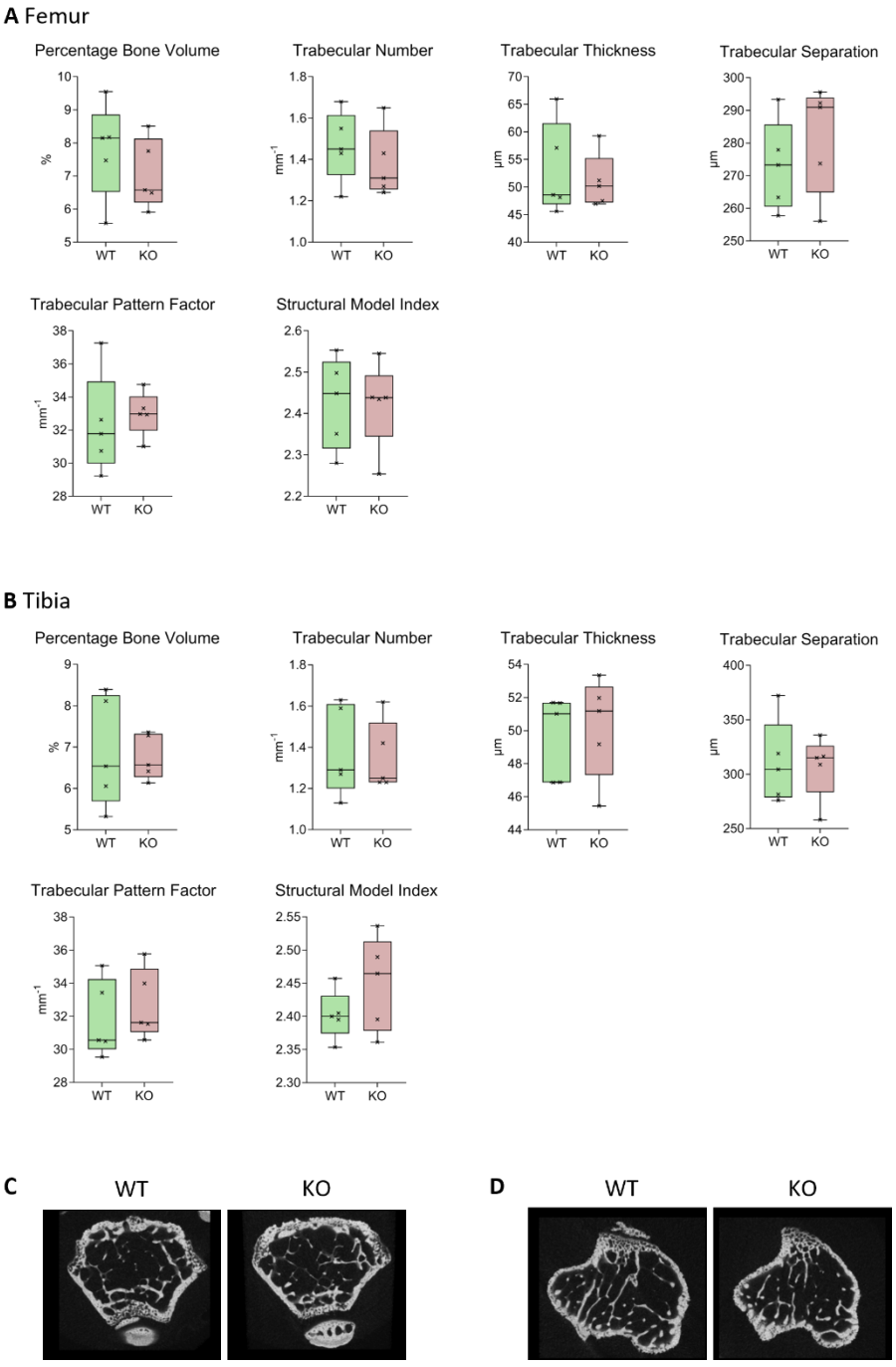

Figure 54. Deletion of Asporin in all tissues has no effect on the microarchitecture of trabecular bone at 3 months of age.

*No difference was found in any uCT trabecular parameter in the femur or the tibia (**A**, **B**) between the wild-type (WT) (green) and the Asporin knockout (KO) (red) mice. uCT images were reconstructed in Nrecon, Volume of Interest (VOI) was determined in DataViewer 100 slices distal of the femoral growth plate and 100 slices proximal to the tibial growth plate. The VOI was analysed in CtAn using the trabecular macro detailed in Appendix X. Student t-test were carried out between WT and KO (n=5) and denoted by *=p<0.05. Representative images of WT and KO*

*trabecular bone from CtVox of reconstructed VOI for femur (**C**) and tibia (**D**). Error bars represent min to max.*

5.2.2 Global loss of Asporin has no effect on cortical bone microarchitecture at 3 months of age.

Cortical bone is the dense compact bone that surrounds trabecular bone and bone marrow and contributes to the bone mechanical strength and fracture healing. Investigation of the cortical bone phenotype in Asporin null mice stemmed from the confirmed expression of Asporin in the prenatal and postnatal (Chapter 4) mouse perichondrium and periosteum[175]. The parameters used for cortical bone analysis include percentage bone volume (the volume of bone calculated as a percentage of the whole tissue volume, excluding trabecular bone), the endosteal circumference, which is a determinant of the long bones width, the cortical thickness (a measure of how thick the cortical bone is). All these parameters are used to calculate the mean moment of inertia (MMI), this gives a prediction of the likelihood of the bone to break under load, the lower the MMI the less force is needed to break the bone. The SMI from the trabecular analysis and the MMI can be considered together to get an overall indicator of the strength of the bone.

Surprisingly, no difference was found in the cortical analysis of the 12-week old tibiae and femur from the global knockouts mice compared to the wild type controls (Figure 55). Loss of Asporin in all tissues had no effect on μCT parameters of cortical formation and microarchitecture.

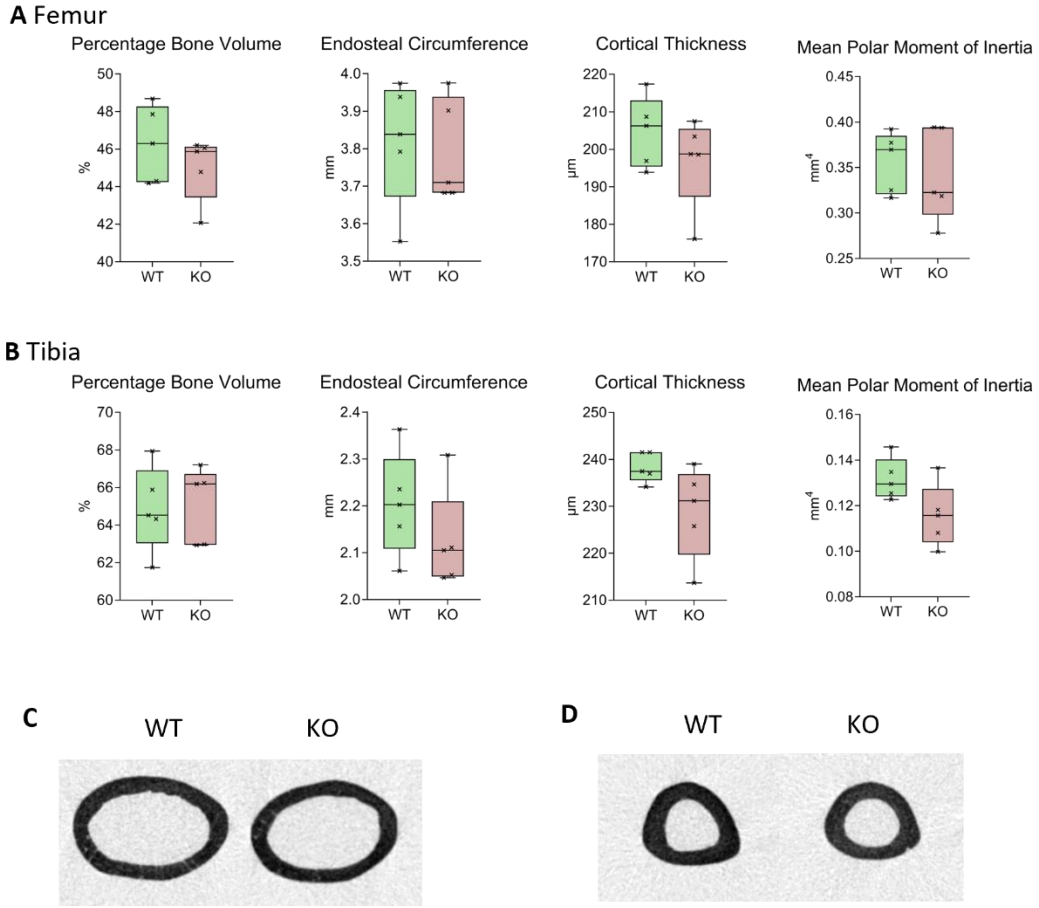

Figure 55. Global knockout of Asporin has no effect on the microarchitecture of cortical bone. *No difference was found in any of the uCT cortical parameters in the femur (**A**) or the tibia (**B**) between the wild-type (WT) (green) and the Asporin knockout (KO) (red) bones. uCT images were reconstructed in NRecon, Volume of Interest (VOI) was determined in DataViewer 100 slices distal of the femoral growth plate and 100 slices proximal to the tibial growth plate. The VOI was analysed in CtAn using the trabecular macro detailed in Appendix X. Student t-test were carried out between WT and KO (n=5) and denoted by *=p<0.05. Representative images of WT and KO cortical bone from CtVox of reconstructed VOI for femur (**C**) and tibia (**D**). Error bars represent min to max.*

5.2.3 Global loss of Asporin results in less stiff tibia at 3 weeks of age.

The most crucial role of the skeletal system is to provide support for the body and to protect the internal organs. For bones to fulfil this role they must be strong and able to withstand external forces. The mechanical properties of connective tissues are dictated by their extracellular matrix strength and integrity. Asporin was shown to modulate mineralisation but also proteoglycan deposition. Therefore, to further determine an overall effect of the loss of Asporin in the bone, destructive 3-point-bend tests were carried out on global knockout tibia and compared to wild-type controls.

Interestingly, the three-point bending of Asporin null tibia showed that Asporin null bones were 36.4 % less stiff than wildtype tibiae ($p=0.0186$, Figure 56 B), however surprisingly the maximum force needed to break the bones was not different between the wild type and knock-out samples (Figure 56 A). This indicates the bones although flexible are still able to withstand equal force to that of the wildtype.

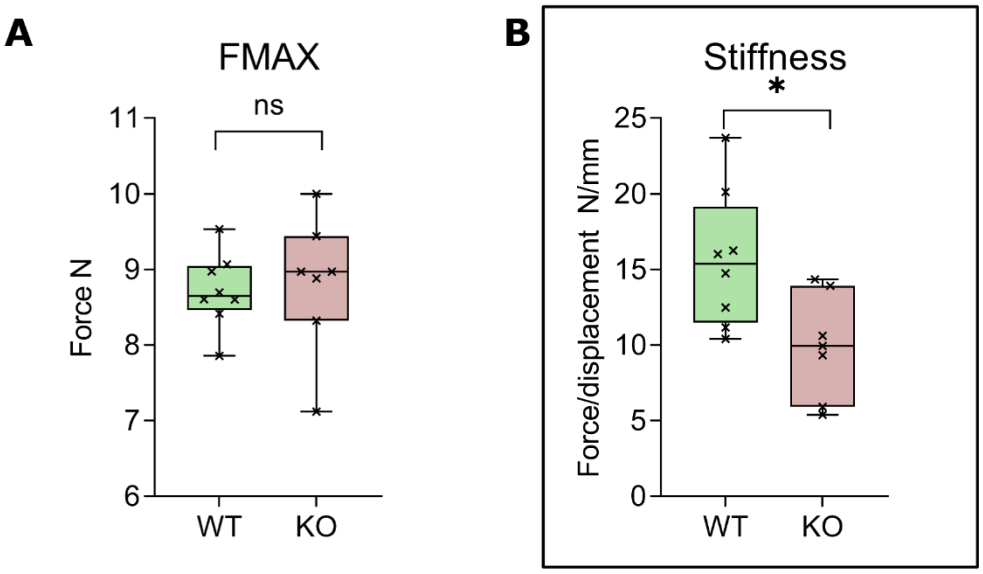

Figure 56. Global knockout of Asporin reduces stiffness of 12-week tibiae. *Destructive three-point bed tests were performed on wild type and global knockout female tibiae sections and maximum force to break (Fmax), and stiffness were calculated (**A** and **B**). Asporin knockout mice show no difference in the Fmax relative to the wild-type control. However, the stiffness of the tibia was significantly reduced in the Asporin knockout tibia relative to the wild type. Standard deviation plotted error bars. Student t-test were carried out between WT and KO (n=3) and denoted by *=p<0.05. Error bars represent min to max.*

5.2.4 Bone marrow adipocyte content is unchanged in Asporin null bones.

Bone marrow fat is an accumulation of fat originating from the bone marrow adipocytes (BMATs) within the core of long bones. Alike to osteoblasts, bone marrow adipocytes are derived from the mesenchyme. Studies have shown BMATs are unlike other fat cells, as within the bone in addition to being an energy source they are also capable of secreting adipokines, cell-signalling cytokines that regulate metabolism and inflammation. These include leptin, adiponectin, and tumour necrosis factor amongst others. Bone marrow adipocytes also play a key role in haematopoiesis, regulating the proliferation and differentiation of blood cell lineages. Increased bone marrow fat has been identified in metabolism and bone diseases. In osteoporosis, elevated bone marrow fat is observed in the weaker bones. The increase of bone marrow adipocytes reduces the space for other key cells of the bone marrow, the bone marrow stem cells necessary to produce osteoblasts, and haematopoietic cells which can have implications on the immune system. The effect of decreased bone morrow adipocytes is less understood, bone marrow fat provides energy stores for bone activity, and decrease in the bone marrow fat may alter the balance of bone resorption and formation.

Assessment of the role of Asporin in bone marrow fat deposition has not been investigated in published work, however due to the connection made between loss of Asporin and counteracting high fat diet-induced metabolic disorder, as well as decreased stiffness of the Asporin-null bones, it was an avenue worth investigating[192]. The high fat diet study focused on the role of Asporin in adipose tissue expansion in epidermal fat but not in bone marrow fat. Recombinant Asporin was found to promote adipocyte differentiation in *in vitro* study using 3T3-L1 cells[192]. Bone marrow fat is linked to diseases of metabolism including obesity and anorexia nervosa, the link made between Asporin and epidermal fat, was interesting as this may alter bone marrow fat[192].

To determine changes in the bone marrow deposition, the 3 month old methacrylate-embedded tibiae sections were stained with Goldner's trichrome to highlight the fat deposits (white) (Figure 57). Number of fat deposits and area of fat deposits were measured, distribution was also assessed by Mann-Whitney U test analysis. Perilipin immunohistochemistry was used to confirm that the counted areas were indeed comprised of adipose tissue.

Contrary to the epidermal fat study, no difference was found in the number or area of fat deposits in the global Asporin knockout mice in comparison to the wild-type mice at 3 months of age (Figure 57).

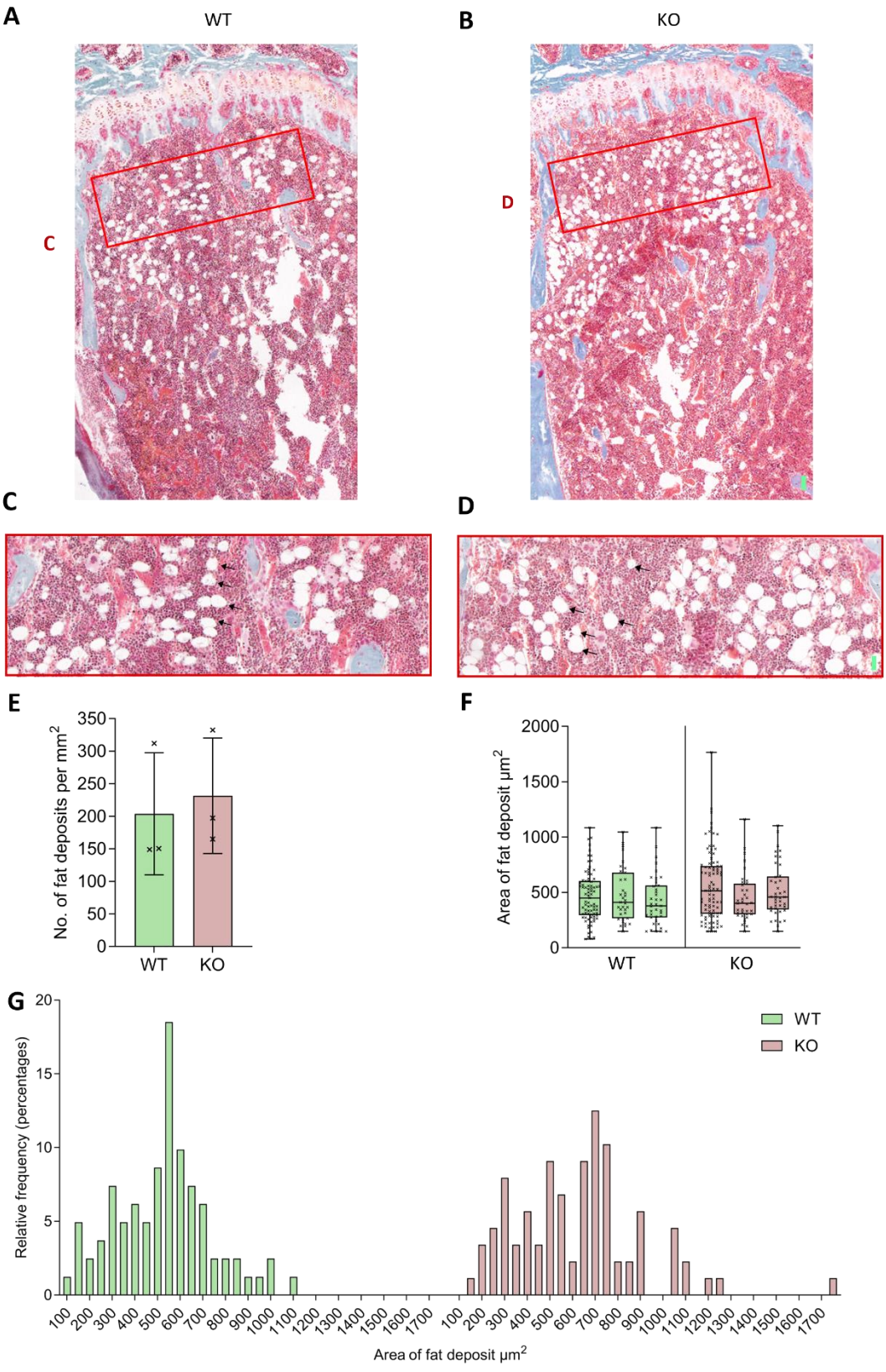

Figure 57. Global knockout of Asporin has no effect on the number of fat deposits in 12-week tibiae.

*Wild type and global knockout female tibiae sections were stained with Goldner's Trichrome to visualise fat deposits (**A** and **B**) Magnified regions with black arrows to highlight example of fat*

*deposits in the tissue (**C** and **D**). Scale bar 20 nm and 10 nm respectively. Asporin knockout mice show no difference in the number of fat deposit per mm^2 of tissue relative to the wild-type control, error bars represent standard deviation(**E**). Area of fat deposits (um^2) for each section, error bars represent min to max (**F**) Histogram of all fat deposit counts display distribution of fat deposits by size, bins 50 um^2. Student t-test (E) and Mann-Whitney U analysis (F) were carried out between WT and KO (n=3) and denoted by *=p<0.05.*

5.2.5 Osteoblast numbers in the tibia are unaffected by the global knockout of Asporin at 3 weeks of age.

The homeostasis of cortical bone appositional growth is balanced by the activity of osteoblasts and osteoclasts in the bone. Changes in this balance can result in overall loss in bone mass or too much bone being laid down.

To assess the effect of the knockout of Asporin on osteoblast numbers in the tibiae, sections were stained with Toluidine Blue to visualise and count osteoblasts number at the bone surface[193].Quantification of the osteoblast number per bone surface area in the global knockout of Asporin found there was no difference in the number of osteoblasts per the bone surface area, in comparison to the wild-type tibiae (Figure 58).

The lack of difference in osteoblast number is in line with the μCT data, where no difference in trabecular bone or cortical bone parameters was found. Changes in osteoblast numbers would be expected to modulate the volume of bone laid down. To explain the difference in the bone stiffness, the osteoclast activity, which is also a crucial part of appositional growth, was next investigated.

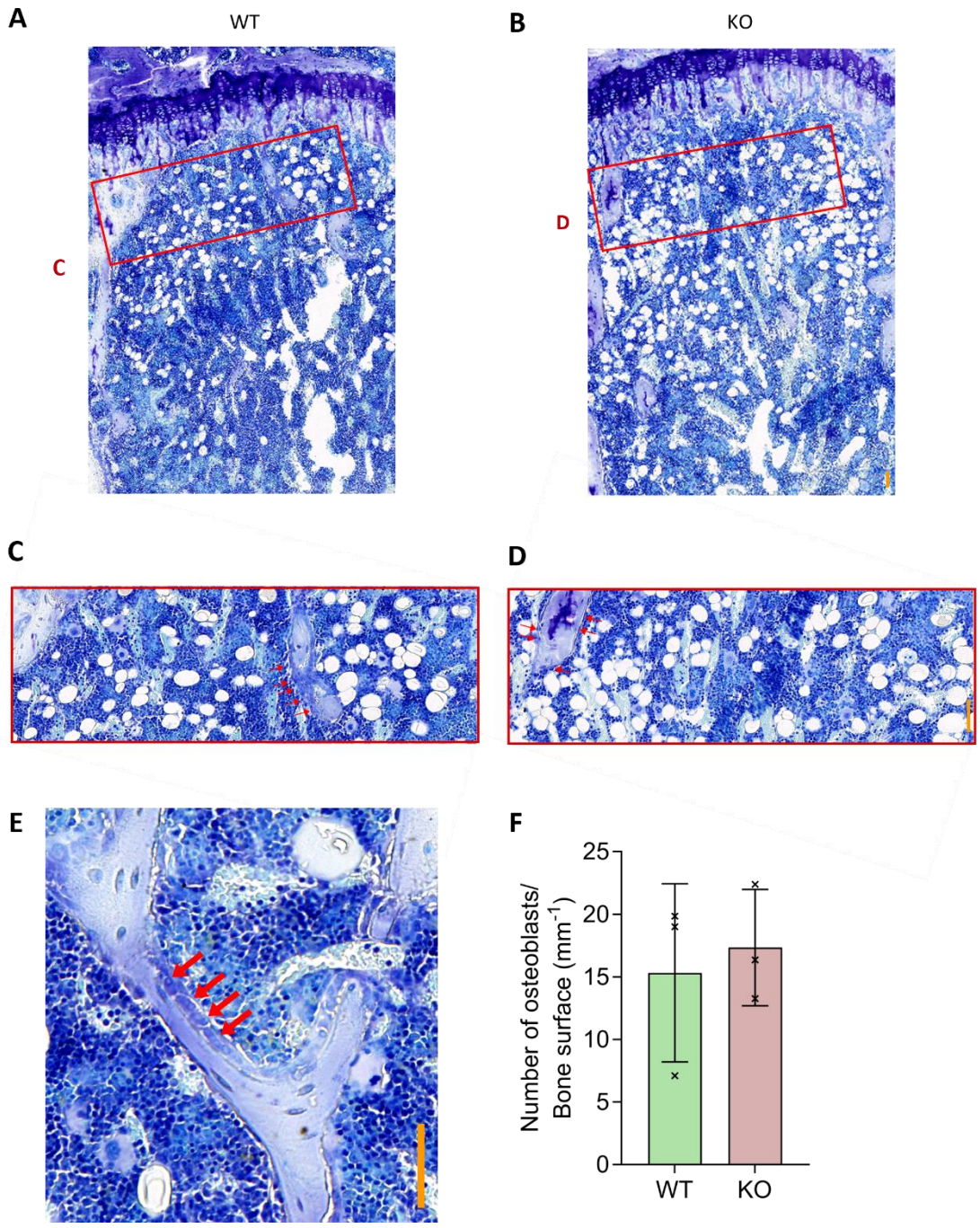

Figure 58. Global knockout of Asporin has no effect on the number of osteoblasts in 12-week tibiae. *Wild type and global knockout female tibiae sections were stained with Toluidine Blue to visualise osteoblasts (**A** and **B**). Magnified regions with red arrows to highlight example of osteoblasts along the bone surface in WT (**C** and **E**) and KO (**D**) Asporin knockout mice show no difference in the number of osteoblasts per bone surface relative to the wild-type control. Standard deviation plotted error bars. Student t-test were carried out between WT and KO (n=3) and denoted by *=p<0.05. Scale bar 20 nm.*

5.2.6 Osteoid deposition is not affected by the deletion of Asporin in 3 month old tibiae.

During bone formation, the osteoblasts secrete osteoid, the unmineralised matrix that is the precursor to mineralised bone, made up predominantly of type I collagen. This is the scaffold that is mineralised by the binding of calcium, to form hydroxyapatite crystals. Abnormal osteoid formation disrupts normal bone formation. Osteomalacia is a disease which shows the effect of improper osteoid mineralisation. In osteomalacia, osteoid accumulation occurs as there is impaired mineralisation, so although the scaffold for bone is secreted, as it is not mineralised, bone is not laid down resulting in weakened bones and increased risk of bone fracture. Asporin has been previously shown to play a role in mineralisation of type I collagen by the osteoblasts and in hydroxyapatite formation[123]. The possibility that a changed osteoid deposition may play a role in the decreased stiffness of the Asporin null bones was therefore investigated.

To assess the osteoid deposition, 3 month old methacrylate embedded tibiae sections were stained with Von Kossa to visualise calcified bone in black and with Van Gieson staining which stains the unmineralised collagen dense osteoid pink/red. The osteoid surface relative to bone surface was measured to assess the amount of active bone surface producing the osteoid and secondly the osteoid area to bone area was measured to assess the volume of osteoid laid down by the osteoblasts. Increased ratio of osteoid/bone volume would indicate either increased production of osteoid or accumulation of osteoid due to reduced mineralisation.

Surprisingly, there was no difference in the deposition of osteoid between the wild type and Asporin null bones (Figure 59). To assess whether there is difference in the mineralisation of the osteoid, time dependent experiments looking at mineralisation will be necessary. The dynamics of bone growth can also be assessed through dynamic histomorphometry, which was performed next.

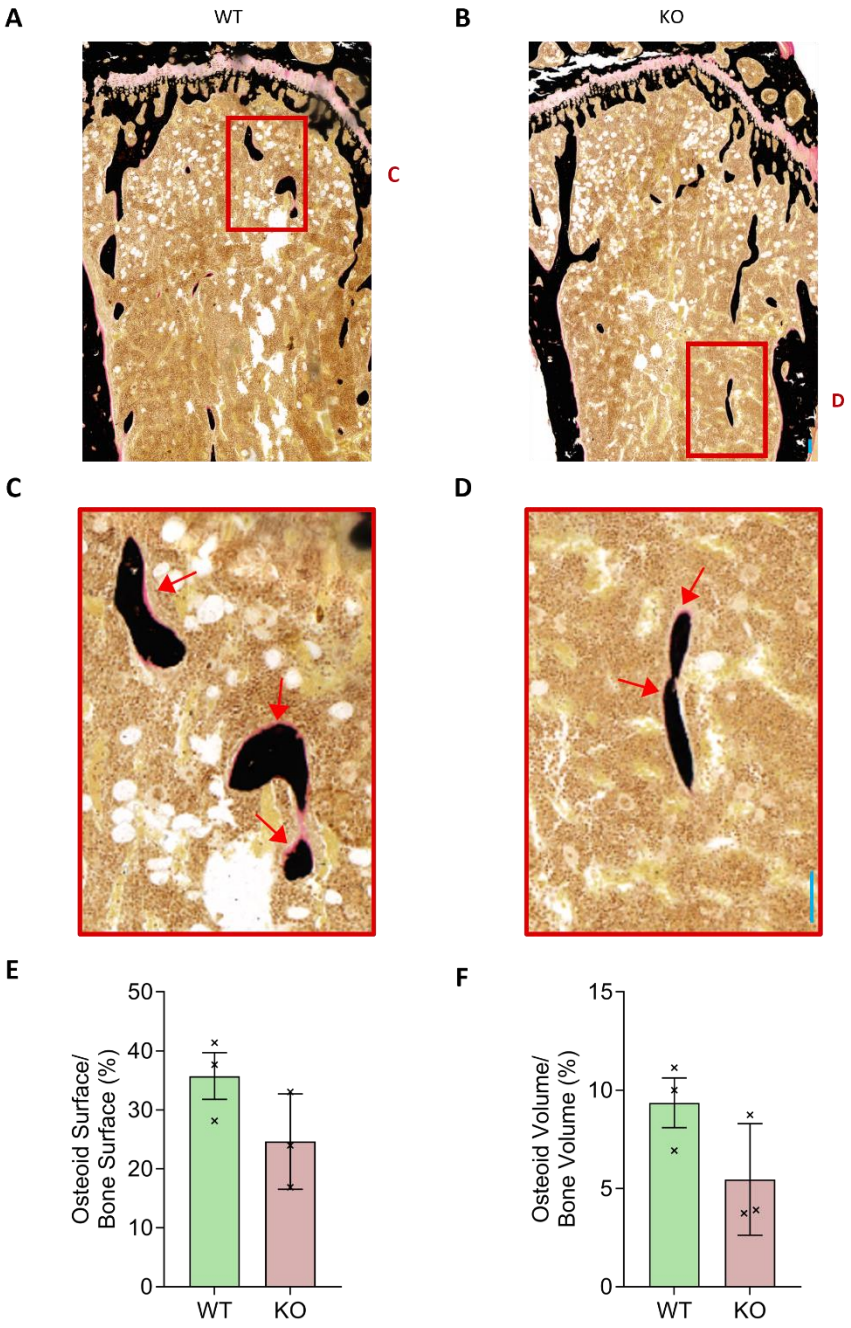

Figure 59. Global knockout of Asporin has no effect on the osteoid surface or volume of osteoid 12-week tibiae. *Wild type and global knockout female tibiae sections were stained with Von Kossa and Van Gieson to visualise bone (black) and osteoid deposition (red/pink) (**A** and **B**). Magnified regions with red arrows to highlight example of osteoid deposition along the bone surface (**C** and **D**) Asporin knockout mice show no difference in the percentage of osteoid surface to bone surface and the volume of osteoid to bone volume relative to the wild-type control. Standard deviation plotted error bars. Student t-test were carried out between WT and KO (n=3) and denoted by *=p<0.05. Scale bar 20 nm.*

5.2.7 Global knockout of Asporin has no effect on osteoclast numbers in 3 month old tibiae.

Osteoclasts are the key cells that orchestrate the bone resorption. Throughout healthy bone growth and homeostasis, the osteoblast (bone deposition) and osteoclast (bone resorption) activity is constantly regulated to allow and maintain the bone turnover. Appositional growth, or the growth of bone widthwise, is responsible for the maintenance of the bone's mechanical strength. As the load on the bone increases through growth or exercise, the bones must also grow in width to strengthen and thicken in order to support and withstand the increased load[65]. Osteoblasts on the outside layer of the long bones, the periosteum, orchestrate the creation of concentric layers of bone increasing the bones diameter on the outside layer of the bone[69].

Alongside this, osteoclasts lining the inner layer of the bone, the endosteum, resorb the mineralised bone tissue. This resorption is important to expand the bone marrow space to allow for continued healthy bone growth and maintenance, without this activity the cortical bone would become too thick, and the bone marrow cavity too small. Conversely, overactivity of osteoclasts in the endosteum can result in cortical bone becoming too thin and resulting in weaker bones.

Osteoclast activity is also important in the trabecular bone, to resorb old or damaged trabecular bone whilst osteoblasts replace it with new bone matrix. This is a tightly regulated and important process. Increased osteoclast activity has been implicated in osteoporosis, where there is increased bone resorption of mineralised bone matrix leading to more porous bones that are weaker and more susceptible to fractures. A decrease in osteoclast activity can also dysregulate bone remodelling and repair. When bone resorption is reduced, it can lead to the accumulation of aged or damaged mineralised bone tissue.

To quantify the number of osteoclasts in the bone, the Tartrate Resistant Acid Phosphatase (TRAcP) staining was caried out on the methacrylate embedded 3 month old tibiae allowing the osteoclasts to be visualised (in red), Aniline blue counterstain was used for contrast to distinguish bone from tissue in the TrapHisto programme. Figure 60. Globally knocking out Asporin had no effect on the number of osteoclasts in the tibiae or on the number of osteoclasts relative to bone area, in comparison to the wild-type tibiae.

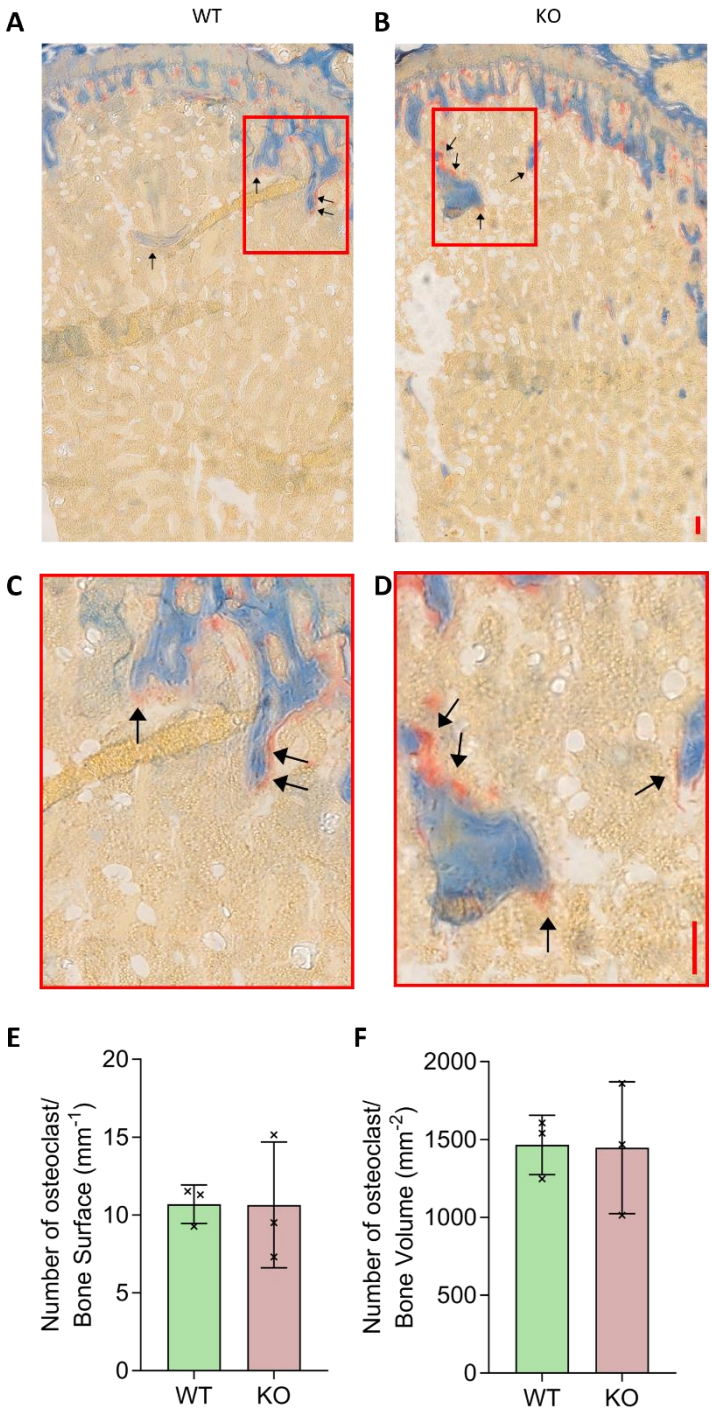

Figure 60. Global knockout of Asporin has no effect on the number of osteoclasts in 12-week tibiae. *Tartrate-resistant acid phosphatase (TRACP) staining was carried out on wild-type and global knockout female tibiae sections to visualise osteoclasts (**A** and **B**) Magnified regions with red arrows to highlight example of osteoclasts (red/pink) along the bone surface (**C** and **D**) Asporin knockout mice show no difference in the number of osteoclasts per bone surface or number of osteoclasts per mm^2 bone volume, relative to the wild-type control. Standard deviation plotted error bars. Student t-test were carried out between WT and KO (n=3) and denoted by *=p<0.05. Scale bar 20 nm.*

5.2.8 Bone turnover is unchanged in the 3 month old Asporin null tibiae compared to the wild type controls.

Dynamic histomorphometry is an experiment used to investigate bone metabolism and homeostasis, the dynamic process of bone formation and resorption. Fluorescent labelling injections with Alizarin complexone and Calcein green, were performed intraperitoneally into mice at 11 weeks of age and at 11 weeks and 6 days before sacrifice at 12 weeks. The fluorescent dye is incorporated into the bone as it forms, the alizarin complexone dye results in a line label in the bone formed at 11 weeks and 6 days and the second dye, calcein green, is incorporated into the bone in the 24 hours prior to sacrifice, this allows enough time for the dye to be incorporated, resulting in a second label of the newly formed bone. This allows the assessment of the bone turnover during 1 week of growth leading up to the 12-week age, which is the age of the tibiae previously examined.

Following sectioning and counterstaining with Calcein blue to highlight the overall bone tissue, the fluorescent labels can be used to measure the Mineral Apposition Rate (MAR) (Figure 61 A,B). MAR is a measure of the speed at which new mineralised bone matrix is deposited along the existing bone surface, and a measure of bone formation. This is calculated by the difference between the two fluorescent labels that were delivered at two separate time points as mentioned and expressed as a distance (μm per day). A higher MAR is indicative of faster bone formation over the time period and a lower MAR is indicative of a slower bone formation.

Mineralising surface per bone surface (MS/BS) is a measure of the active bone surface in the section and the bone formation rate/bone surface (BFR/BS) is a measure of the amount of new bone formed per day per unit of bone surface, calculated by multiplying the MS by the MAR.

In the global knockout mice, there was no difference in any of the histomorphometry parameters in comparison to the wild type (Figure 61 E-G). This is consistent with the lack of differences observed in the other bone

histology experiments, however, the change in the global knock-out bone stiffness remains to be explained.

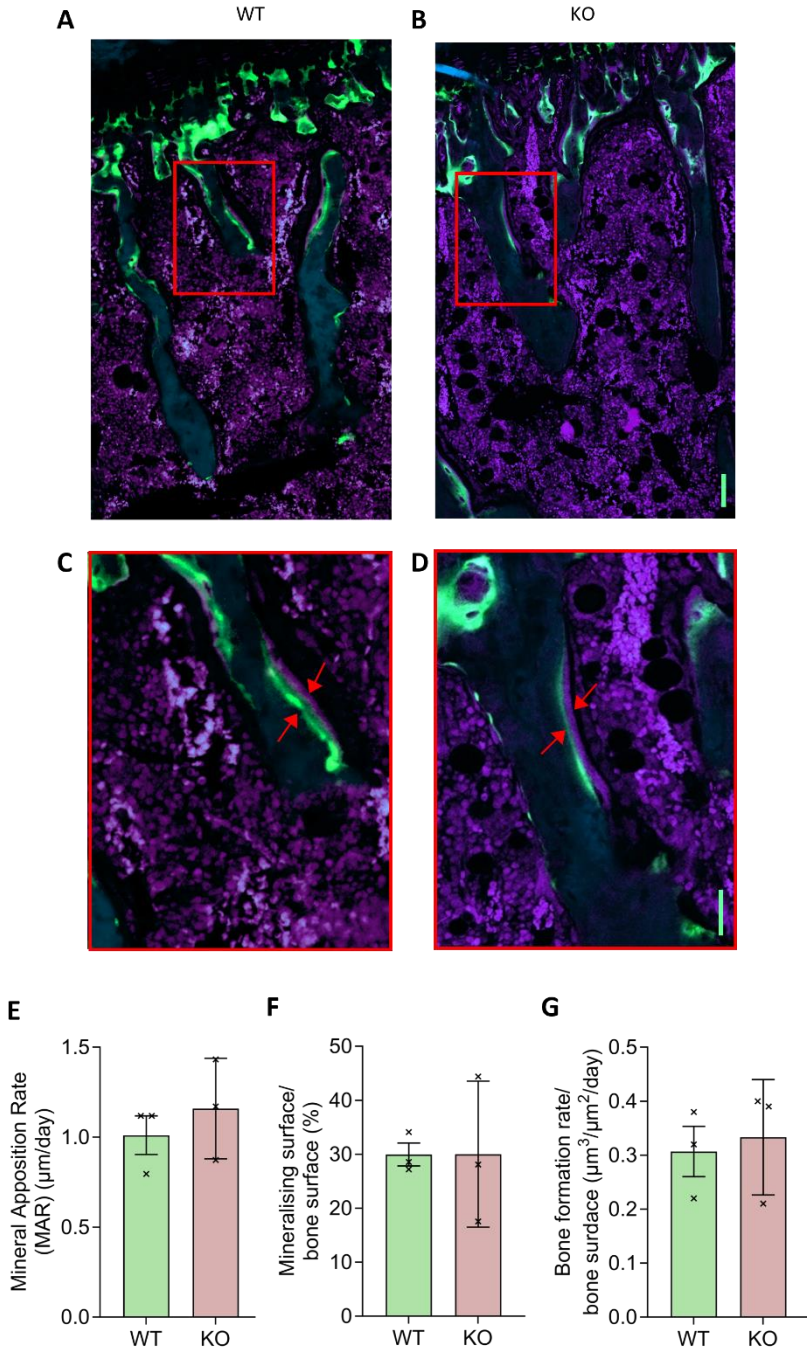

Figure 61. Global knockout of Asporin has no effect on histomorphometry parameters in 12-week tibiae. *Double labelling injections of alizarin complexone (purple) and calcein green (purple) counterstained with calcein blue (blue) and imaged using fluorescent microscope (**A** and **B**) Magnified regions to show distinct double label at the bone surface (**C** and **D**) Asporin knockout mice show no difference in the mineral apposition rate (MAR) (**E**), mineralising surface per bone surface (MS/BS) (**F**) and bone formation rate per bone surface (BFR/BS) (**G**), relative to the wild-type control. Standard deviation plotted error bars. Student t-test were carried out between WT and KO (n=3) and denoted by *=p<0.05. Scale bar 20 nm and 10 nm respectively.*

5.3 Analysis of the effect of the global deletion of Asporin on primary cell.

5.3.1 The global loss of Asporin does not affect the osteogenic differentiation of primary bone marrow derived mesenchymal stem cells (BM-MSCs).

To assess role of Asporin in the osteogenic differentiation axis, primary bone marrow derived mesenchymal stem cells (BM-MSCs) were collected from 3 month old mice and differentiated in osteogenic media for 21 days. Quantitative real time PCR was used to assess gene changes as a result of the loss of Asporin (Figure 62).

To look at the osteogenic axis (Figure 3), *Runx2* the master regulator of osteogenesis was assessed alongside *Spp1* (osteopontin), important for the mineralisation of the matrix which has ability to bind hydroxyapatite and is regulated by *Runx2,* and *Bglap* - a marker of the end stage osteogenic differentiation.

No significant differences were found in the osteogenic gene expression at day 7, 14 or 21 of BM-MSC osteogenesis. This further confirms the lack of effect of the global loss of Asporin on bone formation.

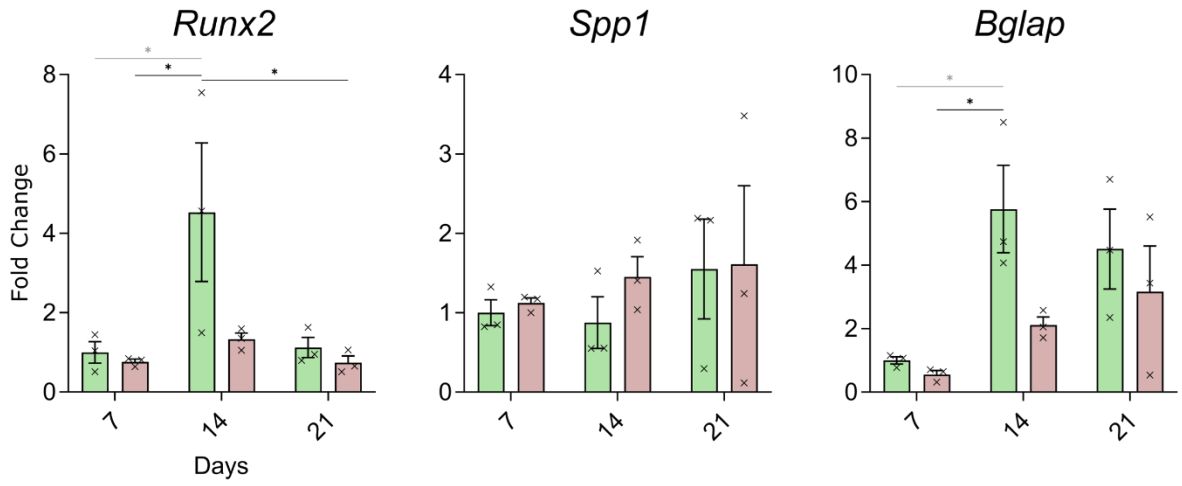

Figure 62. Loss of Asporin has no effect on markers of osteogenesis.

*Osteogenic markers were assessed by rt-qPCR. Runx2 expression, Bglap and Sp7 showed no change in expression at any time point. Expression levels were normalised to 18s.Fold change was calculated to the day 7 wild-type BM-MSCs Standard deviation was plotted, and 2-way ANOVA was carried out between WT and OE and across each timepoint, between WT and OE (Black *) and within the genotype between each time point (Grey *), (n=3) and denoted by *=p<0.05, **=p<0.01, ***=p<0.001.*

Bone marrow derived mesenchymal stem cells were extracted from 3 month old tibia and cultured in osteogenic differentiation media for 21 days. At day 7, 14 and 21 cells were fixed and stained with Alizarin red to quantify the calcium deposition in the monolayer (Figure 63).

There were no significant differences in the concentration of Alizarin red stain at any time point when comparing the osteoblasts extracted from the global Asporin knockout to the wild-type osteoblasts.

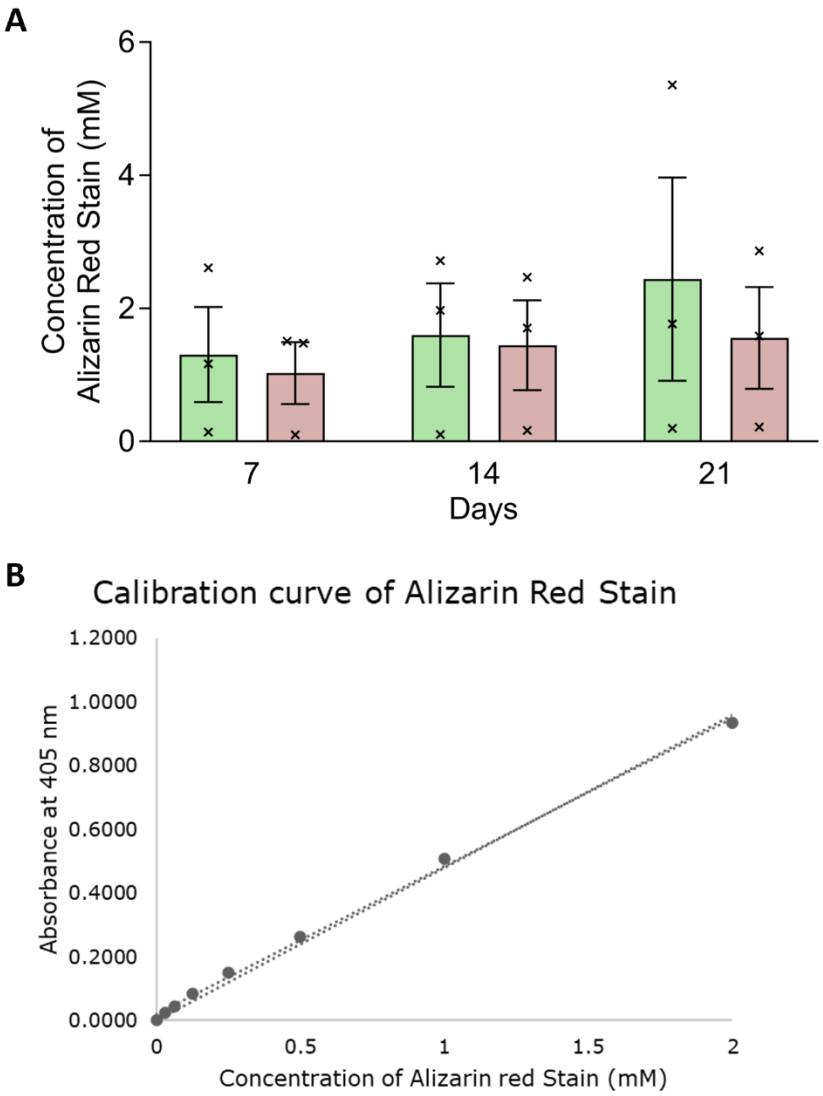

Figure 63. Knockout of Asporin has no effect on mineralisation in MSCs through osteogenic differentiation. *Alizarin Red staining of monolayer Primary MSC cells throughout mineralising 21-day cell culture in osteogenic medium. Comparison of wild-type (WT) and Asporin knockout (KO). Cells were stained with 40mM Alizarin Red stain (ARS). Semi-quantitative measurement of calcium deposition through quantification of Alizarin red stain read by spectrophotometry at 405 nm(**A**). Concentration of stains were calculated from calibration curve of standards of serial dilutions of Alizarin red stain (**B**). Standard error of the mean was calculated and plotted, and 2-way ANOVA was carried out between WT and OE and across each timepoint, between WT and OE (Black *) and within the genotype between each time point (Grey *), (n=3) and denoted by *=p<0.05.*

5.3.2 ALP activity is unaffected in primary osteoblasts derived from Asporin knockout mice.

As previously discussed, alkaline phosphatase hydrolyses beta-glycerophosphate, a crucial component of mineralising media, releasing the inorganic orthophosphate which is converted to hydroxyapatite by the sodium phosphate co-transporters[167]. Binding of hydroxyapatite, the mineral form of calcium apatite, is part of the process of bone mineralisation.

Primary osteoblasts extracted from 3 month old tibiae were cultured in complete alpha-MEM media while they migrated from the bone chips. Migrated primary osteoblasts were subsequently cultured in mineralising media for 21 days, and the ALP activity was assessed at day 7 and 14 of culture (Figure 64).

Global knockout of Asporin did not affect alkaline phosphate (ALP) activity in primary osteoblasts.

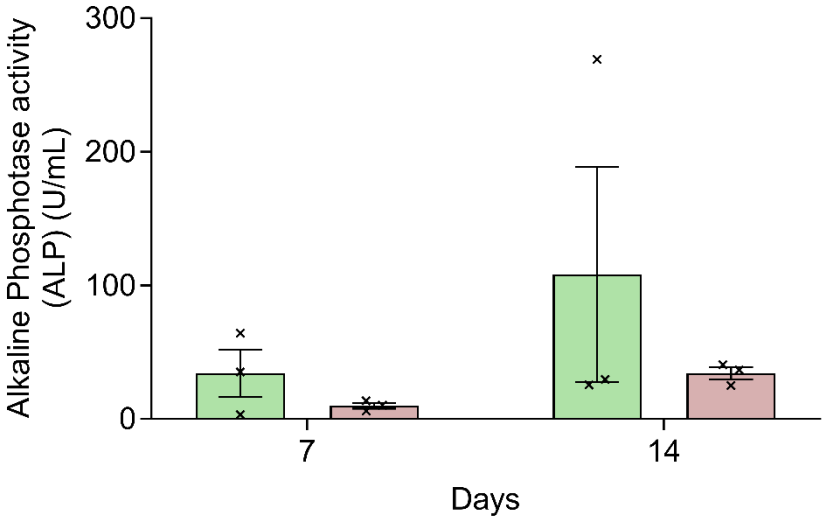

***Figure 64. Global knockout of Asporin has no effect on* alkaline phosphatase activity in primary osteoblasts.** *ALP activity of primary osteoblasts measured at day 7 and 14 of mineralising 21-day cell culture in osteogenic medium. Comparison of wild-type (WT) (green) and Asporin knockout (KO) (red). ALP activity was measured using a colorimetric assay kit read by spectrophotometry. Respective ALP activity was calculated from calibration curve of standards for ALP activity. Standard error of the mean was calculated and plotted, and 2-way ANOVA was carried out between WT and OE and across each timepoint, between WT and OE (Black *) and within the genotype between each time point (Grey *), (n=3) and denoted by *=p<0.05.*

5.4 The effect of deletion of Asporin in Col2 lineage on bone homeostasis

5.4.1 Col2cre-driven knockout of Asporin has no effect on the microarchitecture of mouse trabecular bone at 3 months of age.

As discussed in the introduction, the localisation of Asporin to the periosteum, the populations of type II collagen positive cells in the skeletal progenitor cells of the periosteum, makes this an interesting line of enquiry, as this will explore not only the effect of the loss of Asporin in cartilage but also considering the loss of Asporin in some populations of the periosteal cells. Periosteal cells are involved in fracture repair, bone remodelling and appositional growth.

As previously explained, 12-week tibiae and femur were scanned for uCT analysis and trabecular bone parameters were measured. Alike to the global knockout of Asporin, the conditional loss of Asporin in the Col2cre knockout also showed no difference in the formation and structure of trabecular bone microarchitecture at 12 weeks of age when compared to the conditional wild type (cWT mice are Asporin wild type mice positive for *Col2Cre* expression) controls (Figure 65).

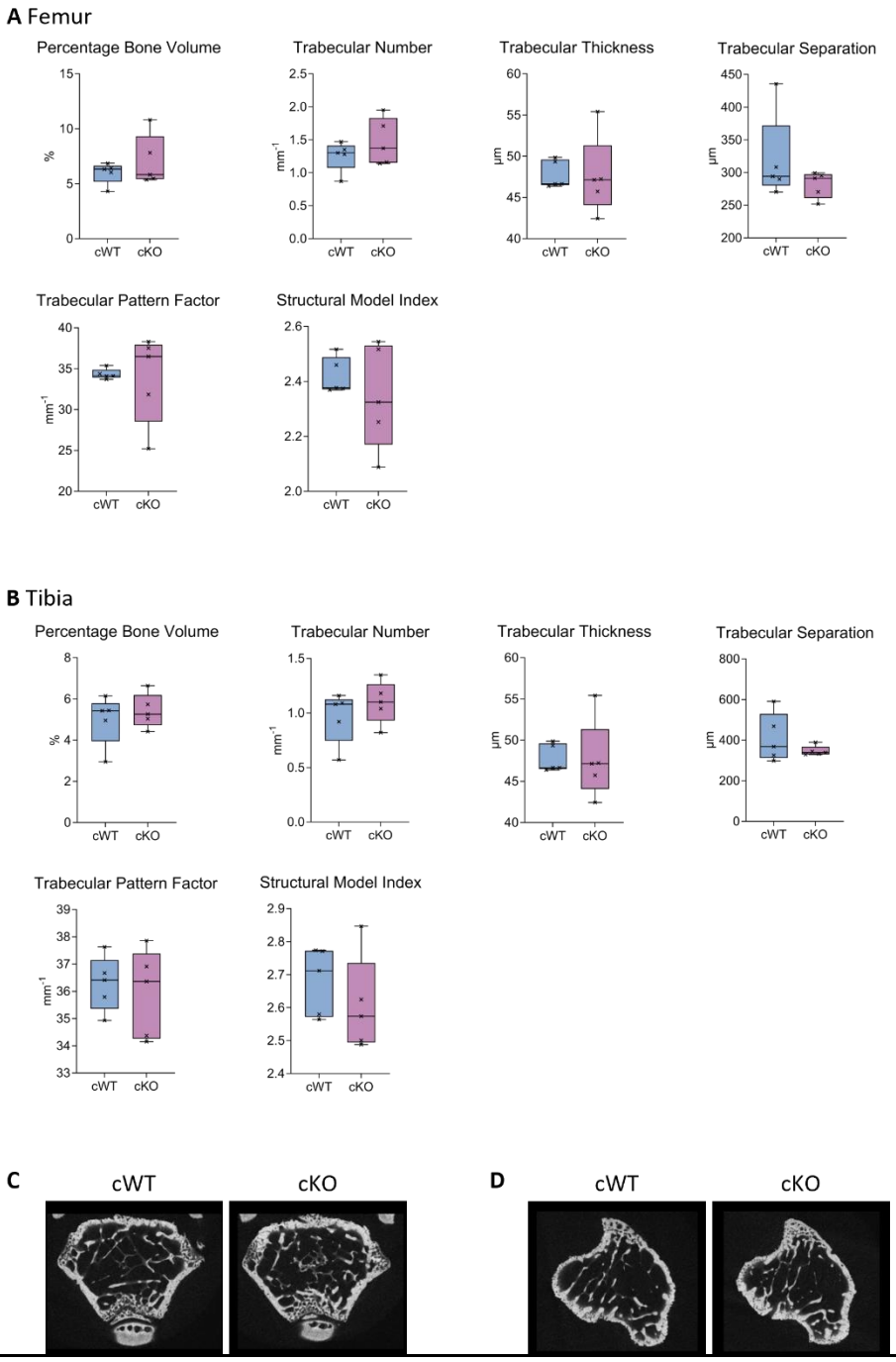

Figure 65. Col2cre knockout of Asporin had no effect on the microarchitecture of trabecular bone.

*No difference was found in any uCT trabecular parameter in the femur or the tibia (**A, B**) between the conditional wild-type (cWT) (blue) and the col2cre conditional Asporin knockout (cKO) (purple) bones. uCT images were reconstructed in NRecon, Volume of Interest (VOI) was determined in DataViewer 100 slices distal of the femoral growth plate and 100 slices proximal to the tibial growth plate. The VOI was analysed in CtAn using the trabecular macro detailed in Appendix X. Student t-test were carried out between WT and KO (n=5) and denoted by *=p<0.05. Representative*

*images of WT and KO trabecular bone from CtVox of reconstructed VOI forfemur (**C**) and tibia (**D**). Error bars represent min to max.*

5.4.2 Col2cre knockout of Asporin affects the bone cortical thickness at 3 months of age and is predicted to result in weaker bones.

Interestingly there were striking differences in the μCT analysis of the cortical bone in the conditional Asporin knockout (cKO) mouse bones (Figure 66). The cortical bone of the femur had a 9.33 % smaller endosteal circumference than the conditional wild-type femur (p=0.00773). The endosteal circumference is calculated from the cross-sectional tissue perimeter and the bone perimeter, both these measurements were significantly reduced in the cKO femur, by 8.38 % (p=0.00281) and 8.79 % (p=0.00449) respectively. The femur bones of the cKO mice were therefore overall thinner.

Additionally, the mean moment of inertia (MMI) is 27.2 % lower in the cKO femur (p=0.000838). This is a significant reduction suggesting that the conditional bones would likely need less force to fracture and therefore are expected to be weaker.

The tibia bones also showed differences, the cortical bone was 3.27 % thinner in the tibia from the 3 month old cKO mice (p=0.00031) compared to cWT controls, similarly to the femur the tibia was also predicted to be weaker, and the MMI was 18.32 % lower in the conditional knockout than the wild type (p=0.0164).

To conclude, Col2cre knockout of Asporin results in thinner and potentially weaker bones. Histological methods were applied next, to determine the reason for the narrower bone and thinner cortical bone. Destructive three-point bending was carried out to confirm the predicted weakness in the bone.

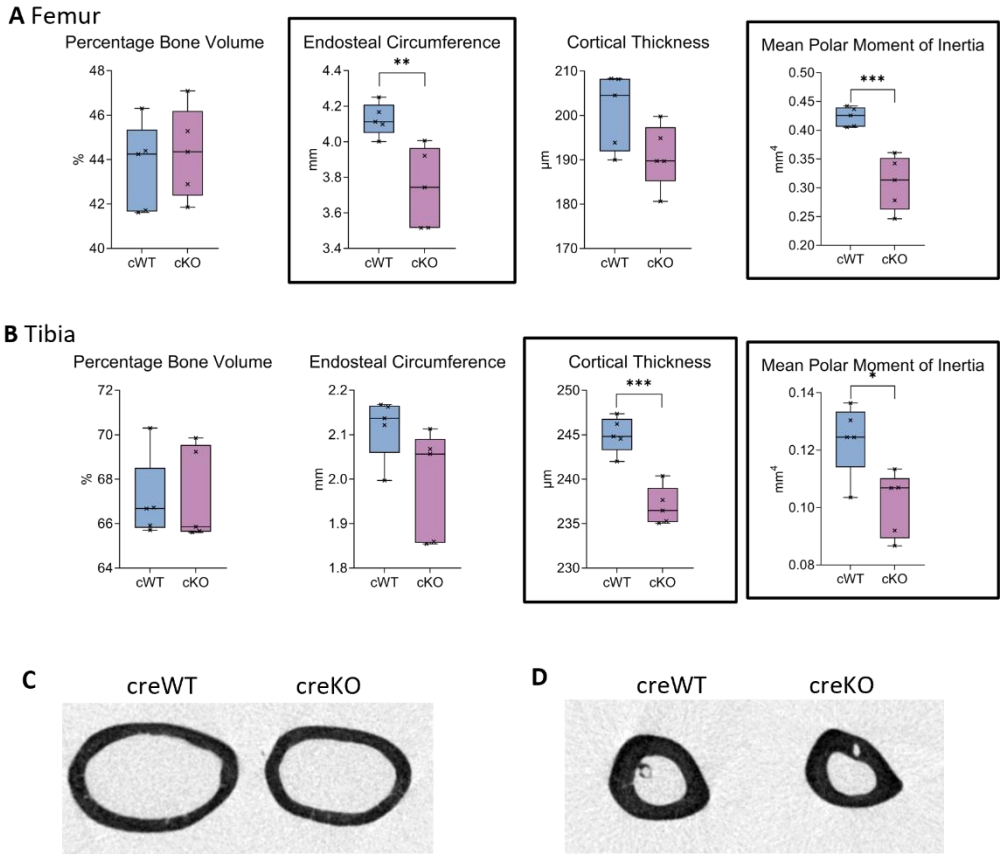

Figure 66. Col2cre knockout of Asporin produced weaker bones, smaller endosteal circumference of the femur and thinner cortical bone in the tibia. *uCT cortical parameters in the femur or the tibia (**A**, **B**) between the conditional wild-type (cWT) (blue) and the col2cre conditional Asporin knockout (cKO) (purple) bones. The endosteal circumference of the femur was smaller in the cKO than cWT and the MMI was lower, predicting weaker bones. The cortical bone of the tibia was thinner and similarly the MMI was lower in the cKO bones. uCT images were reconstructed in NRecon, Volume of Interest (VOI) was determined in DataViewer 100 slices distal of the femoral growth plate and 100 slices proximal to the tibial growth plate. The VOI was analysed in CtAn using the trabecular macro detailed in Appendix X. Student t-test were carried out between cWT and cKO (n=5) and denoted by *=p<0.05, **=p<0.01, ***=p<0.001. Representative images of cWT and cKO cortical bone from CtVox of reconstructed VOI of femur (**C**) and tibia (**D**). Error bars represent min to max.*

5.4.3 Col2cre conditional knockout of Asporin results in weaker and less stiff tibiae at 3 months of age.

The mean polar moment of inertia (MMI) was significantly decreased in the cKO bones and is a predictor of the likelihood the bone is to fracture under load. To determine an overall effect of the *Col2cre*-driven conditional loss of Asporin in the bone, destructive 3-point-bend tests were carried out on conditional knockout tibia and compared to tibiae of the conditional wild-types.

The destructive 3-point bending experiment supported the μCT data MMI result (Figure 67). The cKO tibiae were 47.0 % less stiff than conditional wild-type controls ($p=0.00627$), moreover the maximum force needed to break the cKO tibiae was 18.0 % less in the conditional knockout tibiae ($p= 0.0126$).

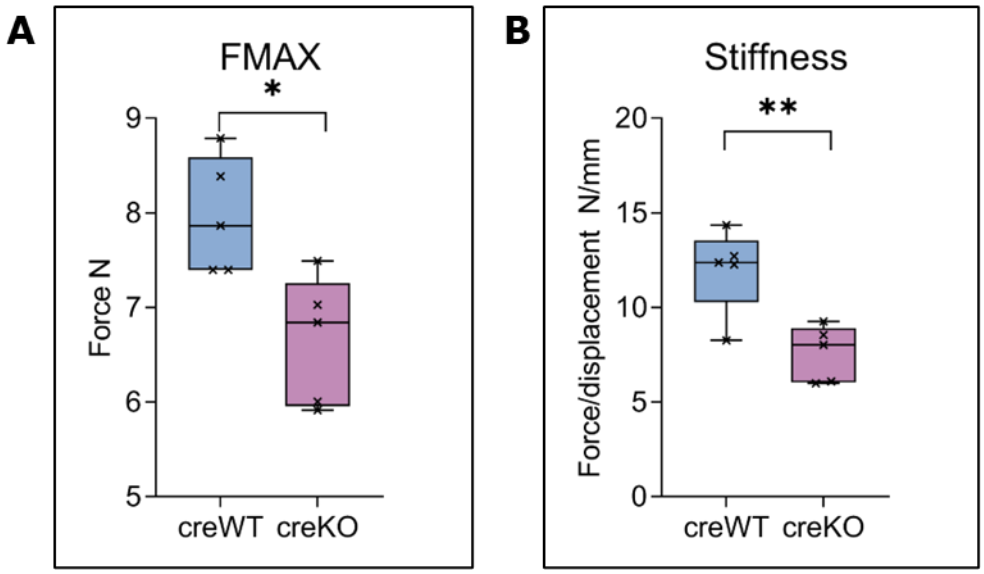

Figure 67. Col2cre knockout of Asporin reduces the strength and the stiffness of 12-week tibiae. *Destructive three-point bed tests were performed on conditional wild type and Col2cre Asporin knockout female tibiae and maximum force to break (Fmax) and stiffness were calculated (**A** and **B**). Col2cre Asporin knockout mice show significantly decreased FMAX relative to the conditional wild-type control. Additionally, the stiffness of the tibia was significantly reduced in the Col2cre Asporin knockout tibia relative to the conditional wild type. Error bars represent min to max. Student t-test were carried out between WT and KO (n=3) and denoted by *=p<0.05 and **=p<0.01.*

5.4.4 Higher number of smaller fat deposits are present in the Col2cre Asporin knockout tibiae at 3 months of age.

As previously discussed, the bone marrow adipocytes (BMATs) are not solely space filling or energy storage but also have an important function in the regulation of the bone marrow niche for haematopoiesis and bone cells production. Moreover, Asporin has previously been shown to control epidermal adipose tissue expansion[192].

In *Col2cre* Asporin knockout tibiae (cKO) at 3 months of age, although there was no significant difference in the overall number of the fat deposits per mm^2 of tissue or in the percentage area of fat relative to total tissue area (Figure 68 E and F). There was a significant difference in the distribution of the fat deposit size in the conditional knockout compared to the conditional wild-type. The conditional knockout tibiae had a higher proportion of smaller fat deposits ($p = 0.373$)without an effect to overall area of fat deposits. No published work has described any effect on the size of fat deposits on bone structure and function as historically the focus has been on the overall area of fat deposits, and the volume of bone marrow fat within the bone.

As there are higher numbers of smaller deposits in the cKO bones and adipocytes are secretory cells that can influence the niche of the bone marrow and coordinate changes in bone homeostasis, there may be some effect due to the increase in the diffusion rate as the surface of the deposit in contact with the bone marrow tissue is increased.

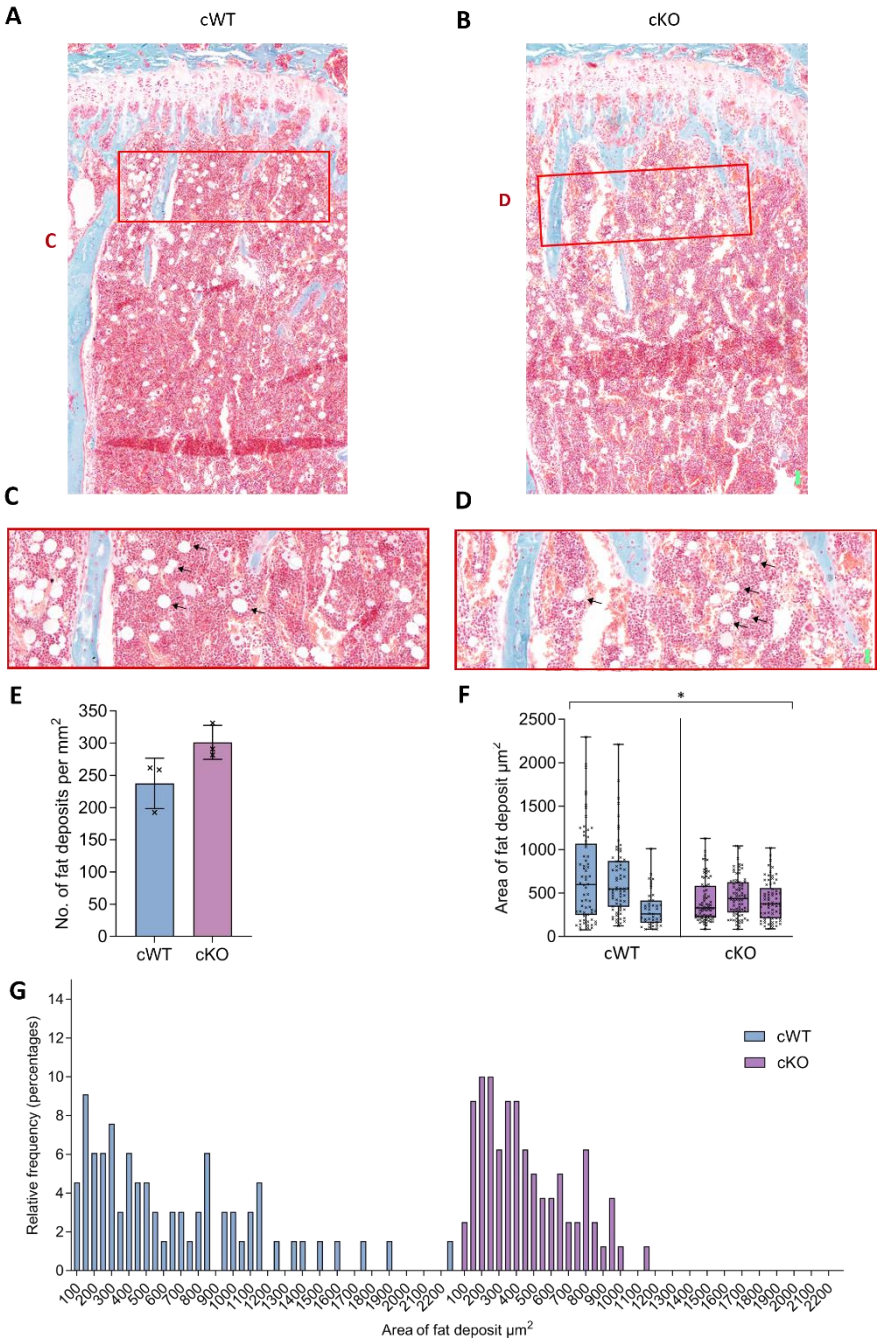

Figure 68. Col2cre knockout of Asporin have a higher proportion of smaller fat deposits in 12-week tibiae. *Conditional wild type and conditional knockout female tibiae sections were stained with Goldner's Trichrome to visualise fat deposits (A and B) Magnified regions with black arrows to highlight example of fat deposits in the tissue (C and D) Col2cre Asporin knockout mice show no difference in the number of fat deposit per mm² of tissue relative to the wild-type control. Area of fat deposits (µm²) for each section, error bars represent min to max (**F**) Conditional knockout tibiae has a smaller median fat deposit size than conditional mice, cWT median =520 µm², cKO median = 404.3 µm², p=0.0373. Histogram of all fat deposit counts display distribution of fat deposits by size, bins 50 um² (**G**) Student t-test (**E**) and Mann-Whitney U*

*analysis (F) were carried out between cWT and cKO (n=3) and denoted by *=p<0.05.. Student t-test (E) and one-way*

5.4.5 Osteoblast numbers are decreased in the Asporin cKO tibiae at 3 months of age.

To assess the effect of the *Col2cre*-driven knockout of Asporin on osteoblast numbers in the tibiae, methacrylate embedded sections were stained with Toluidine Blue to visualise and count osteoblasts number at the bone surface.

Interestingly, there was a 46.66 % decrease in osteoblast number per bone surface in the cKO bones at 3 months of age ($p=0.035$) (Figure 69) relative to the conditional wild type controls.

This decrease in bone formation is in line with the µCT data, which showed that the cKO cortical bone is thinner. A decrease in the osteoblast number would result in less bone being laid down. Moreover, the smaller overall bone size and endosteal circumference may also be a result of the lower osteoblast number. However, Asporin deletion under Col2cre may also impact osteoblast activity and osteoclast activity and function. The thinner bone may trigger bone remodelling to compensate for this, through osteocyte signalling to the periosteum and endosteum to promote osteoblast differentiation from periosteal cells and drive bone formation. If Asporin is deleted in the type II collagen positive skeletal progenitor cells of the periosteum, this could be a stage where Asporin is modulating the capacity of this process. Osteoblast and osteoclast activity will be investigated next to determine potential changes to the bone remodelling balance were investigated next.

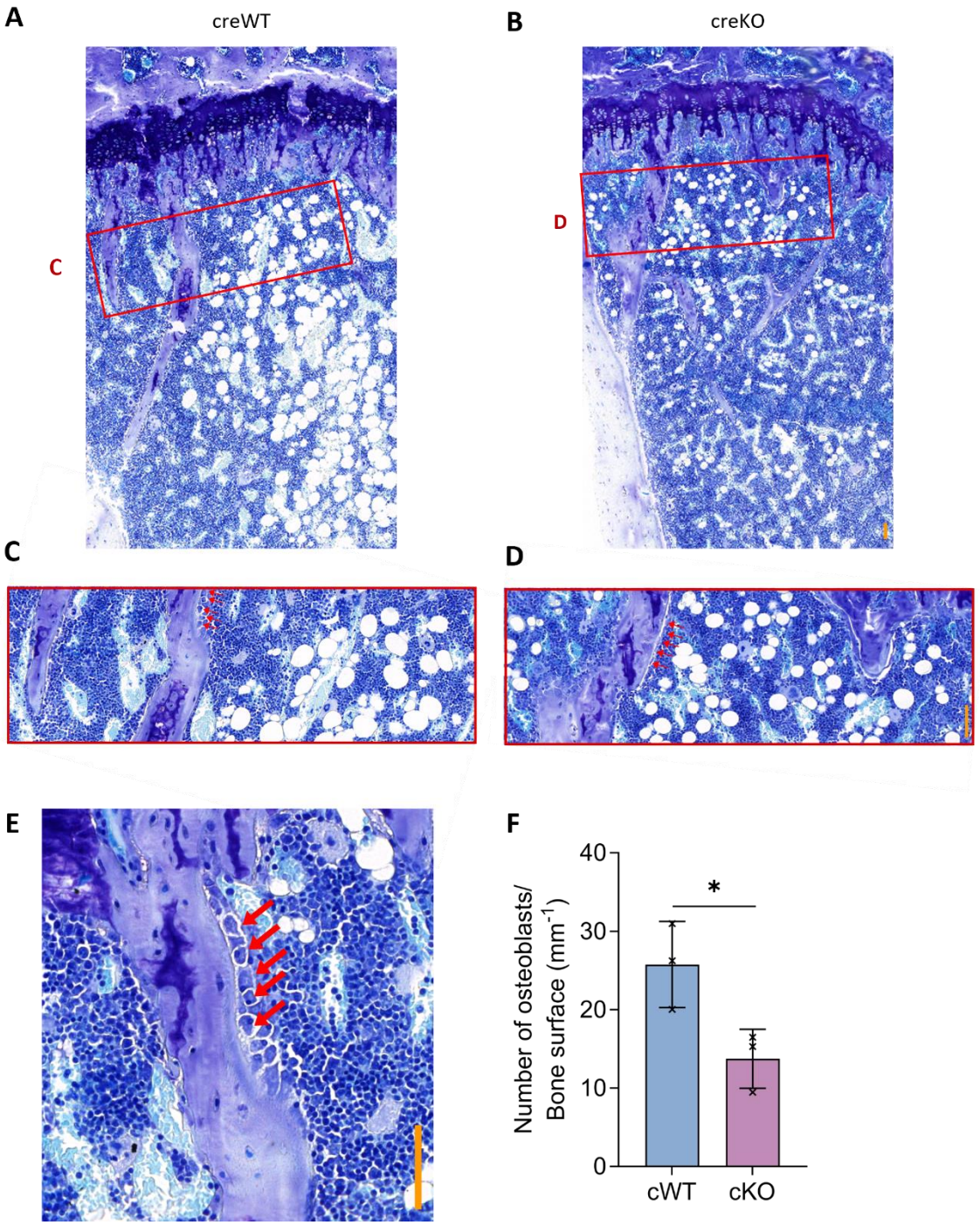

Figure 69. Col2cre knockout of Asporin decreased the number of osteoblasts in 12-week tibiae. *Conditional wild type and conditional knockout female tibiae sections were stained with toluidine blue to visualise osteoblasts (**A** and **B**) Magnified regions with red arrows to highlight example of osteoblasts along the bone surface in cWT (**C** and **E**) and cKO (**D**) Col2cre Asporin knockout show significant reduction of 46.66 % in the number of osteoblasts per bone surface relative to the conditional wild-type control. Standard deviation plotted error bars. Student t-test were carried out between cWT and cKO (n=3) and denoted by *=p<0.05. Scale bar 20 nm.*

5.4.6 There were no differences in the osteoid deposition in Asporin cKO tibiae at 3 months of age.

Briefly, osteoid is the unmineralised scaffold for the formation of new bone, it is secreted by osteoblasts and made up predominantly of Collagen type I fibres. The mineralisation of osteoid is the binding of hydroxyapatite crystals, the mineral form of calcium, to the collagen I fibres. Asporin has been previously implicated in this process by Kalamajski et. al. where Asporin has been shown to bind and mineral type I collagen fibres, the only SLRP capable of this[123].

As previously discussed, there was a reduced number of osteoblasts in the *Col2cre* Asporin knockout bones. However, there was no difference in the osteoid surface to bone surface or in the osteoid volume relative to the bone volume in the cKO tibiae at 3 months of age compared to the cWT controls (Figure 70).

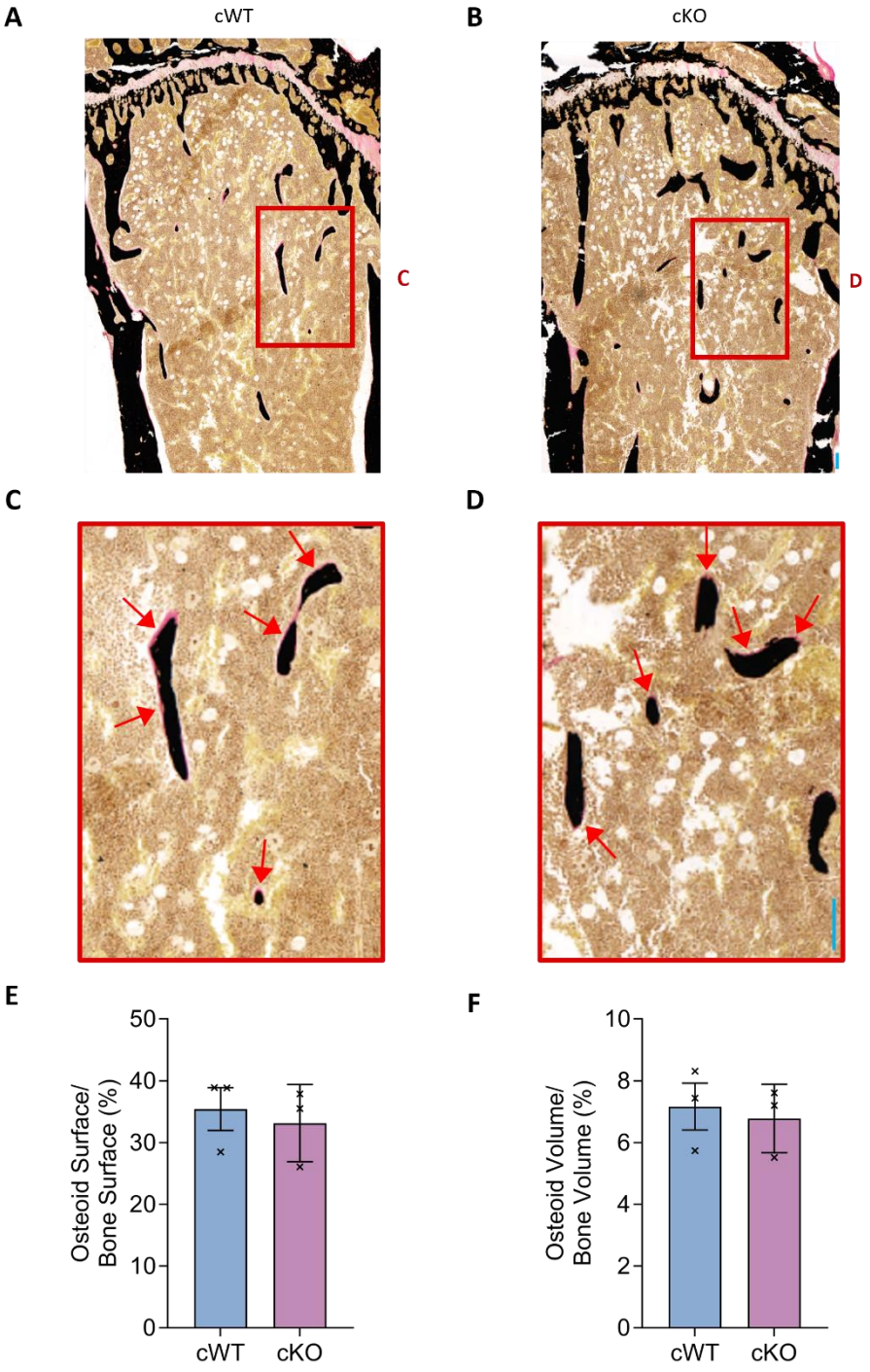

Figure 70. Col2cre knockout of Asporin has no effect on the osteoid surface or volume of osteoid 12-week tibiae. *Wild type and conditional knockout female tibiae sections were stained with Von Kossa and Van Gieson to visualise bone (black) and osteoid deposition (red/pink)(**A** and **B**) Magnified regions with red arrows to highlight example of osteoid deposition along the bone surface (**C** and **D**) Col2cre Asporin knockout mice show no difference in the percentage of osteoid surface to bone surface and the volume of osteoid to bone volume relative to the wild-type control. Standard deviation plotted error bars. Student t-test were carried out between cWT and cKO (n=3) and denoted by *=p<0.05. Scale bar 20 nm.*

5.4.7 Col2cre knockout of Asporin increases osteoclast numbers in 3 month old tibiae.

Osteoclasts are the bone resorbing cells important for bone turnover and removal of old and damaged bone. Osteoclasts work alongside the bone producing osteoblasts to maintain healthy bone mass and appositional growth.

Interestingly, in the *Col2cre* Asporin knockout tibiae at 3 months of age, the number of osteoclasts in the tibia per bone surface (mm) measured using the TRAcP assay, was significantly increased by 246.9 % ($p=0.0069$) and the number of osteoclasts per mm^2 of bone area was significantly increased by 257.96 % ($p=0.047$) relative to the conditional wild type controls (Figure 71).

This increase in osteoclast activity can result in disturbed bone homeostasis. A change in the bone turnover rate can have significant effects on bone health and strength. To assess dynamic homeostasis within the bone, histomorphometry studies have therefore been carried out to determine changes to the homeostasis.

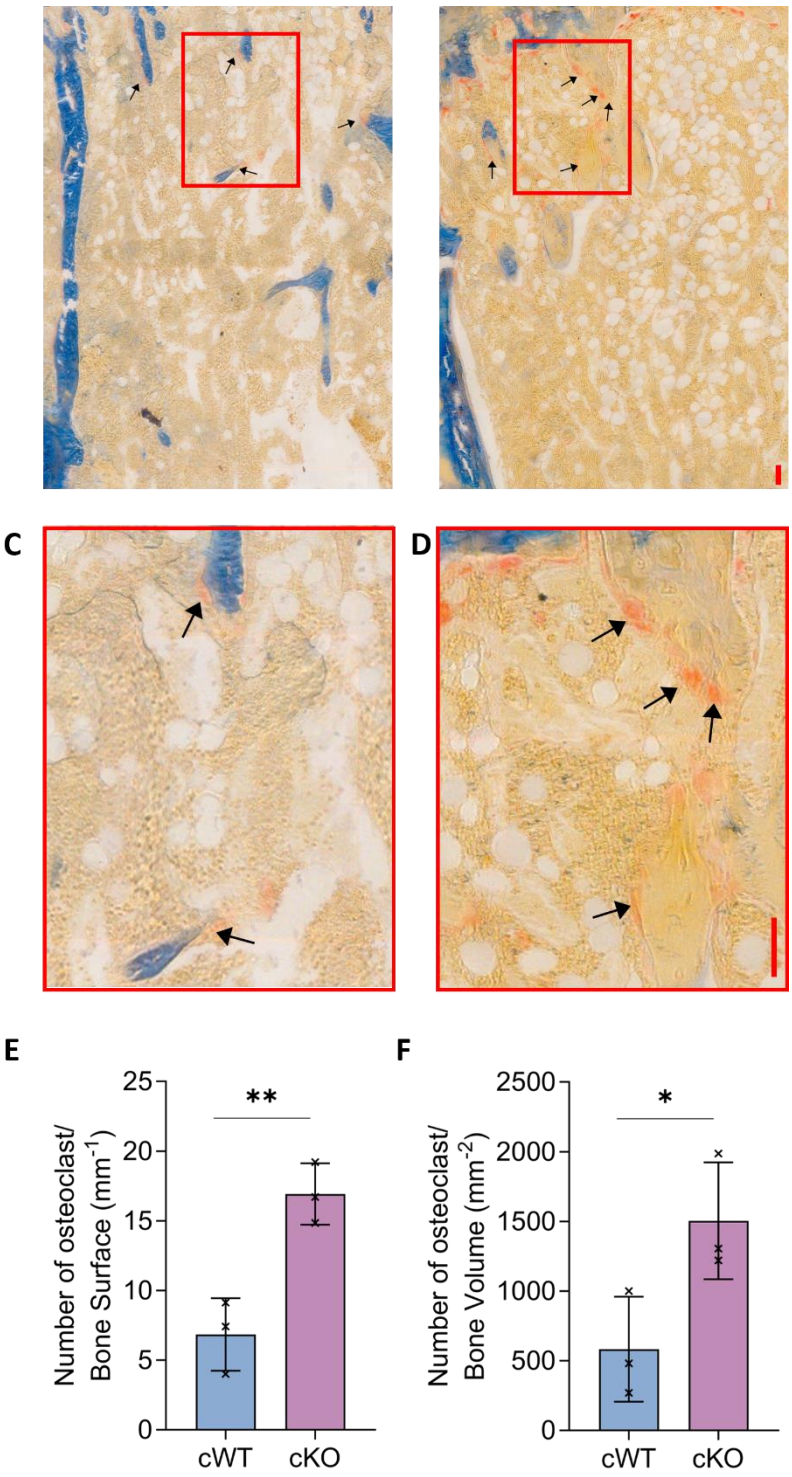

Figure 71. Number of osteoclasts was increased in the Col2cre knockout of Asporin in 12-week tibiae. *Tartrate-resistant acid phosphatase (TRACP) staining was carried out on conditional wild-type and conditional knockout female tibiae sections to visualise osteoclasts (**A** and **B**) Magnified regions with red arrows to highlight example of osteoclasts (red/pink) along the bone surface (**C** and **D**) Col2cre Asporin knockout mice show significantly more osteoclasts per bone surface and number of osteoclasts per mm^2 bone volume, relative to the conditional wild-type control. Standard deviation plotted error bars. Student t-test were carried out between cWT and cKO (n=3) and denoted by *=p<0.05.Scale bar 20 nm.*

5.4.8 Col2cre-driven loss of Asporin impedes mineralisation of the osteoid seam and reduces the bone formation rate at 3 months of age.

A histomorphometry experiment was performed by double labelling of mice at 12-weeks of age via peritoneal injections of Alizarin red and Calcein green, as described previously. The bones were methacrylate embedded, sectioned and counterstained with Calcein blue. The distance between the two stains (Figure 72) was measured using ImageJ and used to calculate the bone dynamics. The results (Figure 72) show a reduction of the mineral apposition rate (MAR) and the bone formation rate per bone surface (BFR/BS) in the Col2cre Asporin knockout tibiae, relative to the conditional wild-type.

A reduction in the MAR is indicative of slower bone formation as mineralisation of the osteoid seam is reduced. The BFR/BS reduction confirms less bone is formed per day per unit of bone surface. The MS/BS is unchanged in the *Col2cre* Asporin knockout relative to the conditional wild type controls, indicating that there is a comparable mineralising surface, however, the mineralisation is reduced.

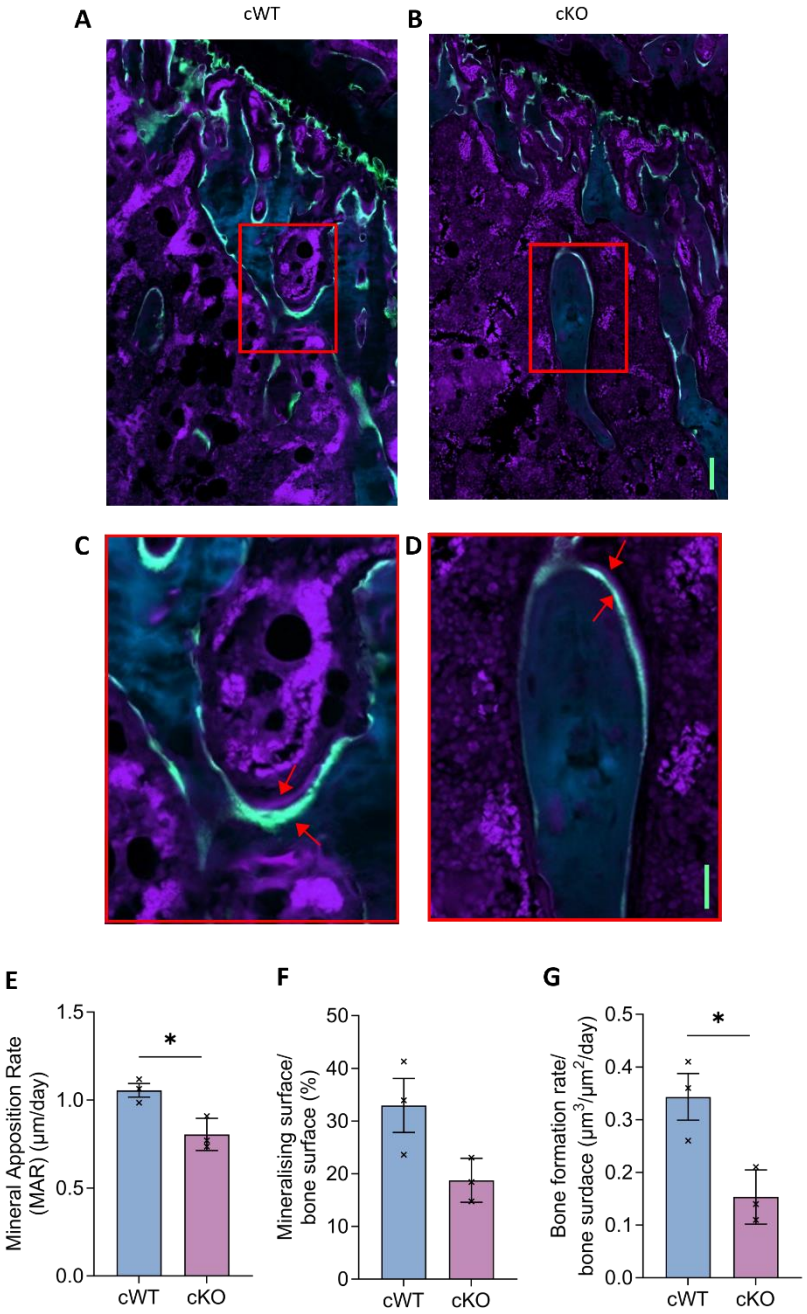

Figure 72. Col2cre knockout of Asporin reduces MAR and the Bone formation rate per bone surface. *Double labelling injections of alizarin complexone (purple) and calcein green (green) counterstained with calcein blue (blue) and imaged using fluorescent microscope (**A** and **B**) Magnified regions to show distinct double label at the bone surface (**C** and **D**) Col2cre Asporin knockout mice show significant reduction in the mineral apposition rate (MAR) (**E**), no difference in the mineralising surface per bone surface (MS/BS) (**F**) and significantly reduced bone formation rate per bone surface (BFR/BS) (**G**), relative to the wild-type control. Standard deviation plotted error bars. Student t-test were carried out between WT and KO (n=3) and denoted by *=p<0.05. Scale bar 20 nm and 10 nm respectively.*

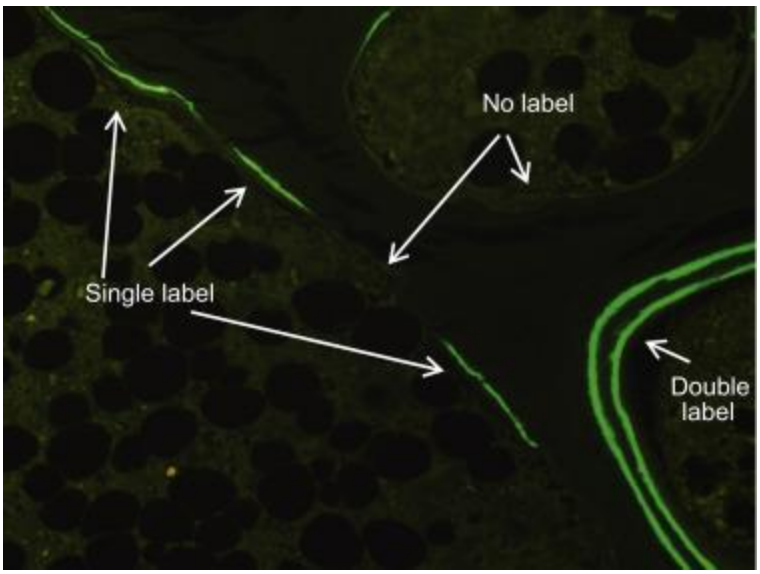

Figure 73. Example image of double labelling in bone. *Double labelling injections both of calcein green (green) counterstained to demonstrate the selection of the single and double labelling. Measurement of the MAR is calculated by the distance between two lines. As a smaller window between injections and at 12-weeks the growth plate is less active therefore the distance is smaller than on the example, 2 labels were used alizarin complexone and alizarin green to allow better discretion identifying the double labels. Image obtained from Basic and Applied Bone Biology -Chapter 8, Allen et al*[194].

5.5 ALP activity is decreased in primary osteoblasts derived from Col2cre Asporin knockout mice, consistent with reduced osteoblast numbers.

Alkaline phosphatase is an enzyme necessary for the mineralisation of the bone matrix, and important for the hydrolysis and release of hydroxyapatite which is bound to the collagen fibres in bone mineralisation. ALP activity is a commonly used biomarker of osteoblast activity.

Interestingly, the *Col2cre*-driven knockout of Asporin resulted in significantly reduced ALP activity at day 7 of primary osteoblast culture, 80.376 % reduction in the conditional knockout relative to their conditional wild-type ($p<0.05$).

Osteoblasts and hypertrophic chondrocytes produce ALP. As previously shown, the osteoblast numbers are significantly reduced in the conditional knockout of Asporin tibiae. The reduction of ALP is consistent with this phenotype, reduced numbers of osteoblasts would result in reduced ALP activity.

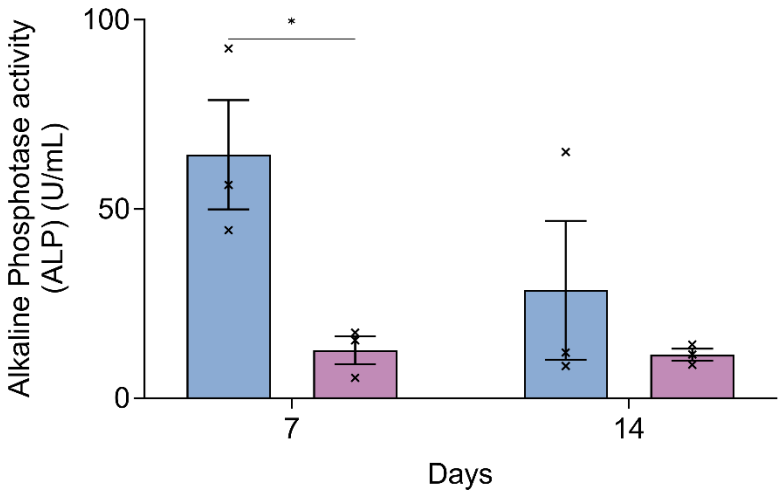

Figure 74. Col2cre knockout of Asporin reduced **alkaline phosphatase activity in primary osteoblasts.** *ALP activity of primary osteoblasts measured at day 7 and 14 of mineralising 21-day cell culture in osteogenic medium. Comparison of conditional wild-type (cWT) (blue) and Col2cre Asporin knockout (cKO) (purple). ALP activity was significantly reduced at day 7 in the conditional knockout osteoblasts. ALP activity was measured using a colorimetric assay kit read by spectrophotometry. Respective ALP activity was calculated from calibration curve of standards for ALP activity. Standard error of the mean was calculated and plotted, and 2-way ANOVA was carried out between WT and OE and across each timepoint, between WT and OE (Black *) and within the genotype between each time point (Grey *), (n=3) and denoted by *=p<0.05.*

Discussion

Asporin is an SLRP with the unique capability in its family to bind calcium and mineralise collagen fibrils and has previously been shown to play a role in regulation of the collagen fibre diameter in skin, and in osteoblast differentiation and in mineralisation of the bone cells *in vitro*[123]. The previous experiments in Chapter 3 determined a role of Asporin in mineralising the ECM of ATDC5 cells and reduced sulphated proteoglycan, possibly due to the downregulation in decorin disruption the aggrecan and type II collagen network in the ECM. Chapter 4 determined that Asporin does not show changes to the growth plate or the articular cartilage in structure or in the expression of ECM proteins. Overall, the mice grew normally, alike to the respective wild-type mice. This suggests, there was no disruption to endochondral ossification. However, the novel data presented here highlights a clear effect of the conditional knockout of Asporin in type II collagen expressing cells on bone remodelling and cortical bone.

Interestingly, a global deletion of Asporin in all mouse tissues had no effect on the bone structural and mechanical parameters nor on the numbers or activity of BMATs, MSCs, osteoblasts and osteoclasts. The only difference detected in the global knock-out bones at 3 months of age was a difference in the stiffness of the tissue, potentially meaning that the Asporin null bones are more elastic. The periosteum and endosteum are responsible for appositional growth, ensuring the bone is strong enough to withstand mechanical forces exerted onto it, the bone is mechanoresponsive and can remodel to accommodate the mechanical force. If Asporin is involved in the periosteal cells differentiation into osteoblasts for bone formation this could explain the difference in the increased elasticity of the global knockout tibiae

However, the targeted knockout of Asporin under the *Col2* promoter resulted in weaker bones with thinner cortical bone. Type II collagen is expressed by mesenchymal precursors of the osteoblast lineage,

chondrocytes, but also in early differentiating osteoblasts and a subset of cells in the periosteum[195]. As the conditional knockout works under the type II collagen promoter, Asporin will be knocked out in these cells.

The reduction in osteoblast numbers in the cKO bones, reduced ALP activity, and increased osteoclast numbers, demonstrate a clear disruption in bone homeostasis, which is further supported by decreased bone deposition rate, demonstrated by the histomorphometry studies. A reduction of bone formation would limit replacement of new trabecular bone, but additionally it would limit appositional growth of the bone. This compromise in bone formation has been shown in previous studies to weaken the structural integrity of the bone and implicated in osteoporosis, where bone density is found to be decreased.

Most interestingly there was no difference found in the osteoid surface of the *Col2cre* Asporin knockout mice however the mineral apposition rate and the bone formation rate per bone surface was reduced. It would be expected that with a reduction in osteoblast numbers and activity, there would be a reduction in osteoid deposition as well as in mineralisation. With the reduction in osteoblasts but no difference in the osteoid this could be suggestive of an accumulation of osteoid rather than an increased rate of osteoid production. Conditions such as Osteomalacia where osteoid mineralisation is impaired, the osteoid accumulates and results in weakened long bones and additionally abnormal levels of calcium and phosphorus in the serum of individuals with osteomalacia[196]. This is further supported by the histomorphometry data, where the mineralisation rate is significantly reduced in the cKO mice. Taken together, the presence of Asporin in the wild-type calcification zone and the cartilage specific knockout of Asporin in the growth plate where type II collagen expressing cells are present, the reduced osteoblast numbers without a decrease in osteoid and furthermore the reduced MAR it could be suggested that there is a disruption to the osteoblasts ability to mineralise the type I collagen osteoid and therefore the osteoid accumulates.

This dysregulation in the bone formation and the increased osteoclast activity highlight a role for Asporin in the mineralisation of osteoid. These defects in the bone mineralisation are similar to those observed in osteomalacia and the increase in osteoclast activity alike to that observed in osteoporosis, both conditions have damaging effects on bone strength, with bones being found to be weaker and more likely to fracture. As shown in the 3-point bend tests, the Col2cre bones were also found to be weaker and needing less force to break the bones. This novel finding suggests a role for Asporin in fracture repair, the cells of the periosteum have been shown to be involved in fracture repair, the presence of type II collagen positive cells in the periosteum confirming Asporin will be deleted in populations of the periosteal cells, may be an explanation for the changes shown to the cKO bones, where the bones are weakened, and bone remodelling is hindered. .

In the type X collagen specific knockout of *Runx2* to delete Runx2 specifically in the hypertrophic chondrocytes, by Qin et. al. it was found that the mice trabeculae developed abnormally prenatally due to a reduction in transdifferentiation of the chondrocytes to osteoblasts however by 6 and 20 weeks the trabeculae was normal, they determined through cell lineage tracing that there was sufficient osteoblasts from the perichondrium that could remodel and build up the trabecular bone to normal[177]. This highlights the importance of the perichondral and periosteal cells in contributing to bone remodelling and strength. The mouse bones develop as normal however there is a clear disruption to remodelling, this may suggest that Asporin is dispensable in endochondral ossification as demonstrated in Chapter 4 however it is important in the remodelling. The converse to this work by Qin et. al may be happening in the Asporin knockouts where transdifferentiation and initial growth is normal however the periosteal and perichondral cells with Asporin knocked out, under the type II collagen promoter, cannot function correctly in the mineralisation and deposition of new bone to remodel.

The thinner cortical bones is very interesting there is a reduction in the cortical thickness and the endosteal circumference, these are two parameters modified by appositional growth. This further alludes to a role of Asporin in the periosteum/perichondrium. This may be in the initial formation of the bone collar where the perichondrium differentiates to osteoblasts and produces mineralising bone encompassing the growth plate, or later in the appositional growth of the cortical bone.

Further study will be essential to study this in more detail, transverse sections of the tibia cold be used to assess cortical parameters with histology using the techniques employed here. It would be interesting to see if the osteoid is also accumulating at the periosteum or endosteum and whether there are changes in the histomorphometry parameters in the cortical bone.

Interestingly the primary osteoblasts came from bone chips, where the chips were cultured and migrate out of the bone. This is predominantly cortical bone as most trabecular bone is removed during the bone marrow removal steps. These cortical bone derived osteoblasts show reduced ALP activity in the conditional knockout mouse cells. ALP is crucial for the formation of mineralised bone tissue, ALP hydrolyses pyrophosphates, such as BGP used in the Chapter 3 mineralisation studies [197]. The hydrolysis of the pyrophosphate produces the inorganic phosphate hydroxyapatite, the molecule incorporated for the mineralisation of bone and cartilage. In Chapter 3 mineralisation of the ECM containing type I collagen increased with the overexpression of Asporin in the presence of BGP; here we see a decrease in ALP expression and in the bone reduced mineralisation of the osteoid, made up of predominantly type I collagen. Considering these together there is a possibility of Asporin modulating ALP activity. However, this would need further testing to ascertain a clear pathway of Asporin and ALP interaction.

However, mouse numbers have significantly hindered the strength of this research, with changes being subtle it would be necessary to increase

the number of the mice to bring it to publishable quality and to be able to draw meaningful conclusions from the data. Using the data here for global μCT data, for the MMI in the cortical tibia analysis, through power calculations it was determined a sample size of 10 would be sufficient to find a significant difference, this would coincide with the significant reduction in the tibia stiffness in the global knockout, in this study an n of 5 was measured. However, using the osteoclast data of the wild-type and global knockout, which was a significant finding in the conditional knockout, it was determined a sample size of 56,000 would be needed to find significance, this estimated sample size may be skewed slightly as only n=3 was used in the plastic histology, nevertheless the difference in global was so subtle that this lack of significance is likely to be a real no difference and not due to a low number of samples.

Chapter 6. Role of Asporin in Development of the Spine

6.1 Introduction

The spine is a critical structure of the central skeleton which acts as support for the entire skeleton and the vital organs. Alike to long bones, the spinal vertebrae also form through endochondral ossification with a singular ossification centre, separating in to 2 ossification centres by calcified bone forming two growth plates (the end plates) at the top and bottom of each vertebra. As a result of this similarity, mutations affecting long bone formation often also present with a spinal phenotype, as all growth plates of the skeleton are disrupted. This is seen in spondyloepiphyseal dysplasia congenita, where both the spine and the long bones growth and formation are disrupted as a result of a Type II Collagen mutation[198].

In addition to abnormalities within the vertebrae, there can be changes to the intervertebral disc (IVD). Alike to the articular cartilage, protecting the end of long bones in the knee and hip joints, the ends of the vertebrae in the spinal column are covered by cartilage protective layer, formed by the fusing of the secondary ossification centres to for cartilaginous end plates. Intervertebral discs (IVD) also a key element of the spinal structure, cartilage discs between the vertebrae which absorb forces on the spine and cushion the vertebrae. As discussed, the IVD is made up of the annulus fibrosus (AF), which is separated into the outer annulus and the inner annulus, the cartilage endplates which connect the IVD to the vertebrae and the nucleus pulposus (NP)[199, 200]. The annulus fibrosis is made up of predominantly collagens and fibroblast cells, the inner and outer annulus can be distinguished by the ratio of type I to type II collagens, the inner annulus made up of majority type II collagen and rounded fibrocartilage cells and the outer annulus made up of majority type I collagen and elongated fibroblast-like cells[201].

Alike to the knee joints, the degradation of the cartilage in the spine results in inflammation, loss of cartilage and damage to the underlying bone,

similar to that of OA, this is referred to as intervertebral disc disease (IDD). As previously discussed, Asporin has been implicated in osteoarthritis, further studies found the D14 polymorphism was linked to lumbar disc degeneration in an Asian population[202]. This makes it interesting to investigate the role of Asporin within the spine and IVD if modulation of Asporin was to be used as a therapeutic target in OA or IDD.

Chapter aims:

- To determine the role of Asporin in development of the spine by histology analysis of 12-week old wild type and Asporin null spines.
- To carry out micro-CT analysis of 12-week old spines with the global knockout of Asporin, conditional Col2cre knockout of Asporin and the respective wild type control spines

6.2 Global and conditional loss of Asporin has no effect on proteoglycan distribution of the spinal cartilage and bone tissue.

To investigate the role of Asporin in spinal development, 12-week old plastic embedded spinal sections of the L5 and adjacent IVD were stained with Safranin O to visualise the structure of the tissue and the presence of cartilage in the end plates and the IVD structure.

The annulus fibrosis surrounds the nucleus pulposus, as mentioned is subdivided into the inner annulus and the outer annulus[200]. The annulus is crucial for the structure of the spine, absorbing compression and protecting the spine under tension and torsion.

Safranin O stains cartilage by staining proteoglycans of the cartilage ECM. Commonly, Safranin O is used in OA studies as it can be used for semi-quantitative data by scoring of loss of staining being proportional to the loss of cartilage[203].

In the global knockout of Asporin the overall structure of the knockout was comparable to that of the wild type spine. The safranin O staining of the cartilage end plates and annulus fibrosis, was alike to that of the wild type. However, in the Col2Cre conditional knockout of Asporin there was a subtle difference in the staining of the inner annulus of the upper IVD, however this may be an artifact as it was not consistent in the conditional knockout IVD, whilst the overall structure of the vertebrae is not different to that of the conditional wildtype. (Figure 75)

To gain more insight into any structural changes to the bone and the development and to confirm whether the difference in conditional knockout staining within the IVD was real or artifact, Goldner's Trichrome was employed. This uses multiple stains outlined in 2.7.5.4 to visualise particular features of the bone, this combination stains the bone marrow

dark red and the uncalcified cartilage and uncalcified bone (osteoid) stains red and light green stains the bone pale green/blue.

No differences were observed in the global knockout L5 vertebrae in comparison to the WT in the Goldner's trichrome staining. The IVD of the conditional knockout of Asporin appeared to have reduced staining in the inner annulus, however the follow up staining with Goldner's did not support this and the difference in staining is likely to be an artefact than a true difference. However, interestingly, observing the osteoid deposition in the conditional knockout vertebrae, (pink/bright red in the bone marrow adjacent to the bone), there appears to be increased osteoid, unmineralised bone matrix made up of type I collagen in the cKO vertebrae in comparison to the cWT where there is essentially no osteoid deposition. (Figure 76)

Although there were no obvious differences in the structures of the global knockout and conditional knockout vertebrae compared to the relative wild type controls, this is qualitative data. To investigate, quantitative parameters of the L5 vertebrae structure, a μCT analysis was carried out on the L5.

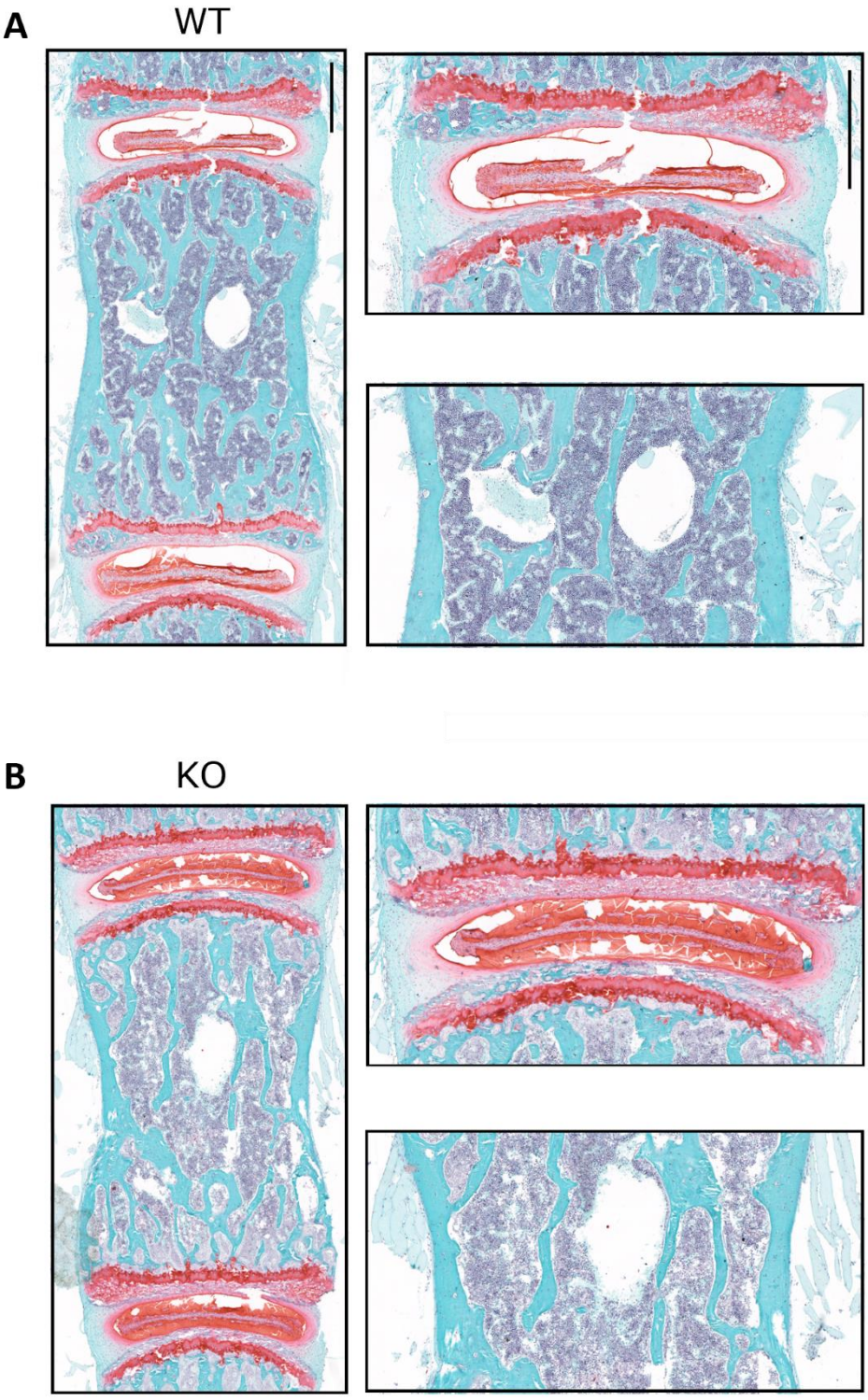
A
WT
B
KO

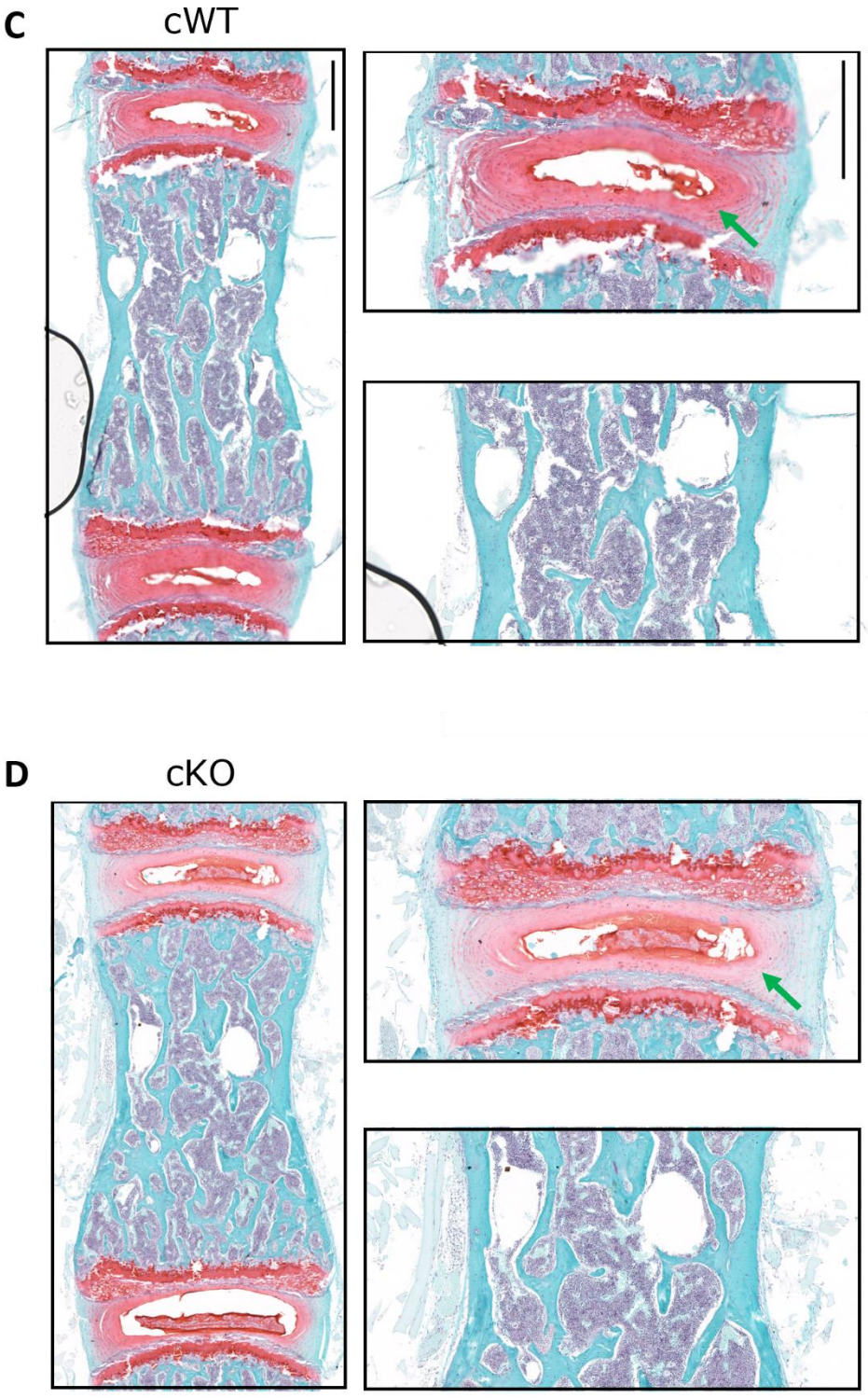

Figure 75. No apparent difference in the cartilage of L5 endplates and the IVD in the global and conditional knockout of Asporin. *Safranin O/ Fast green staining of the L5 vertebrae to visualise, cartilage (red), bone tissue (blue) and the nuclei (black). No overt differences in the tissues and structure of the L5 vertebrae in the global knockout of Asporin (**B**) in comparison*

*to the wild-type vertebrae (**A**), or in the conditional knockout (**D**) in comparison to the conditional wild-type vertebrae (**C**). Green arrows indicate the inner annulus where a subtle difference in staining is observed. Sections were matched between WT and KO, and cWT and cKO .Magnified images of the IVD and the vascularisation entrances of the spinal arteries into the vertebrae (white circles). Scale bar = 5 nm.*

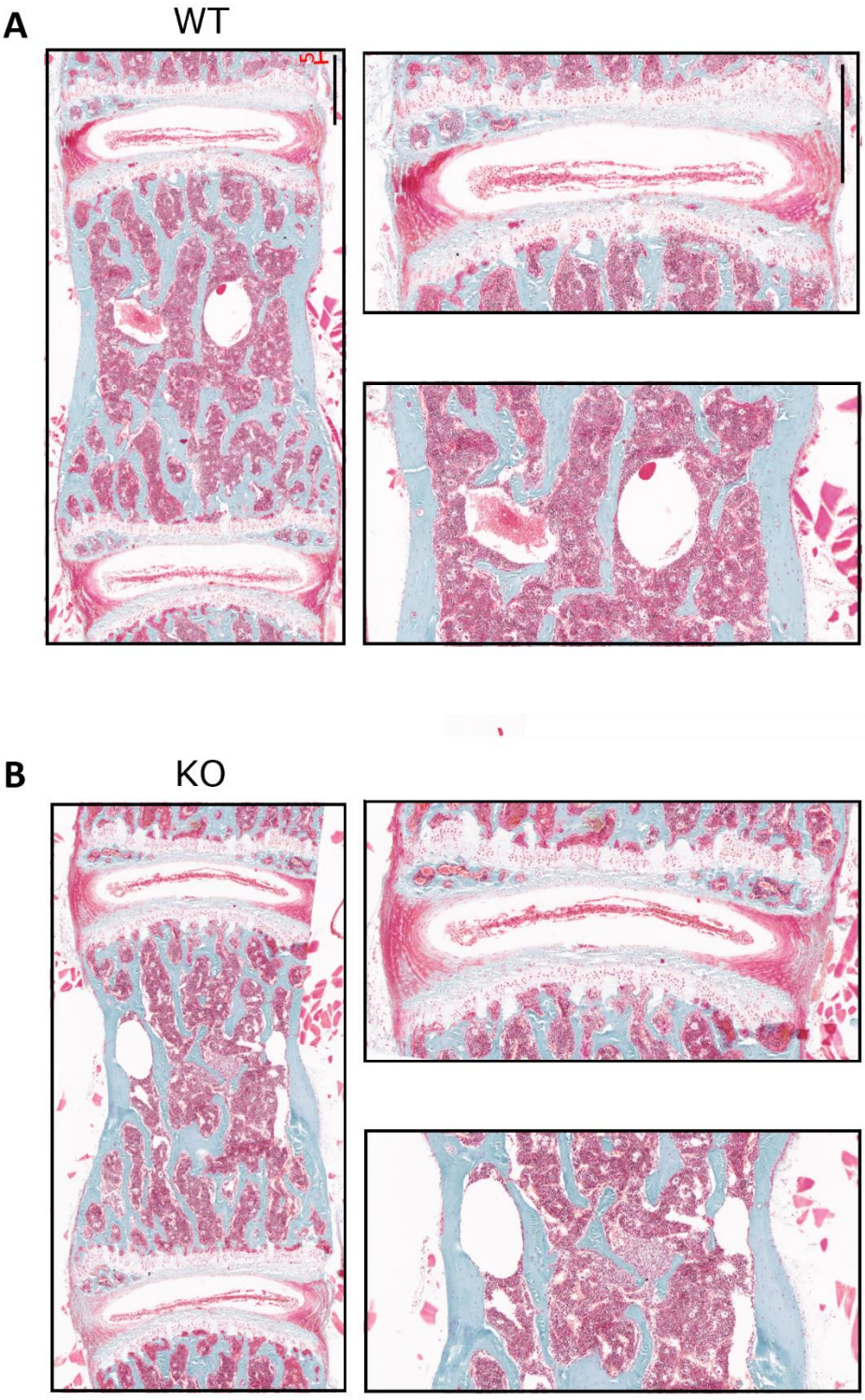
A
WT
B
KO

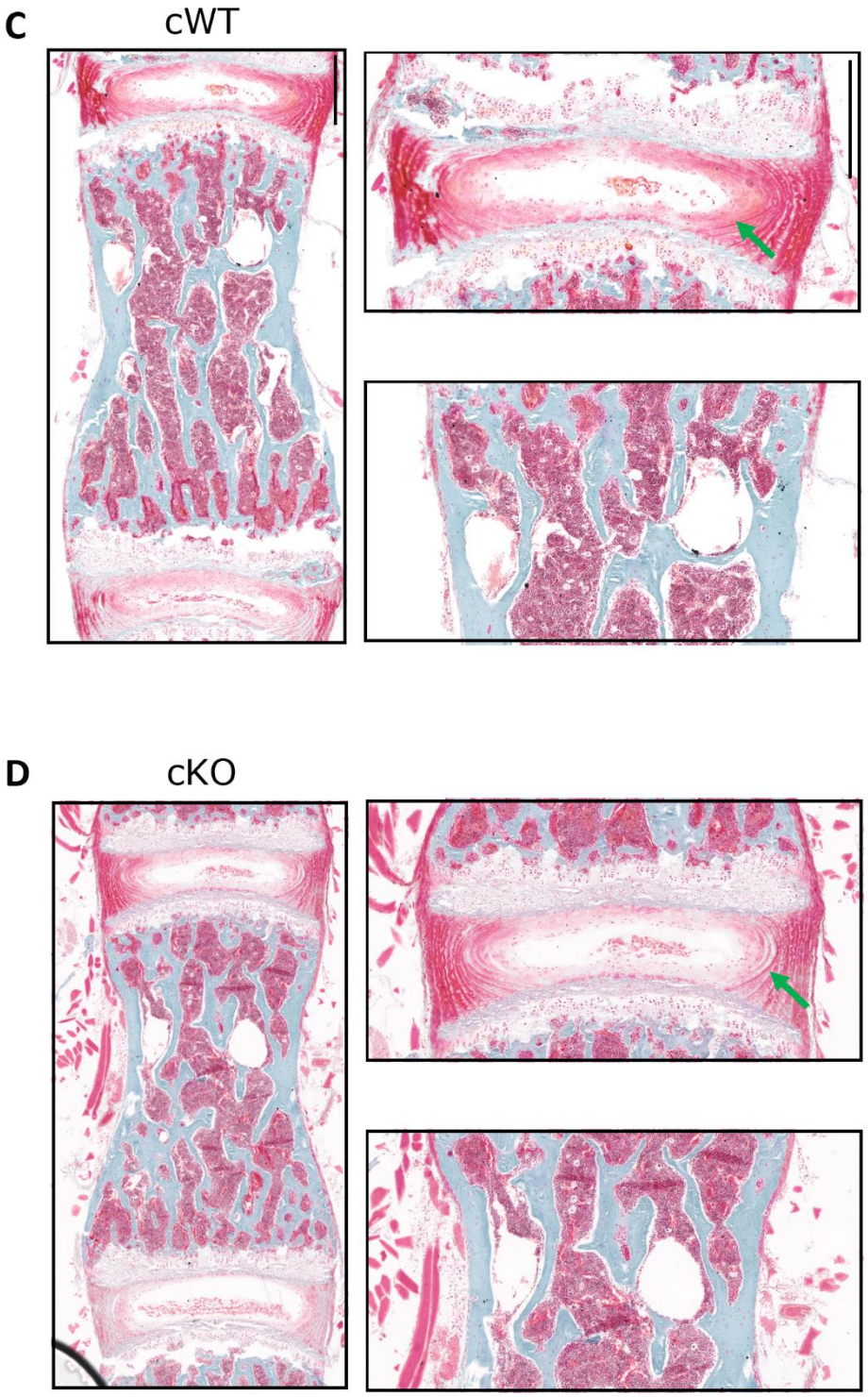

Figure 76. Osteoid deposition is increased as a result of the conditional knockout of Asporin. L5 endplates, spinal tissue and the IVD in the global and conditional knockout of Asporin. *Goldner's trichrome staining of the L5 vertebrae to visualise, cartilage and osteoid (pink/red), bone tissue*

*(blue) and the bone marrow (dark red). No overt differences in the tissues and structure of the L5 vertebrae in the global knockout of Asporin (**B**) in comparison to the wild-type vertebrae (**A**). However, osteoid deposition was increased in the conditional knockout (**D**) in comparison to the conditional wild-type vertebrae (**C**). Sections were matched between WT and KO, and cWT and cKO. Magnified images of the IVD and the vascularisation entrances of the spinal arteries into the vertebrae (white circles). Scale bar = 5 nm.*

6.3 Trabecular bone of the L5 vertebrae was not different in the global or conditional knockout of Asporin.

uCT analysis of the L5 has not been carried out on Asporin null and conditional mice previously. The parameters used for trabecular analysis cover percentage bone volume this is the volume of bone calculated as a percentage of the whole tissue volume, excluding cortical bone as that is analysed separately. Trabeculae are the rods and planes of bone that form the interconnected network of cancellous bone, these trabeculae surround bone marrow. Trabecular number is the total number of trabecular, thickness is the average thickness of the trabeculae, and the trabecular separation is the distance between trabeculae. The number, thickness and separation all impact the strength of the bone and health of the bone due to changes in the bone volume to bone marrow volume ratio. Enough bone mass is crucial for strength but too much bone can result in less bone marrow which is necessary for bone homeostasis and recovery. The pattern factor is a determinant of the shape of the trabeculae, lower number means a higher proportion of rod like trabeculae and a higher number indicates a higher proportion of plane like trabeculae. Finally, the Structure Model Index (SMI) is calculated based on the previous parameters and gives an overall prediction of the likelihood of the bone to snap. Cortical bone is not studied in the vertebrae, vertebrae are predominantly trabecular bone with only a thin layer of cortical bone at the surface of the vertebrae. uCT analysis macro have not been developed for cortical analysis and the thin nature of the cortical makes it challenging to do so.

Despite the Asporin's involvement in the IDD, no difference was found in the trabecular analysis of the 12-week mice vertebrae in the global or conditional knockouts. Loss of asporin has no effect on uCT parameters of trabecular formation and cancellous bone microarchitecture at 12 weeks.

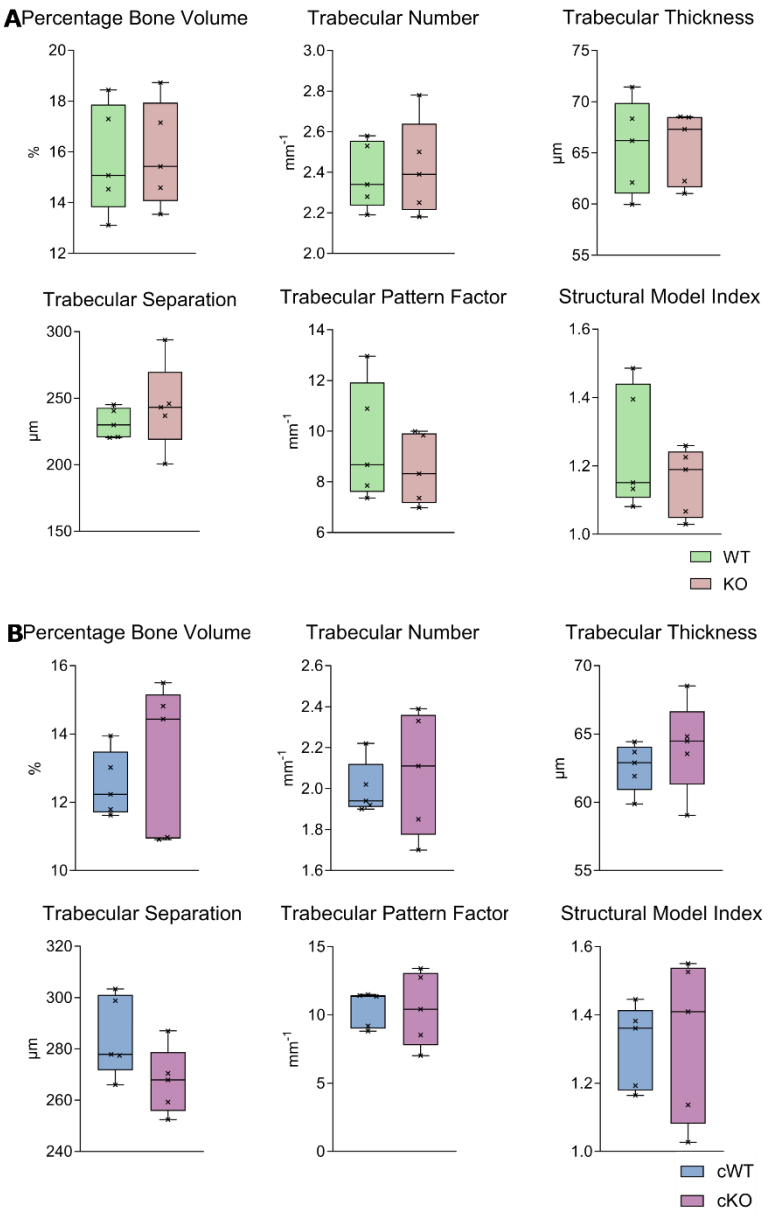

Figure 77. Global and Col2cre conditional knockout of Asporin had no effect on the microarchitecture of trabecular bone of the L5. *No difference was found in any uCT trabecular parameter in the L5 between the wild type (WT) (green) and the global Asporin knockout (KO) (red) mice (**A**) or between the conditional wild type (WT) (blue) and the col2cre conditional Asporin knockout (cKO) (purple) mice (**B**). uCT images were reconstructed in NRecon, Volume of Interest (VOI) was determined in DataViewer immediately distal to the femoral growth plate up to immediately proximal to the tibial growth plate. The VOI was analysed in CtAn using the L5 macro detailed in Appendix X. Student t-test were carried out between WT and KO and cWT and cKO(n=5) and denoted by *=p<0.05. Representative images of WT and*

*KO trabecular bone from CtVox of reconstructed VOI for WT and KO L5 vertebrae (**C**) and cWT and cKO L5 vertebrae (**D**).Error bars represent min to max.*

6.4 Discussion

As Asporin has been implicated in intervertebral disc (IVD) biology and in the bone changes observed in the conditional knockout (cKO) mice described in Chapter 5, it is important to consider a role of Asporin in spinal growth which shares similarities with long bone development. Both processes involve a growth plate and undergo mechanisms similar to endochondral ossification[140]. The changes observed in the legs highlighted an accumulation of osteoid in the long bones and a reduction in its mineralisation. There were no changes to endochondral ossification observed in Chapter 3, however the identification of Asporin in IVD, makes studying the spine separately very interesting[140].

No difference was observed in any of the features studied in the spine this suggests although Asporin may be implicated in IVD cartilage, it is not involved in the development of the spine.

The OARSI system for scoring of cartilage for OA progression using safranin O is well respected and validated as the standard for OA scoring. However, the IVD scoring using Safranin O is not as clear. Although a subtle difference is observed in the conditional Asporin knockout inner annulus, this would not appear a different score in the IVD scoring. For full confirmation and semi-quantitative study of the IVD, it would require multiple scorers and multiple sections throughout the spine. This preliminary data however is novel and interesting for further investigation of the role of Asporin in the IVD, specifically the inner annulus.

The inner annulus is predominantly made up of type II collagen, as the conditional knockout is targeted for the knockout of Asporin under the type II collagen promoter, it is therefore understandable for the effect of the loss of Asporin to be localised to the inner annulus[201].

However, interestingly in the Goldner's trichrome staining, there was presence of osteoid in the conditional knockout vertebrae and not observed

in any other genotype. This is consistent with the presence of accumulated osteoid in the cKO tibiae. However, further experiments are necessary to determine the reason for this osteoid, including counting osteoblast in the vertebrae. It would be interesting to look at histomorphometry of the spines to determine if there is a difference in the mineralisation rate of osteoid in the spine and also OsteoidHisto staining and quantification to confirm if this is a true increase in osteoid deposition[153]. Additionally if cortical analysis of the spine would be possible that would be very interesting to determine if there was a difference to the cortical tissue of the bone alike to the leg bones, as there is no periosteum it would give further insight if the changes observed in the tibiae are a result of periosteum if the spine does not show the same or if there is another possible pathway explaining the differences in the tibia and vertebrae. Some of this study could be achieved with using transverse sections of the vertebrae to visualise the cortical bone employing the techniques to measure bone parameters discussed in Chapter 5.

Chapter 7. Role of Asporin in Tendon structure.

7.1 Introduction

The musculoskeletal system is the collection of tissues that form the system allowing for movement and support of the body. This includes the bones which will be discussed further in the following chapter, the muscles, and the joints. Additionally, the cartilage, tendons and ligaments are also essential components of the musculoskeletal system. The previous chapter explored the role of Asporin within the cartilage, this chapter will investigate the role of Asporin within the tendons.

Tendons, also made up of collagen fibrils, the hierarchical structure of tendons is discussed in Chapter 1. Tendons are responsible for the attachment of muscles to the bone and to convert the contractile forces of the muscle to move the bones for movement. They also provide stability across the joint, securing the muscles to the bones of the joint. A well-known tendon is the Achilles tendon located at the back of the heel, attaching the calf muscle to the heel bone (calcaneus bone). This tendon is responsible for flexion of the foot, allowing the pointing of the foot downwards, necessary for walking/running and contributes to the stability of the ankle bone.

Asporin has been shown to be expressed in tendons and ligaments[175, 204], previous studies have also explored the role of Asporin in skin. Asporin null mice have been shown to have tougher skin, and the collagen fibrils of the skin imaged through transmission electron microscopy (TEM) showed potentially thinner collagen fibril diameters in the Asporin null mice. Mechanical testing of the tensile strength of the Asporin KO skin showed that only 75% of the energy required to rear the wild type skin was required to achieve failure of the KO samples.

Although the expression of Asporin has been detected in tendons, studies have not been carried out on the role of Asporin in tendon structure and mechanical properties.

Chapter aims:

- To assess the wild type and Asporin KO tendon structure through TEM imaging of collagen fibrils of the Achilles tendons.
- To determine the mechanical properties of Asporin null Achilles tendons compared to those of wild type Achilles tendon controls.

7.2 Loss of Asporin had no observable effect on the diameter of collagen fibrils.

To assess the structure of the Achilles tendon following the loss of Asporin. Achilles tendons were dissected from 9-week wild type and Asporin null mice, processed and cross-sectioned for imaging by transmission electron microscopy (TEM).

Several areas of the tendons containing the collagen fibrils were imaged, and nearby tenocytes were imaged to identify potential differences in collagen fibrils and tenocyte structure (Figure 78). Round collagen fibrils of varied diameters were observed in both wild type and Asporin KO samples with no overt differences were identified in the Asporin null Achilles tendon collagen fibril diameters. There was also no clear difference in the structure of the wild type and KO tenocytes at 9-weeks.

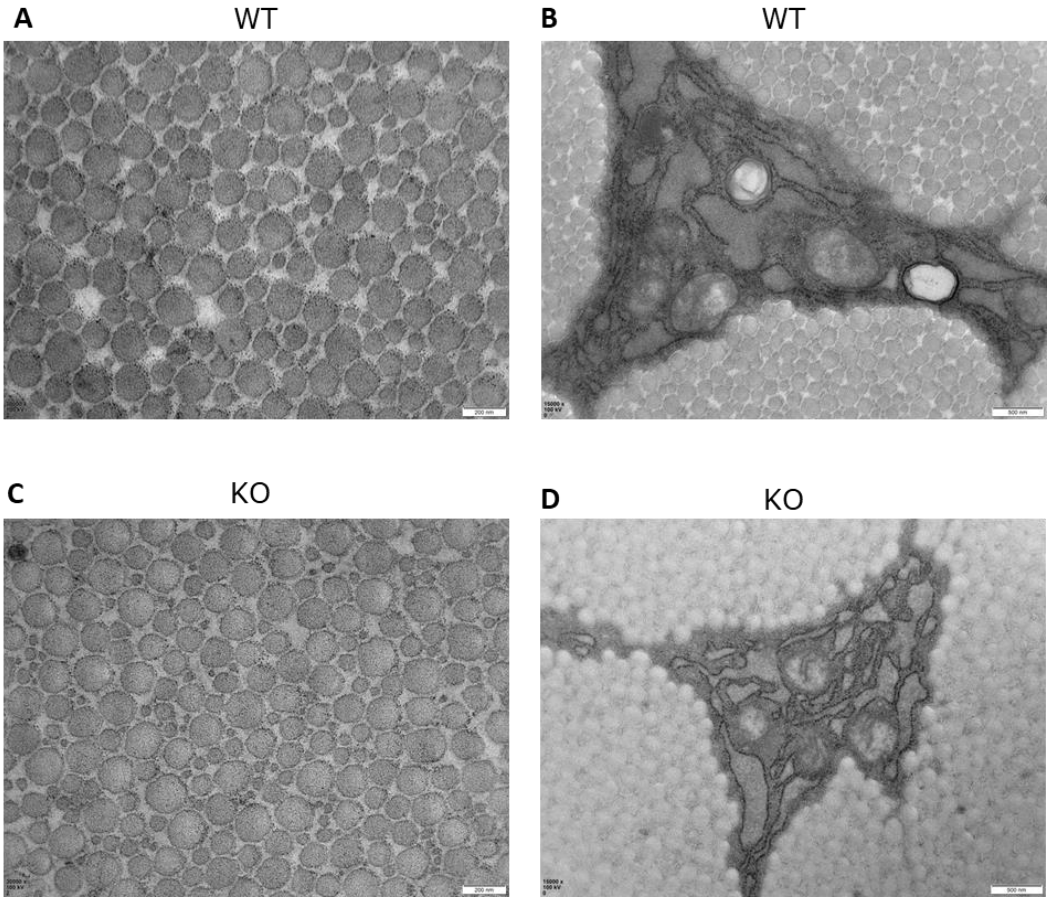

Figure 78. No apparent difference in the distribution of collagen fibril diameter of Asporin null tendons. *Transmission electron microscopy images of wild type (**A**)and Asporin knockout (**C**) collagen fibrils of the Achilles tendon, and TEM images of tenocytes embedded within the collagen fibrils of wildtype (**B**) and Asporin knockout mice (**D**).Scale bars 200 nm (A and C) and 500 nm (B and D) respectively.*

7.3 Loss of Asporin has no effect on the strength of the 9-week old Achilles tendons.

To assess the stretch and the strength of the 9-week tendons in the global knockout mice, test to failure tests were carried out on the PBS frozen Achilles tendon of wild type mice and global Asporin knockout mice.

Fmax was calculated as the maximum force exerted on the tendon at the point the tendon snaps. Due to the composition of tendons, where they are formed of bundles of collagen fibrils that form strands, tendons do not snap as a whole unit, instead the tendons snap by individual collagen fibrils snapping, this makes the snap more gradual, the maximum force is therefore calculated at the point it begins to fail.

No difference was found in the Fmax of the global knockout tendon in comparison to the wild type tendon.

Secondly, the stiffness (N/ mm) was calculated by the force required to stretch (displace) the tendon 1 mm. The stiffness was used as a measure of the stretch capacity of the tendon, a lower N/ mm value means less force is required to stretch the tendon 1 mm, and therefore they are less stiff and easier to stretch. A higher N/ mm value would mean more force is required to stretch the tendon 1 mm and therefore these tendons are stiffer and harder to stretch.

No difference was found in the stiffness of the global knockout tendon in comparison to the wild type tendon. (Figure 79)

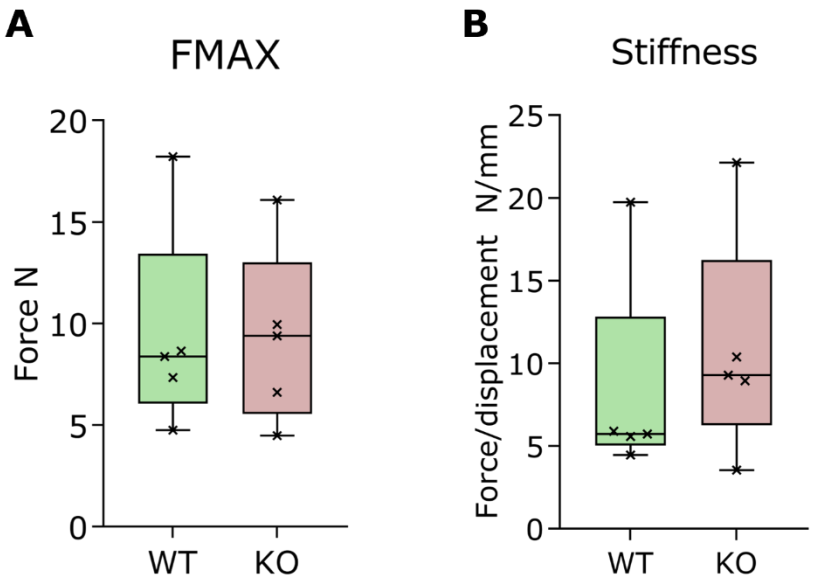

Figure 79. Global knockout of Asporin has no effect stiffness or strength of 9-week tendons. *Destructive test to failure tests were performed on wild type and global knockout female Achilles tendons maximum force to snap tendon (FMax) and stiffness were calculated (**A** and **B**). Asporin knockout mice show no difference in the Fmax or stiffness relative to the wild type control. Student t-test were carried out between WT and KO (n=5) and denoted by *=p<0.05.Error bars represent min to max.*

7.4 Discussion

The Achilles tendon, alike to most, is made up of mainly type I collagen fibrils. The structure of a tendon as discussed in the Chapter 1, is made up of bundles of collagen fibrils, these are stabilised by non-collagenous proteins, such as Asporin. As discussed, a characteristic of some skeletal dysplasia is changes to tendons, joint laxity, where the recoil ability of tendons is reduced, resulting in joint instability and hypermobility, as observed in SEMD-JL2[205]. Due to the ability of Asporin to bind collagen and the composition of tendons being fibres of bundles of collagen and the expression of Asporin within tendons, it was novel and interesting to explore the effect of a global knockout of Asporin on the tendon. The TEM images did not appear to be overtly different however quantification of the fibrils could be caried out in future work to determine fibril diameters and the distribution in fibril sizes as changes to collagen fibril diameter has been shown to affect the tendon strength[206]. Tensile strength is positively associated with the collagen fibril diameter[206].

The lack of difference in collagen fibrils would correlate with the lack of difference observed in the mechanical testing of the tendons where both the Fmax and the stiffness, the force required to stretch (displace) the tendon. However, the process of tendon stretching is challenging and involves freezing before testing which may change the properties of the tendon. Nevertheless, it still gives insight into the role of Asporin, although it is detected in tendons and in ligaments, such as the periodontal ligament, the global ablation of Asporin has no effect on the mechanical properties of the tendons. Cyclic testing would be interesting in future work, skeletal dysplasias sometimes present with a tendon or ligament phenotype, such as KIF22 mutations resulting in SEMD-JL2 where tendons are more lax and do not contract as well as their normal tendons[91].

Asporin expression in the Achilles is significantly increased in younger tendons and decreases with age, these studies were carried out on 9-week old tendons, future work would look at younger tendons to see if the loss

of Asporin when it is at a stage where it is normally expressed at a higher level shows a difference in the WT and KO.

Chapter 8. Discussion

8.1 Asporin as a therapeutic target for OA

The data presented here is strong data for the potential use of Asporin as a therapeutic target in OA. In these chapters it has been demonstrated that the loss of Asporin does not disrupt endochondral ossification or long bone growth. There is no damage to the articular cartilage both in the expression of type II collagen or in OA hallmarks of increased proliferation or apoptosis. This demonstrates the loss of Asporin would have no off-target effects in the cartilage or exacerbate the OA pathogenicity.

8.2 Asporin is important for bone remodelling.

The conditional loss of Asporin has further confirmed that Asporin is not needed for endochondral ossification as the cKO mice developed normally with no changes to the growth plate or long bone growth. However, there was clear differences in the case of bone remodelling. The hypothesis that Asporin being knockout out in the periosteum in the type II collagen positive skeletal progenitor cells is supported by the changes to only the bone remodelling parameters and not the initial growth[63]. Most interestingly the cortical bone has formed normally in structure however it is thinner and smaller the width-wise growth of bone is controlled by the periosteum and the endosteum, furthermore the osteoid accumulation on the trabeculae and mineral appositional rate is reduced highlighting again a system of bone remodelling coordinated by the periosteum of trabecular bone adaptations and thickening through the suppression of osteoclastogenesis and promotion of osteoblastogenesis is impeded by the conditional loss of Asporin[22, 62, 71].

Furthermore, the changes to the bone cells in the conditional knockout where there is a decrease in osteoblast in the trabecular bone and the increase in osteoclasts in the bone highlight a clear imbalance in the bone homeostasis compared to the conditional wild-type. These changes may be due to crosstalk between the cells, which is known to occur

throughout development in the maintenance of bone homeostasis and remodelling[36]. However, it is interesting that there is no difference in the μCT data for trabecular bone which would be expected if this change was causing an imbalance in bone formation or degradation. Power calculations indicate this lack of difference is not due to low numbers of mice. Interestingly, the TGF-β superfamily and signalling have been shown to influence osteoblast and osteoclast differentiation and activity[207]. Asporin has been shown to dampen TGF-β1 signalling, with the loss of Asporin, there is a potential this has allowed TGF- β1 signalling to be higher in the conditional knockout from the cells expressing type II collagen[157].

Therefore, the effect of the loss of Asporin on TGF-β signalling in the bone would be very interesting for not only investigating the changes observed in the bone here but also in the role in OA, where TGF-β signalling is often implicated[175]. This could be achieved through IHC on the tissues and looking at downstream proteins of the signalling pathway It could also be investigate *in vitro* using primary cells. By obtaining osteoblasts and osteoclasts from the conditional mice, they could be cultured together or through transferring conditioned media from each cell type to look at the cross talk and influence between the two cell types and determine if there are any changes in this activity, or the factors secreted by these cell types.

8.3 Asporin is not needed for early skeletal development.

The loss of Asporin, has not proved harmful to the mice. No phenotypic changes are observed in the global mice and only the cortical bone remodelling changes to the conditional knockout. The overall growth of the mouse is not affected, and macrostructure of the body is not disrupted. The spine and vertebrae of the global and conditional knockout develop indistinguishably to their respective wild types. The global loss of Asporin does not have a pathogenic phenotype.

This result was surprising, with its role in type I collagen mineralisation, a major process in bone development, however there are

other proteins available and still expressing that may compensate for the loss of Asporin, or although Asporin has this capability it is likely to not be the main protein, or one of the main proteins to mineralise bone during development the most known proteins in mineralisation by hydroxyapatite crystal formation are osteopontin and bone sialoprotein[124,123]. Osteopontin, as previously discussed is a protein sharing the same aspartic acid repeat as the Asporin protein, which acts as a calcium ion binding site to modulate mineralisation of bone and teeth[122].

8.4 Possible pathogenicity of the upregulation of Asporin in OA the decreased ECM integrity.

The overexpression of Asporin, drives mineralisation of the ECM, the calcification of cartilage is a hallmark of OA however the lack of type I collagen in the articular cartilage would not support the hypothesis for Asporin to induce calcification of the articular cartilage, as Asporin binds and mineralises type I collagen, not type II collagen which is abundant in the articular cartilage[41]. However, the suppression of decorin by the overexpression of Asporin may be important in the progression of OA, the *in vitro* study demonstrated a clear loss in the sulphated proteoglycan deposition and suppression of decorin. The role of decorin as a physical linker in the ECM, forming type II collagen-aggrecan and aggrecan-aggrecan constructs is an important role within the ECM the suppression of decorin and may result in a lack of these constructs being formed and reduce the anchoring of the aggrecan and type II molecules in the ECM, resulting in an unstable and malformed ECM[181]. To study this further it would be interesting to investigate Asporin-decorin interaction or the mechanism that leads to this suppression of decorin. Decorin has been shown in other studies to inhibit TGF-β and biglycan, another protein within the Class I SLRPs, which results in overactive TGF-β signalling by decreased sequestration of TGF-β[124, 136]. In DMM surgery models of decorin null mice, it was found that loss of decorin, accelerated OA progression. Where it has been highlighted that Asporin is upregulated in OA articular cartilage, this

may be a route to investigate of whether the suppression of decorin is present in the OA cartilage and as a result this may be accelerating OA, possibly through modulation of TGF-β signalling. Future work could focus on determining if there is a change in decorin expression on the DMM surgery mice between the WT and Asporin null mice and looking at targeting Asporin being possibly chondroprotective if it results in decorin expression being maintained.

The overexpression study would be important to repeat, as the WT cells do not appear to follow a clear chondrogenic differentiation pattern. Therefore, conclusions that are drawn from this study should be with the consideration of this caveat. If clear chondrogenesis is not occurring, can it be determined a role or lack of role is due to the biology or due to the differentiation. There may be multiple reasons for this, passage number of the ATDC5 cells and does this impact differentiation capacity, have they begun to differentiate already with age, are the growth factors still effective in driving differentiation. These all need to be investigated in future work to draw meaningful conclusions from this experiment, however this initial study has highlighted the interesting connection between Asporin and decorin and a role for Asporin in matrix mineralisation.

8.5 Future Work

The most interesting difference was the cortical changes, the cortical bone is both thinner and narrower, the bones are easier to break. Exploration into the reason for these changes is critical for understanding the role of Asporin in the musculoskeletal system. Currently, two hypotheses are considered for the mechanism of this difference, the type II collagen positive cells residing in the periosteum and the potential of transdifferentiation of hypertrophic chondrocytes to osteoblasts and osteocytes.

The type II collagen positive cells of the periosteum are important in fracture repair. Within the periosteum the inner layer of the periosteum, the

"cambium" layer, there is a reserve of skeletal progenitor cells, osteoblasts, fibroblasts and blood vessels[195]. In the Col2cre KO mouse, Asporin is not expressed in any cell expressing type II collagen, therefore these cells containing that have been shown to be type II collagen positive would not express Asporin. The cells are a cohort of skeletal progenitor cells, which are employed in fracture repair and also appositional growth, where cortical bone grows in thickness[195].

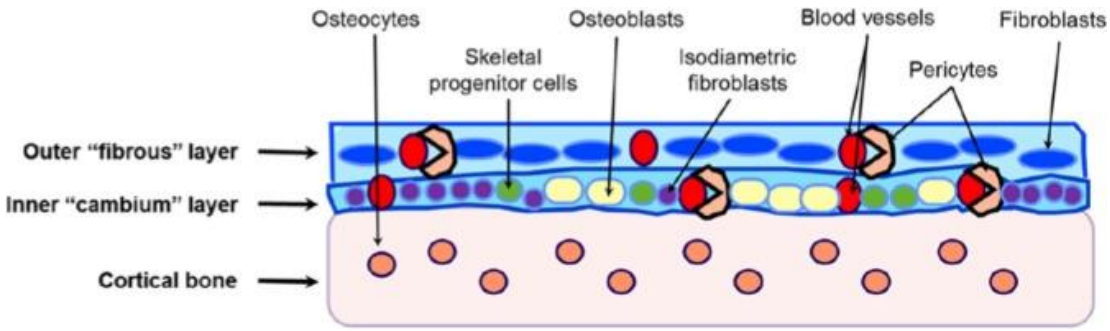

Figure 80. Structure of the periosteum and cells present in the cells. *The structure of the periosteum is organised into two layers, the outer layer, which is more fibrous containing fibroblasts, blood vessels. The inner layer contains the skeletal progenitor cells and this is where the type II collagen progenitor cells are located and this lies against the cortical bone.*

The lack of Asporin taken with the increased accumulation of osteoid and lack of mineralisation of the osteoid, may indicate cortical bone growth is hindered. The change observed the thinner bone that is observed in the cKO mice may therefore be as a result of these progenitor cells lacking in Asporin expression with its capability to mineralise type I collagen, the main component of osteoid[123].

This would be interesting to explore further, the formation of osteophytes has similar developmental milestones to fracture repair[160]. It would therefore be interesting to explore if Asporin is involved in the osteophyte formation, as Asporin is found to be upregulated in OA cartilage, if Asporin is involved in osteophyte formation this could be an explanation for Asporin in the surrounding tissues. IHC analysis of the DMM sections of the WT and KO tissues would confirm or nullify its role, this could also contribute to the chondroprotective role that is present in the WT and KO mice post DMM surgery. Furthermore, developing of the histomorphometry research, if the orientation of the bone is changed and embedded to allow for sectioning through the bone to look at the ring of cortical bone, the mineralisation rate and osteoid accumulation could be studied at the periosteum.

Alternatively, there is a cohort of hypertrophic chondrocytes that can undergo transdifferentiation to generate osteoblasts and osteocytes that are important for trabecular and cortical bone formation[16]. This is very interesting as they initially start as chondrocytes which are type II collagen expressing, they will differentiate lacking Asporin expression. Subsequently, when they differentiate to osteoblasts if they still retain the expression of type II collagen they will continue to lack Asporin, which in a way similar to that described for the periosteal cells above, may result in hindered bone mineralisation of the cortical bone during appositional growth and may therefore explain the reduced cortical thickness and weaker bones.

To explore both these hypotheses, cell lineage tracing could be employed, where the cells lacking Asporin are tracked through to assess if

they do contribute to the cortical bone development and how further investigate the changed as a result of the conditional knockout. Whether this is through type II positive cells from the periosteum or through the transdifferentiation of hypertrophic chondrocytes.

Additionally, primary cell culture of periosteal cells would be interesting to determine if there is a real difference in the periosteal cells ability to mineralise or differentiate. This could be through assessing gene expression by qPCR and alizarin red staining of monolayer to assess calcium deposition during mineralisation which would indicate its role or lack of role in the cortical bone maintenance and growth through the periosteal progenitor cells.

To explore the transdifferentiation hypotheses driving primary chondrocytes of conditional wild-type and conditional knockout mice to hypertrophic chondrocytes and then drive osteogenesis to mimic transdifferentiation, it could be assessed if there is a change in their capacity to transdifferentiate.

Additionally, the mouse work was carried out on solely female mice, this is not common in mouse work, however due to the early ages studied in these experiments, it reduces the concern for oestrogen impact. Repeating these experiments on male mice would be important to eliminate a gender impact on the changes observed or whether there is a presence of a phenotype in male Asporin global and conditional knockout mice. Furthermore, the number of the mice is lower than would be optimal for this type of study, and this is important to consider when no change is observed whether this due to the low numbers of mice and therefore larger variability in data sets or there is no real difference as a result of loss of Asporin. This is particularly important for the global mice where there is no changes observed, or appear to tend towards significance.

Overall, the study has been thorough exploring multiple avenues of bone development, however, further refinement must be carried out to

confirm a lack of change in these mice cohorts. This would be through the increase in mouse numbers, studying both male and female and to further investigate the only real difference that was observed which was the cortical bone changes.

References

1. Muhr J, Arbor TC, Ackerman KM. Embryology, Gastrulation. StatPearls. Treasure Island (FL): StatPearls Publishing Copyright © 2023, StatPearls Publishing LLC.; 2023.

2. Caplan AI. The mesengenic process. Clinics in plastic surgery. 1994;21(3):429-35.

3. Ghimire S, Mantziou V, Moris N, Martinez Arias A. Human gastrulation: The embryo and its models. Developmental Biology. 2021;474:100-8.

4. Goswami R. Primer on the metabolic bone diseases and disorders of mineral metabolism. Indian J Med Res. 144: Copyright: © 2017 Indian Journal of Medical Research.; 2016. p. 489-90.

5. Gilbert S. Osteogenesis: The Development of Bones. 6th ed2000.

6. Zhou G, Zheng Q, Engin F, Munivez E, Chen Y, Sebald E, et al. Dominance of SOX9 function over RUNX2 during skeletogenesis. Proceedings of the National Academy of Sciences. 2006;103(50):19004-9.

7. Sadler TW. The embryologic origin of ventral body wall defects. Seminars in Pediatric Surgery. 2010;19(3):209-14.

8. Goldring MB. Chondrogenesis, chondrocyte differentiation, and articular cartilage metabolism in health and osteoarthritis. Therapeutic advances in musculoskeletal disease. 2012;4(4):269-85.

9. Lefebvre V, Dvir-Ginzberg M. SOX9 and the many facets of its regulation in the chondrocyte lineage. Connect Tissue Res. 2017;58(1):2-14.

10. Inada M, Yasui T, Nomura S, Miyake S, Deguchi K, Himeno M, et al. Maturational disturbance of chondrocytes in Cbfa1-deficient mice. Dev Dyn. 1999;214(4):279-90.

11. Yap SP, Xing X, Kraus P, Sivakamasundari V, Chan HY, Lufkin T. Generation of mice with a novel conditional null allele of the Sox9 gene. Biotechnol Lett. 2011;33(8):1551-8.

12. Mansour S, Hall CM, Pembrey ME, Young ID. A clinical and genetic study of campomelic dysplasia. J Med Genet. 1995;32(6):415-20.

13. Bi W, Huang W, Whitworth DJ, Deng JM, Zhang Z, Behringer RR, et al. Haploinsufficiency of Sox9 results in defective cartilage primordia and premature skeletal mineralization. Proc Natl Acad Sci U S A. 2001;98(12):6698-703.

14. Han Y, Lefebvre V. L-Sox5 and Sox6 drive expression of the aggrecan gene in cartilage by securing binding of Sox9 to a far-upstream enhancer. Mol Cell Biol. 2008;28(16):4999-5013.

15. Kozhemyakina E, Lassar AB, Zelzer E. A pathway to bone: signaling molecules and transcription factors involved in chondrocyte development and maturation. Development. 2015;142(5):817-31.

16. Zhou X, von der Mark K, Henry S, Norton W, Adams H, de Crombrugghe B. Chondrocytes transdifferentiate into osteoblasts in endochondral bone during development, postnatal growth and fracture healing in mice. PLoS Genet. 2014;10(12):e1004820.

17. Komori T. Regulation of osteoblast differentiation by transcription factors. J Cell Biochem. 2006;99(5):1233-9.

18. Komori T, Yagi H, Nomura S, Yamaguchi A, Sasaki K, Deguchi K, et al. Targeted disruption of Cbfa1 results in a complete lack of bone formation owing to maturational arrest of osteoblasts. Cell. 1997;89(5):755-64.

19. Nakashima K, Zhou X, Kunkel G, Zhang Z, Deng JM, Behringer RR, et al. The novel zinc finger-containing transcription factor osterix is required for osteoblast differentiation and bone formation. Cell. 2002;108(1):17-29.

20. Chen X, Wang L, Zhao K, Wang H. Osteocytogenesis: Roles of Physicochemical Factors, Collagen Cleavage, and Exogenous Molecules. Tissue Eng Part B Rev. 2018;24(3):215-25.

21. Qin L, Liu W, Cao H, Xiao G. Molecular mechanosensors in osteocytes. Bone Research. 2020;8(1):23.

22. Dallas SL, Prideaux M, Bonewald LF. The osteocyte: an endocrine cell ... and more. Endocr Rev. 2013;34(5):658-90.

23. Holmbeck K, Bianco P, Pidoux I, Inoue S, Billinghurst RC, Wu W, et al. The metalloproteinase MT1-MMP is required for normal development and maintenance of osteocyte processes in bone. J Cell Sci. 2005;118(Pt 1):147-56.

24. Zhang K, Barragan-Adjemian C, Ye L, Kotha S, Dallas M, Lu Y, et al. E11/gp38 selective expression in osteocytes: regulation by mechanical strain and role in dendrite elongation. Mol Cell Biol. 2006;26(12):4539-52.

25. Verbruggen SW, Sittichokechaiwut A, Reilly GC. Osteocytes and Primary Cilia. Curr Osteoporos Rep. 2023;21(6):719-30.

26. van Bezooijen RL, Roelen BA, Visser A, van der Wee-Pals L, de Wilt E, Karperien M, et al. Sclerostin is an osteocyte-expressed negative regulator of bone formation, but not a classical BMP antagonist. J Exp Med. 2004;199(6):805-14.

27. Cui Y, Niziolek PJ, MacDonald BT, Zylstra CR, Alenina N, Robinson DR, et al. Lrp5 functions in bone to regulate bone mass. Nat Med. 2011;17(6):684-91.

28. Tresguerres FGF, Torres J, López-Quiles J, Hernández G, Vega JA, Tresguerres IF. The osteocyte: A multifunctional cell within the bone. Annals of Anatomy - Anatomischer Anzeiger. 2020;227:151422.

29. Feng X, Teitelbaum SL. Osteoclasts: New Insights. Bone Res. 2013;1(1):11-26.

30. Suda T, Takahashi N, Udagawa N, Jimi E, Gillespie MT, Martin TJ. Modulation of osteoclast differentiation and function by the new members of the tumor necrosis factor receptor and ligand families. Endocr Rev. 1999;20(3):345-57.

31. Dougall WC, Glaccum M, Charrier K, Rohrbach K, Brasel K, De Smedt T, et al. RANK is essential for osteoclast and lymph node development. Genes Dev. 1999;13(18):2412-24.

32. Wiktor-Jedrzejczak W, Bartocci A, Ferrante AW, Jr., Ahmed-Ansari A, Sell KW, Pollard JW, et al. Total absence of colony-stimulating factor 1 in the macrophage-deficient osteopetrotic (op/op) mouse. Proc Natl Acad Sci U S A. 1990;87(12):4828-32.

33. Insogna KL, Sahni M, Grey AB, Tanaka S, Horne WC, Neff L, et al. Colony-stimulating factor-1 induces cytoskeletal reorganization and c-src-dependent tyrosine phosphorylation of selected cellular proteins in rodent osteoclasts. J Clin Invest. 1997;100(10):2476-85.

34. Trouvin AP, Goëb V. Receptor activator of nuclear factor-κB ligand and osteoprotegerin: maintaining the balance to prevent bone loss. Clin Interv Aging. 2010;5:345-54.

35. Boyce BF, Xing L. Functions of RANKL/RANK/OPG in bone modeling and remodeling. Arch Biochem Biophys. 2008;473(2):139-46.

36. Glass DA, 2nd, Bialek P, Ahn JD, Starbuck M, Patel MS, Clevers H, et al. Canonical Wnt signaling in differentiated osteoblasts controls osteoclast differentiation. Dev Cell. 2005;8(5):751-64.

37. Kobayashi Y, Maeda K, Takahashi N. Roles of Wnt signaling in bone formation and resorption. Japanese Dental Science Review. 2008;44(1):76-82.

38. Hawkes CP, Mostoufi-Moab S. Fat-bone interaction within the bone marrow milieu: Impact on hematopoiesis and systemic energy metabolism. Bone. 2019;119:57-64.

39. Chang LR, Marston G, Martin A. Anatomy, Cartilage. StatPearls. Treasure Island (FL): StatPearls Publishing

40. Mow VC, Ratcliffe A, Robin Poole A. Cartilage and diarthrodial joints as paradigms for hierarchical materials and structures. Biomaterials. 1992;13(2):67-97.

41. Sophia Fox AJ, Bedi A, Rodeo SA. The basic science of articular cartilage: structure, composition, and function. Sports health. 2009;1(6):461-8.

42. Fisher M, Ackley T, Richard K, Oei B, Dealy CN. Osteoarthritis at the Cellular Level: Mechanisms, Clinical Perspectives, and Insights From Development. In: Narayan R, editor. Encyclopedia of Biomedical Engineering. Oxford: Elsevier; 2019. p. 660-76.

43. Buckwalter JA, Mow VC, Ratcliffe A. Restoration of Injured or Degenerated Articular Cartilage. J Am Acad Orthop Surg. 1994;2(4):192-201.

44. Rutkovskiy A, Stensløkken KO, Vaage IJ. Osteoblast Differentiation at a Glance. Med Sci Monit Basic Res. 2016;22:95-106.

45. Pearson Education I. Human Anatomy & Physiology. 9th ed2016.

46. Olsen BR, Reginato AM, Wang W. Bone development. Annual review of cell and developmental biology. 2000;16:191-220.

47. Gerber H-P, Vu TH, Ryan AM, Kowalski J, Werb Z, Ferrara N. VEGF couples hypertrophic cartilage remodeling, ossification and angiogenesis during endochondral bone formation. Nature Medicine. 1999;5(6):623-8.

48. Stickens D, Behonick DJ, Ortega N, Heyer B, Hartenstein B, Yu Y, et al. Altered endochondral bone development in matrix metalloproteinase 13-deficient mice. Development. 2004;131(23):5883-95.

49. Page-McCaw A, Ewald AJ, Werb Z. Matrix metalloproteinases and the regulation of tissue remodelling. Nat Rev Mol Cell Biol. 2007;8(3):221-33.

50. Cheung JO, Grant ME, Jones CJ, Hoyland JA, Freemont AJ, Hillarby MC. Apoptosis of terminal hypertrophic chondrocytes in an in vitro model of endochondral ossification. J Pathol. 2003;201(3):496-503.

51. Börjesson AE, Windahl SH, Karimian E, Eriksson EE, Lagerquist MK, Engdahl C, et al. The role of estrogen receptor-α and its activation function-1 for growth plate closure in female mice. American journal of physiology Endocrinology and metabolism. 2012;302(11):E1381-9.

52. Ağırdil Y. The growth plate: a physiologic overview. EFORT Open Rev. 2020;5(8):498-507.

53. Lian JB, McKee MD, Todd AM, Gerstenfeld LC. Induction of bone-related proteins, osteocalcin and osteopontin, and their matrix

ultrastructural localization with development of chondrocyte hypertrophy in vitro. J Cell Biochem. 1993;52(2):206-19.

54. Vortkamp A, Lee K, Lanske B, Segre GV, Kronenberg HM, Tabin CJ. Regulation of rate of cartilage differentiation by Indian hedgehog and PTH-related protein. Science. 1996;273(5275):613-22.

55. Maeda Y, Nakamura E, Nguyen MT, Suva LJ, Swain FL, Razzaque MS, et al. Indian Hedgehog produced by postnatal chondrocytes is essential for maintaining a growth plate and trabecular bone. Proc Natl Acad Sci U S A. 2007;104(15):6382-7.

56. Pajni-Underwood S, Wilson CP, Elder C, Mishina Y, Lewandoski M. BMP signals control limb bud interdigital programmed cell death by regulating FGF signaling. Development. 2007;134(12):2359-68.

57. Nilsson O, Parker EA, Hegde A, Chau M, Barnes KM, Baron J. Gradients in bone morphogenetic protein-related gene expression across the growth plate. J Endocrinol. 2007;193(1):75-84.

58. Wang JS, Mazur CM, Wein MN. Sclerostin and Osteocalcin: Candidate Bone-Produced Hormones. Frontiers in Endocrinology. 2021;12.

59. Mizokami A, Kawakubo-Yasukochi T, Hirata M. Osteocalcin and its endocrine functions. Biochem Pharmacol. 2017;132:1-8.

60. Si J, Wang C, Zhang D, Wang B, Zhou Y. Osteopontin in Bone Metabolism and Bone Diseases. Med Sci Monit. 2020;26:e919159.

61. Nakamura H, Yukita A, Ninomiya T, Hosoya A, Hiraga T, Ozawa H. Localization of Thy-1-positive cells in the perichondrium during endochondral ossification. J Histochem Cytochem. 2010;58(5):455-62.

62. Duchamp de Lageneste O, Julien A, Abou-Khalil R, Frangi G, Carvalho C, Cagnard N, et al. Periosteum contains skeletal stem cells with high bone regenerative potential controlled by Periostin. Nature Communications. 2018;9(1):773.

63. Matthews BG, Novak S, Sbrana FV, Funnell JL, Cao Y, Buckels EJ, et al. Heterogeneity of murine periosteum progenitors involved in fracture healing. Elife. 2021;10.

64. Black DM, Rosen CJ. Clinical Practice. Postmenopausal Osteoporosis. N Engl J Med. 2016;374(3):254-62.

65. Birkhold AI, Razi H, Duda GN, Weinkamer R, Checa S, Willie BM. The Periosteal Bone Surface is Less Mechano-Responsive than the Endocortical. Sci Rep. 2016;6:23480.

66. Wang L, You X, Zhang L, Zhang C, Zou W. Mechanical regulation of bone remodeling. Bone Res. 2022;10(1):16.

67. Caillot-Augusseau A, Lafage-Proust MH, Soler C, Pernod J, Dubois F, Alexandre C. Bone formation and resorption biological markers in cosmonauts during and after a 180-day space flight (Euromir 95). Clin Chem. 1998;44(3):578-85.

68. O'Leary TJ, Wardle SL, Gifford RM, Double RL, Reynolds RM, Woods DR, et al. Tibial Macrostructure and Microarchitecture Adaptations in Women During 44 Weeks of Arduous Military Training. Journal of Bone and Mineral Research. 2021;36(7):1300-15.

69. Iles RK, Docherty SM, editors. Biomedical sciences : essential laboratory medicine2012.

70. Boskey AL, Coleman R. Aging and bone. J Dent Res. 2010;89(12):1333-48.

71. Wang JS, Wein MN. Pathways Controlling Formation and Maintenance of the Osteocyte Dendrite Network. Current Osteoporosis Reports. 2022;20(6):493-504.

72. Deutsch U, Dressler GR, Gruss P. Pax 1, a member of a paired box homologous murine gene family, is expressed in segmented structures during development. Cell. 1988;53(4):617-25.

73. Scaal M. Early development of the vertebral column. Seminars in Cell & Developmental Biology. 2016;49:83-91.

74. Smits P, Lefebvre V. Sox5 and Sox6 are required for notochord extracellular matrix sheath formation, notochord cell survival and development of the nucleus pulposus of intervertebral discs. Development. 2003;130(6):1135-48.

75. Takimoto A, Mohri H, Kokubu C, Hiraki Y, Shukunami C. Pax1 acts as a negative regulator of chondrocyte maturation. Exp Cell Res. 2013;319(20):3128-39.

76. Jia M, Chen S, Zhang B, Liang H, Feng J, Zong Z. Effects of Constitutive β-Catenin Activation on Vertebral Bone Growth and Remodeling at Different Postnatal Stages in Mice. PLOS ONE. 2013;8(9):e74093.

77. Blom HJ, Shaw GM, den Heijer M, Finnell RH. Neural tube defects and folate: case far from closed. Nature Reviews Neuroscience. 2006;7(9):724-31.

78. Meunier P, Aaron J, Edouard C, VlGnon G. Osteoporosis and the Replacement of Cell Populations of the Marrow by Adipose Tissue: A Quantitative Study of 84 Iliac Bone Biopsies. Clinical Orthopaedics and Related Research®. 1971;80.

79. Caruso S, Bernardi S, Pasini M, Giuca MR, Docimo R, Continenza MA, et al. The process of mineralisation in the development of human tooth. Eur J Paediatr Dent. 2016;17(4):322-6.

80. Lin Y, Yan Z, Liu L, Qiao J, Jing W, Wu L, et al. Proliferation and pluripotency potential of ectomesenchymal cells derived from first branchial arch. Cell Prolif. 2006;39(2):79-92.

81. Balic A, Thesleff I. Chapter Seven - Tissue Interactions Regulating Tooth Development and Renewal. In: Chai Y, editor. Current Topics in Developmental Biology. 115: Academic Press; 2015. p. 157-86.

82. Smith AJ, Cooper PR. Chapter 32 - Cellular Signaling in Dentin Repair and Regeneration. In: Vishwakarma A, Sharpe P, Shi S, Ramalingam M, editors. Stem Cell Biology and Tissue Engineering in Dental Sciences. Boston: Academic Press; 2015. p. 405-17.

83. Mortazavi H, Baharvand M. Common conditions associated with periodontal ligament widening. Imaging science in dentistry. 2016;46(4):229-37.

84. Dean R. The Periodontal Ligament: Development, Anatomy and Function. OHDM. 2017;16(6).

85. Ueda M, Goto T, Kuroishi KN, Gunjigake KK, Ikeda E, Kataoka S, et al. Asporin in compressed periodontal ligament cells inhibits bone formation. Archives of oral biology. 2016;62:86-92.

86. Lewiecki EM. Role of sclerostin in bone and cartilage and its potential as a therapeutic target in bone diseases. Therapeutic advances in musculoskeletal disease. 2014;6(2):48-57.

87. Ikegawa S. Expression, regulation and function of asporin, a susceptibility gene in common bone and joint diseases. Current medicinal chemistry. 2008;15(7):724-8.

88. Nikolaus A, Currey JD, Lindtner T, Fleck C, Zaslansky P. Importance of the variable periodontal ligament geometry for whole tooth mechanical function: A validated numerical study. Journal of the mechanical behavior of biomedical materials. 2017;67:61-73.

89. Cho H, Tarafder S, Fogge M, Kao K, Lee CH. Periodontal ligament stem/progenitor cells with protein-releasing scaffolds for cementum formation and integration on dentin surface. Connect Tissue Res. 2016;57(6):488-95.

90. de Jong T, Bakker AD, Everts V, Smit TH. The intricate anatomy of the periodontal ligament and its development: Lessons for periodontal regeneration. Journal of periodontal research. 2017;52(6):965-74.

91. Min BJ, Kim N, Chung T, Kim OH, Nishimura G, Chung CY, et al. Whole-exome sequencing identifies mutations of KIF22 in spondyloepimetaphyseal dysplasia with joint laxity, leptodactylic type. Am J Hum Genet. 2011;89(6):760-6.

92. Goudouri O-M, Kontonasaki E, Boccaccini AR. 17 - Layered scaffolds for periodontal regeneration. In: Tayebi L, Moharamzadeh K, editors. Biomaterials for Oral and Dental Tissue Engineering: Woodhead Publishing; 2017. p. 279-95.

93. Dubrulle J, Pourquie O. Welcome to Syndetome: A New Somitic Compartment. Developmental Cell. 2003;4(5):611-2.

94. Miyabara S, Yuda Y, Kasashima Y, Kuwano A, Arai K. Regulation of Tenomodulin Expression Via Wnt/β-catenin Signaling in Equine Bone Marrow-derived Mesenchymal Stem Cells. Journal of equine science. 2014;25(1):7-13.

95. Muench JR, Thelen DG, Henak CR. Interfibrillar shear behavior is altered in aging tendon fascicles. Biomechanics and modeling in mechanobiology. 2020;19(3):841-9.

96. Robey PG, Boskey AL, Leikin S. Chapter 8 - The regulatory role of matrix proteins in mineralization of bone. In: Dempster DW, Cauley JA, Bouxsein ML, Cosman F, editors. Marcus and Feldman's Osteoporosis (Fifth Edition): Academic Press; 2021. p. 165-87.

97. Wood ML, Luthin WN, Lester GE, Dahners LE. Tendon creep is potentiated by NKISK and relaxin which produce collagen fiber sliding. The Iowa orthopaedic journal. 2003;23:75-9.

98. Kastelic J, Galeski A, Baer E. The multicomposite structure of tendon. Connect Tissue Res. 1978;6(1):11-23.

99. Screen H, Bader D, Lee D, Shelton J. Local strain measurement within tendon. Strain. 2004;40(4):157-63.

100. Olsen BR, Reginato AM, Wang W. Myogenesis: The Development of Muscle. Annual review of cell and developmental biology. 2000;16:191-220.

101. Bentzinger CF, Wang YX, Rudnicki MA. Building muscle: molecular regulation of myogenesis. Cold Spring Harb Perspect Biol. 2012;4(2).

102. Yue B. Biology of the extracellular matrix: an overview. Journal of glaucoma. 2014;23(8 Suppl 1):S20-3.

103. Lu Y, Parker KH, Wang W. Effects of osmotic pressure in the extracellular matrix on tissue deformation. Philosophical transactions Series A, Mathematical, physical, and engineering sciences. 2006;364(1843):1407-22.

104. Hynes RO, Naba A. Overview of the matrisome--an inventory of extracellular matrix constituents and functions. Cold Spring Harb Perspect Biol. 2012;4(1):a004903.

105. von Marschall Z, Fisher LW. Decorin is processed by three isoforms of bone morphogenetic protein-1 (BMP1). Biochemical and Biophysical Research Communications. 2010;391(3):1374-8.

106. Verma RP, Hansch C. Matrix metalloproteinases (MMPs): chemical-biological functions and (Q)SARs. Bioorg Med Chem. 2007;15(6):2223-68.

107. Ricard-Blum S. The collagen family. Cold Spring Harb Perspect Biol. 2011;3(1):a004978.

108. Shoulders MD, Raines RT. Collagen structure and stability. Annu Rev Biochem. 2009;78:929-58.

109. Poole AR, Kobayashi M, Yasuda T, Laverty S, Mwale F, Kojima T, et al. Type II collagen degradation and its regulation in articular cartilage in osteoarthritis. Annals of the Rheumatic Diseases. 2002;61(suppl 2):ii78.

110. Schaefer L, Iozzo RV. Biological functions of the small leucine-rich proteoglycans: from genetics to signal transduction. The Journal of biological chemistry. 2008;283(31):21305-9.

111. Sommarin Y, Wendel M, Shen Z, Hellman U, Heinegård D. Osteoadherin, a Cell-binding Keratan Sulfate Proteoglycan in Bone, Belongs to the Family of Leucine-rich Repeat Proteins of the Extracellular Matrix *. Journal of Biological Chemistry. 1998;273(27):16723-9.

112. Johnson HJ, Rosenberg L, Choi HU, Garza S, Höök M, Neame PJ. Characterization of epiphycan, a small proteoglycan with a leucine-rich repeat core protein. The Journal of biological chemistry. 1997;272(30):18709-17.

113. Reardon AJ, Le Goff M, Briggs MD, McLeod D, Sheehan JK, Thornton DJ, et al. Identification in vitreous and molecular cloning of opticin, a novel member of the family of leucine-rich repeat proteins of the extracellular matrix. The Journal of biological chemistry. 2000;275(3):2123-9.

114. Gregg RG, Kamermans M, Klooster J, Lukasiewicz PD, Peachey NS, Vessey KA, et al. Nyctalopin expression in retinal bipolar cells restores visual function in a mouse model of complete X-linked congenital stationary night blindness. J Neurophysiol. 2007;98(5):3023-33.

115. Sodhi H, Panitch A. Glycosaminoglycans in Tissue Engineering: A Review. Biomolecules. 2021;11(1):29.

116. Kamma-Lorger CS, Pinali C, Martínez JC, Harris J, Young RD, Bredrup C, et al. Role of Decorin Core Protein in Collagen Organisation in Congenital Stromal Corneal Dystrophy (CSCD). PLoS One. 2016;11(2):e0147948.

117. Svensson L, Aszódi A, Reinholt FP, Fässler R, Heinegård D, Oldberg A. Fibromodulin-null mice have abnormal collagen fibrils, tissue organization, and altered lumican deposition in tendon. The Journal of biological chemistry. 1999;274(14):9636-47.

118. Chakravarti S, Magnuson T, Lass JH, Jepsen KJ, LaMantia C, Carroll H. Lumican regulates collagen fibril assembly: skin fragility and corneal opacity in the absence of lumican. J Cell Biol. 1998;141(5):1277-86.

119. Jepsen KJ, Wu F, Peragallo JH, Paul J, Roberts L, Ezura Y, et al. A Syndrome of Joint Laxity and Impaired Tendon Integrity in Lumican- and Fibromodulin-deficient Mice *. Journal of Biological Chemistry. 2002;277(38):35532-40.

120. Boskey AL, Robey PG. Chapter 11 - The Regulatory Role of Matrix Proteins in Mineralization of Bone. In: Marcus R, Feldman D, Dempster DW, Luckey M, Cauley JA, editors. Osteoporosis (Fourth Edition). San Diego: Academic Press; 2013. p. 235-55.

121. Lorenzo P, Aspberg A, Onnerfjord P, Bayliss MT, Neame PJ, Heinegard D. Identification and characterization of asporin. a novel member of the leucine-rich repeat protein family closely related to decorin and biglycan. The Journal of biological chemistry. 2001;276(15):12201-11.

122. Hunter GK, Kyle CL, Goldberg HA. Modulation of crystal formation by bone phosphoproteins: structural specificity of the osteopontin-mediated inhibition of hydroxyapatite formation. Biochem J. 1994;300 (Pt 3)(Pt 3):723-8.

123. Kalamajski S, Aspberg A, Lindblom K, Heinegård D, Oldberg A. Asporin competes with decorin for collagen binding, binds calcium and promotes osteoblast collagen mineralization. Biochem J. 2009;423(1):53-9.

124. Xu L, Li Z, Liu SY, Xu SY, Ni GX. Asporin and osteoarthritis. Osteoarthritis and Cartilage. 2015;23(6):933-9.

125. Murphy S, Ohlendieck K. The biochemical and mass spectrometric profiling of the dystrophin complexome from skeletal muscle. Comput Struct Biotechnol J. 2016;14:20-7.

126. Önnerfjord P, Khabut A, Reinholt FP, Svensson O, Heinegård D. Quantitative proteomic analysis of eight cartilaginous tissues reveals characteristic differences as well as similarities between subgroups. The Journal of biological chemistry. 2012;287(23):18913-24.

127. BioGPS. ASPN - Gene Report 2021 [10/5/21]. Available from: http://biogps.org/#goto=genereport&id=54829.

128. Mouse Genome Informatics (MGI) MGDM, Gene Expression Database (GXD). MGI - Aspn Gene Detail 2021 [10/5/21]. Available from: http://www.informatics.jax.org/marker/MGI:109233.

129. Consortium S. STRING ASPN Protein Human 2021 [10/5/21]. Available from: https://string-db.org/cgi/network?taskId=b3BnJzmdWHVy&sessionId=bludjR4eShuL.

130. Wang Y, Fan X, Xing L, Tian F. Wnt signaling: a promising target for osteoarthritis therapy. Cell Communication and Signaling. 2019;17(1):97.

131. Swain S, Sarmanova A, Mallen C, Kuo CF, Coupland C, Doherty M, et al. Trends in incidence and prevalence of osteoarthritis in the United Kingdom: findings from the Clinical Practice Research Datalink (CPRD). Osteoarthritis and Cartilage. 2020;28(6):792-801.

132. Neogi T. The epidemiology and impact of pain in osteoarthritis. Osteoarthritis Cartilage. 2013;21(9):1145-53.

133. Chen D, Shen J, Zhao W, Wang T, Han L, Hamilton JL, et al. Osteoarthritis: toward a comprehensive understanding of pathological mechanism. Bone Res. 2017;5:16044.

134. Gruber HE, Ingram JA, Hoelscher GL, Zinchenko N, Hanley EN, Jr., Sun Y. Asporin, a susceptibility gene in osteoarthritis, is expressed at higher levels in the more degenerate human intervertebral disc. Arthritis research & therapy. 2009;11(2):R47.

135. Kizawa H, Kou I, Iida A, Sudo A, Miyamoto Y, Fukuda A, et al. An aspartic acid repeat polymorphism in asporin inhibits chondrogenesis and increases susceptibility to osteoarthritis. Nature genetics. 2005;37(2):138-44.

136. Sakao K, Takahashi KA, Arai Y, Saito M, Honjyo K, Hiraoka N, et al. Asporin and transforming growth factor-β gene expression in osteoblasts from subchondral bone and osteophytes in osteoarthritis. Journal of Orthopaedic Science. 2009;14(6):738-47.

137. Nakajima M, Kizawa H, Saitoh M, Kou I, Miyazono K, Ikegawa S. Mechanisms for asporin function and regulation in articular cartilage. The Journal of biological chemistry. 2007;282(44):32185-92.

138. Sciences N-NCfAT. Intervertebral disc disease 2012 [10/5/21]. Available from: https://rarediseases.info.nih.gov/diseases/8572/intervertebral-disc-disease.

139. Rustenburg CME, Emanuel KS, Peeters M, Lems WF, Vergroesen PA, Smit TH. Osteoarthritis and intervertebral disc degeneration: Quite different, quite similar. JOR spine. 2018;1(4):e1033.

140. Wang S, Liu C, Sun Z, Yan P, Liang H, Huang K, et al. IL-1β increases asporin expression via the NF-κB p65 pathway in nucleus pulposus cells during intervertebral disc degeneration. Sci Rep. 2017;7(1):4112.

141. Yu X, Liu H, Liu S, Chen X, Zhao X, Du Y, et al. Periodontal ligament-associated protein-1 gets involved in experimental periodontitis. Journal of periodontal research. 2019;54(2):180-9.

142. Yamada S, Tomoeda M, Ozawa Y, Yoneda S, Terashima Y, Ikezawa K, et al. PLAP-1/Asporin, a Novel Negative Regulator of Periodontal Ligament Mineralization*. Journal of Biological Chemistry. 2007;282(32):23070-80.

143. Könönen E, Gursoy M, Gursoy UK. Periodontitis: A Multifaceted Disease of Tooth-Supporting Tissues. Journal of clinical medicine. 2019;8(8).

144. BioSigma. Fast-Read® 102 - Product Information [Available from: https://www.biosigma.com/fast-read-reg-102.html.

145. Sakai K, Hiripi L, Glumoff V, Brandau O, Eerola R, Vuorio E, et al. Stage-and tissue-specific expression of a Col2a1-Cre fusion gene in transgenic mice. Matrix Biol. 2001;19(8):761-7.

146. Schneider CA, Rasband WS, Eliceiri KW. NIH Image to ImageJ: 25 years of image analysis. Nature Methods. 2012;9(7):671-5.

147. Johnson de Sousa Brito FM, Butcher A, Pisconti A, Poulet B, Prior A, Charlesworth G, et al. Syndecan-3 enhances anabolic bone formation through WNT signaling. Faseb j. 2021;35(4):e21246.

148. Dempster DW, Compston JE, Drezner MK, Glorieux FH, Kanis JA, Malluche H, et al. Standardized nomenclature, symbols, and units for bone histomorphometry: a 2012 update of the report of the ASBMR Histomorphometry Nomenclature Committee. J Bone Miner Res. 2013;28(1):2-17.

149. Zhang J, Wang JHC. The Effects of Mechanical Loading on Tendons - An In Vivo and In Vitro Model Study. PLOS ONE. 2013;8(8):e71740.

150. Schonk DM, Kuijpers HJH, van Drunen E, van Dalen CH, Geurts van Kessel AHM, Verheijen R, et al. Assignment of the gene(s) involved in the expression of the proliferation-related Ki-67 antigen to human chromosome 10. Human Genetics. 1989;83(3):297-9.

151. Almubarak A, Berry FB. Assessment of Growth Plate Chondrocytes Proliferative Activity in Embryonic Endochondral Ossification via Ki-67 Immunofluorescence. Methods Mol Biol. 2022;2579:227-33.

152. Stähelin BJ, Marti U, Solioz M, Zimmermann H, Reichen J. False positive staining in the TUNEL assay to detect apoptosis in liver and intestine is caused by endogenous nucleases and inhibited by diethyl pyrocarbonate. Mol Pathol. 1998;51(4):204-8.

153. van 't Hof RJ, Rose L, Bassonga E, Daroszewska A. Open source software for semi-automated histomorphometry of bone resorption and formation parameters. Bone. 2017;99:69-79.

154. Torgersen JS, Takle H, Andersen O. Localization of mRNAs and proteins in methyl methacrylate-embedded tissues. J Histochem Cytochem. 2009;57(9):825-30.

155. Zhu X, Jiang L, Lu Y, Wang C, Zhou S, Wang H, et al. Association of aspartic acid repeat polymorphism in the asporin gene with osteoarthritis of knee, hip, and hand: A PRISMA-compliant meta-analysis. Medicine. 2018;97(12):e0200.

156. Arellano RD, Hernández F, García-Sepúlveda CA, Velasco VM, Loera CR, Arguello JR. The D-repeat polymorphism in the ASPN gene and primary knee osteoarthritis in a Mexican mestizo population: a case-control study. J Orthop Sci. 2013;18(5):826-31.

157. Liu L, Zhao C, Zhang H, Lu Y, Luo B, Yao Z, et al. Asporin regulated by miR-26b-5p mediates chondrocyte senescence and exacerbates osteoarthritis progression via TGF-β1/Smad2 pathway. Rheumatology. 2021;61(6):2631-43.

158. Tomoaia G, Pasca RD. On the Collagen Mineralization. A Review. Clujul Med. 2015;88(1):15-22.

159. Chawla S, Mainardi A, Majumder N, Dönges L, Kumar B, Occhetta P, et al. Chondrocyte Hypertrophy in Osteoarthritis: Mechanistic Studies and Models for the Identification of New Therapeutic Strategies. Cells. 2022;11(24):4034.

160. Hsia AW, Emami AJ, Tarke FD, Cunningham HC, Tjandra PM, Wong A, et al. Osteophytes and fracture calluses share developmental milestones and are diminished by unloading. Journal of Orthopaedic Research. 2018;36(2):699-710.

161. Yu L, Wei M. Biomineralization of Collagen-Based Materials for Hard Tissue Repair. Int J Mol Sci. 2021;22(2).

162. Yao Y, Wang Y. ATDC5: an excellent in vitro model cell line for skeletal development. J Cell Biochem. 2013;114(6):1223-9.

163. Burmester A, Luthringer B, Willumeit R, Feyerabend F. Comparison of the reaction of bone-derived cells to enhanced MgCl2-salt concentrations. Biomatter. 2014;4(1):e967616.

164. Newton PT, Staines KA, Spevak L, Boskey AL, Teixeira CC, Macrae VE, et al. Chondrogenic ATDC5 cells: An optimised model for rapid and physiological matrix mineralisation. International Journal of Molecular Medicine. 2012;30(5):1187-93.

165. Hanna H, Mir LM, Andre FM. In vitro osteoblastic differentiation of mesenchymal stem cells generates cell layers with distinct properties. Stem Cell Research & Therapy. 2018;9(1):203.

166. Langenbach F, Handschel J. Effects of dexamethasone, ascorbic acid and β-glycerophosphate on the osteogenic differentiation of stem cells in vitro. Stem Cell Research & Therapy. 2013;4(5):117.

167. Michigami T, Ozono K. Roles of Phosphate in Skeleton. Frontiers in endocrinology. 2019;10.

168. Lindahl U, Couchman J, Kimata K, Esko JD. Proteoglycans and Sulfated Glycosaminoglycans. In: Varki A, Cummings RD, Esko JD, Stanley P, Hart GW, Aebi M, et al., editors. Essentials of Glycobiology. Cold Spring Harbor (NY): Cold Spring Harbor Laboratory Press. Copyright 2015-2017 by The Consortium of Glycobiology Editors, La Jolla, California. All rights reserved.; 2015. p. 207-21.

169. Roughley PJ, Mort JS. The role of aggrecan in normal and osteoarthritic cartilage. Journal of Experimental Orthopaedics. 2014;1(1):8.

170. Chen H, Ghori-Javed FY, Rashid H, Adhami MD, Serra R, Gutierrez SE, et al. Runx2 regulates endochondral ossification through control of chondrocyte proliferation and differentiation. J Bone Miner Res. 2014;29(12):2653-65.

171. Zhou J, Wei X, Wei L. Indian Hedgehog, a critical modulator in osteoarthritis, could be a potential therapeutic target for attenuating cartilage degeneration disease. Connect Tissue Res. 2014;55(4):257-61.

172. Wei F, Zhou J, Wei X, Zhang J, Fleming BC, Terek R, et al. Activation of Indian hedgehog promotes chondrocyte hypertrophy and upregulation of MMP-13 in human osteoarthritic cartilage. Osteoarthritis and Cartilage. 2012;20(7):755-63.

173. Hu Q, Ecker M. Overview of MMP-13 as a Promising Target for the Treatment of Osteoarthritis. Int J Mol Sci. 2021;22(4).

174. Kwan Tat S, Amiable N, Pelletier J-P, Boileau C, Lajeunesse D, Duval N, et al. Modulation of OPG, RANK and RANKL by human chondrocytes and their implication during osteoarthritis. Rheumatology. 2009;48(12):1482-90.

175. Kou I, Nakajima M, Ikegawa S. Expression and regulation of the osteoarthritis-associated protein asporin. The Journal of biological chemistry. 2007;282(44):32193-9.

176. Chen D, Kim DJ, Shen J, Zou Z, O'Keefe RJ. Runx2 plays a central role in Osteoarthritis development. J Orthop Translat. 2020;23:132-9.

177. Qin X, Jiang Q, Nagano K, Moriishi T, Miyazaki T, Komori H, et al. Runx2 is essential for the transdifferentiation of chondrocytes into osteoblasts. PLoS Genet. 2020;16(11):e1009169.

178. Houben A, Kostanova-Poliakova D, Weissenböck M, Graf J, Teufel S, von der Mark K, et al. β-catenin activity in late hypertrophic chondrocytes locally orchestrates osteoblastogenesis and osteoclastogenesis. Development. 2016;143(20):3826-38.

179. Fujita T, Azuma Y, Fukuyama R, Hattori Y, Yoshida C, Koida M, et al. Runx2 induces osteoblast and chondrocyte differentiation and enhances their migration by coupling with PI3K-Akt signaling. Journal of Cell Biology. 2004;166(1):85-95.

180. Lee KS, Lam TK, Song YQ, Cheah KSE, Cheung KMC, Chan D. In-Vivo Study of Asporin in Cartilage Tissues. Global Spine Journal. 2014;4(1_suppl):s-0034-1376609-s-0034-.

181. Han B, Li Q, Wang C, Patel P, Adams SM, Doyran B, et al. Decorin Regulates the Aggrecan Network Integrity and Biomechanical Functions of Cartilage Extracellular Matrix. ACS Nano. 2019;13(10):11320-33.

182. Zhu Z, Zhong L, Li R, Liu Y, Chen X, Li Z, et al. Study of Osteoarthritis-Related Hub Genes Based on Bioinformatics Analysis. Biomed Res Int. 2020;2020:2379280.

183. Chen N, Wu RWH, Lam Y, Chan WCW, Chan D. Hypertrophic chondrocytes at the junction of musculoskeletal structures. Bone Reports. 2023;19:101698.

184. Jiao Z, Chai H, Wang S, Sun C, Huang Q, Xu W. SOST gene suppression stimulates osteocyte Wnt/β-catenin signaling to prevent bone resorption and attenuates particle-induced osteolysis. J Mol Med (Berl). 2023;101(5):607-20.

185. Ağırdil Y. The growth plate: a physiologic overview. EFORT Open Reviews. 2020;5(8):498-507.

186. Briggs MD, Bell PA, Wright MJ, Pirog KA. New therapeutic targets in rare genetic skeletal diseases. Expert Opin Orphan Drugs. 2015;3(10):1137-54.

187. Mullan LA, Mularczyk EJ, Kung LH, Forouhan M, Wragg JM, Goodacre R, et al. Increased intracellular proteolysis reduces disease severity in an ER stress-associated dwarfism. J Clin Invest. 2017;127(10):3861-5.

188. Kyrylkova K, Kyryachenko S, Leid M, Kioussi C. Detection of Apoptosis by TUNEL Assay. In: Kioussi C, editor. Odontogenesis: Methods and Protocols. Totowa, NJ: Humana Press; 2012. p. 41-7.

189. Sandell LJ, Aigner T. Articular cartilage and changes in arthritis. An introduction: cell biology of osteoarthritis. Arthritis Res. 2001;3(2):107-13.

190. Wilson K, Usami Y, Hogarth D, Scheiber AL, Tian H, Oichi T, et al. Analysis of Association between Morphometric Parameters of Growth Plate and Bone Growth of Tibia in Mice and Humans. Cartilage. 2021;13(2_suppl):315s-25s.

191. Reddy Mh R. Osteopetrosis (Marble Bone Disease): A Rare Disease in Children. Int J Clin Pediatr Dent. 2011;4(3):232-4.

192. Sakashita H, Yamada S, Kinoshita M, Kajikawa T, Iwayama T, Murakami S. Mice lacking PLAP-1/asporin counteracts high fat diet-induced metabolic disorder and alveolar bone loss by controlling adipose tissue expansion. Sci Rep. 2021;11(1):4970.

193. Dobson PF, Dennis EP, Hipps D, Reeve A, Laude A, Bradshaw C, et al. Mitochondrial dysfunction impairs osteogenesis, increases osteoclast activity, and accelerates age related bone loss. Sci Rep. 2020;10(1):11643.

194. Allen MR, Burr DB. Chapter 8 - Techniques in Histomorphometry. In: Burr DB, Allen MR, editors. Basic and Applied Bone Biology (Second Edition): Academic Press; 2019. p. 141-58.

195. Li X, Yang S, Yuan G, Jing D, Qin L, Zhao H, et al. Type II collagen-positive progenitors are important stem cells in controlling skeletal development and vascular formation. Bone Research. 2022;10(1):46.

196. King TC. 6 - Skin and Musculoskeletal Pathology. In: King TC, editor. Elsevier's Integrated Pathology. Philadelphia: Mosby; 2007. p. 145-68.

197. Vimalraj S. Alkaline phosphatase: Structure, expression and its function in bone mineralization. Gene. 2020;754:144855.

198. Anderson IJ, Goldberg RB, Marion RW, Upholt WB, Tsipouras P. Spondyloepiphyseal dysplasia congenita: genetic linkage to type II collagen (COL2AI). Am J Hum Genet. 1990;46(5):896-901.

199. Waxenbaum JA, Reddy V, Futterman B. Anatomy, Back, Intervertebral Discs. StatPearls. Treasure Island (FL): StatPearls Publishing. Copyright © 2023, StatPearls Publishing LLC.; 2023.

200. Wagner S, Tintle S, Gwinn D. 16 - Intervertebral Disc Process of Degeneration: Physiology and Pathophysiology. In: Steinmetz MP, Benzel EC, editors. Benzel's Spine Surgery, 2-Volume Set (Fourth Edition). Philadelphia: Elsevier; 2017. p. 165-75.e4.

201. Torre OM, Mroz V, Bartelstein MK, Huang AH, Iatridis JC. Annulus fibrosus cell phenotypes in homeostasis and injury: implications for regenerative strategies. Ann N Y Acad Sci. 2019;1442(1):61-78.

202. Song YQ, Cheung KM, Ho DW, Poon SC, Chiba K, Kawaguchi Y, et al. Association of the asporin D14 allele with lumbar-disc degeneration in Asians. Am J Hum Genet. 2008;82(3):744-7.

203. Glasson SS, Chambers MG, Van Den Berg WB, Little CB. The OARSI histopathology initiative – recommendations for histological assessments of osteoarthritis in the mouse. Osteoarthritis and Cartilage. 2010;18:S17-S23.

204. Henry SP, Takanosu M, Boyd TC, Mayne PM, Eberspaecher H, Zhou W, et al. Expression pattern and gene characterization of asporin. a newly discovered member of the leucine-rich repeat protein family. The Journal of biological chemistry. 2001;276(15):12212-21.

205. Tsirikos AI, Mason DE, Scott CI, Jr., Chang WN. Spondyloepimetaphyseal dysplasia with joint laxity (SEMDJL). Am J Med Genet A. 2003;119a(3):386-90.

206. Erisken C, Zhang X, Moffat KL, Levine WN, Lu HH. Scaffold fiber diameter regulates human tendon fibroblast growth and differentiation. Tissue Eng Part A. 2013;19(3-4):519-28.

207. Jann J, Gascon S, Roux S, Faucheux N. Influence of the TGF-β Superfamily on Osteoclasts/Osteoblasts Balance in Physiological and Pathological Bone Conditions. Int J Mol Sci. 2020;21(20).